

**New Approaches to Casting Hypereutectic  
Al-Si Alloys to Achieve Simultaneous  
Refinement of Primary Silicon and  
Modification of Eutectic Silicon**

A thesis submitted for the degree of Doctor of  
Philosophy

by

Kawther W. A. Al-Helal

Brunel Centre for Advanced Solidification Technology  
(BCAST), Brunel University

October 2013

*This thesis is dedicated to  
my family for their  
love, support and encouragement*

بِسْمِ اللَّهِ الرَّحْمَنِ الرَّحِيمِ

أَتُونِي زُبَرَ الْحَدِيدِ ۖ حَتَّىٰ إِذَا سَلَوَىٰ بَيْنَ الصَّدَقَيْنِ قَالَ انفُخُوا ۖ حَتَّىٰ إِذَا جَعَلَهُ نَارًا  
قَالَ أَتُونِي أُفْرِغُ عَلَيْهِ قِطْرًا ۚ فَمَا اسْطَاعُوا أَن يَظْهَرُوهُ وَمَا اسْتَطَاعُوا لَهُ نَفْبًا.

صدق الله العظيم

الكهف: من الآية 95

In the name of Allah, the Entirely Merciful, the Especially Merciful

"Bring me blocks of iron, when he had filled up the space between the two steep mountain-sides, He said, "Blow (with your bellows)" Then, when he had made it (red) as fire, he said: "Bring me molten lead, that I may pour over it. So Gog and Magog were unable to pass over it, nor were they able (to effect) in it any penetration".

Surat Al-Kahf: 95

Holy Quran

## **Abstract**

Hypereutectic Al-Si alloys are of increasing interest for applications that require a combination of light weight and high wear resistance, such as pistons, liner-less engine blocks and pumps. The wear resistance of this class of alloys is due to the presence of hard primary Si particles formed during casting. The objective of this work was to develop one or more methods of refining primary silicon in cast hypereutectic Al-Si alloys to compete with the conventional process of adding phosphorous and to achieve the simultaneous modification of silicon in the Al-Si eutectic.

A robust sampling/casting technique was developed to minimise macro-segregation of primary silicon during solidification of hypereutectic Al-Si alloys by using water cooled steel mould with cooling rate in excess of 15 K/s.

The morphology of silicon phases was found to change with increasing melt temperature and cooling rate. The high cooling rate and superheat temperature produces a good distribution of polyhedral primary silicon particles in a refined lamellar eutectic matrix in solidification of commercial purity Al-Si alloys.

Removing Ca by fluxing with  $K_2SiF_6$  prior to casting can improve the refinement and modification effect of Mg and Sb respectively. Effects of various inoculants were studied. Microstructural analysis showed that Mg and ZnS refined primary Si whereas MgO, CaO and Na<sub>2</sub>S coarsened the primary Si together with a modification effect on the eutectic Si. Adding Zn had no effect on morphology of Si phases. Refinement of both primary and eutectic silicon phases was observed for the Al-15Si alloy with Mg content  $\leq 0.3$  wt%.

P-doped  $\gamma$ -Al<sub>2</sub>O<sub>3</sub> was found to be a potent substrate to nucleate primary silicon whilst good modification of the eutectic matrix is retained during solidification of hypereutectic Al-Si alloys. On using P-doped  $\gamma$ -Al<sub>2</sub>O<sub>3</sub> could be a perfect and clean source of P without additional impurities.

A new solid-liquid duplex casting process was devised to achieve simultaneous refinement and modification of Si phases in hypereutectic Al-Si alloys with improvement in mechanical properties. The static mechanical properties of Al-Si produced by the solid-liquid duplex casting process are significantly better than conventionally cast untreated Al-Si and slightly better than conventionally cast Al-Si treated with P and/or Sr.

A novel Al-ZnS master alloy was developed by *in situ* reaction of Zn and Na<sub>2</sub>S in the Al melt. The results from this study leave little doubt that this novel Al-ZnS master alloy is a promising refiner in solidification of hypereutectic Al-Si alloys. It refines primary silicon to the same extent as that achieved by adding P via Cu-P following the same refinement mechanism.

## **Preface**

This thesis is a description of work that I performed in the Brunel Centre for Advanced Solidification Technology, Brunel University, West London from 22<sup>nd</sup> October 2009 to 30<sup>th</sup> October 2013. To the best of my knowledge, this work is original, except where suitable references are made to previous work. Neither this, nor any substantially similar dissertation has been submitted to any other institution nor is it the result of my own work. The content of the dissertation does not exceed 60,000 words.

## Related Publications

### International Journal Papers

- Kawther W. Al-Helal, Ian C. Stone and Zhongyun Fan, “*Simultaneous Primary Si Refinement and Eutectic Modification in Hypereutectic Al-Si Alloys*”, Trans. Indian Inst. Metals. (December 2012) 65(6):663–667.
- Kawther W. Ahmed Al-Helal, Yun Wang, Ian C. Stone and Zhongyun Fan, ‘*Effect of Ca Level on the Formation of Silicon Phases During Solidification of Hypereutectic Al-Si Alloys*’, Mat. Sci. Forum Vol. 765 (2013) pp 117-122.
- Kawther Al-Helal, Ian C. Stone and Z. Fan, ‘*Morphology of Silicon Phases in Solidification of High Purity Hypereutectic Al-15Si Alloy*’, 2013. The paper is in preparation.
- Kawther Al-Helal, Ian C. Stone and Z. Fan, ‘*Novel Al-ZnS Master Alloy for Refinement of Primary Silicon Crystals in Solidification of Hypereutectic Al-Si Alloys*’, 2013. The paper is in preparation.
- Kawther Al-Helal, Ian C. Stone and Z. Fan, “*Effect of Solidification Rate on Macro Segregation and Morphologies of Silicon phases in Solidification of Hypereutectic Al-15Si Alloy*”, 2013. The paper is in preparation.

## Conferences

- The John Hunt International Symposium, Brunel University, UK, December 12 -14, 2011.
- National Student Conference in Metallic Materials, Manchester Conference Centre, UK, June 25-26, 2012.
- Fifth International Conference on Solidification Science and Processing, Bhubaneswar, India, November 19-22, 2012 / Poster.
- Sixth International Light Metals Technology Conference (LMT2013), Windsore, UK, July 24-26, 2013.

## **Acknowledgements**

I would like to express my sincere gratitude and grateful admiration to my supervisors Prof. Zhongyun Fan and Dr. Ian Stone for their encouragement, continuous guidance, utmost effort and interest through the work that contributed in its completeness.

I am grateful to the EPSRC, UK for funding this project and my special thanks and sincere gratitude to Prof. Paul Harris / Wolfson Materials Processing Centre, Prof. Andy Feest and Dr. Kumar Sundaram / Oxford University for their help and useful discussion throughout my PhD programme. My thanks to Aura Metals Ltd for supplying the CuP shot that I used during my research.

I am in great debt to Prof. Dmitry Eskin and Dr. Hari-babu Nadendla for their obliging and fruitful support on all topics and through all stages of this work.

I have received technical help/suggestions from many people at BCAST during the course of this work. I want to specially mention Dr. Yun Wang, Dr. Jayesh Patel, Dr. Yubo Zuo, Dr. Magdalena Nowak, Dr. H-T Li, Dr. Anil Midathada and Dr. Prasadd Ayyagari for their scientifically helpful and discussions. My special thanks to Mr. Stephen Cook, Mr. Peter Lloyd and Mr. Carmelo Nunez for their technical support.

I wish to express my thanks to my colleagues at BCAST for their support and letting me fell part of the team whenever we worked together.

Finally, I wish to express my deepest respect and sincere appreciation to my family for their encouragement, patience and great understanding.

## Table of Contents

Abstract .....	iii
Preface .....	iv
Related Publications .....	v
Conferences .....	v
Acknowledgements.....	vi
Table of Contents .....	vii
List of Figures .....	xii
List of Tables .....	xxii
Nomenclature .....	xxiv

<b>Chapter 1 Introduction.....</b>	<b>1</b>
1.1 Background .....	1
1.2 Objectives and Scope.....	3
1.3 Outline of Thesis .....	4
<b>Chapter 2 Literature Review .....</b>	<b>5</b>
2.1 Introduction to Al-Si Alloys .....	5
2.2 The Al-Si Alloy System and Properties.....	6
2.3 Hypereutectic Al-Si Alloys.....	9
2.4 Inclusions and Oxides.....	13
2.5 Calcium in Al-Si Alloys .....	14
2.6 Fluxing .....	16
2.7 Eutectic Modification .....	18
2.8 Primary Si Refinement and Morphology.....	21
2.9 Simultaneous Refinement of Primary Si and Modification of Eutectic Si.....	26
2.10 Mechanism of Nucleation of Primary Si.....	27
2.10.1 Classical nucleation theory.....	27

2.10.2 Nucleation on potent substrates by adsorption .....	29
2.11 Nucleation-Adsorption Model .....	31
2.12 Segregation of Primary Si .....	32
2.13 Mechanical Properties .....	32
2.14 Casting Processes .....	33
2.14.1 Conventional casting .....	34
2.14.2 Semi-solid processing .....	36
2.14.3 Duplex casting processes.....	38
<b>Chapter 3 Experimental Techniques and Procedures.....</b>	<b>41</b>
3.1 Materials Preparation.....	41
3.2 Effect of Cooling Rate on Primary and Eutectic Si .....	42
3.2.1 TP-1 test procedure .....	43
3.3 Effect of Melt Superheat on Primary and Eutectic Si .....	44
3.4 Refinement and Modification in a High Purity Hypereutectic Al-Si Alloy .....	44
3.5 Effect of Ca Level on Primary and Eutectic Si.....	45
3.6 Effect of Chemical Additions on Primary and Eutectic Si.....	45
3.7 Refinement of Primary Si using Zincblende ZnS .....	46
3.7.1 ZnS micron scale particles .....	46
3.7.2 Synthesised ZnS nanoparticles .....	47
3.7.3 <i>In situ</i> preparation of ZnS .....	48
3.7.4 Preparation of an Al-ZnS master alloy .....	48
3.8 Nucleation and Growth of Primary Si on Al <sub>2</sub> O <sub>3</sub> .....	49
3.9 A New Solid-Liquid Duplex Casting Process.....	49
3.10 Characterisation Methods .....	55
3.10.1 Preparation of samples.....	55
3.10.2 Chemical composition analysis.....	55
3.10.3 Optical microscopy (OM) .....	55

3.11 Scanning Electron Microscopy (SEM) .....	56
3.12 Mechanical Property Tests.....	56
<b>Chapter 4 Results .....</b>	<b>57</b>
4.1 Effect of Solidification Rate on Primary and Eutectic Si.....	57
4.1.1 Effect of cooling rate.....	57
4.1.2 Effect of melt superheat.....	58
4.2 Refinement and Modification in a High Purity Hypereutectic Al-Si Alloy .....	62
4.2.1 Unmodified/unrefined high purity Al-15Si alloy .....	62
4.2.2 High purity Al-15Si alloy refined with P .....	63
4.2.3 High purity Al-15Si alloy modified with Ca .....	64
4.3 Effect of Ca Level on Primary and Eutectic Si.....	65
4.3.1 Removal of Ca by $K_2SiF_6$ flux .....	65
4.3.2 High Ca content.....	68
4.3.3 Effect of Ca in the presence of Mg or Sb .....	69
4.4 Effect of Chemical Additions on Primary and Eutectic Si.....	72
4.4.1 Magnesium (Mg) .....	73
4.4.2 Mg and Ca oxides .....	77
4.4.3 Zincblende ZnS .....	78
4.4.3.1 ZnS micron scale particles .....	78
4.4.3.2 ZnS nanoparticles .....	79
4.4.3.3 <i>In situ</i> prepared ZnS .....	81
4.4.3.4 Characterisation of an Al-ZnS master alloy .....	83
4.4.3.5 Effect of the Al-ZnS master alloy.....	84
4.4.4 Sodium Sulphide ( $Na_2S$ ).....	89
4.4.5 Zinc (Zn).....	89
4.5 Nucleation and Growth of Primary Si on $Al_2O_3$ .....	90
4.6 The New Solid-Liquid Duplex Casting Process .....	96

4.6.1 Conventional casting .....	96
4.6.2 The Solid-liquid duplex casting process.....	98
4.6.2.1 Optimum P and Sr for P-treated and Sr-treated alloys .....	98
4.6.2.2 Optimum Si content in Sr-treated Al-Si alloy .....	113
4.6.2.3 Effect of casting temperature .....	117
4.6.2.4 Comparison between the solid-liquid duplex and conventional casting processes.....	121
4.6.2.5 Application of the solid-liquid duplex process for producing Al-18Si alloy .....	123
4.6.3 Mechanical properties .....	125
<b>Chapter 5 Discussion.....</b>	<b>127</b>
5.1 Effect of Solidification Rate on Primary and Eutectic Si.....	127
5.1.1 Effect of cooling rate.....	127
5.1.2 Effect of melt superheat.....	129
5.1.3 Summary.....	130
5.2 Refinement and Modification in a High Purity Hypereutectic Al-Si Alloy .....	130
5.2.1 Unmodified/unrefined high purity Al-15Si alloy .....	130
(1) Homogeneous nucleation and growth mechanism of primary Si in unrefined hypereutectic Al-Si alloys .....	131
(2) Growth of unmodified eutectic Si in Al-Si alloy.....	132
5.2.2 High purity Al-15Si alloy refined with P .....	133
5.2.3 High purity Al-15Si alloy modified with Ca .....	134
5.2.4 Summary.....	135
5.3 Effect of Ca Level on Primary and Eutectic Si.....	135
5.3.1 Removal of Ca by $K_2SiF_6$ flux .....	135
5.3.2 High Ca content.....	136
5.3.3 Effect of Ca in the presence of Mg or Sb .....	139
5.3.4 Summary.....	140

5.4 Effect of Chemical Additions on Primary and Eutectic Si.....	141
5.4.1 Magnesium (Mg) .....	141
5.4.2 Mg and Ca oxides .....	142
5.4.3 Refinement of primary Si crystals by zincblende ZnS .....	144
5.4.4 Summary.....	146
5.5 Nucleation and Growth of Primary Si on Al <sub>2</sub> O <sub>3</sub> .....	147
5-5-1 Summary .....	148
5.6 The New Solid-Liquid Duplex Casting Process .....	148
5.6.1 Optimum P and Sr content for P-treated and Sr-treated alloys .....	149
5.6.2 Optimum Si content in Sr-treated Al-Si alloy.....	150
5.6.3 Effect of casting temperature.....	150
5.6.4 The mechanism of refinement and modification in solid-liquid duplex casting process .....	152
5.6.5 Summary.....	153
<b>Chapter 6 Conclusions .....</b>	<b>155</b>
6.1 Effect of Solidification Rate on Primary and Eutectic Si.....	155
6.2 Refinement and Modification in a High Purity Hypereutectic Al-Si Alloy .....	156
6.3 Effect of Ca Level on Primary and Eutectic Si.....	156
6.4 Effect of Chemical Additions on Primary and Eutectic Si.....	157
6.5 Nucleation and Growth of Primary Si on Al <sub>2</sub> O <sub>3</sub> .....	158
6.6 The New Solid-Liquid Duplex Casting Process .....	159
<b>Chapter 7 Recommendations for further work .....</b>	<b>160</b>
7.1 Refinement of Primary Si Crystals by Zincblende ZnS .....	160
7.2 Nucleation and Growth of Primary Si on Al <sub>2</sub> O <sub>3</sub> .....	160
7.3 The New Solid-Liquid Duplex Casting Process .....	160
<b>References .....</b>	<b>161</b>

## List of Figures

<b>Figure 2.1</b> Equilibrium Al-Si phase diagram with typical microstructure of hypoeutectic and hypereutectic Al-Si Alloys.....	5
<b>Figure 2.2</b> Microstructure of Al-Si Alloys etched by Weck's Reagent; (a) Hypoeutectic (b) Hypereutectic.....	6
<b>Figure 2.3</b> Standard Gibbs energy of formation of several sulphides, oxides, chlorides, and fluorides at 723 °C.....	17
<b>Figure 2.4</b> Exchange equilibrium between aluminium and different metal chlorides or metal fluorides at 723 °C.....	17
<b>Figure 2.5</b> Eutectic growth modes suggested by Dahle <i>et al.</i> (84). (a) nucleation and growth on primary $\alpha$ -Al dendrites; (b) independent nucleation of eutectic grains, and (c) planar-front growth. .....	19
<b>Figure 2.6</b> Eutectic silicon morphology in Al-Si Alloys: (a) unmodified, (b) Fibrous structure (c) Lamellar structure.....	20
<b>Figure 2.7</b> Silicon crystal morphologies: (a) Fish-bone like structure, (b) Large star shaped crystal and (c) Large plates structure.....	22
<b>Figure 2.8</b> SEM micrographs of star shaped crystals in 25 wt% Si alloy: (a) fully developed star with five arms growing in length and thickness from a common nucleus. (b) a star crystal at an early stage of development.....	22
<b>Figure 2.9</b> The crystal structures of (a) AlP; (b) Si.....	24
<b>Figure 2.10</b> The optical micrographs of: (a) Al-30Si alloy, (b) Al-30Si with the addition of 400 ppm P.....	24
<b>Figure 2.11</b> A schematic representation of (a) homogenous nucleation and (b) heterogeneous nucleation on foreign substrate.....	27
<b>Figure 2.12</b> The formation of a spherical nucleus of solid phase on the surface of a foreign substrate.....	28
<b>Figure 2.13</b> A schematic illustration of the 'high pressure die-casting' (HPDC) machine.....	35

<b>Figure 2.14</b> Schematic illustration of the MCAST (melt conditioning by advanced shearing technology) unit.....	38
<b>Figure 2.15</b> Relationship between the content of the first liquid $C_1$ and the Si particle size $d$ of the primary Si in a stepwise cast ingot .....	39
<b>Figure 2.16</b> Relationship between the content of the second liquid $C_2$ and the Si particle size $d$ of the primary Si in a stepwise cast ingot.....	39
<b>Figure 2.17</b> Diagram of the swirl enthalpy equilibration device (SEED process).....	40
<b>Figure 3.1</b> Cooling curve of Al-15Si alloy sampled using boron nitride coated steel mould: (a) water cooled with cooling rate of 15 K/s, and (b) air cooled with cooling rate of 1 K/s.....	42
<b>Figure 3.2</b> Scanning graphs showing the segregation of primary Si at the top of the TP-1 test casting in solidification of hypereutectic Al-15Si alloy at: (a) 1150 °C, (b) 720 °C and (c) 620 °C.....	43
<b>Figure 3.3</b> Schematic diagram of American Association Standard, TP-1 test mould ladle.....	43
<b>Figure 3.4</b> XRD pattern of ZnS prepared by the solid-liquid chemical reaction. The peaks associated with diffraction from crystallographic phases of zincblende ZnS are labelled.....	47
<b>Figure 3.5</b> Preparation of Al-19Si (Target Alloy) by mixing the melt of Sr-treated Al-8Si (Alloy 1) with P-treated Al-30Si solid chips (Alloy 2) and casting at 610 °C.....	50
<b>Figure 4.1</b> Optical micrographs of Al-15Si alloy to show the morphology of primary Si and the eutectic structure cast at 750 °C for different cooling rates; (a,b) air cooled steel mould (1K/s), (c,d) TP-1 test ( about 3.5 K/s) and (e,f) water cooled steel mould (15 K/s), at (a, c, e) low magnification and (b, d, f) high magnification.....	58
<b>Figure 4.2</b> Comparison of primary Si morphologies of Al-15Si alloy cast from different melt temperatures .....	59
<b>Figure 4.3</b> Comparison of eutectic silicon morphologies of Al-15Si alloy at different melt temperatures.....	60

<b>Figure 4.4</b> Particle size distribution of primary Si in Al-15Si alloy cast from: (a) 650 °C; (b) 700 °C; (c) 730 °C; (d) 750 °C; (e) 845 °C and (f) 1150 °C.....	61
<b>Figure 4.5</b> Effect of melt temperature on: (a) primary Si particle size; (b) shape factor, (c) particle number density and (d) primary Si volume fraction of Al-15Si alloy.....	62
<b>Figure 4.6</b> Optical micrographs of Al-15Si alloys solidified from 800°C: (a,b) high purity alloy; (c,d) commercial purity alloy. (a,c) low magnification and (b,d) high magnification.....	63
<b>Figure 4.7</b> Optical micrographs of Al-15Si+20ppm P alloy solidified from 800 °C: (a,b) high purity alloy; (c,d) commercial purity alloy. (a,c) low magnification and (b,d) high magnification.....	64
<b>Figure 4.8</b> Optical micrographs of high purity Al-15Si+30ppm Ca alloy solidified from 800 °C. (a) low magnification and (b) high magnification.....	65
<b>Figure 4.9</b> Optical micrographs of Al-15Si alloy solidified from 800 °C: (a,b) without K <sub>2</sub> SiF <sub>6</sub> flux; (c,d) with 0.5 wt% K <sub>2</sub> SiF <sub>6</sub> flux. (a,c) low magnification; (b,d) high magnification.....	66
<b>Figure 4.10</b> Optical micrographs of Al-18Si alloy solidified from 800 °C: (a,b) without K <sub>2</sub> SiF <sub>6</sub> flux; (c,d) with 0.5 wt% K <sub>2</sub> SiF <sub>6</sub> flux. (a,c) low magnification; (b,d) high magnification.....	67
<b>Figure 4.11</b> Particle size distribution of primary Si in: (a) Al-15Si Alloy; (b) Al-15Si with 0.5 wt% K <sub>2</sub> SiF <sub>6</sub> flux; (c) Al-18Si alloy and (d) Al-18Si with 0.5 wt% K <sub>2</sub> SiF <sub>6</sub> flux.....	67
<b>Figure 4.12</b> Vertical section of the Al-Si-Ca phase diagram for Al-15Si-xCa (x=0-1wt%) .....	68
<b>Figure 4.13</b> Optical micrographs of the typical morphology of primary Si and an Al-Si-Ca phase, in the Al-15Si-0.5Ca alloy, formed in association with each other and with oxide particles (a) and bifilms (b).....	69
<b>Figure 4.14</b> Vertical section of the Al-Si-Mg phase diagram for Al-15Si-xMg (x=0-1wt%).....	70
<b>Figure 4.15</b> Optical micrographs of: (a,b) Al-15Si alloy (c,d) Al-15Si alloy with 0.5 wt% Mg; (e,f) Al-15Si alloy fluxed with 0.5 wt% AP1 then alloyed with	

0.5 wt% Mg cast from 800 °C. (a,c & e) low magnification to show the size and distribution of primary Si and (b,d & f) high magnification to show the eutectic structure.....	71
<b>Figure 4.16</b> Optical micrographs of: (a,b) Al-15Si alloy; (c,d) with 0.5 wt% Sb and (e,f) fluxed with 0.5 wt% AP1 then alloyed with 0.5 wt% Sb cast from 800 °C. (a,c & e) low magnification to show the size and distribution of primary Si and (b,d & f) high magnification to show the eutectic structure.....	72
<b>Figure 4.17</b> Optical micrographs of the Al-15Si alloy cast from 800 °C. (a) low magnification and (b) high magnification.....	73
<b>Figure 4.18</b> Optical micrographs of Al-15Si alloy with the addition of (a,b) 0.1 wt% Mg, (c,d) 0.3 wt% Mg, (e,f) 0.4 wt% Mg. (g,h) 0.5 wt% Mg, (i,j) 0.75 wt% Mg and (k,l) 1%wt Mg. (a,c,e,g,I & k) low magnification to show the size and distribution of primary Si; (b,d,f,h,j & l) high magnification to show the eutectic structure.....	74
<b>Figure 4.19</b> Plot of primary Si particle size as a function of Mg addition (wt%) to commercial purity Al-15Si alloy.....	75
<b>Figure 4.20</b> Particle size distribution of primary Si in Al-15Si alloys with: (a) 0.0; (b) 0.1; (c) 0.3; (d) 0.4; (e) 0.5 and (f) 0.75 wt% Mg additions.....	76
<b>Figure 4.21</b> Optical micrographs of Al-15Si alloys as cast from 800 °C: (a,b) Al-15Si alloy; (c,d) Al-15Si with 0.5 wt% MgO and (e,f) Al-15Si with 0.5 wt% CaO. (a,c & e) low magnification to show the size and distribution of primary Si and (b,d & f) high magnification to show the eutectic structure.....	77
<b>Figure 4.22</b> Optical micrographs of Al-18Si alloy. (a) low magnification to show the size and distribution of primary Si and (b) high magnification to show the eutectic structure.....	78
<b>Figure 4.23</b> Optical micrographs of: (a, b) Al-18Si with the addition of 0.5 wt% ZnS ( $\leq 44 \mu\text{m}$ in size); (c, d) Al-18Si alloy with the addition of 100 ppm P. (a, c) low magnification and (b, d) high magnification.....	79
<b>Figure 4.24</b> Optical micrographs of as-cast alloys: (a,b) Al-18Si alloy; (c,d) Al-18Si with the addition of 0.5 wt% ZnS nanoparticles. (e,f) Al-18Si alloy with the	

addition of 100 ppm P. (a,c&e) low magnification to show the size and distribution of primary Si and (b,d&f) high magnification to show the eutectic structure.....	80
<b>Figure 4.25</b> Particle size distribution of primary Si in Al-18Si alloys: (a) without addition; (b) with 100ppm P; (c) with 0.5 wt% ZnS <44 µm and (d) with 0.5 wt% ZnS nanoparticles.....	81
<b>Figure 4.26</b> Optical micrographs of Al-18Si with nominally 0.27 wt% ZnS formed <i>in situ</i> . (a) low magnification, and (b) high magnification .....	82
<b>Figure 4.27</b> Particle size distribution of primary Si in: (a) Al-18Si alloy; (b) Al-18Si with the addition of 0.27 wt% ZnS zincblende; and (c) Al-18Si with the addition of 100 ppm P.....	83
<b>Figure 4.28</b> SEM micrographs and EDS spectrum showing the formation of precipitated ZnS particles. (a) low magnification to show the size and distribution of ZnS particles, and (b) high magnification to show the morphology of ZnS particles .....	83
<b>Figure 4.29</b> Optical micrographs of: (a, b) Al-22Si alloy: (c, d) Al-22Si with the addition of 0.05 wt% ZnS cast after 20 min; (e,f) Al-22Si with the addition of 0.1 wt% ZnS cast after 20 min; (g,h) Al-22Si with the addition of 0.16 wt% ZnS cast after 20 min; (a,c,e & g) low magnification and (b,d,f & h) high magnification. ZnS was added in the form of the Al-ZnS master alloy.	85
<b>Figure 4.30</b> Plot of primary Si particle size as a function of ZnS addition (wt%), in the form of Al-ZnS master alloy, to commercial purity Al-22Si alloy.....	86
<b>Figure 4.31</b> Particle size distributions of primary Si in Al-22Si alloys: (a) without addition; (b) with 0.05 wt% ZnS; (c) with 0.1 wt% ZnS; and (d) 0.16 wt% ZnS addition.....	87
<b>Figure 4.32</b> Optical micrographs of Al-22Si with the addition of 0.1% ZnS cast after 1.5 hr holding time prior to casting. (a) low magnification and (b) high magnification.....	87
<b>Figure 4.33</b> Optical micrographs of Al-20Si alloy with the addition of 200 ppm P. (a) low magnification and (b) high magnification.....	88

<b>Figure 4.34</b> Particle size distribution of primary Si in: (a) Al-22Si alloys with 0.1 wt% ZnS; (b) Al-20Si with 200 ppm P.....	88
<b>Figure 4.35</b> Optical micrographs of Al-18Si with the addition of 0.5 wt% Na <sub>2</sub> S. (a) low magnification to show the size and distribution of primary Si and (b) high magnification to show the eutectic structure.....	89
<b>Figure 4.36</b> Optical micrographs of as-cast alloys: (a,b) Al-22Si alloy; (c,d) Al-22Si with the addition of 0.5 wt% Zn. (a,c) low magnification to show the size and distribution of primary Si and (b,d) high magnification to show the eutectic structure.....	90
<b>Figure 4.37</b> Optical micrographs showing example of the association of primary Si with oxide bifilms in Al-18Si alloy cast from 800 °C. (a) low magnification and (b) high magnification.....	90
<b>Figure 4.38</b> Optical micrographs of as-cast alloys: (a,b) Al-18Si alloy; (c,d) Al-18Si with the addition of 0.5 wt% $\alpha$ -Al <sub>2</sub> O <sub>3</sub> (0.5 $\mu$ m); and (e,f) Al-18Si with the addition of 0.5 wt% $\gamma$ -Al <sub>2</sub> O <sub>3</sub> (0.5 $\mu$ m). (a,c & e) low magnification to show the size and distribution of primary Si and (b,d & f) high magnification to show the eutectic structure.....	92
<b>Figure 4.39</b> Optical micrographs of as-cast alloys: (a,b) Al-18Si alloy; (c,d) Al-18Si with the addition of 0.5wt% P-doped $\alpha$ -Al <sub>2</sub> O <sub>3</sub> (0.5 $\mu$ m in size); and (e,f) Al-18Si with the addition of 0.5wt% P-doped $\gamma$ -Al <sub>2</sub> O <sub>3</sub> (0.5 $\mu$ m in size). (a,c & e) low magnification to show the size and distribution of primary Si and (b,d & f) high magnification to show the eutectic structure.....	93
<b>Figure 4.40</b> Optical micrographs of as-cast alloys: (a,b) Al-18Si alloy; (c,d) Al-18Si with the addition of 0.5 wt% P-doped $\gamma$ -Al <sub>2</sub> O <sub>3</sub> (3 $\mu$ m); and (e,f) Al-18Si with the addition of 100ppm P. (a,c & e) low magnification to show the size and distribution of primary Si and (b,d & f) high magnification to show the eutectic structure.....	94
<b>Figure 4.41</b> Particle size distribution of primary Si in: (a) Al-18Si alloys; (b) with 0.5wt% P-doped $\gamma$ -Al <sub>2</sub> O <sub>3</sub> (0.5 $\mu$ m in size); (c) with 0.5wt% P-doped $\gamma$ -Al <sub>2</sub> O <sub>3</sub> (3 $\mu$ m in size) addition; and (d) with 100ppm P .....	95

<b>Figure 4.42</b> Optical micrographs of conventionally cast Al-19Si alloy without P or Sr addition at (a) low magnification to show the size and distribution of primary Si and (b) high magnification to show the eutectic structure.....	96
<b>Figure 4.43</b> Optical micrographs of conventionally cast Al-19Si alloy: (a,b) Al-19Si+200ppm P and (c,d) Al-19Si+200ppm Sr at (a,c) low magnification to show the size and distribution of primary Si and (b,d) high magnification to show the eutectic structure.....	97
<b>Figure 4.44</b> Optical micrographs of conventionally cast Al-19Si+200ppm P+200ppm Sr at (a) low magnification and (b) high magnification.....	97
<b>Figure 4.45</b> Optical micrographs of Al-8Si alloy cast from 800 °C, at: (a) low magnification and (b) high magnification.....	98
<b>Figure 4.46</b> Optical micrographs of Al-30Si: (a) without added P; (b) with 50 ppm added P; (c) with 100 ppm added P; (d) with 200 ppm added P; (e) with 300 ppm added P; and (f) with 400 ppm added P.....	99
<b>Figure 4.47</b> Particle size distribution of primary Si in Al-30Si alloys: (a) with no addition; (b) with 50 ppm P; (c) with 100 ppm P; (d) with 200 ppm P; (e) 300 ppm P; and (f) with 400 ppm P addition.....	100
<b>Figure 4.48</b> Plot of particle size of primary Si against the amount of P added to commercial purity Al-30Si Alloy.....	101
<b>Figure 4.49</b> Optical micrographs of Al-19Si+P produced by mixing Al-8Si with: (a,b) Al-30Si alloy (SLD1), (c,d) Al-30Si+50ppm P alloy (SLD2) and (e,f) Al-30Si+100ppm P (SLD3). (a,c & e) low magnification and (b,d & f) high magnification.....	102
<b>Figure 4.50</b> Particle size distribution of primary Si in Al-19Si+P produced by mixing Al-8Si liquid alloy with solid: (SLD1) Al-30Si alloy; (SLD2) Al-30Si+50ppm P alloy and (SLD3) Al-30Si+100ppm P.....	103
<b>Figure 4.51</b> Optical micrographs of Al-8Si+400ppm Sr alloy cast from 800 °C, at (a) low magnification and (b) high magnification.....	104

- Figure 4.52** Optical micrographs of Al-19Si+200ppm Sr alloy produced by mixing liquid Al-8Si+400ppm Sr and solid Al-30Si alloys (SLD4), cast from 610 °C, at (a) low magnification and (b) high magnification. ....104
- Figure 4.53** Optical micrographs of Al-19Si+200ppm Sr+P produced by mixing liquid Al-8Si+400ppm Sr with solid (a,b) Al-30Si+50ppm P (SLD5); (c,d) Al-30Si+100ppm P (SLD6); (e,f) Al-30Si+200ppm P (SLD7); (g,h) Al-30Si+300 ppm P (SLD8) and (i,j) Al-30Si+400ppm P (SLD9). (a,c,e,g&i) low magnification and (b,d,f,h&j) high magnification. ....105
- Figure 4.54** Plot of primary Si particle size in the target alloy against P content of the Al-30Si solid starting alloy when mixed with Al-8Si+400ppm Sr alloy and cast from 610 °C (SLD5-SLD9).....106
- Figure 4.55** Particle size distribution of primary Si in Al-19Si+200ppm Sr+P produced by mixing liquid Al-8Si+400ppm Sr with solid: (SLD4) Al-30Si; (SLD5) Al-30Si+50ppm P; (SLD6) Al-30Si+100ppm P; (SLD7) Al-30Si+200ppm P; (SLD8) Al-30Si+300ppm P and (SLD9) Al-30Si+400ppm P.....107
- Figure 4.56** Optical micrographs of Al-19Si+Sr+200ppm P alloy produced by mixing solid Al-30Si+400ppm P with liquid (a,b) Al-8Si+300ppm Sr (SLD10); (c,d) Al-8Si+200ppm Sr (SLD11). (a,c) low magnification and (b,d) high magnification.....108
- Figure 4.57** Optical micrographs of Al-19Si+150ppm Sr+150ppm P alloy produced by mixing solid Al-30Si+300ppm P and liquid Al-8Si+300ppm Sr (SLD12) at (a) low magnification and (b) high magnification.....109
- Figure 4.58** Particle size distribution of primary Si in Al-19Si+Sr+200ppm P alloy produced by mixing solid Al-30Si+400ppm P with liquid: (SLD10) Al-8Si+300ppm Sr and (SLD11) Al-8Si+200ppm Sr.....109
- Figure 4.59** Particle size distribution of primary Si in Al-19Si+150ppm Sr+150ppm P alloy produced by mixing solid Al-30Si+300ppm P and liquid Al-8Si+300ppm Sr (SLD12).....109
- Figure 4.60** Optical micrographs of Al-19Si+252ppm P+200ppm Sr alloy produced by mixing solid Al-30Si+400ppm P alloy with liquid CPAI+540ppm Sr alloy cast from 610 °C (SLD13). (a) low magnification and (b) high magnification.....113

**Figure 4.61** Optical micrographs of Al-19Si+200ppm P+200ppm Sr alloy produced by mixing solid Al-30Si+400ppm P alloy with liquid Al-8Si+400ppm Sr alloy cast from 610 °C (SLD9). (a) low magnification and (b) high magnification.....114

**Figure 4.62** Optical micrographs of Al-19Si+148ppm P+200ppm Sr alloy produced by mixing solid Al-30Si+400ppm P alloy with liquid Al-12.6Si+317ppm Sr alloy cast from 610 °C (SLD14). (a) low magnification and (b) high magnification.....114

**Figure 4.63** Optical micrographs of Al-19Si+108ppm P+200ppm Sr alloy produced by mixing solid Al-30Si+400ppm P alloy with liquid Al-15Si+274ppm Sr alloy cast from 610 °C (SLD15). (a) low magnification and (b) high magnification.....114

**Figure 4.64** Plot of average primary Si particle size in the Al-19Si target alloy against Si content of liquid Sr-treated Al-Si starting alloy (SLD13, 9, 14, 15) .....

.....115

**Figure 4.65** Particle size distribution of primary Si in Al-19Si+P+Sr alloy cast from 610 °C produced by mixing: (SLD13) solid Al-30Si+400ppm P alloy with liquid CPAI+540ppm Sr alloy; (SLD9) solid Al-30Si+400ppm P alloy with liquid Al-8Si+ 400ppm Sr alloy; (SLD14) solid Al-30Si+400ppm P alloy with liquid Al-12.6Si+317ppm Sr alloy and (SLD15) solid Al-30Si+400ppm P alloy with liquid Al-15Si+274ppm Sr alloy.....115

**Figure 4.66** Optical micrographs of Al-19Si+148ppm P+200 ppm Sr alloy produced by mixing solid Al-30Si+400ppm P with liquid Al-12.6Si+317ppm Sr cast from: (a,b) 610 °C (SLD14); (c,d) 710 °C (SLD16); and (e,f) 750 °C (SLD17). (a,c & e) low magnification and (b,d & f) high magnification...117

**Figure 4.67** Particle size distribution of primary Si in Al-19Si+148ppm P +200ppm Sr alloy produced by mixing solid Al-30Si+400ppm P with liquid Al-12.6Si+317ppm Sr cast from: (SLD9) 610 °C; (SLD16) 710 °C and (SLD17) 750 °C.....118

**Figure 4.68** Plot of average primary Si particle size in Al-19Si+148ppm P +200ppm Sr alloy produced by solid-liquid duplex casting process against casting temperature(SLD14, 16, 17).....120

<b>Figure 4.69</b> Optical micrographs of Al-19Si+200ppm P+200ppm Sr alloy produced by: conventional casting process of Al-19Si+200ppm P cooled down from 800 °C to 700 °C then adding 200 ppm Sr, cast from 610 °C. (a) low magnification and (b) high magnification.....	121
<b>Figure 4.70</b> Particle size distribution of primary Si in Al-19Si+200ppm P+200ppm Sr produced by conventional casting process of Al-19Si+200ppm P cooled down from 800 °C to 700 °C then adding 200 ppm Sr, cast from 610 °C.....	121
<b>Figure 4.71</b> Optical micrographs of Al-19Si+200 ppm P+200 ppm Sr alloy produced by: (a,b) conventional casting process at 800 °C, (c,d) solid-liquid duplex casting process 610 °C (SLD18). (a,c) low magnification and (b,d) high magnification.....	122
<b>Figure 4.72</b> Particle size distribution of primary Si in Al-19Si+200ppm P+200ppm Sr produced by the solid-liquid duplex (SLD18) and conventional casting processes.....	123
<b>Figure 4.73</b> Optical micrographs of conventionally cast Al-18Si alloy: (a,b) Al-18Si without P and Sr and (c,d) Al-18Si+50ppm P+200ppm Sr. (a,c) low magnification to show the size and distribution of primary Si, (b,d) high magnification to show the eutectic structure.....	124
<b>Figure 4.74</b> Optical micrographs of Al-18Si+50ppm P+200ppm Sr produced by the solid-liquid duplex casting process cast at 610 °C. (a) low magnification and (b) high magnification.....	124
<b>Figure 4.75</b> Particle size distribution of primary Si in Al-18Si+50ppm P+200ppm Sr produced by the solid-liquid duplex and conventional casting processes.....	125
<b>Figure 4.76</b> Ultimate tensile strength and elongation of Al-18Si produced by the solid-liquid duplex (SLD) and conventional casting processes (without and with P and Sr addition cast from 800 °C).....	126
<b>Figure 5.1</b> A schematic diagram illustrating the different growth sequences of octahedral primary Si in unmodified Al-Si alloys.....	131

<b>Figure 5.2</b> A schematic diagram illustrating the vector relationship between the growth rate $V_{[100]}$ along the [100] growth direction, growth rate $V_{[E]}$ normal to the edges and the growth rate $V_{[111]}$ normal to the {111} facets .....	132
<b>Figure 5.3</b> Coupled zones in (a) symmetrical and (b) asymmetrical phase diagrams. The Al-Si system has a typical asymmetrical phase diagram .....	133
<b>Figure 5.4</b> Optical micrographs of the typical morphology of primary Si and the Al-Si-Ca phase, in the Al-15Si-0.5Ca alloy. (a) Entrained oxide bifilm and (b) primary Si and Al-Si-Ca phase formed in association with each other and with oxide bifilms.....	136
<b>Figure 5.5</b> (a) Back scattered SEM micrograph showing the high level of entrained oxide in the Al-15Si-0.5Ca alloy, and the association of Al-Si-Ca dispersoids with the oxide bifilms; and (b) typical EDS point analysis spectrum from the Al-Si-Ca dispersoids.....	137
<b>Figure 5.6</b> Ellingham diagram plots showing the standard free energy of a reaction as a function of temperature.....	143
<b>Figure 5.7</b> Comparative oxidation losses caused by the addition of various elements to an aluminium melt.....	143
<b>Figure 5.8</b> Viscosity of Al-Si alloys as a function of Si content.....	150
<b>Figure 5.9:</b> Viscosity of Al-Si alloys as a function of temperature .....	152

## List of Tables

<b>Table 2.1</b> Hypereutectic Al-Si Alloy Designations and Nominal Compositions .....	10
<b>Table 2.2</b> Typical classification of Al-Si eutectic microstructures.....	21
<b>Table 3.1</b> Composition of commercial purity Al (LM0) and Al-50Si master alloy raw materials (wt%).....	41
<b>Table 3.2</b> Properties and suppliers of chemicals used in alloying experiments.....	46

<b>Table 3.3</b> Experimental parameters to produce Al-19Si alloy from solid Al-30Si alloy with varying P additions and liquid Al-8Si melt varying Sr additions. The mass ratio of the two alloys was fixed of 1:1 and the casting temperature was fixed at 610 °C.....	52
<b>Table 3.4</b> Experimental parameters to produce Al-19Si alloy from solid Al-30Si and liquid alloys of different Si% lower Si content or varying casting temperature.....	54
<b>Table 4.1</b> Effect of different form and size of Al <sub>2</sub> O <sub>3</sub> without and with P on the average particle size of primary Si and compared with P addition.....	94
<b>Table 4.2</b> Alloying parameters and key microstructural results for solid-liquid duplex casting of a target Al-19Si alloy cast from 610 °C using fixed solid : liquid alloy ratio of 1:1 (by mass). .....	111
<b>Table 4.3</b> Alloying parameters and key microstructural results for solid-liquid duplex casting of a target Al-19Si alloy cast from 610 °C varying Si content of the low Si liquid alloy and the associated solid alloy : liquid alloy mass ratio.....	116
<b>Table 4.4</b> Alloying parameters and key microstructural results for solid-liquid duplex casting of a target Al-19Si alloy produced by mixing solid Al-30Si+400ppm P with liquid Al-12.6Si+317ppm Sr cast from different casting temperatures. In addition to SLD18 in which Al-19Si+200ppm P+200ppm Sr alloy produced by solid-liquid duplex process, cast from 610 °C.....	119
<b>Table 5.1</b> Calculated lattice misfit <i>f</i> between Si and some substrates.....	138
<b>Table 5.2</b> Calculated lattice misfit <i>f</i> between Al <sub>2</sub> CaSi <sub>2</sub> and some substrates.....	139

## Nomenclature

A list of symbols is given with a brief description

Symbol	Definition
Al	Aluminium
$\alpha\text{-Al}_2\text{O}_3$	Alpha Alumina
$\gamma\text{-Al}_2\text{O}_3$	Gamma Alumina
$\text{AlCl}_3$	Aluminium chloride
$\text{AlF}_3$	Aluminium fluoride
AlP	Aluminium phosphide
As	Arsenic
Ba	Barium
Be	Beryllium
BeO	Beryllium oxide
Bi	Bismuth
$\text{C}_2\text{Cl}_6$	Carbon hexachloride
Ca	Calcium
CaO	calcium oxide
Cd	Cadmium
$\text{Cl}_2$	Chloride
Cu	Copper
$e_{ijkl}$	Bond energies between ij and kl atoms
Er	Rare earth
$f(\theta)$	Catalytic efficiency
$\text{F}_2$	Fluoride
Fe	Iron
Ga	Gallium
Ge	Germanium
$\text{H}_3\text{PO}_4$	Phosphoric acid
Hf	Hafnium
K	Potassium
$\text{K}_2\text{SiF}_6$	Potassium Silicon fluoride
La	Lanthanum
Li	Lithium
m	Fractional coordination numbers parallel to the surface
Mg	Magnesium

---

$\text{MgCl}_2$	Magnesium chloride
$\text{MgO}$	Magnesium oxide
$\text{Mg}_2\text{Si}$	Magnesium silicide
Mn	Manganese
Mo	Molybdenum
MR	Modification rating concept
n	Fractional coordination numbers perpendicular to the surface
$N_0$	Avogadro's number
Na	Sodium
$\text{Na}_2\text{S}$	Sodium sulphide
$\text{NaOH}$	Sodium hydroxide
Ni	Nickel
P	Phosphorus
PB	Pilling-Bedworth ratio
Pb	Lead
R	Embryo radius
<i>R</i>	Gas constant
Rb	Rubidium
S	Sulphur
Sb	Antimony
Se	Selenium
$\text{SF}_6$	Sulphur hexafluoride
Si	Silicon
Sn	Tin
Sr	Strontium
Te	Tellurium
$\text{Ti}_2\text{Cl}_6$	Titanium hexachloride
$\text{TiAl}_3$	Titanium aluminide
$\text{TiB}_2$	Titanium diboride
$T_m$	Monotectic temperature
$T_{mA}$	Catalyst melting point
V	Vanadium
$w_L$	Interaction parameters in the liquid
$w_S$	Interaction parameters in the solid
Yb	Ytterbium

---

---

$z$	Coordination number
Zn	Zinc
ZnS	Zinc sulphide
Zr	Zirconium
$ZrO_2$	Zirconium oxide
$\gamma_{ml}$	Interface energy of substrate-liquid
$\gamma_{ms}$	Interface energy of substrate-solid
$\gamma_{sl}$	Interface energy of solid-liquid
$\Delta G_{het}$	Total free energy for heterogeneous nucleation
$\Delta G_{hom}$	Total free energy for homogenous nucleation
$\Delta G_v$	Difference in Gibbs free energy per unit volume
$\mu$	Equilibrium chemical potential
$\mu_0$	Standard state chemical potential
$\chi'_{ij}$	Interface concentration
$\phi$	Fraction of a monolayer adsorbed on the surface

---

## Abbreviations

---

Symbol	Definition
BCAST	Brunel Centre for Advanced Solidification Technology
BSE	Back Scattered Electron
DC	Direct Chill
EDX	Energy-Dispersive X-ray analysis
HPDC	High Pressure Die-Casting
MC-HPDC	Melt Conditioned-High Pressure Die-Casting
OM	Optical Microscope
PM	powder Metallurgy
ppm	Part per million
RS	Rapid Solidification
SEED	Swirl Enthalpy Equilibration Device
SEM	Scanning Electron Microscopy
SSM	Semi-Solid Metal
TP-1	Test Process-1
WAS	Worldwide Analysis System
SLD	Solid-Liquid Duplex process

---

# **Chapter 1**

## **Introduction**

### **1.1 Background**

Over a number of decades, considerable effort has been made towards the development of lightweight engineering materials. Among the aluminium alloys, Al-Si alloys are widely used in transportation and other industrial sectors due to their combination of adequate mechanical properties and excellent castability [1-3]. Al-Si alloys that contain more than 12wt%Si exhibit hypereutectic microstructures, normally consisting of primary silicon particles in an Al-Si eutectic matrix. Hypereutectic Al-Si alloys are of increasing interest for applications that require a combination of low density, thermal stability, good corrosion resistance, good thermal conductivity and high wear resistance such as pistons, liner-less engine blocks and pumps [4-6].

The wear resistance of this class of alloys is due to the presence of hard primary silicon particles formed during casting, but comes at the expense of poor machine tool life. Generally, the machinability of unrefined and unmodified hypereutectic Al-Si alloy is worse due to the presence of coarse primary silicon and long needle-like eutectic silicon in the matrix. To both minimise excessive machine tool wear and meet the strict operating targets of automotive engine applications, the load bearing primary silicon phase must be present as fine, well dispersed particles [7].

To increase the industrial applicability of hypereutectic Al-Si alloys, various methods have been used to refine primary silicon. It has been reported that the primary silicon particle size can be affected by the cooling rate during solidification [8-10], and on using a thermal rate treatment [11] or melt superheating [12-13], the primary silicon particles are refined substantially. The addition and refinement effects of phosphorus [9], boron [14], strontium [15], rare earth metals [16], scandium [17] and  $\gamma$ -Al<sub>2</sub>O<sub>3</sub> nanoparticles [18-19] on primary Si have also been studied. Melt treatments using a magnetic field [20], an electrical field [21], shear loading [22], the melt conditioned high pressure die casting (MC-HPDC) process [23], electromagnetic stirring [24] and ultrasonic vibrations [25] have all been found to be effective for refinement of primary silicon particles and their distribution. The effect of vibration on the solidifying melt has been investigated and shown to be successful in refining the microstructure [26-27]. Of all these methods, only the addition of phosphorous is widely applied. The remaining processes have achieved only limited refinement of primary silicon, are not thoroughly

investigated, and/or are impractical or not cost effective. In commercial practice refinement is currently achieved by the addition of ~50 ppm phosphorous in the form of Cu-P, Al-Cu-P or Al-Fe-P master alloys to the Al-Si melt before casting. The widely accepted explanation of the refining effect of phosphorus is the formation of aluminium phosphide (AlP) particles which act as potent substrates for heterogeneous nucleation of primary silicon. The crystal structure and lattice parameter of AlP are close to those of silicon with minimal mismatch between them, less than 1% [28].

It is a common practice in the casting of hypoeutectic and near eutectic Al-Si alloys to modify eutectic Si using certain elemental additions, typically Na, Sr or Sb. The modified morphology of the eutectic Si is of a fine fibrous or coral-like form rather than a coarse acicular form typical of unmodified Al-Si alloys. Modification leads to enhanced fluidity during casting, and improved ductility and fracture toughness.

Despite the capability of refining primary silicon in hypereutectic alloys and modifying eutectic silicon in hypoeutectic or near eutectic alloys, it is not possible to achieve both refinement of primary silicon and modification of eutectic silicon in hypereutectic alloys by the addition of phosphorous and a modifying element simultaneously. This is due to the mutual interaction between phosphorous and the modifying element.

For hypereutectic Al-Si alloys, the final properties in the cast component are controlled by the size and distribution of the primary silicon phase in addition to the degree of modification of the eutectic silicon matrix. The microstructures and mechanical properties of Al-Si alloys are strongly affected by the casting process. A good casting process is to fill the mould cavity without any defects. In slowly cooled castings of Al-Si alloys with more than 15% silicon, it is reported that the primary silicon segregates to the upper parts of a casting. This phenomenon is assumed to be caused by gravity segregation, i.e. less dense silicon particles float in the aluminium melt during solidification [29]. Furthermore, segregation and depletion of silicon on the outer surface of cast components are common problems in high pressure die casting and squeeze casting [30].

Apart from conventional casting processes, such as die casting, squeeze casting, permanent mould casting, and sand casting; semi-solid processing and duplex processing are two relatively new casting techniques [7]. Currently the semi-solid metal (SSM) technique represents one of the commercially feasible technologies for production of high integrity, complex shaped metallic components with improved mechanical properties and tight dimensional control [31]. The attractive advantage of semi-solid processing is that it requires a lower temperature and less force, i.e. less energy consumption [30]. The disadvantage of semi-solid processing is less suitable

for alloys with small solidification ranges and strict temperature control is needed in most processes. Duplex casting involves the mixing of two alloys of different composition or temperature prior to solidification of the component [32]. A number of duplex casting techniques have been investigated to refine the primary silicon without the use of inoculants, but with limited success [33]. Aspects of the research in this thesis draw upon these two processes.

## 1.2 Objectives and Scope

The main aims of this study are:

1. To develop one or more methods of refining primary silicon in cast hypereutectic Al-Si alloys to compete with the conventional process of adding phosphorous.
2. To develop a technique which, in addition to refining primary Si, also achieves the secondary goal of simultaneous modification of silicon in the Al-Si eutectic.

To achieve these two key objectives, a number of steps were taken during the course of the research for this thesis:

- (i) As noted above, in hypereutectic Al-Si alloys with more than 15% silicon, it has been reported that the primary silicon tends to segregate by flotation to the upper parts of the casting. Thus, for accurate microstructure analysis and evaluation of different solidification conditions and methods; a robust casting and sampling procedure was developed.
- (ii) The effect of cooling rate and melt superheat on the size and morphology of primary Si was carried out in a more systematic way than in previous investigations.
- (iii) The role of Ca, present at various levels as an impurity in commercial purity alloys, on the morphologies of primary and eutectic silicon was studied.
- (iv) The zincblende form of ZnS is isostructural with AlP, and has almost identical lattice parameter. The potential for the zincblende form of ZnS to act as a heterogeneous nucleant for primary Si, without the problem of interaction with modifier added for the purposes of eutectic modification from which AlP suffers, was investigated.
- (v) As stated above, there is some evidence that  $\text{Al}_2\text{O}_3$  may be a suitable substrate for nucleation of primary silicon. An attempt was made to improve the suitability of alumina by doping  $\alpha\text{-Al}_2\text{O}_3$  and  $\gamma\text{-Al}_2\text{O}_3$  powders with phosphorous and then adding them to hypereutectic Al-Si melts prior to casting.

- (vi) As an alternative to chemical approaches, a physical approach to simultaneous refinement of primary Si and eutectic modification was developed through a new solid-liquid duplex casting process. In this process pre-refined primary silicon particles are retained when a solid highly hypereutectic alloy is added to a liquid eutectic alloy that contains an element to achieve eutectic modification.

### 1.3 Outline of Thesis

Following the introduction and objectives of this study, Chapter 2 of this thesis is a review of literature relevant to the scope of research. It will provide an introduction to Al-Si alloys and go on to describe aspects of their microstructure including the refinement of primary Si and modification of the Al-Si eutectic. It will also discuss the relevance of particular casting processes.

The experimental work in Chapter 3 focuses on the development of a new inoculant or method of refining primary Si in cast hypereutectic Al-Si alloys to compete with the conventional casting process of adding phosphorous and then to achieve the simultaneous refinement of primary silicon and modification of eutectic Si. The procedure for the preparation of the Al-Si alloys and synthesised inoculants such as ZnS and P-doped  $\text{Al}_2\text{O}_3$  for different casting conditions, and the characterisation with mechanical property measurement techniques will be presented. In Chapter 3 experiments to observe the effect of solidification rate, chemical additions and casting techniques on morphologies of silicon during solidification of hypereutectic Al-Si alloys are described.

In Chapter 4 the metallographic studies on the effect of solidification rate, melt purity, Ca level and various inoculants such as Mg,  $\text{MgO}$ ,  $\text{CaO}$ , ZnS,  $\text{Na}_2\text{S}$ , Zn and P-doped  $\text{Al}_2\text{O}_3$ , on silicon morphologies are presented and quantitatively compared to the binary hypereutectic Al-Si base alloy. The results of a new solid-liquid duplex casting process for simultaneous refinement of primary Si and eutectic modification with its optimum operating conditions are investigated in detail.

Chapter 5 offers discussions on the effect of all the above parameters, including melt superheat, cooling rate, chemical additions and casting techniques on the refinement of primary Si and modification of eutectic Si in solidification of hypereutectic Al-Si alloys. The main conclusions of the study and suggestions for future work are presented in Chapter 6 and Chapter 7, respectively.

# Chapter 2

## Literature Review

### 2.1 Introduction to Al-Si Alloys

Alloys with silicon as the major alloying element are the most important of the aluminium casting alloys, primarily because of their excellent casting characteristics. Additions of silicon to pure aluminium report good feeding characteristics, high fluidity, low shrinkage and good hot cracking resistance [34]. The Al-Si casting alloys can be classified commercially into three groups:

- (a) Hypoeutectic alloys, with 5 to 11 wt% silicon,
- (b) Eutectic and near eutectic alloys with 11 to 13 wt% silicon,
- (c) Hypereutectic alloys, with 13 to 25 wt% silicon.

The Al-Si binary system forms a simple eutectic at 577 °C and 12.6 wt% Si. Typical Al-Si binary alloy microstructures are also illustrated in Figure 2.1.

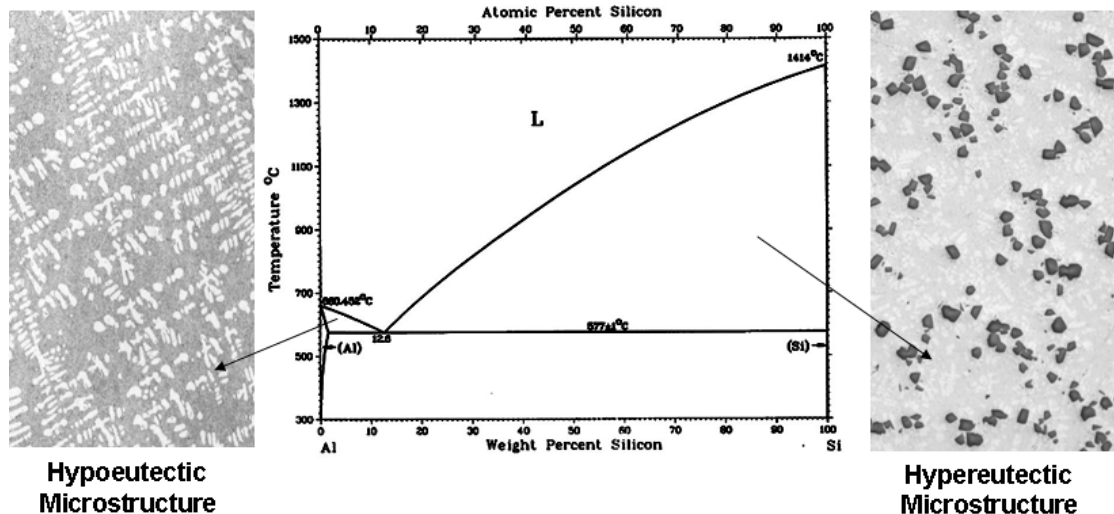


**Figure 2.1** Equilibrium Al-Si phase diagram with typical microstructures of hypoeutectic and hypereutectic Al-Si alloys [30].

The aluminium-silicon system is a simple binary eutectic with negligible solubility of aluminium in silicon and limited solubility of silicon in aluminium. The solubility of silicon in aluminium reaches a maximum of 1.5 at% at the eutectic temperature. Al-Si alloys differ from a "standard" eutectic phase diagram in that aluminium has virtually zero solid solubility in silicon at any temperature. This means that there is no  $\beta$ -Si solid solution phase and this phase is "replaced" by pure silicon. So, for Al-Si alloys, the eutectic is a structure of  $\alpha$ -Al + Si rather than  $\alpha$ -Al +  $\beta$ -Si [35].

The hypoeutectic alloys consist of a soft, ductile primary  $\alpha$ -Al phase and a very hard, brittle Si phase associated with the eutectic reaction [36-38]. The microstructure greatly depends on the solidification rate and the presence of modifying elements (the process of Al-Si eutectic modification is described in section 2.7). Large eutectic flakes of silicon and large  $\alpha$ -Al dendrites with large dendrite arm spacing are produced at a low solidification rate or for unmodified hypoeutectic alloy, while at a high solidification rate or in a modified alloy, a fibrous morphology of the eutectic silicon and small dendrites of  $\alpha$ -Al will be produced [39].

The microstructure of hypereutectic Al-Si alloys consists of primary Si particles dispersed in a matrix of aluminium and silicon eutectic. These primary Si particles impart excellent wear resistance to the alloys. For a given silicon concentration, the morphology of silicon particles depends greatly on the solidification rate and on the alloying elements [9, 37, 39]. Typical micrographs of hypo- and hypereutectic alloys that conducted in this thesis are shown in Figure 2.2.

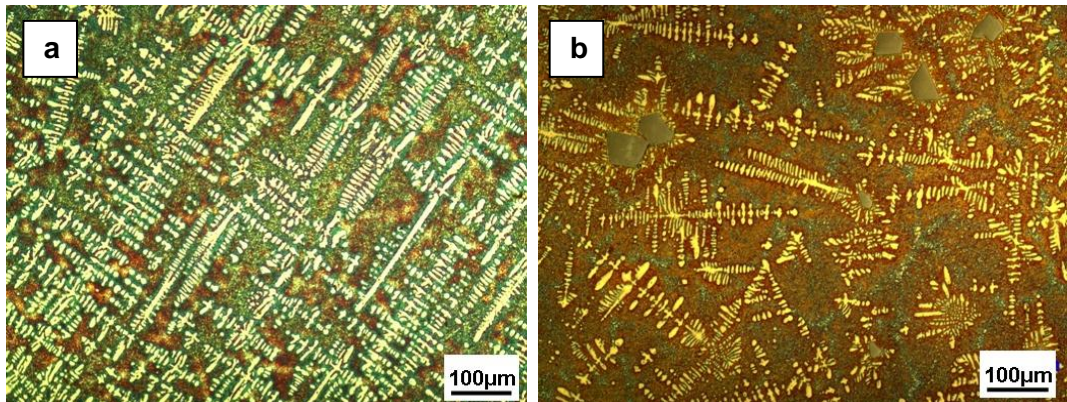


**Figure 2.2** Microstructure of Al-Si alloys etched by Weck's Reagent; (a) Hypoeutectic (b) Hypereutectic.

## 2.2 The Al-Si System and Properties

The great effect of silicon in aluminium alloys is the improvement of casting characteristics. Additions of silicon to pure aluminium dramatically improve feeding characteristics, fluidity and hot tear resistance [40]. Adding silicon is also accompanied by a reduction in specific gravity and coefficient of thermal expansion.

In general, an optimum range of silicon content can be assigned to casting processes. For slow cooling rate processes (such as sand casting), the range is 5 to 7wt%, for permanent mould casting it is 7 to 9wt%, and for die casting it is 8wt% and higher. The bases for these recommendations are the relationship between cooling rate and fluidity and the effect of percentage of eutectic on feeding [41]. In addition to

silicon which is a eutectic-forming element, other elements are present in commercial Al-Si alloys. They are either added as minor alloying elements to strengthen the material or are present as impurities. Formation of second-phase precipitates, grain refinement, influence on porosity and phase modification are the major mechanisms responsible for the effects of alloying elements on the properties of Al-Si alloys. The most known alloying elements used in the Al-Si alloys include Mg, Fe, Cu, Mn, Zn, Ni and P and eutectic modifying elements such as Sb, Ca, Na, and Sr [7].

**Magnesium** is the basis for strength and hardness development in heat-treated Al-Si alloys and is commonly used in more complex Al-Si alloys containing nickel, copper, and other elements for the same purpose. Addition of Mg leads to formation of the  $Mg_2Si$  phase, which contributes towards the properties of high silicon alloys as well as altering the nature and quantity of primary silicon formed [42-43]. The hardening phase  $Mg_2Si$  displays a useful solubility limit corresponding to approximately 0.70 wt% Mg, beyond which either no further strengthening occurs or matrix softening takes place. The solution heat treatment concentrates Mg and some Si from the solid solution phase, which is retained by quenching. Subsequent aging, with both time and temperature being variables, allows controlled precipitation of  $Mg_2Si$  in the  $\alpha$ -Al matrix resulting in significant increased strength [44]. Further details on the effect of Mg on the microstructure of hypereutectic Al-Si alloys are discussed in sections 4.3.1 and 5.3.1.

**Iron** is the most common element in Al-Si alloys and it can be tolerated up to level of 1.5 to 2.0 wt% Fe. The presence of Fe in Al-Si alloys introduces as many as six different Al-Fe-Si based intermetallic phases. Commercial Al-alloys always contain Fe, often as an undesirable impurity and occasionally as a useful minor alloying element [45-46]. The most common intermetallics are hexagonal  $\alpha$ -AlFeSi ( $Al_8Fe_2Si$ ) and monoclinic  $\beta$ -AlFeSi ( $Al_5FeSi$ ) phases. Other iron-bearing phases such as  $Al_6Fe$  and  $Al_3Fe$  can also be found in these alloys [46]. These insoluble phases, especially at elevated temperature, are responsible for improvements in strength but can also be responsible for poor ductility and fatigue resistance. As the fraction of insoluble phase increases with increased iron content, fluidity and feeding characteristics are negatively affected [36].

**Copper** is the most common alloying element for improved wear resistance Al-Si alloys. The maximum equilibrium solid solubility of Cu in Al is up to 6wt% at 546 °C [36]. Cu additions impart additional strengthening of the matrix through precipitation hardening process ( $Al_2Cu$  phase) or through the modification of the hard, brittle Al-Fe-Si phases by substitution in these intermetallics phases [38]. As the strength of these alloys increase with the addition of Mg and Cu, some sacrifice in ductility and corrosion resistance occurs [36]. The  $Al_2Cu$  precipitation is controlled by heat

treatment. To obtain optimum corrosion resistance in aluminium based HPDC alloy, Cu additions are limited to less than 0.1wt%.

**Manganese** is commonly added to commercial Al-Si alloys, typically at a level of more than 1wt%. Mn is commonly used to reduce the tendency for die soldering and to neutralize the detrimental effect of iron impurity [47]. Mn addition favours the formation of intermetallics such as  $\text{Al}_{15}(\text{Fe},\text{Mn})_3\text{Si}_2$  rather than the  $\text{Al}_9\text{Fe}_2\text{Si}_2$  type. The  $\text{Al}_{15}(\text{Fe},\text{Mn})_3\text{Si}_2$  intermetallics is typically cubic in structure, and as a result gives improved mechanical properties [46].

**Nickel** can enhance the strength and hardness of Al-Si Alloys at elevated temperature in the presence of copper [7] due to the formation of  $\text{Al}_7\text{Cu}_4\text{Ni}$  phase. This precipitated phase would make contribution to the microhardness of the Al-Si alloy as it has a higher microhardness values than that of Al matrix [48].

**Phosphorus** is added to hypereutectic Al-Si alloys and combines with molten aluminium to form tiny, insoluble AlP particles which act as effective heterogeneous nucleants for primary Si (AlP and Si both have diamond-like cubic crystal structures with similar lattice parameters) [28]. More details of the refinement mechanism of primary Si by Phosphorus are provided in section 2.8.

**Antimony** at concentration levels equal to or greater than 0.05 wt% modifies eutectic silicon in the aluminium-silicon alloy in a lamellar form. The effectiveness of antimony in altering the eutectic structure depends on an absence of phosphorus and on an adequately rapid rate of solidification. Antimony also reacts with sodium, calcium or strontium to form coarse intermetallics with adverse effects on castability and eutectic structure. Antimony is classified as a heavy metal with potential toxicity and hygiene implications, especially if the melt contains hydrogen since  $\text{SbH}_3$  formation is possible. This gas is highly toxic and can pose an environmental problem [49].

**Calcium** is known as a weak aluminium-silicon eutectic modifier. Calcium, entering the Al-Si alloys along with the addition of silicon, is often responsible for casting porosity due to increased hydrogen solubility even at trace concentration levels [6]. The effect of Ca is investigated in this thesis and further literature on the role of Ca in Al-Si alloys is discussed in section 2.5.

**Sodium** is specified as an optional modifier for Al-Si eutectic. Sodium can successfully modify eutectic silicon morphology with significantly enhanced mechanical properties [50]. Sodium interacts with phosphorus to reduce their effectiveness in modifying the eutectic and in the refinement of the primary Si phase [51].

**Strontium** is widely used to modify the Al-Si eutectic. Effective modification can be achieved at very low addition levels, but a range of recovered Sr of 0.008 to 0.04 wt% is commonly used. Higher levels of Sr are associated with casting porosity, especially

in processes in which solidification occurs more slowly. Degassing efficiency may also be negatively affected at higher strontium levels [15].

### 2.3 Hypereutectic Al-Si Alloys

More than 50 years ago, hypereutectic Al-Si alloys were employed for casting heavy-duty diesel engine pistons. Despite those many years of casting experience, understanding hypereutectic alloys and the special requirements for controlling their microstructure, casting soundness, cycle time and tool life continues to evade many foundries. In reality, hypereutectic Al-Si alloys can be considered as important aluminium metal matrix composite (MMC) systems; they are *in situ* composites of primary Si crystals distributed throughout an Al-Si eutectic matrix. Thus, hypereutectic Al-Si alloys share many of the properties of other aluminium MMC systems, for instance, systems that incorporate such hard second-phases as SiC, Al<sub>2</sub>O<sub>3</sub> or B<sub>4</sub>C [30].

For a specific application, the selection of a hypereutectic Al-Si alloy depends on its castability, the casting process, the required mechanical and physical properties and the use of the casting. Therefore, parameters such as the percentage of Si, its shape and distribution play an important role on the mechanical properties. The higher the silicon content, the harder and stronger material, but at the expense of ductility.

The major Al-Si alloy groups used commercially are [43]:

- Al-Si-Cu alloys: provide good casting properties with moderate strength and hardness.
- Al-Si-Mg alloys: offer good permanent mould casting properties and with heat treatment give improved strength and hardness.
- Al-Si-Cu-Mg alloys: offers good wear resistance and are commonly used as engine parts.

The compositions of the most common Al-Si alloys with its application are given in Table 2.1 [30, 52-56].

A good alloying example is the so-called 3HA alloy. The typical composition of 3HA is Al-14Si-2Cu-0.5Mg-0.5Mn-0.05Zr with 0.05% strontium used as the modifier. It has been reported to have a unique combination of improved high temperature strength, corrosion resistance, wear resistance, fluidity and good machinability, thus becoming an alternative Al-Si alloy that can be used to make linerless engine blocks [7].

**Table 2.1:** Hypereutectic Al-Si Alloy Designations and Nominal Compositions [30, 52-56]

Designation	Owner	Si	Cu	Mg	Fe	Ni	Others		Applications	Notes
LM28	BS1490:1988	18	1.5	1		1		Nom.	Pistons	
LM28	BS1490:1988	17 - 20	1.3- 1.8	0.8- 1.5	≤0.7	0.8- 1.5	≤0.6Mn, ≤0.2Zn, ≤0.1Pb, ≤0.1Sn, ≤0.2Ti, ≤0.6Cr, ≤0.5Co, ≤0.1Others (each), ≤0.3 Others (total)	Spec.		
LM29	BS1490:1988	23	1	1		1		Nom.	Pistons	
LM29	BS1490:1988	22 - 25	0.8- 1.3	0.8- 1.3	≤0.7	0.8- 1.5	≤0.6Mn, ≤0.2Zn, ≤0.1Pb, ≤0.1Sn, ≤0.2Ti, ≤0.6Cr, ≤0.5Co, ≤0.1Others (each), ≤0.3 Others (total)	Spec.		
LM30	BS1490:1988	17	4.5	0.5				Nom.	Linerless engine blocks	
LM30	BS1490:1988	16 - 18	4-5	0.4- 0.7	≤1.1	≤0.1	≤0.3Mn, ≤0.2Zn, ≤0.1Pb, ≤0.1Sn, ≤0.2Ti, ≤0.1Others (each), ≤0.3 Others (total)	Spec.		
Alusil	KS Aluminium Technologie AG	17	4	1				Nom.	Linerless engine blocks (Porsche Cayenne, Audi V6 and V8, BMW)	

Designation	Owner	Si	Cu	Mg	Fe	Ni	Others		Applications	Notes
A390	AI Assoc.	17	4.5	0.6	<0.4		0.5Zn	Nom.	Primary sand and permanent mould alloy. For die castings 390 is used (higher Fe content to prevent die-soldering).	
B390	AI Assoc.	16 - 18	4-5	0.45-0.65	<1.3	<0.1	<0.5Mn, <1.5Zn, <0.2Ti, ≤0.1Others (each), ≤0.2 Others (total)		Engine blocks, pistons, pumps, compressors. Secondary (scrap-based) alloy. Workhorse alloy 99.5% of all 390 series applications)	
391 (Mercasil)	Mercury Marine	18 - 20	<0.2	0.4-0.7	<1.2		<0.3Mn		Die-casting. Marine Engine Blocks (low Cu to improve corrosion resistance). A391 for permanent mould (<0.4Fe). B391 for sand casting (<0.2Fe)	
393 (Vanasil)		21 - 23	0.7-1.1	0.7-1.3	<1.3	2.0-2.5	<0.1Mn, <0.1Zn, 0.1-0.2Ti, 0.08-0.15V, ≤0.15 Others (total)		Diesel pistons. Very early hypereutectic alloy (introduced more than 50 years ago), and continues to be used.	
DISPAL S250	Peak	20			5	2		Nom.	Cylinder liners	Spray formed
DSIPAL S260	Peak	25	4	1				Nom.	Cylinder liners	Spray formed
MSFC-398	NASA								Pistons	
M174+	MAHLE								Pistons	

Table 2.1 continued

## **Forged Pistons**

AA 4032      Al-12.2Si-0.9Cu-1.0Mg-0.9Ni

AA 2618      Al, 0.1-0.25Si, 1.9-2.7Cu, 1.3-1.8Mg, 0.8-1.3Fe, 0.9-1.2Ni, ≤0.05Mn, ≤0.1Zn, ≤0.05Cr, 0.04-0.1Ti

## **Other Al-Si Alloys for Engine Components**

A332    Al-12Si-1Cu-1Mg-2Ni (Pistons)

3HA    Al-14Si-2Cu-2Ni-0.5Mg-0.5Mn-0.05Zr-0.05Sr

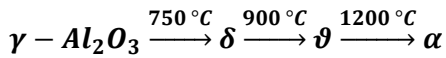
Australian experimental (fully eutectic) alloy

## 2.4 Inclusions and Oxides

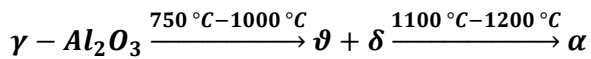
It is well established that a large variety of inclusions are present in small quantities in commercial aluminium and aluminium alloys. The common inclusions in commercial aluminium are oxides, carbides, borides, nitrides, chlorides, and fluorides. These inclusions play an important and crucial role in facilitating the crystal nucleation process of the matrix phase and other primary phases [57-58], since the high-energy crystal/liquid interface is partly replaced by an area of low-energy crystal/inclusion interface [59]. However, these inclusions differ in their nucleation catalytic activity.

Aluminium readily oxidizes in the presence of air or moisture forming a strong, thin film of protective oxide on the exposed metal surface. The detrimental effects of the oxides on the microstructure and properties have been extensively investigated in aluminium alloys. Studies have shown that oxide films, particularly formed at liquid state at high temperatures, are frequently associated with the casting porosity, hot tearing and cracks, resulting in decreased strength, ductility and corrosion resistance of the castings [60].

Most of the IA and IIA elements also readily form very stable oxides. These oxides have lower densities than the corresponding parent metal and so tend to be broken and porous to both air and moisture ( $\text{BeO}$  is an exception). Elements with Pilling-Bedworth (PB) ratios (oxide density to metal density) less than one form discontinuous and non-protective oxides, while those with PB ratios  $> 1$  form continuous and protective oxides. The PB ratios of  $\text{BeO}$ ,  $\text{ZrO}_2$ ,  $\gamma\text{-Al}_2\text{O}_3$ ,  $\alpha\text{-Al}_2\text{O}_3$ ,  $\text{MgO}$  and  $\text{CaO}$ , are 1.70, 1.56, 1.31, 1.28, 0.80 and 0.64 respectively [61]. Thus, a melt containing Ca and Mg cannot maintain its continuous protective  $\text{Al}_2\text{O}_3$  skin even when the melt is quiescent. Instead, it will be subjected to a rapid and continuous oxidation leading to formation of more oxides. Alumina  $\text{Al}_2\text{O}_3$  is one of the most common oxides found in aluminium alloys. It exists in eight different polymorphs: seven metastable phases ( $\gamma$ ,  $\delta$ ,  $\kappa$ ,  $\rho$ ,  $\eta$ ,  $\theta$ , and  $\chi$ ) as well as the thermodynamically stable  $\alpha$ -phase. The metastable (also known as transition) phases of alumina are basically nano crystalline in nature and can be easily synthesized by a variety of methods. The usual way to synthesize the  $\alpha$ -phase, however, is to heat the transition alumina phases at relatively high temperatures, e.g., 1000-1200 °C. The transformation sequence may be illustrated as follows [62]:



or



$\gamma$ -Al<sub>2</sub>O<sub>3</sub> is one of the metastable polytypes of Al<sub>2</sub>O<sub>3</sub> that is used extensively as a catalytic support material because of its high porosity and large surface area. At temperatures in the range 1000-1200°C  $\gamma$ -alumina transforms rapidly into the thermodynamically stable  $\alpha$ -alumina phase (corundum), significantly reducing the surface area and thus suppressing the catalytic activity of the system. The phase transformation can be shifted to higher temperatures by doping  $\gamma$ -alumina with one of many elements such as La, Ba, P, or Si [63].

In the case of unalloyed aluminium, the oxide film is initially  $\gamma$ -Al<sub>2</sub>O<sub>3</sub>. It is a thin film that inhibits further oxidation through prolonged heating at higher temperatures (~800 °C). After an incubation period, this oxide transforms to  $\alpha$ -Al<sub>2</sub>O<sub>3</sub>. The  $\gamma$ -Al<sub>2</sub>O<sub>3</sub> has been found to have the highest occurrence level in the  $\alpha$ -Al phase and is believed to be a very potent substrate for the crystallization of the matrix phase [57, 64].

There is much experimental evidence to conclude that some Si particles nucleate and grow on oxide particles or bifilms during solidification of hypereutectic Al-Si alloys. Observation by Campbell and Cao [65-66] showed that Si particles formed on long oxide films and they also interpreted cracks in eutectic Si to be due to short bifilms on which the Si nucleated. The bifilm concept is the enfolding of the liquid surface into the bulk melt. As the surface usually has a surface film, the film is entrained, being folded double; hence, the name “bifilm.” The dry film on surface of the liquid metal becomes folded together, the dry faces now opposed in the folding action, and without bond [67]. Early work by Zhang *et al.* [68] show that Si particles formed on oxide particles on solidification of Al-15Si alloy. They believe that enhanced nucleation is likely to be due to the distribution of oxide films as well dispersed, discrete, nano scale oxide particles which act as potent/efficient heterogeneous substrates for primary Si.

## 2.5 Calcium in Al-Si Alloys

Attention has been given to the effect of Ca content on the microstructure of Al-Si alloys. Ca has been reported to cause modification of the Al-Si eutectic from a flake-like to a fine fibrous silicon structure [69].

Calcium enters aluminium casting alloys as impurities with the addition of Si, appearing as calcium silicides, phosphides and nitrides, which are considered to be harmful, and requires removal of Ca to levels of 30 ppm, and preferably 10 ppm [70].

Calcium is expected to affect the casting characteristics of aluminium casting alloys because of its significant influence on the viscosity and surface tension of the melt [71].

P, Ca and Sb are among the various trace elements in aluminium alloys reported to react with Sr to neutralize its modifying effect on the eutectic Si. Suzuki and Oshir [72] have invented an efficient method of eliminating P and/or Sb from molten aluminium by addition of Ca at a temperature of 923 to 1123 K followed by blowing chlorine gas or a chloride flux to remove calcium phosphide or Ca-Sb compound with the forming dross to improve modification of hypoeutectic Al-Si alloys.

Nakae *et al.* [73] studied the influence of impurity elements such as Ca on modification of eutectic Si in Al-Si alloys treated with Sr. They observed that in using commercial grade Al-Si alloys, a reduction in modification of eutectic Si is due to the reaction between Sr and Ca. Perfect modification could be obtained in high purity Al-Si alloy melted in a high purity alumina tube and treated with Sr. The mechanism proposed is that Ca forms  $\text{CaSi}_2$ , which reacts with Sr forming strontium-calcium-silicide.

EI-Hadad *et al.* [74] have investigated the effect of Ca content on the microstructure of eutectic Si particles in Sr modified 319 alloy. They found that a Ca concentration of 50 ppm and higher coarsened the primary Si particles due to the formation of Al-Si-Ca-Sr compounds.

Kwon *et al.* [75] investigated the effects of increasing Ca content on the modification of Al-7Si-0.3Mg alloy with Sr. They observed weakening of the eutectic modification rate in 50 ppm Sr treated alloy and decreased UTS and elongation. Meanwhile, coexistence of Ca and P has been found to increase eutectic modification rate and to depress the eutectic temperature, due to the interaction between them.

Preliminary studies of the modification process in hypereutectic Al-Si alloys found that Ca content affects primary Si particle size in addition to modification of the eutectic [76]. A calcium level of less than 500 ppm in Al-Si alloys improves the mechanical properties through modification of the eutectic Si from an acicular or plate-like to a fine fibrous morphology. The formation of  $\text{CaSi}_2$  in Al-Si alloys with Ca concentrations of more than 500 ppm detrimentally influences the mechanical properties. Ca at very low levels may also tie up hydrogen present in the melt as hydride, so reducing porosity. However, above a critical Ca content, the protective  $\text{Al}_2\text{O}_3$  film on the melt may become weakened and rupture, leading to more rapid pick-up of hydrogen [6].

Kim [77] studied the relationship between Ca content and primary Si particle size in B390 hypereutectic alloy through control of Ca content by the addition of  $\text{Ti}_2\text{Cl}_6$  in the melts. Calcium was found to have a significant effect on the size of primary Si particles

of B390 aluminium casting alloy. Primary Si particles were refined as Ca content decreased.

Liu *et al.* [78] investigated the effect of Ca impurity on solidification structure of a near eutectic Al-Si piston alloy (ZL109). They found that Ca can lead to P refinement inefficiency and many kinds of Ca compounds exist in commercial purity silicon, which are the main source of the Ca impurity in ZL109 alloy. This inefficiency of primary Si refinement is due to the formation of  $\text{Ca}_x\text{Si}_y\text{P}_z$  compounds which are more stable than the AlP phase in the melt. The P refinement efficiency can be recovered after addition of  $\text{C}_2\text{Cl}_6$  which removes Ca. Fluxing, remelting and holding the melt for a certain time are the most efficient methods to remove Ca. Chloride and fluoride compounds are used for fluxing aluminium alloy melts to remove alkali metals [77]. Most previous studies used chloride compounds such as  $\text{C}_2\text{Cl}_6$  or  $\text{Ti}_2\text{Cl}_6$  for melt treatment.

## 2.6 Fluxing

A flux is a material added to molten metal that reacts with impurities to form dross or slag, which floats to the surface of the metal and can be removed by skimming. The uses of salt fluxes fall into five categories: cover, cleaning, drossing, refining and wall-cleaning. Cover fluxes prevent oxidation of the molten bath and cause the agglomeration of metal droplets in the dross to form larger drops that then sink back into the bath. Cleaning fluxes facilitate keeping furnace or crucible walls above and below the melt line free of build-up. Drossing fluxes are used to reduce the rich metallic content of drosses that may contain up to 60-80% free metal. Refining fluxes contain compounds that break down and are thermodynamically favourable to react with certain metallic elements in the aluminium. For example, certain chlorine or fluorine-containing fluxes will react with Mg, Ca, Li, Na and K in the molten aluminium to form compounds that will partition to the dross phase, where they can be removed by skimming [5].

Fluxing is a useful means of obtaining clean metal, preventing formation of too much oxide, removing non metallic inclusions from the melt and removing oxide build-up from furnace walls. Fluxes may be grouped into two classes: gaseous or solid. Gaseous fluxes may be a mixture of an inert gas with a chemically active gas that is injected into the molten bath. Solid fluxes are mixtures of salts, and seem to be the most favoured type of fluxes used in foundries [79]. In general fluxes can be broadly categorized as passive or active. Passive fluxes protect the surface of the molten bath from oxidation and prevent hydrogen pick up by the melt. Active fluxes react chemically with the aluminium oxide and clean the melt more effectively [80].

According to Pacz in his patent for alkali fluorides [81], typically sodium fluoride can be added to the aluminium-silicon melt to modify the eutectic silicon. Jeffries [82] reported that addition of fluxes to Al-Si alloys affects the morphology and dispersion of the silicon in the eutectic. In 1922 Guillet and Search proposed that the change in the Al-Si eutectic structure with the addition of sodium fluoride and potassium fluoride is due to the removal of oxides and impurities, such as alumina and silica, by the fluxing effect of these compounds [39].

Current technologies for alkali/alkaline earth removal involve treatment with reactive halides either in gaseous form (e.g. chlorine) or as salts ( $MgCl_2$ ,  $AlF_3$ ,  $K_2SiF_6$  etc.). In addition to removing the targeted elements (Li, Na, Ca or Mg) these treatments also generally promote the removal of non-metallic inclusions by dewetting/ floatation [83]. The metal chlorides that have a standard Gibbs energy value more negative than  $AlCl_3$  are more stable than  $AlCl_3$ . This means that when  $Cl_2$  is injected into aluminium containing various metallic elements, the chlorine will preferentially react with these metallic impurities. The same also applies to fluorides. Li, Na, K, Ca, Mg, and Ba all form more stable chlorides and fluorides than aluminium and can, therefore, be removed by  $Cl_2$ ,  $F_2$ , or  $SF_6$  injection or halide salts [6] as shown in Figure 2.3.

The equilibrium constant for reactions such as  $Al + 3MeX = 3Me + AlX_3$  ( $X = Cl$  or  $F$ , and  $Me = Li, Na, K$ ) and  $Al + 1.5MeX_2 = 1.5Me + AlX_3$  ( $X = Cl$  or  $F$  and  $Me = Ca, Mg, Ba, Sr$ ) is shown in Figure 2.4 for different metals. An equilibrium constant much less than one indicates that at equilibrium the reaction is shifted to the left, while a value much greater than one implies that the reaction is shifted to the right. Therefore, according to Figure 2.4, to an alkali or alkali-earth chloride electrolyte has no tendency to react with aluminium. Corresponding metal-fluorides are slightly more reactive than metal-chlorides [5].

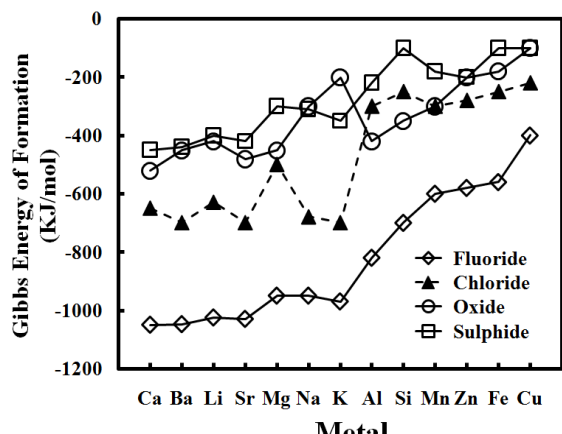


**Figure 2.3** Standard Gibbs energy of formation of several sulphides, oxides, chlorides, and fluorides at 723 °C [5].

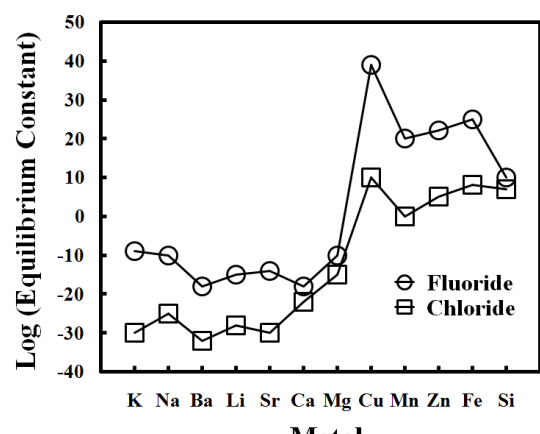


**Figure 2.4** Exchange equilibrium between aluminium and different metal chlorides and metal fluorides at 723 °C [5].

## 2.7 Eutectic Modification

The term 'modification' describes the change in scale and morphology of the eutectic Si from a coarse flake-like structure to a fibrous or fine flake structure in Al-Si alloys. It is necessary to modify the eutectic Al-Si to improve strength, ductility, pressure tightness and machinability [84]. The growth form of the faceting Si phase is such as to produce a three-dimensional skeletal crystal pattern rather than thin sheets. The silicon plates appear to be separate crystals but they are in fact interconnected. In as-cast Al-Si foundry alloys eutectic Si often has a very coarse and plate-like morphology, leading to poor mechanical properties, particularly ductility [85]. In most foundry applications modification occurs by adding small concentrations of elements such as Sr, Na or Sb [86]. Modification of the Al-Si eutectic can be achieved by two processes [51, 84]:

- Chemically induced modification by trace addition of specific elements.
- Quench modification, which refers to rapid freezing.

Knuutinen *et al.* [87] investigated the modifying action of Ca, Ba, Y, and Yb in Al-7Si-0.3Mg alloy. They found that Ba and Ca produce a fibrous silicon structure, similar to the effects caused by additions of Na or Sr, while Y and Yb cause a plate-like structure.

Kumari *et al.* [70] studied the modification of Al-7Si-0.3Mg alloy by Ca and Sr. They found that the optimum level of Ca for achieving modification and best mechanical properties lies in the range of 0.0085-0.017 wt%. They also found that a higher amount of Ca leads to the formation of higher porosity and Al-Ca-Si intermetallics, and that Sr modification leads to more porosity than Ca at a fixed 0.018 wt% level in the alloy.

Prasad [88] reported that for a given addition level of Sb, modification of eutectic silicon was more effective after longer melt holding than after short holding following inoculation.

Ho and Cantor [89] studied the modification of Al-Si eutectic microstructure using the entrained droplet technique with different levels of P and Na. They found that modification from coarse-faceted silicon particles to clusters of fine-scale silicon particles was enhanced by increasing the purity of the alloy, increasing the cooling rate or adding Na; where increasing alloy purity removes P and prevents the formation of AlP; adding Na leads to the formation of  $\text{Na}_3\text{P}$  in preference to AlP; and increasing cooling rate allows insufficient time for the precipitation of AlP from low levels of dissolved P.

For a given eutectic microstructure there is an optimum level of modifier. A higher level of modifier results in over-modification. For instant, Sr over-modification,

coarsening and reversion of the fine fibrous silicon structure to an interconnected plate form will take place [84].

Several studies have recently shown that widely different eutectic solidification modes can occur in hypoeutectic Al-Si alloys as a result of the addition of modifying elements. The three theoretically expected eutectic solidification modes suggested by Dahle *et al.* [90] are shown in Figure 2.5:

- (a) nucleation and growth on the primary  $\alpha$ -Al dendrites;
- (b) independent nucleation of eutectic grains in interdendritic spaces;
- (c) planar-front growth opposite to the thermal gradient.

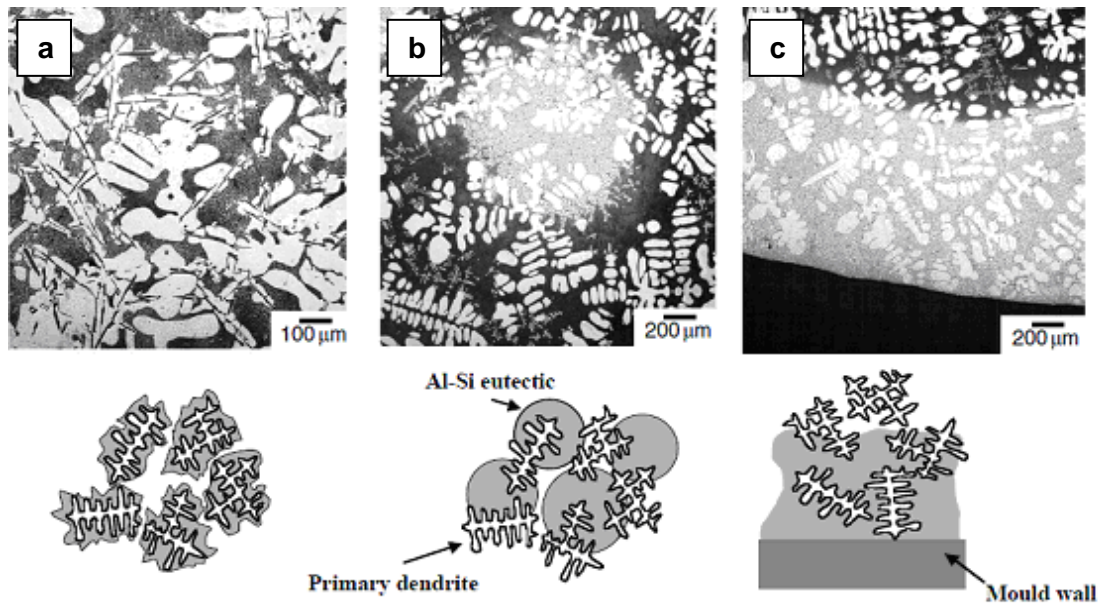


**Figure 2.5** Eutectic growth modes suggested by Dahle *et al.* [90]. (a) nucleation and growth on primary  $\alpha$ -Al dendrites; (b) independent nucleation of eutectic grains, and (c) planar-front growth.

Basically two classes of theories have been suggested to explain the mechanism of modification [91]. These are:

- restricted nucleation theory; and
- restricted growth theory.

According to the restricted nucleation theory, the modifier neutralizes the heterogeneous nuclei of AIP or it reduces the diffusion coefficient of Si in the melt. This suppresses the undercooling in the melt before eutectic solidification and modification takes place. For the restricted growth theories, the modifying element is adsorbed on twin re-entrant grooves or growing surfaces of the Si phase, thus the normal growth of

Si is inhibited and twinning is promoted. For growth to proceed the modification process, the number of twins increases in comparison with the unmodified eutectic silicon which has few or no twins [84].

Several elements are known to cause chemical modification. A growth twin is created at the interface when the atomic radius of the element relative to that of silicon exceeds a value of about 1.65 [87]. In the presence of a chemical modifier, the twinning frequency and the angle of branching increase with cooling rate. Na is the ideal modifier because it produces the greatest number of twins and also the finest modified structures at the lowest concentrations [51]. But the choice of modifier also depends on other factors such as ease of dissolution, vapour pressure, stability in the melt etc. Figure 2.6 shows the three morphologies of eutectic Si. Figure 2.6a shows unmodified eutectic Si. Some chemical modifiers: such as Na, K, Rb, Ca, Sr, Ba, La, Yb produce a fibrous structure as shown in Figure 2.6b. Elements such As, Sb, Se and Cd when used as a modifier, produce modified lamellar structure as shown in Figure 2.6c.

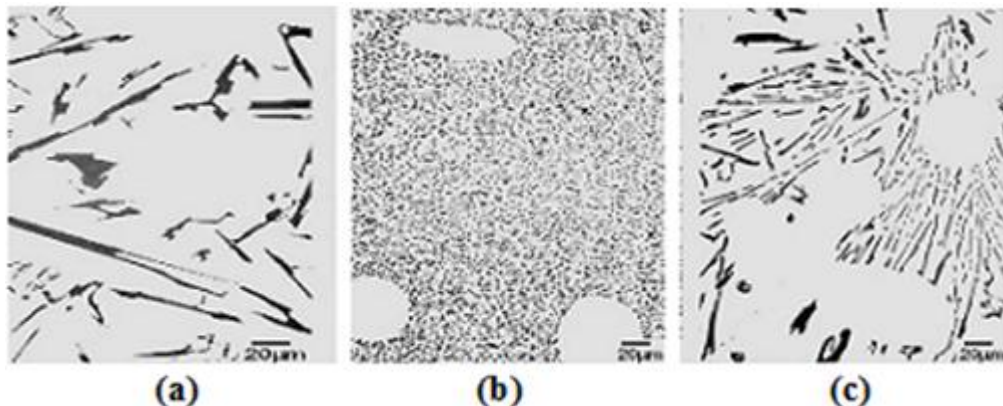


**Figure 2.6** Eutectic silicon morphology in Al-Si Alloys (a) unmodified, (b) modified fibrous structure (c) modified lamellar structure [92].

The modification rating concept (MR) is used to characterise the modified structure.

$$MR = \sum (\text{fraction of class} \times \text{class number})$$

The class number refers to the scale of rating from 1 to 6 for the range of structures observed in modified Al-Si alloys [84]. The various classes with their description are presented in the Table 2.2.

**Table 2.2** Typical classification of Al-Si eutectic microstructures.

Class number	Structure	Description
1	Fully unmodified	Silicon is present in the form of large plates as well as in acicular form.
2	Lamellar	A finer lamellar structure, though some acicular Si may be present (but no large plates).
3	Partially modified	The lamellar structure starts to break up into smaller pieces.
4	Absence of lamellae	Complete disappearance of lamellar Si. Some acicular Si may still be present.
5	Fibrous Si eutectic (Fully modified)	Acicular Si is completely absent.
6	Very fine eutectic (Super modified)	The fibrous Si becomes so small that individual particles cannot be resolved under an optical microscopy.

## 2.8 Primary Si Refinement and Morphology

Primary Si in hypereutectic Al-Si alloys is very hard, imparting wear resistance, but decreasing tool life during machining. Controlling the size, shape and distribution of the primary Si particles in hypereutectic Al-Si alloy castings is commonly known as refinement. It is based on maximizing the number of sites on which primary Si crystals can nucleate [30].

Primary Si in hypereutectic Al-Si alloys exhibits a variety of morphologies such as star-like, polygonal, coarser platelet, etc. Generally, the machinability of hypereutectic Al-Si alloys is worse due to the presence of coarser primary Si [93].

Ullah *et al.* [94] studied the silicon crystal morphologies during solidification refining from Al-Si melts in the range of 17-38 wt% Si, they found that at lower silicon contents the silicon morphologies have a fish-bone or star-like shape but at the highest Si contents the growth habit changed to large plates that have a tendency to grow in layers and thus form Al inclusions in the Si crystals. Examples of these primary Si morphologies are shown in Figure 2.7.

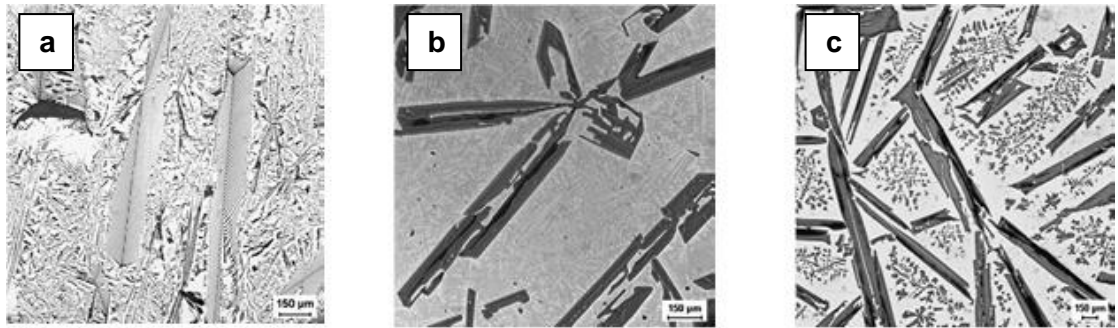


**Figure 2.7** Primary silicon crystal morphologies: (a) Fish-bone-like structure, (b) Large star shaped crystal and (c) Large plate structure [94].

The strong tendency of Si to grow in the (111) plane through the twin plane re-entrant angle edge mechanism (TPRE) combined with different nucleation conditions is the reason for the formation of the different morphologies. However, at increasing super saturation a specific type of hopper crystal grows, where the edges and corners grow fast, which, together with the preferred growth in the (111) plane, results in the five-fold star. Figure 2.8 shows SEM micrographs of five-fold primary Si crystals.

Xu and Jiang [13] conclude that the morphologies of primary Si are a strong function of the solidification conditions such as melt superheat and cooling rate. As the melt temperature increases, the morphologies of primary Si change from star-like and other irregular primary Si to octahedral primary Si and the size of primary Si will gradually decrease. Also they found that the cooling rate plays an important role in determining the morphologies of primary Si in the solid state. The size of primary Si will gradually decrease with increasing cooling rate. In general, the size of the primary Si increases with increasing Si content and with decreasing cooling rate. Larger superheating seems to promote the formation of the fish bone structure.

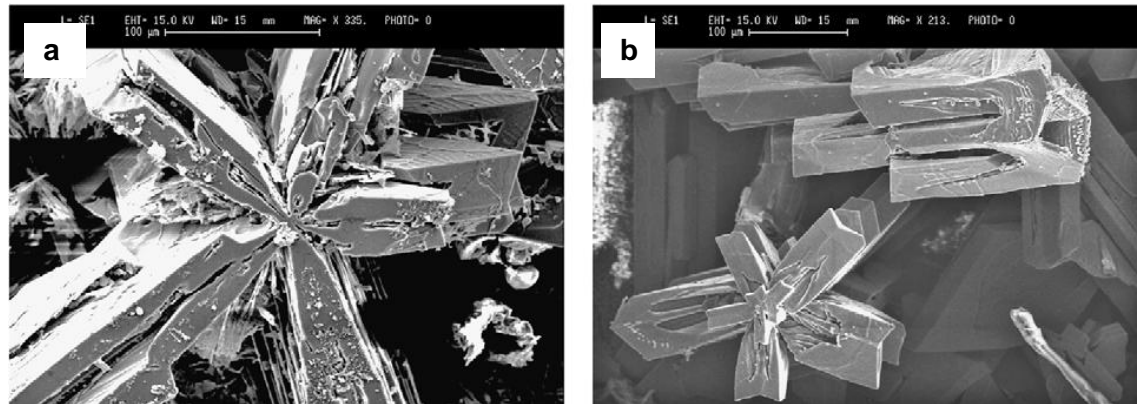


**Figure 2.8** SEM micrographs of star shaped crystals in Al-25wt%Si alloy: (a) fully developed star with five arms growing in length and thickness from a common nucleus; (b) a star crystal at an early stage of development [94].

It has been reported that high melt superheating and quick cooling to a pouring temperature significantly refine the primary Si of Al-Si alloys without addition of refinement elements [12-13, 95] and the microstructure in the solid state is influenced by the liquid structure before solidification [96].

Li *et al.* [12] investigated the effect of cooling rate and superheat on Si morphology. Al-16wt%Si alloy was heated to 720, 880, 960 and 1050 °C then cooled back to 720°C in air (at 60-70 K/s) and cast into sand and metal moulds. Also, the alloy was cooled back to 720 °C at 150-200 K/s (by adding solid samples to the melt) and cast into metal moulds. In each case the primary Si shaw greater refinement (and a more compact morphology) with increasing melt superheat. The effect was more dramatic in the sand castings than in the metal mould castings, the latter being more refined as a result of the higher solidification rate in the metal moulds, although the primary Si was always more refined in the metal mould castings than in the sand castings. Greater refinement was also achieved by cooling from the superheated temperature to the pouring temperature at a higher rate. Their explanation for the refinement process was little.

The effect of superheat and cooling rate on the microstructure of hypereutectic Al-Si alloy is investigated in this thesis and further literature and discussion are illustrated in sections 4.1 and 5.1.

Microstructure control using minor element additions has been the most popular method due to its simplicity. Phosphorus or phosphorus compounds are normally used for the refinement of primary Si in hypereutectic Al-Si alloys. Aluminium phosphide (AlP) particles are commonly accepted to be the nucleation site for primary silicon hypereutectic Al-Si alloys, since both have similar crystal structures as shown in Figure 2.9 and the lattice parameters of Si and AlP are very close with a lattice mismatch of less than 1% [28]. The primary Si nucleates and then grows by wrapping around the AlP nucleant to develop as a compact particle [65], examples of compact particles are shown in Figure 2.10b. The compound AlP may also be a common nucleus for eutectic Si in unmodified alloys, but becomes less active in the presence of the modifying element, e.g. Na, or Sr. The mechanism for this transition is unclear but may relate to the reaction of P with intermetallic formed between the modifying element and Al, Mg and Si [84]. Thus an excess of P will lead to refinement of primary Si and little or no eutectic modification, and an excess of Sr will lead to eutectic modification without substantial refinement of primary Si.

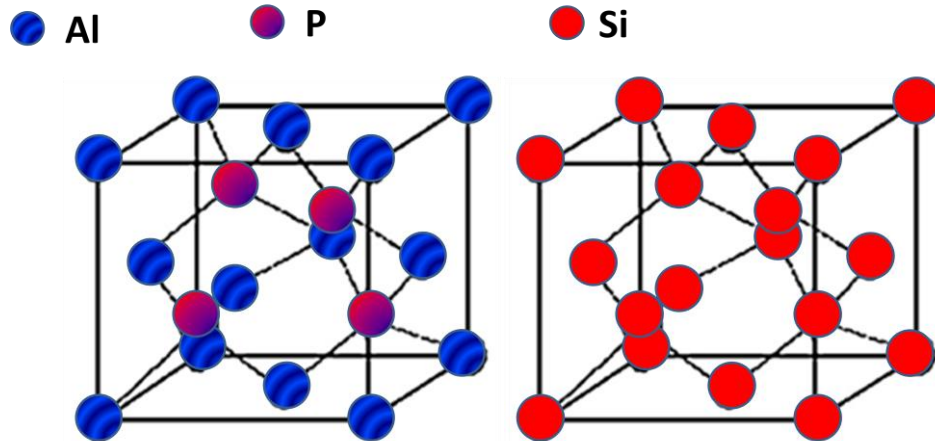


**Figure 2.9** The crystal structures of AlP and Si [97].

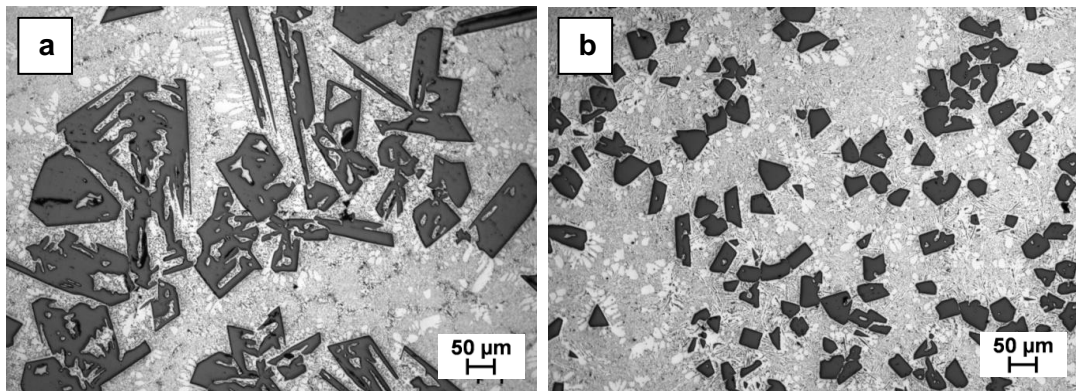


**Figure 2.10** Optical micrographs of as-cast alloys that conducted in this thesis: (a) Al-30Si alloy, (b) Al-30Si with the addition of 400 ppm P.

AIP has the zinblend crystal structure with a lattice constant of 5.4310 Å at 300 K. It is thermodynamically stable up to 1,000 °C. P is most effectively added in the form of Cu-P, Al-Cu-P or Al-Fe-P master alloys [68]. The eutectic Cu-8%P dissolves quickly and completely at 714 °C, thus it is the preferred product for use in the foundry [30].

AIP particles have an affinity for each other and agglomerate into clusters that are no longer effective as nucleants. Agglomerates then rise to the melt surface, oxidize and are removed in the dross. Melt agitation (stirring, ladling) enhances agglomeration. Large melts (tonnes) lose effective refinement over many hours or even days. While, small melts (a few kg) can lose effective refinement within 4-5 h. Refinement can be reactivated by heating the melt to above ~900 °C to dissolve the AIP agglomerates and cool the melt back down to its working temperature to precipitate new dispersed particles. This practice can have the consequences of greater melt oxidation (especially Mg burn-out) and an increased amount of dissolved hydrogen [30].

Zhang *et al.* [98] have shown that reprecipitation can lead to AlP with varying morphologies which in turn affect the morphology of primary Si particles, e.g. reprecipitation during cooling from 1500 °C led to coarse flake AlP particles which led to coarse elongated primary Si particles.

Significant refinement of primary Si in 390 alloy has been reported by the use of Germanium, Gallium, Selenium, Tellurium, Lithium, Cadmium, and Lithium Chloride [99] but the refinement efficiency was less than that of using phosphorus.

Xing *et al.* [100] have investigated the effect of rare earth RE elements on the hypereutectic Al-Si alloys. They found that the size of the primary Si is considerably decreased with suitable addition of the RE on solidification of the hypereutectic Al-17.5Si and Al-25Si alloys. The addition of RE the primary Si changed from a coarse shape to a fine faceted shape, changes the size distribution of the primary Si and improves the mechanical properties of the Al-Si alloys.

Youn *et al.* [101] studied the refinement of primary Si in A390 alloy by applying ultrasound. The ultrasound was injected through a horn inserted into the melt. Primary Si size decreased from 80 µm to ~8 µm after 10 min ultrasound injection, but no further refinement with even longer ultrasound injection. They thought that both cavitation (formation and collapse of bubbles) and propagation of ultrasonic waves (causing melt streaming) contributed to vigorous mixing. In the ultrasonic technique, the compression and relaxation of high frequency ultrasonic waves have effect on melt. The transient cavitations could produce an impact strong enough to break up the clusters and disperse them more uniformly through the entire matrix without forming any clusters. In addition, acoustic cavitations accelerate heat and mass transfer processes such as diffusion, dispersion, emulsification, etc., which helps local undercooling during solidification and further helps to refine primary Si particles [102].

Zhang *et al.* [25] studied the effect of ultrasonic melt treatment (UST) on the microstructure of Si phases in solidification of hypereutectic Al-Si alloys. A significant refinement of primary Si crystals was observed when UST was applied to the liquid phase close to the liquidus of the primary Si phase.

Feng *et al.* [103] applied ultrasound to Al-23Si melt by making the crucible part of the horn, which should provide a more even distribution of the ultrasound. Ultrasound was applied at 500W for 10 min. They reported a degassing effect, and refined primary Si.

Zhang *et al.* [68] investigated an alternative, physical means of refining primary Si by intensive melt shearing using the twin-screw device prior to casting. They found that intensive melt shearing led to greater refinement of the primary Si particles than the common practice of refining with P. This refinement of primary Si is likely to be due to

the distribution of oxide films as well dispersed, discrete, nano scale oxide particles which act as potent/efficient heterogeneous substrates.

Physical refinement method with the application of intensive melt shearing during solidification was proposed and its effect on the microstructure of a hypereutectic aluminium-silicon alloy was studied by Zuo *et al.* [104]. The intensive melt shearing was achieved by the use of a rotor-stator unit. They found that intensive melt shearing has different effects on the microstructure of hypereutectic Al-Si alloy, depending on the treatment temperature. When shearing above the liquidus temperature, the primary Si particles were slightly refined. While, shearing below the liquidus, there was a significant refinement of the primary Si particles and the optimum shearing temperature for refining primary Si particles of Al-20wt%Si alloy was at 660 °C.

Spray forming is an alternative approach to refine the primary silicon particle size in hypereutectic alloys (see section 2.14.2). Which results in homogeneous, fine-scale microstructures, with low levels of segregation. Al-Si alloys manufactured by this process exhibit microstructures consist of equiaxed silicon particles approximately 1 to 10 µm in size, dispersed in a matrix of  $\alpha$ -Al solid solution [105].

## 2.9 Simultaneous Refinement of Primary Si and Modification of Eutectic Si

Due to the interaction between P and the modification chemicals such as Sr, Na and Ca, it is not possible to achieve both refinement of primary Si and modification of eutectic Si simultaneously in hypereutectic alloys [18].

Zarif *et al.* [106] found that, unlike P, Sr does not promote nucleation. Where, increasing Sr additions depressed the eutectic nucleation temperature and this could be a result of the formation of a  $\text{Al}_2\text{Si}_2\text{Sr}$  intermetallic phase that could consume or detrimentally affect potent AIP nucleation sites.

Research on hypereutectic Al-Si alloys has shown that additions of rare earth elements RE are a potential chemical alternative to P in refinement of primary Si. However the refinement of primary Si appears to be only moderate but may have the advantage of producing modified Al-Si eutectic simultaneously [16, 107]. Furthermore it is not clear that the refinement evident in binary alloys will translate to commercial multi-component alloys. The modification of eutectic silicon in RE-treated hypereutectic Al-Si alloys is supposed to be due to the suppression of the nucleation temperature of eutectic silicon and limited growth due to the decrease in diffusion rate of Si with the decrease in growth temperature

A group at Shanghai Jiao Tong University found that the addition of La to Al-17wt%Si and Al-25wt%Si resulted in both refinement of primary Si and eutectic modification [107], whereas similar addition to A390 alloy (containing 17.5% Si and

4.8% Cu) [108] resulted in no significant refinement of primary Si or modification of the eutectic Si. The La was present as a phase with the nominal composition  $\text{Al}_7\text{Si}_7\text{Cu}_2\text{La}_{3.5}$  which the authors asserted was formed late in solidification and was often associated with  $\text{Al}_2\text{Cu}$ . The La-rich phase was coarse and acicular, and may be detrimental to properties especially ductility. Despite a lack of thorough research, and although the effects appear to be moderate, there does appear to be some evidence that RE elements do simultaneously refine primary Si and modify eutectic Si.

Refining agents like Ga, Ge, Se, Be, Te, Li, Cd, Zn, Mn, V, Cb, Bi, Mo, Hf and S either individually or in combination have also been studied. These agents along with Na would give simultaneous silicon refinement and eutectic modification [109]. Moderately refined primary Si particles dispersed in a partially modified Al-Si eutectic matrix was achieved.

Melt treatments by a magnetic field [20], electrical field [21], shear loading [22], melt conditioning high pressure die casting (MC-HPDC) processing [23], electromagnetic stirring [24] ultrasonic vibrations [25] and vibration on the solidifying melt [26-27] have been found to be effective for simultaneous refinement and modification of the Si phases in hypereutectic Al-Si alloys, but either to only a limited extent or using a technique that requires significant further development.

## 2.10 Mechanism of Nucleation of Primary Si

### 2.10.1 Classical nucleation theory

Homogenous nucleation can occur in pure metals. It can be realized only under special conditions (i.e. levitation cooling, ultra high purity materials, etc). In practice nucleation usually starts on solid nucleants or on oxide layers in the melt. Nucleation on a solid substrate is known as heterogeneous nucleation, Figure 2.11 [59].

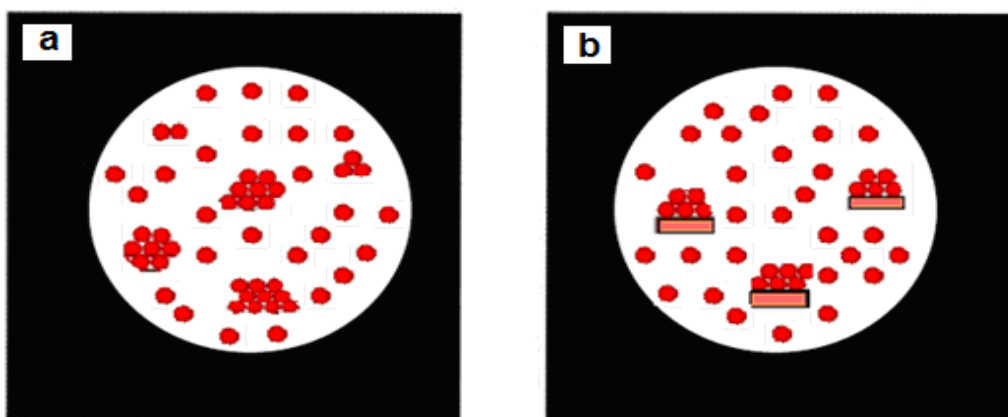


**Figure 2.11** A schematic representation of (a) homogenous nucleation and (b) heterogeneous nucleation on a foreign substrate [59].

The nucleation efficiency of a foreign solid substrate depends on the interaction between the solid surface and the melt, called wetting [110]. The wetting is characterized by the wetting angle  $\theta$  as shown in Figure 2.12. For a cap-shaped embryo of radius  $r$  wetting the substrate with a wetting angle  $\theta$ , the lateral area, the base area and the volume of the cap are:  $2\pi r^2(1-\cos(\theta))$ ;  $\pi r^2 \sin^2(\theta)$  and  $(2+\cos(\theta))(1-\cos(\theta))^2 (\pi r^3)/3$  respectively.

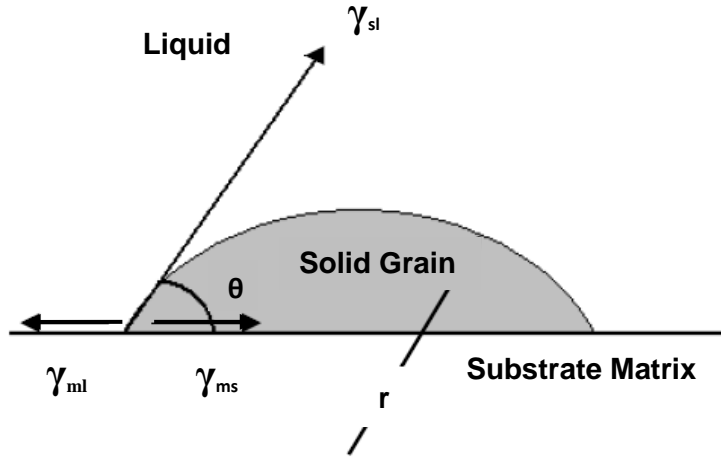


**Figure 2.12** The formation of a spherical nucleus of solid phase on the surface of a foreign substrate.

The total free energy change for embryo formation, taking into account the net interfacial free energy terms and the volume free energy change, is

$$\Delta G_{het} = \frac{4\pi r^3}{3} \Delta G_v \{(1/4)(2 + \cos(\theta))(1 - \cos(\theta))^2\} + 2\pi r^2(1 - \cos(\theta))\gamma_{sl} + \pi r^2 \sin^2(\theta)(\gamma_{ms} - \gamma_{ml}) \quad ... (2.1)$$

where  $\gamma_{ms}$ ,  $\gamma_{sl}$  and  $\gamma_{ml}$  are the interface energies of substrate-solid, solid-liquid and substrate-liquid interfaces respectively as shown in Figure 2.12 and  $\Delta G_v$  is the difference in Gibbs free energy per unit volume between the liquid and the solid. Applying the criterion for critical radius i.e.  $(d\Delta G/dr)_{r=r^*} = 0$  and using the Young equation for the wetting angle  $\theta$ ,

$$\gamma_{ml} = \gamma_{ms} + \gamma_{sl} \cos(\theta) \quad ... (2.2)$$

then the relation for critical radius to be  $r^* = (-2 \gamma_{sl}/\Delta G_v)$ . By substituting equation (2.2) into equation (2.1) and the value of  $r^*$ , we can obtain:

$$\Delta G_{het}^* = \frac{16\pi}{3} \left( \frac{\gamma_{sl}^3}{\Delta G_v^2} \right) \cdot \left( \frac{1}{4} \right) (2 + \cos(\theta)) (1 - \cos(\theta))^2 \quad \dots (2.3)$$

$$\Delta G_{het}^* = \frac{16\pi}{3} \left( \frac{\gamma_{sl}^3}{\Delta G_v^2} \right) \cdot f(\theta) \quad \dots (2.4)$$

where  $f(\theta) = (1/4)(2 + \cos(\theta))(1 - \cos(\theta))^2$  is the catalytic efficiency which varies between 0 and 1 depending on the wetting angle [59, 111-113].

### 2.10.2 Nucleation on potent substrates by adsorption

There are considerable problems with the classical heterogeneous nucleation theory, particularly when the catalytic efficiency is high, i.e. when  $\theta$ ,  $f(\theta)$  and  $\Delta G^*$  approach zero [114]. In 1954, Yang and co-workers [115] used the classical model to consider the formation of thin films by condensation of sodium vapour on different substrates. They found that the critical nucleus size ( $2r^*$ ) is just about the size of a unit cell of sodium. This gave an indication of just how small a nucleus could be. Walton [116] remarked that for nuclei of this low magnitude the uncertainties concerned with the classical model and the concept of surface energy become serious, because the critical nucleus size approaches the atomic level or is actually planar under such conditions. He then considered the formation of thin metal films through using the partition function and kinetic theory on the basis of an adsorption mechanism, followed by atomic rearrangement to achieve a preferred configuration. Walton's approach avoided the use of the spherical-cap assumption and the concept of surface energy.

Sundquist [117] considered heterogeneous nucleation of the solidification of tin at low undercooling. He pointed out that the spherical-cap assumption is no longer applicable in such cases, thus he proposed that the nucleus formed at low supercooling should be considered as "a monolayer of atoms occupying the atomic sites on the catalyst surface". He derived an expression for the nucleation rate to explain the reported experimental observations. Accordingly, in 1964 Chalmers [118] made the following remarks about nucleation on potent substrates:

*"A monolayer of atoms on the surface of a substrate cannot be regarded as a group of atoms brought together by a fluctuation in the liquid; it is more reasonable to regard it as an adsorbed layer in which the atoms can be arranged in many ways. The groupings of the atoms in the adsorbed layer play the same part as the embryo in the liquid; some have the structure of the crystal and, if large enough, can provide the starting point for further growth".*

Recently, evidence of the adsorption mechanism has been revealed using high-resolution transmission electron microscopy. This evidence includes Al nucleation by a

monolayer of catalytic  $TiAl_3$  on  $TiB_2$  substrates in Al-based glasses [119] and Si nucleation by a monolayer of catalytic AIP on Al crystals in Al-Si-P alloys [120]. It has been shown that substrates that preferentially adsorb the nucleating species are favourable for nucleation, and for sufficiently strong adsorption nucleation could become barrierless [121]. It has also been shown that if the sum of the substrate/solid and solid/liquid interfacial free energies were less than the substrate/liquid interfacial energy, then an adsorbed solid layer would be stable even above the liquidus [122].

Kim and Cantor [123] developed an adsorption model for the initial formation of solid phase, in which a monolayer of liquid at a substrate/melt interface was considered in a binary system. It was suggested that this monolayer could have a similar structure and composition to the solid phase at small undercooling. In general, adsorption has become an accepted mechanism for nucleation on potent/wettable substrates. Notable examples include Si nucleation by a monolayer of AIP on Al.

Ho and Cantor [124] measured undercooling for solidification of Si catalysed by Al doped with up to 2 ppm P and 850 ppm Na and they found that high-purity Al is a poor catalyst, and multiple nucleation at a high undercooling of 45-60 K leads to a fine-scale sub micrometre Si microstructure. Ho and Cantor [89] also found that catalysis is improved dramatically by doping with P at levels as low as 0.5-2 ppm. P is adsorbed onto the Al surface to form a catalytic AIP layer, and at high P levels AIP particles precipitate within the liquid, nucleating large twinned single crystals of Si at a few degrees of undercooling. Nucleation takes place with cube-cube orientation relationships between Al, AIP and Si. Na additions poison the catalytic effect, probably by a preferential reaction to form  $Na_3P$ , and high liquid undercoolings are restored, together with a modified fine-scale Si microstructure.

Cantor [125] concluded that when catalysis is efficient with contact angles below  $10-20^\circ$  and undercooling below 10-20K, nucleation takes place by a microscopic atom-by-atom adsorption process at the catalyst surface, rather than by the formation of a bulk spherical cap.

Fan [126] has recently developed an epitaxial model for heterogeneous nucleation on potent substrates. In this model, the liquid atoms order on the substrate layer by layer then nucleation takes place forming a solid phase with a crystal structure resembling that of the substrate (the pseudomorphous phase) and a coherent interface with the substrate. He found that the epitaxial nucleation model can explain a number of nucleation related phenomena, such as solute effects, hyper-nucleation and edge-to-edge matching.

## 2.11 Nucleation-Adsorption Model

When catalysis is efficient, it seems more reasonable to regard heterogeneous nucleation as an adsorption process. Nucleation takes place by dynamic atom-by-atom adsorption at the catalyst surface, rather than by the formation of a bulk spherical cap. Coudurier *et al.* [127] and Cantor [125] have shown that the surface energy  $\gamma$  of a catalyst **A** adsorbing atoms from a solidifying liquid **B** is given by:

$$\gamma = \sum x'_{ij} (\mu_{ij}^0 - \mu_{ij}) + RT x'_{ij} \ln x'_{ij} + \delta_{ijkl} m x'_{ij} x'_{kl} \omega_{ijkl} + \delta_{ijkl} n x_{ij} x'_{kl} \omega_{ijkl} - \delta_{ijkl} m x_{ij} x_{kj} \omega_{ijkj} \quad \dots \dots (2.5)$$

where the summation is over all  $i, k = \mathbf{A}, \mathbf{B}$  and  $j, l = \mathbf{S}, \mathbf{L}$ ;  $S$  and  $L$  are solid and liquid phase;  $\mu^0$  and  $\mu$  are the standard state and equilibrium chemical potentials,  $\delta_{ijkl} = 0$  for  $i = k$  and  $j = l$ ,  $\delta_{ijkl} = 1$  otherwise; and

$$\omega_{ijkl} = \frac{1}{2} z N_0 (2e_{ijkl} - e_{ijij} - e_{klkl}) \quad \dots \dots (2.6)$$

are interaction parameters;  $e_{ijkl}$  are bond energies between  $ij$  and  $kl$  atoms;  $R$  is the gas constant;  $N_0$  is Avogadro's number;  $z$  is the coordination number and  $m$  and  $n$  are fractional coordination numbers parallel and perpendicular to the surface, respectively.

The first term on the right-hand side of equation (2.5) is the chemical energy of removing surface atoms from the liquid and catalyst phases; their entropy of mixing is in the second term; the third term is their internal bond energy; the bond energy between the surface atoms and the catalyst and liquid phases is in the fourth term; and the fifth term is the broken bond energy needed to create a surface within the catalyst and liquid phases.

When the catalyst **A** and the solidifying liquid **B** are immiscible, equation (2.5) can be simplified to [125]:

$$\gamma \approx -\phi R \Delta T + RT \{\phi \ln \phi + (1 - \phi) \ln (1 - \phi)\} + \frac{3}{2} \phi (1 - \phi) RT_m + \frac{1}{4} \{\phi (\omega_s + RT_m) + (1 - \phi) (\omega_L + 3RT_{mA})\} \quad \dots \dots (2.7)$$

where  $\phi = \sum x'_{is}$  is the fraction of a monolayer adsorbed on the surface,  $\omega_s$  and  $\omega_L$  are **A-B** interaction parameters in the solid and liquid, respectively,  $T_m$  is the melting point and  $T_{mA}$  is the catalyst melting point. When a ternary element **C** is added, equation (2.5) for the surface energy must be summed over all  $i, k = \mathbf{A}, \mathbf{B}, \mathbf{C}$  and  $j, l = \mathbf{S}, \mathbf{L}$ . When the catalyst and solidifying liquid are immiscible, and C dissolves only in the catalyst,

equation (2.7) remains valid, with the catalyst melting point replaced by its liquidus temperature.

## 2.12 Segregation of Primary Si

Some experimental studies have shown that there is a tendency for primary Si to segregate to the top of a cast samples [29]. Significant segregation has been observed earlier in slowly solidified castings with more than 15 wt% Si [29]. Buoyancy driven convection was generally considered to be the major cause of primary Si segregation in casting [128]. Hypereutectic Al-Si alloys suffer from macro-segregation, particularly under slow solidifications conditions such as in sand casting from a high pouring temperature. Additions of phosphorous as well as strontium to these alloys may reduce silicon segregation in casting by providing longer floatation time or short primary solidification temperature range. Adding P can refine the primary Si particles, i.e. reduce the undercooling, and adding Sr increases the melt viscosity [129] thus reducing the floatation rate. Cooling the casting at higher solidification rate in excess of 15 K/s was found to reduce segregation of primary Si [130]. The microsegregation of primary Si was observed and overcome in this study and more details are in sections 4.1 and 5.1.

## 2.13 Mechanical Properties

It is well known that, both the structure and properties of Al-Si alloys are extremely sensitive to the fabrication technique. The distribution and morphology of primary Si have an important bearing on the mechanical properties of Al-Si alloys [84]. Both hypo- and hypereutectic Al-Si alloys have shown promise as an engine blocks material due to their adequate wear resistance and higher strength to weight ratio [131]. Wear resistance in Al-Si alloys is primarily due to the presence of silicon in the aluminium matrix. Increasing the silicon content in Al-Si alloys not only increases the wear resistance of the alloy but also the strength [132]. However, the improvement in strength and wear resistance comes at the cost of machinability and castability.

Silicon crystals in hypereutectic Al-Si alloys possess very high hardness and contribute to the abrasive wear resistance of cast parts. Wear resistance of the alloys depends highly on the scale and amount of primary Si. It was found that increasing silicon content in hypereutectic alloys can improve the wear resistance of the castings and small, spherical, uniformly distributed silicon particles enhance the strength properties of Al-Si alloys [7].

Wislei *et al.* [40] studied the effect of microstructure on mechanical properties for Al-9wt% Si, he found that the mechanical properties of casting alloys depend not only

on their chemical composition but are also extensively dependent on microstructural features such as the morphologies of the Al-rich  $\alpha$ -phase and of the eutectic Si particles. Al-Si alloys containing 2-20 wt% Si have been studied by Torabian [133] using a pin-on-disc type wear testing machine at room temperature. He found that the effect of composition on mechanical properties of Al-Si alloys is: as the amount of silicon in the alloy increases, the strength properties of Al-Si alloys also increase up to the eutectic composition, after which they show a decline with further increase in the silicon content. However, with increasing silicon content the hardness increases and the elongation decrease continuously. This may be largely attributed to the shape, size and distribution of silicon particles in the cast structures up to the eutectic composition. If silicon is present as fine particles and is uniformly distributed in the structure, the strength properties will increase. However, when the primary Si appears as coarse particles, the strength properties decrease with increasing silicon content, while the hardness goes on increasing because of the increase in the overall amount of silicon particles [133].

The mechanical properties of hypereutectic Al-Si alloys are mainly determined by the primary and eutectic Si. Cracks are consistently initiated by brittle fracture within the primary Si particles or debonding of Si particles from the eutectic matrix, and then propagate through the matrix and along the grain boundaries during tensile loading. The refinement of primary Si can decrease the probability of crack initiation by premature fracture of primary Si particles, and thus improves the mechanical properties [134]. According to Hong and Suryanarayana [135], the cracks pass around the primary or eutectic Si particles in Al-Si alloys with finer particles, while in the case of larger particles, cracks can pass through the large Si particles. A reasonably high tensile strength, without the loss of elongation, can be achieved in Al-Si alloys by controlling the size of the microstructural features.

Kilicaslan [17] found that addition of Sc produced finer eutectic and primary Si particles along with higher strength and elongation. Therefore, improvement of mechanical properties for the Al-20Si-0.6Sc alloy over Al-20Si alloy can be attributed to the particle size strengthening via Si particle refinement.

## 2.14 Casting Processes

The microstructures and mechanical properties of Al-Si alloys are strongly affected by the casting process. A good casting process is to fill the mould cavity without any defects. Silicon has a high heat of fusion, ~1810 KJ/kg, compared with other commonly cast metals, e.g. ~395 KJ/kg for Al, ~275 KJ/kg for Fe which improves its fluidity i.e. the fluid life. Thus, melt can flow further into a die before it is too cool to flow any further.

This is a result of high release of heat of fusion during the formation of primary Si in the early stages of solidification. The disadvantage of this specification is harder to achieve directional solidification and hence shrinkage feeding can be difficult. This is because the high heat release associated with primary Si heats mould surfaces quickly and reduces the chilling effect of the mould. Where necessary the problem may be overcome by introducing chills in sand moulds, or intense cooling or spraying of dies [30].

In addition to conventional casting processes such as die casting, squeeze casting, permanent mould casting, and sand casting, semi-solid processing and duplex processing are more recently developed casting techniques [7].

Brief descriptions of some of the casting processes of hypereutectic Al-Si alloys are given below.

#### **2.14.1 Conventional casting**

Conventional casting such as high pressure die casting (HPDC), Squeeze casting and permanent mould casting have been successfully used for casting hypereutectic Al-Si alloys. Conventional HPDC is the most popular process for casting small to medium sized hypereutectic alloy components [30]. A schematic diagram of a cold chamber high pressure die-casting machine is shown in the Figure 2.13. High pressure die-casting (HPDC) is a process in which molten metal is injected into a precisely dimensioned steel mould through a shot sleeve, within which pressure is maintained until solidification has been completed. It offers good surface finishing of components with accurate dimensions [136].

HPDC is usually done in relatively cool dies to minimise cycle time and maximise productivity. This seems desirable as a cool die will produce a high cooling rate and lead to refined primary Si, but a die that is too cool at the start of the cycle may lead to premature chilling during flow through the die and an undesirable distribution of primary Si. An appropriate die temperature must be selected in combination with the cavity fill rate in order to achieve the optimum combination of primary Si size and distribution, and then select an appropriate melt temperature to avoid premature Si formation in the shot sleeve or runner. HPDC is a relatively inexpensive process and it is widely used for mass production of components different in size and complexity. Since the cooling rate during solidification plays an important role in the final size of primary Si, the high cooling rate of HPDC solves the problem of primary Si size for small parts but these particles are not necessarily uniformly distributed.

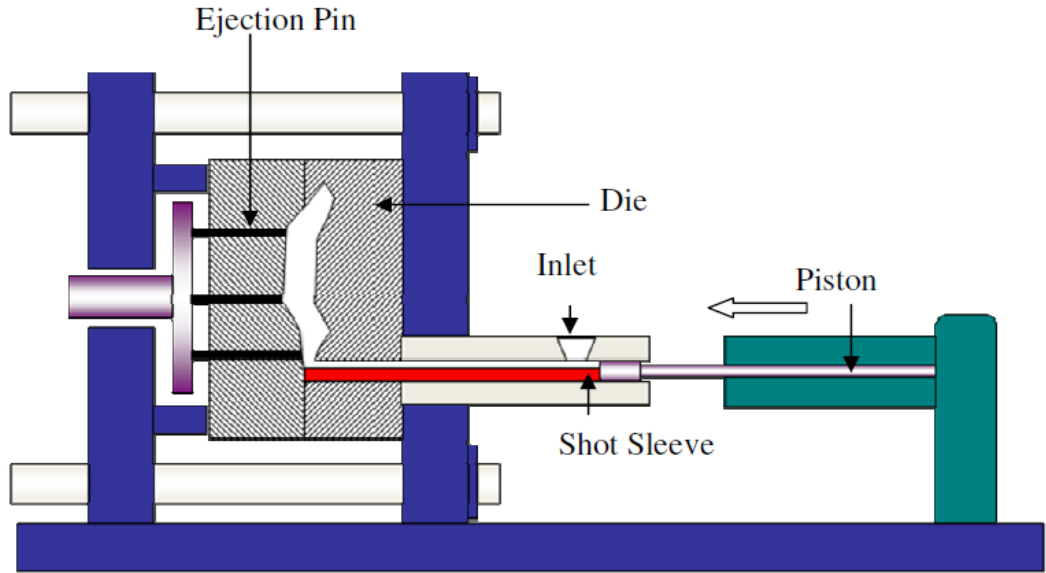


**Figure 2.13** A schematic illustration of a cold chamber high pressure die-casting (HPDC) machine [136].

The surface of HPDC castings are always depleted in primary Si to some depth [137]. This is of most concern for surfaces that will be subject to wear, and such surfaces will require machining to reveal primary Si. The cause of surface depletion is not well understood: (i) some argue that deep undercooling and rapid solidification of melt in intimate contact with cool dies leads to extremely refined primary Si that is indistinct from eutectic Si; (ii) others argue that rapid solidification displaces the eutectic composition so that only eutectic forms at the surface. The depth of primary Si depletion can be controlled by using dies in the temperature range 230-260 °C and avoiding slow cavity fill. Cooling rate alone can be sufficient to refine primary Si in HPDC, although in practice refinement using P additions is frequently used for complete control (a too low melt T, too long a dwell in the shot sleeve, and/or too slow flow before the die cavity may result in the formation of coarse primary Si before the melt enters the die cavity).

In addition to cooling rate, pressure on the melt during solidification is another processing parameter that can be controlled to improve cast microstructure. Feeding of casting by molten alloys can be improved by applying external pressure so that the porosity can be reduced during solidification.

Squeeze casting is a development from HPDC. Although similar to HPDC, it requires melt treatment practices more akin to permanent mould casting. Squeeze casting is used to produce high-integrity parts demanding minimal turbulence during filling, and slow filling requires high melt and die temperatures to prevent premature

chilling during fill. As a result, and because thicker sections may be cast compared with HPDC, squeeze casting always requires primary Si refinement practice i.e. P addition [30]. In the open-die squeeze casting process the molten metal is poured directly into the bottom die, and then the top die is forced down to “forge” the part. Closed-die squeeze casting is more akin to HPDC, but with slower filling to reduce turbulence. The metal solidifies rapidly under considerable pressure in the range of 27.5 to 82.6 MPa depending on the melt alloy. Squeeze-cast parts have no internal porosity and have a fine cast structure if the process parameters are well optimized [138]. Squeeze casting is most widely used to produce high integrity parts such as automobile chassis and suspension components [31]. The low melt velocity in squeeze casting offers a less turbulent flow of the melt into the die than that in HPDC. This lower metal fill rate leads to reduced air entrapment and shrinkage porosity with better dimensional control of the final product compared with HPDC [137].

Generally, HPDC and squeeze cast components exhibit high dimensional accuracy, low roughness as well as higher strength and hardness in comparison to permanent mould cast components [139].

#### **2.14.2 Semi-solid processing**

Semi-solid processing is a promising technique for producing near-net shape components for high performance applications from aluminium alloys, as well as from metal matrix composites. The metal used in this process is a mixture of solid and liquid and the feed material has a consistency similar to butter at room temperature, so it can be injected into a die using relatively low pressures.

Currently, the semi-solid metal (SSM) technique represents one of the commercially feasible technologies for production of complex shaped metallic components with high integrity, improved mechanical properties and tight dimensional control [31]. The parameters that control the processibility and mechanical properties of components produced by SSM process are [140]:

- Temperature range for solidification (freezing range): too wide a solidification range could lead to poor resistance to hot tearing and poor fluidity of the liquid alloy.
- Temperature sensitivity of solid fraction: solid volume fraction of SSM slurry is usually determined by the SSM processing temperature.
- Potential for age hardening: alloys designed for SSM processing need to have large  $\Delta C$ , which is defined as the solid solubility difference between SSM temperature and aging temperature.

- Morphology of the solid phase in semi-solid state: ideal slurry for SSM processing has a controlled volume fraction of fine and spherical solid particles distributed uniformly in a liquid matrix with good fluidity. Such SSM slurry can ensure smooth mould filling and fine and uniform microstructure after solidification.
- Castability of the semi-solid slurry: good fluidity of the liquid phase needs to be ensured through composition selection during alloy design.

When compared to conventional casting (liquid-state processing), the attractive advantages of semi-solid processing are [141]:

- Less energy consumption, where, it requires lower temperature with less force.
- With the use of controlled die filling conditions, the high viscosity of the semi-solid metal ensures that the semi-solid metal fills the die without harmful porosity or other defects.

For the production of SSM slurry, there are two primary routes:

- Rheo-route, which involves preparation of SSM slurry from liquid metal by shearing during solidification and feeding directly into the die cavity or mould for shaping. This route is also known as the Slurry-On-Demand route (SOD).
- Thixo-route, which is basically two steps process, which involving preparation of a feedstock material with thixotropic characteristics, then reheating the feedstock billet to semisolid temperature to produce the SSM slurry and subsequently making a casting in the die cavity.

The process of forming in the semi-solid state is known as "Thixoforming", whereas the production of the feedstock billet (non-dendritic material) is known as "Rheocasting".

Although rheocasting was identified as the production technology at the very beginning of semi-solid processing research, it has not been commercialised to any great extent so far. This is possibly because of the quality of the semisolid slurry produced by such stirring processes, where, mechanical stirring results in the formation of very coarse rosettes with a diameter of a few hundred micrometres or approaching millimetre level. The slurries produced under such conditions do not have adequate thixotropic characteristics for successful direct shaping by either a casting or a forging route. Also, the rheocasting of hypereutectic Al-Si alloy has seldom attained success with acceptable microstructure in an economic and efficient way [142]. Semi-solid processing of hypereutectic Al-Si alloys is mainly limited to the thixocasting route [143-144].

Fan [31] has developed a new rheocasting process. In this process, the overheated liquid metal is poured into a twin screw extruder for continuous shearing with cooling down to below the liquidus temperature as shown in Figure 2.14. The

resulting thixotropic feedstock is transferred to a mould or to a casting machine for shaping. The component produced by this process has a fine grain size, spherical morphology of primary particles and uniform microstructure.

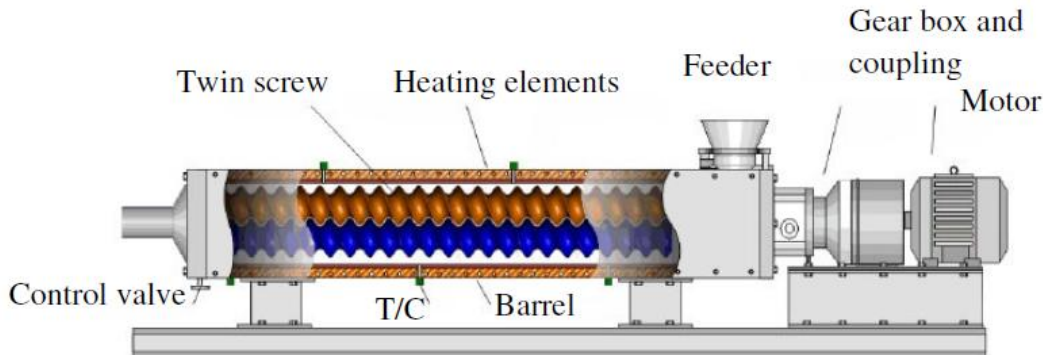


**Figure 2.14** Schematic illustration of the MCAST (melt conditioning by advanced shearing technology) unit [136].

Spray casting is another non-agitation semi-solid process for feedstock production. The molten metal is directed through a nozzle to meet the high pressure inert gas (nitrogen or argon). The liquid metal stream is atomised by the high pressure gas into micrometre sized droplets that experience high cooling rate during their flight, the cooling rate being in the order of  $103 \text{ K s}^{-1}$ . While the large droplets remain fully liquid and the small droplets solidify during atomisation, those of intermediate sizes become semisolid. The droplets are collected on a moving substrate and consolidated to form a coherent preform. It is generally believed that spray cast materials are suitable as feedstock for thixoforming, especially for high temperature alloys, such as steels and superalloys [31]. Spray forming has been developed for the manufacture of Al-Si alloys with Si concentrations up to 70 wt.%. Spray-formed hypereutectic Al-Si alloys have a microstructure consisting of fine (less than  $10 \mu\text{m}$ ), approximately uniformly sized silicon crystals in a matrix of  $\alpha$ -aluminium solid solution [145].

Hogg *et al.* [146] studied the microstructure of a spray formed Si-30wt%Al alloy. They found that the microstructure consisted of  $\sim 5 \mu\text{m}$  equiaxed primary Si grains and a coarse grained Al-rich phase with occasional regions of  $\sim 10 \mu\text{m}$  equiaxed Al-rich grains interpenetrating the Si network with no evidence of a lamellar Al-Si eutectic.

### 2.14.3 Duplex casting processes

The principle of duplex processes is the mixing of two alloys, which are sequentially poured into a mould with a particular time interval between pouring. Careful control of the relative liquidus temperature of the two alloys and cooling conditions provides extra

nucleation sites for silicon and this can lead to significant refinement of primary Si of the resulting alloy [32].

Ohmi *et al.* [147-148] refined the primary Si particles of hypereutectic Al-Si alloy using a duplex process. In this process a relatively low liquidus temperature alloy with a relatively high liquidus temperature alloy are cast in sequence at a given time interval. During the mixing of two alloys, the second alloy melt is rapidly cooled by the first alloy which acts as a coolant. The duplex casting process was used to refine the primary Si without the use of inoculants. The composition of the second liquid was kept constant at 32 wt% silicon and the final solute content after mixing was maintained at 22 wt% silicon by adjusting the volume of the second liquid. The time interval between pouring the first and second liquids was 7 s. Two kinds of mould were used; mould 1 was made of plain graphite and mould 2 was also made of graphite but with a bottom plate made of brick. Solidification in mould 1 was faster than that in mould 2. The primary Si particle size exhibited a minimum value for compositions of the first liquid in the range 12-17 wt% silicon as shown in Figure 2.15. It is usually said that a primary Si particle size below 40  $\mu\text{m}$  is useful in practical terms. In these experiments, the primary Si was refined to below this size.

Alternatively, the composition of the first liquid was maintained at 12 wt% silicon and the composition of the second liquid was varied. The time interval between pouring the first and second liquids was 7s, and moulds 1 and 2 were used as described above. The results are shown in Figure 2.16. The size of primary Si particles decreased, but at a decreasing rate, with increasing second liquid Si content.

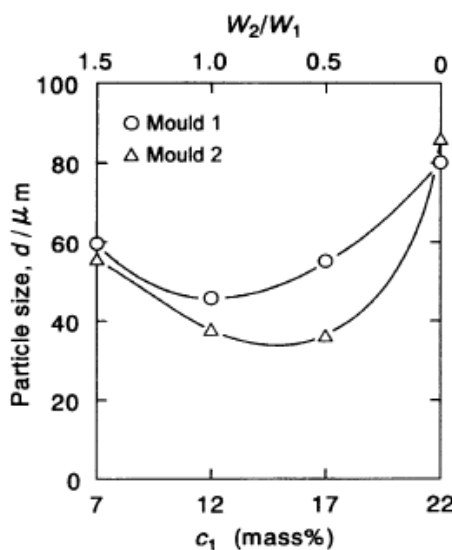


**Figure 2.15** Relationship between the content of the first liquid  $C_1$  and the Si particle size  $d$  of the primary Si in a stepwise duplex cast ingot [4].

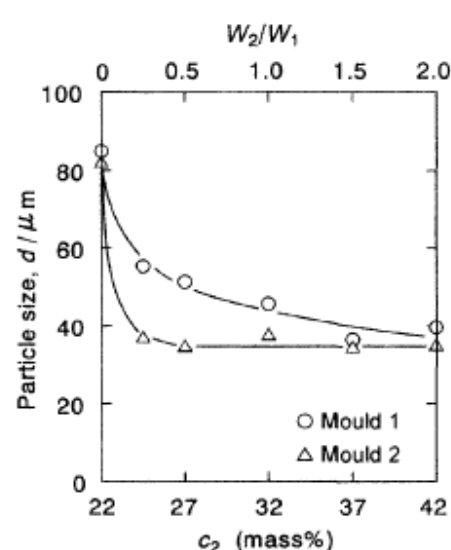


**Figure 2.16** Relationship between the content of the second liquid  $C_2$  and the Si particle size  $d$  of the primary Si in a stepwise duplex cast ingot [4].

The disadvantages of this duplex process are the composition limitations and the technical difficulties [33] where using more complex moulds and thin sections could lead to poor mixing with thin sections that are very lean in solute (and thus low strength). Also, it is not clear how sequential filling could be applied to bottom filling casting processes.

Saha *et al.* [142] have introduced two novel methods using “diffusion solidification” for achieving refined semi-solid cast parts for both hypoeutectic as well as hypereutectic Al-Si alloys. The two concepts are [149]:

- mixing semi-solid hypoeutectic alloy with liquid hypereutectic alloy such that the cooler hypoeutectic alloy rapidly chills the liquid hypereutectic alloy leading to refined primary Si,
- cooling the liquid hypereutectic alloy with the addition of solid particles of the same alloy.

Alcan [150] has developed the “SEED” (swirl enthalpy equilibration device) process which is an effective route for the preparation of feedstock for semi-solid forming processes as shown in Figure 2.17.

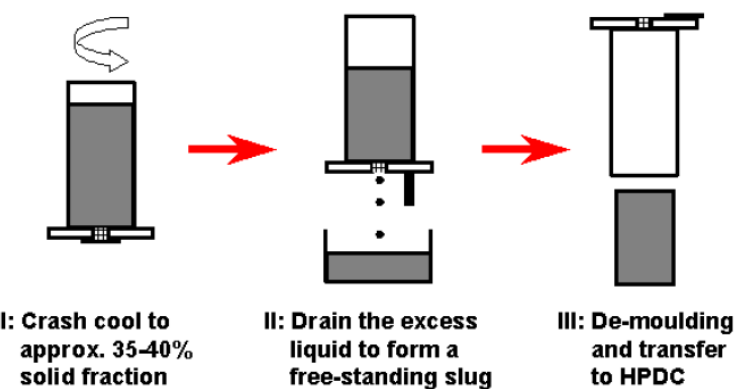


**Figure 2.17** Diagram of the swirl enthalpy equilibration device (SEED process) [151].

The SEED process involves the application of swirling, which allows the extraction of a controlled amount of heat from the molten alloy to generate a modified semi-solid mixture. This method has been applied successfully to the production of A356/A357 Al-Si semi-solid feedstocks. A combination of the SEED process, isothermal holding and addition of solid alloy during swirling was used by Tebib *et al.* [152] to rheoprocess semi-solid A390 alloy. A significant increase in the volume fraction of non-dendritic  $\alpha$ -Al phases with refinement of primary Si was observed when using this process.

# Chapter 3

## Experimental Techniques and Procedures

In this chapter, the procedure for preparation of the Al-Si alloys and inoculants under different casting conditions and the characterisation and mechanical property measurement techniques applied will be presented. The experimental approach was as follows:

1. A more systematic study of the effect of casting conditions (melt superheat and cooling rate) and alloy purity on scale and morphology of primary Si during solidification of hypereutectic Al-Si alloys.
2. A better understanding of the role of Ca content on the refinement of primary and eutectic Si. This was achieved by both melt treated with  $K_2SiF_6$  flux to remove Ca, and by adding Al-Ca master alloy to elevate the Ca content.
3. Refinement of primary Si using different chemicals other than phosphorous. In particular, the addition of ZnS or P-doped  $Al_2O_3$  were investigated as an alternative to AlP.
4. Applying a new solid-liquid duplex casting process to achieve simultaneous primary Si refinement and eutectic modification in hypereutectic Al-Si alloys.

### 3.1 Materials Preparation

Initial batches of each Al-Si alloy used in this research were prepared in an electrical resistance furnace by melting and diluting an Al-50Si master alloy (supplied by Norton Aluminium Ltd, UK) with commercial purity aluminium LM0 (supplied by Coleshill Aluminium Ltd, UK) at 1100 °C for 3 h in a clay-graphite crucible. The compositions of the raw materials are listed in Table 3.1.

**Table 3.1** Composition of commercial purity Al (LM0) and Al-50Si master alloy raw materials (wt%)

Alloy	Cu	Mg	Si	Fe	Mn	Ni	Zn	Pb	Sn	Ti	Cr	Al
LM0	0.03	0.03	0.30	0.40	0.03	0.03	0.07	0.03	0.03	-	-	Bal.
Al-50Si	0.08	0.28	51.0	0.32	0.02	0.01	0.02	0.02	0.01	0.09	0.03	Bal.

To ensure homogeneity, the molten alloys were manually stirred for few seconds and then cast. For each experiment, the Al-Si alloy was melted in a clay-graphite crucible and held for one hour in the furnace at the experiment temperature prior to any addition. All sampling and casting moulds were preheated at 200-350 °C. Different compositions were chosen (e.g. Al-15Si, Al-18Si, Al-19Si and Al-22Si) in order to allow us investigating the effect of different parameters on a wide range of Al-Si alloys. After preparing the melt, different procedures were followed depending on factors to be studied.

### 3.2 Effect of Cooling Rate on Primary and Eutectic Si

To study the effect of cooling rate, castings were made using three different mould/cooling systems to give cooling rates between 1 and 15 K/s. For each experiment, the Al-15Si alloy was heated up to 1150 °C and then cooled down to the experiment pouring temperature. After 30 minutes at the set pouring temperature, samples were taken either: by the American Association Standard TP-1 test mould preheated at 350 °C, which corresponded to a cooling rate of 3.5 K/s at the central region of a cross-section, 38 mm from the base of the TP-1 sample [153]; or by a Boron Nitride coated steel mould (35mm in diameter and 40mm in height with long handle) preheated at 200 °C. The steel mould was cooled either in a water bath with cooling rate of 15 K/s or air cooled with cooling rate of 1 K/s. The cooling rates were confirmed by monitoring the temperature at the centre of the casting during cooling, and typical cooling curves for the water cooled and air cooled moulds are provided in Figure 3.1a and Figure 3.1b, respectively.

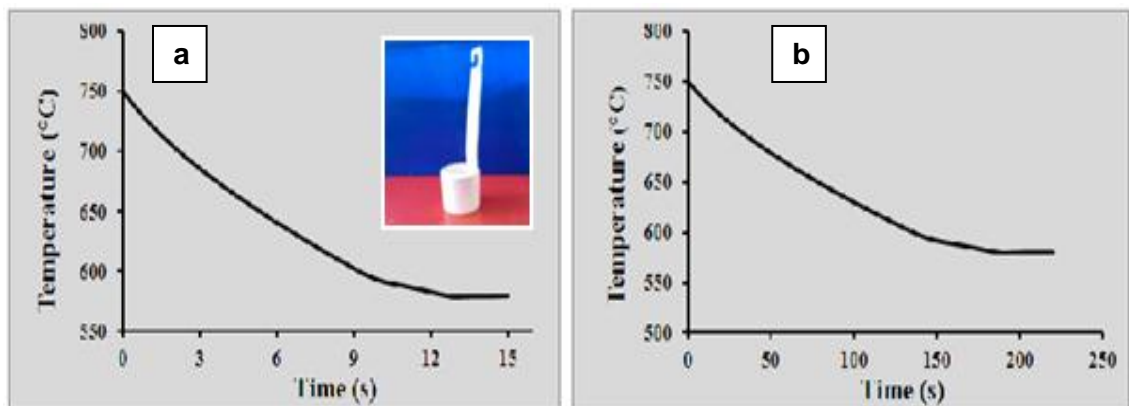


**Figure 3.1** Cooling curve of Al-15Si alloy sampled using the boron nitride coated steel mould: (a) water cooled with cooling rate of 15 K/s, and (b) air cooled with cooling rate of 1 K/s.

Initial experiments to investigate the effect of cooling rate revealed significant or severe segregation of primary Si to the top of casting when the cooling rate was low (i.e. 3.5 K/s in TP-1 samples and 1K/s using the air cooled mould), irrespective of melt superheat. For example Figure 3.2 shows the segregation of primary Si in the Al-15Si alloy TP-1 samples cast from different melt temperatures. The use of the TP-1 and air cooled moulds was subsequently abandoned and all other experiments in this study were carried out using the water cooled cylindrical steel mould to ensure a uniform distribution of primary Si.

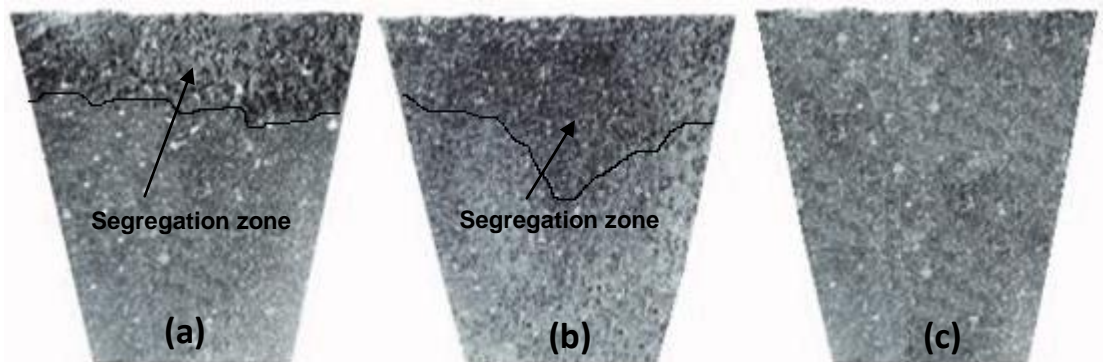


**Figure 3.2** Scanning graphs showing the segregation of primary Si at the top of the TP-1 test casting in solidification of hypereutectic Al-15Si alloy from: (a) 1150 °C, (b) 720 °C and (c) 620 °C.

### 3.2.1 TP-1 test procedure

In order to study the morphology of silicon in hypereutectic Al-Si alloy as a function of cooling rate, the American Association Standard TP-1 test was operated in conditions to provide a consistent cooling rate of 3.5 K/s at the central region of a cross-section, 38 mm from the base of the TP-1 sample. The schematic diagram of TP-1 test mould is shown in Figure 3.3 [153].

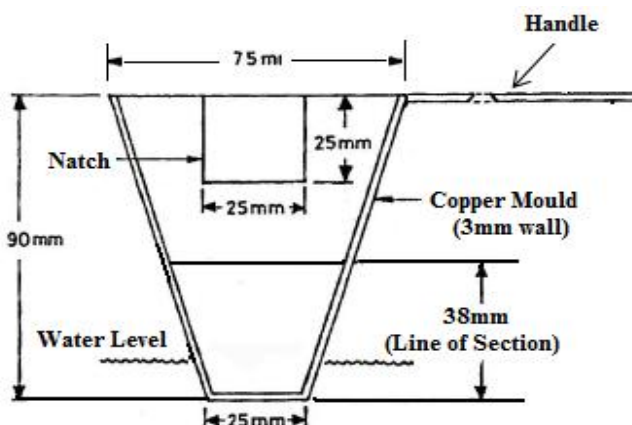


**Figure 3.3** Schematic diagram of the American Association Standard TP-1 test mould ladle [153].

The experimental steps of the TP-1 test are as follows:

- a) The alloy was melted in the electrical resistance furnace and held at the appropriate experiment temperature.
- b) The TP-1 mould ladle was placed in an oven for preheating to 350 °C.
- c) The prepared melt was stirred using a graphite rod for 30 s and poured into the TP-1 mould ladle at the desired temperature and the ladle placed on a quench tank until final solidification was complete.
- d) The water flow rate in the quench tank was set at 3.8 l/min. This flow rate resulted in 3.5 K/s cooling rate at 38 mm from the bottom of the ladle.

### **3.3 Effect of Melt Superheat on Primary and Eutectic Si**

For the effect of superheat, different casting temperatures were selected ranging from 650 °C to 1150 °C for the Al-15Si alloy. For each experiment, the Al-15Si alloy was heated up to 1150 °C and then cooled down to the experiment pouring temperature prior to casting. After 30 min at the set temperature, samples were taken by using the preheated steel mould which was then water cooled at approximately 15 K/s.

### **3.4 Refinement and Modification in a High Purity Hypereutectic Al-Si Alloy**

Because of the potential interaction effect of some impurities such as P and Ca in the commercial purity hypereutectic Al-Si alloys, a series of high purity Al-15Si and Al-15Si-Ca alloys, with and without P additions, were manufactured by using 4N (99.99%) purity Al (supplied by Hydro Aluminium High Purity GmbH, Grevenbroich, Germany) as well as 5N (99.999%) purity Si (supplied by Aldrich). The P content in the 4N Al was determined by glow discharge mass spectroscopy at Evans Analytical Group (Tournefeuille, France) and was  $0.4 \pm 0.08$  ppm [106]. P was added in the form of Cu-P shot (Supplied by Aura Metals Ltd) and Ca was added as 99.9 wt% Ca powder (supplied by Riedel-de Haen). The aluminium was cleaned in NaOH solution followed by distilled water and the silicon cleaned in methanol [89]. The aluminium and silicon were melted under an Argon atmosphere in an electrical resistance furnace, and held at 800 °C for 30 min to ensure a homogeneous melt. For Al-15Si-P and Al-15Si-Ca alloys, Ca powder and Cu-P were wrapped in aluminium foil and inserted into the Al-15Si melt. After 15-20 min following the addition, samples were taken by using the preheated steel mould which was then water cooled at approximately 15 K/s. The same experiments were repeated to prepare commercial purity Al-15Si, Al-15Si-P alloys by melting and diluting an Al-50Si master alloy with commercial purity aluminium LM0 at 1100 °C for 3 h in a clay-graphite crucible.

### **3.5 Effect of Ca Level on Primary and Eutectic Si**

To study the effect of Ca content on scale and morphology of silicon, experiments were conducted by adding  $K_2SiF_6$  (AP1) flux (supplied by Alpha Foundry Supplies, UK) to Al-Si alloys. AP1 is a pink powdered exothermic drossing-off flux providing a dry cover. It is a protective exothermic cover flux which when applied to the surface of the metal minimises oxidation and hydrogen pick-up thereby greatly reducing melting losses. The chemical composition of AP1 is  $K_2SiF_6$  which decomposes at 500 °C to produce the fluoride gases as stated in the specification sheet. AP1 is often chosen to be a fluoride salt flux to remove alkali elements such as Ca, Na and La.

The initial Al-Si alloys were prepared as described in section 3.1. To ensure homogeneity, the molten alloy was manually stirred for a few seconds and then the furnace was set to 800 °C for each experiment. AP1 flux ( $K_2SiF_6$ ) was added to the melt (0.5 wt%) with gentle mixing and skimming off the dross. In the case of studying the effect of high Ca content, Ca was added in the form of Al-10Ca master alloy. After 20 min, samples were taken with and without fluxing by using the preheated steel mould which was then water cooled at approximately 15 K/s. The Ca composition was analysed before and after changing the Ca content using optical emission spectroscopy (OES). Specification of OES is presented in detail in section 3.10.2.

### **3.6 Effect of Chemical Additions on Primary and Eutectic Si**

A number of different elements and compounds were added to study their effect on solidification of hypereutectic Al-Si alloys and the reason for choosing these chemicals are stated in detail in Chapter Four. In studying the effect of alloying on the microstructure of Al-Si Alloys, the chemicals listed in Table 3.2 were wrapped in aluminium foil and added to the Al-Si melt with gentle mixing. 15-20 min after mixing in the added chemicals, samples were taken by using the preheated steel mould which was then water cooled at approximately 15 K/s.

**Table 3.2** Properties and suppliers of chemicals used in alloying experiments.

Material	Properties	Wt% added	Supplier
<b>Mg</b>	Ingot, 99.95%	0.1, 0.3, 0.4, 0.5, 0.75, 1.0	MEL. Manchester, UK
<b>Sb</b>	99.50%	0.5	Aldrich
<b>Ca</b>	Powder, 99.95%	0.5	Riedel-deHaen
<b>Zn</b>	Shot, 99.9%	-	Alfa Aesar
<b>MgO</b>	Powder, 99.90% (0.5 µm)	0.5	Inframmat advanced material
<b>CaO</b>	Powder, 99.99%	0.5	REacton
<b><math>\alpha</math>-Al<sub>2</sub>O<sub>3</sub></b>	Powder, 99.8% (0.5 µm)	0.5	Inframmat advanced material
<b><math>\gamma</math>-Al<sub>2</sub>O<sub>3</sub></b>	Powder, 99.9% (3 µm)	0.5	Alfa Aesar
<b>ZnO</b>	Powder, 99.99%	-	Aldrich
<b>Na<sub>2</sub>S</b>	Powder, 99%	0.5	Alfa Aesar
<b>ZnS</b>	Powder, 99.99% ( $\leq$ 44 µm)	0.5	Alfa Aesar

### 3.7 Refinement of Primary Si Using Zincblende ZnS

Aluminium phosphide (AlP) particles are often suggested to be the nucleation site for primary silicon in hypereutectic Al-Si alloys, as both the crystal structure and lattice parameter of AlP (crystal structure: cubic; lattice parameter: 5.431 Å) are close to that of silicon (crystal structure: cubic; lattice parameter: 5.421 Å), there is minimal mismatch between the AlP and the Si phases (<1%) [28].

Due to the structural similarity of zincblende ZnS and AlP, use as an inoculant to refine primary Si was explored. ZnS occurs in two common polytypes, zincblende (also called sphalerite, cubic with lattice parameter 5.410 Å) and wurtzite (hexagonal with lattice parameters  $a_0 = 3.249$  Å,  $c_0 = 5.207$  Å). ZnS has the cubic zincblende structure below 1020 °C and has the hexagonal wurtzite structure above this phase transition temperature [154].

#### 3.7.1 ZnS micron scale particles

Experiments were conducted by adding 0.5 wt% of 99.99% purity ZnS powder (supplied by Alfa Aesar Ltd, UK) with -325 mesh size (less than 44 µm) to the hypereutectic Al-18Si melt with gentle mixing at 800 °C. After 20 min, samples were taken by using the preheated steel mould which was then water cooled at approximately 15 K/s.

### 3.7.2 Synthesis ZnS nanoparticles

Because of the significant refinement of primary Si using micron scale zincblende ZnS particles (see section 4.4.3.2); nano scale particles were used in an attempt to increase the refinement efficiency. Since ZnS nanoparticles could not be secured from any supplier, they were synthesized in the laboratory.

One synthesis method for zincblende ZnS nanoparticles is by the solid-liquid chemical reaction using ZnO and Na<sub>2</sub>S under ultrasonic treatment [155]. 2 g of ZnO powder (supplied by Aldrich) and 40 ml Na<sub>2</sub>S solution (2.0 mol/l) were mixed and irradiated in an ultrasonic bath for 20 min. The suspension produced was purged with Argon to remove oxygen and then stirred using a magnetic stirrer in a water bath at 90 °C for 2 h. The reaction product was then quenched to room temperature immediately, filtered and washed with distilled water and ethanol several times to remove any residual Na<sub>2</sub>S. The ZnS nanoparticles were finally obtained after drying and grinding. According to this procedure proposed by She *et al.* [155], the prepared ZnS nanoparticles should be crystalline cubic zincblende with a uniform distribution and an average size of 35 nm. The synthesized powder was analysed by X-ray diffractometry (XRD), which was performed using a Bruker D8 Advance X-ray diffractometer with Cu radiation at a voltage of 40 kV and a current of 40 mA. The XRD patterns for the produced ZnS show that it consists of mainly cubic zincblende structure as shown in Figure. 3.4. The synthesized powder was wrapped in aluminium foil and inserted into the Al-Si melt. After 20 min following the addition, samples were taken by using the preheated steel mould which was then water cooled at approximately 15 K/s.

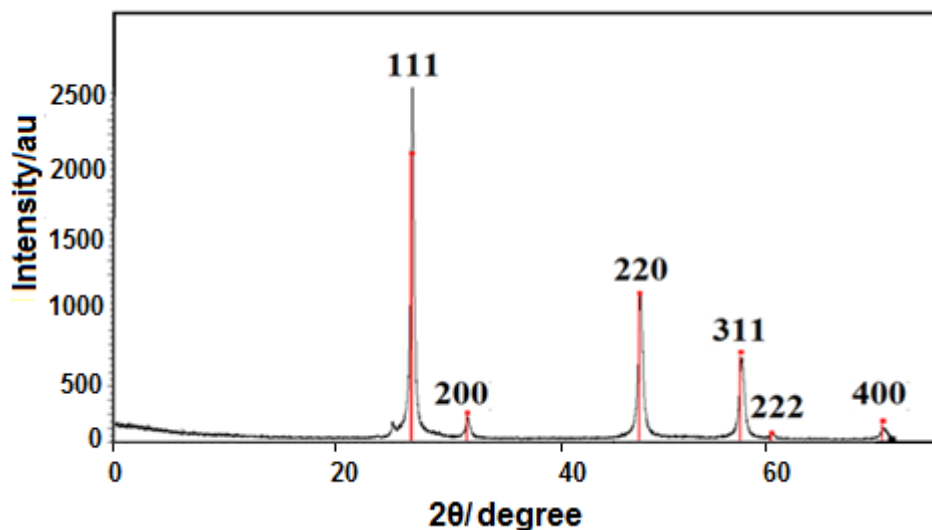


**Figure 3.4** XRD pattern of ZnS prepared by the solid-liquid chemical reaction. The peaks associated with diffraction from crystallographic phases of zincblende ZnS are labelled.

### **3.7.3 *In situ* preparation of ZnS**

In order to overcome the low wettability of ZnS particles with the melt (as discussed in section 4.4.3.2) and thus to improve the refinement of primary Si, experiments were conducted to prepare ZnS *in situ* by adding 0.5 g of the element of Zn to 270 g of Al-18Si melt with gentle stirring at 800 °C, 10 min after which, 1.0 g of Na<sub>2</sub>S powder wrapped in aluminium foil was added to the melt. The formation of ZnS is according to the following chemical reaction [156]:



The molten alloy was manually stirred for a few seconds and after 20 min following the addition, samples were taken by using a preheated steel mould which was then water cooled at approximately 15 K/s. Optical emission spectroscopy (OES) analysis of Zn in the solidified Al-18Si+ZnS alloy suggested that the produced alloy contains 0.27% ZnS.

### **3.7.4 Preparation of an Al-ZnS master alloy**

Experiments were carried out to prepare an Al-ZnS master alloy by adding Na<sub>2</sub>S and Zn to a high purity Al melt. According to equation 3.1, one mole of Zn and one mole of Na<sub>2</sub>S are required to produce one mole of ZnS. The molecular weight of Zn, Na<sub>2</sub>S and ZnS are 65, 78 and 97.5 respectively. Hence, to produce Al-1.5wt%ZnS the stoichiometric amount of Zn metal (2 g) was added with the 50% excess of Na<sub>2</sub>S powder (3.6 g) to 200 g high purity aluminium melt with gentle mixing at 800 °C for 20 min. The use of an excess amount of Na<sub>2</sub>S was needed to ensure that the reaction was driven to completion. The produced master alloy was cast in cylindrical mould pre-heated to 200 °C, and cooling in air at a cooling rate of approximately 16 K/s.

Another set of experiments were conducted to refine Al-22Si alloy by adding different amounts of the Al-1.5wt%ZnS master alloy and casting for two melt holding times of 20 min and 1.5 h. The amounts of Al-1.5wt%ZnS master alloy added to 200 g of Al-22Si alloy were 8, 16 and 24 g to produce alloys with 0.05, 0.1 and 0.16 wt% ZnS respectively.

The chemical composition of Al-22Si alloy after adding the master alloy with 0.1 wt% ZnS analysed using optical emission spectrometry (OES) showed that the Si composition reduced to around 20 wt% Si because of dilution. Hence, to compare with P refinement, an experiment was conducted by adding 200 ppm of P in the form of Cu-P shot to Al-20Si alloy. A sample was taken after 20 min. Samples for all above

experiments were taken using the preheated steel mould which was then water cooled at approximately 15 K/s.

### **3.8 Nucleation and Growth of Primary Si on Al<sub>2</sub>O<sub>3</sub>**

In some experimental results it was noticed that primary Si particles were clearly associated with visible oxide bafilms, as shown for example in Figure 4.37. There is also some experimental evidence in the literature that concluded that some Si particles nucleate and grow on oxide bafilms during solidification of hypereutectic Al-Si alloys. Work by Pennors *et al.* [157] presented clear microstructures in which AIP particles are seen aligning along oxide bafilms.

Experiments were carried out to study the effect of adding  $\alpha$ -Al<sub>2</sub>O<sub>3</sub> and  $\gamma$ -Al<sub>2</sub>O<sub>3</sub> powder on the morphology of Si in hypereutectic Al-Si alloys. In order to use powder having the same impurities and particle size distribution,  $\gamma$ -Al<sub>2</sub>O<sub>3</sub> was prepared from  $\alpha$ -Al<sub>2</sub>O<sub>3</sub> powder in the laboratory as follows [158]:

50 gm of  $\alpha$ -Al<sub>2</sub>O<sub>3</sub> (Supplied by Inframet Advanced Material, 0.5  $\mu\text{m}$  in size) was mulled for 3-5 min with 16 ml of distilled water. A further 10 ml of distilled water was added in 5 ml portions with mulling for 3-5 min after each addition. The powder was left to dry in air at room temperature for approximately 18 h before drying overnight at approximately 120 °C. Finally, the powder was calcined by heating it at 4 °C/min to 500 °C and then maintaining this temperature for 4 h.

In order to enhance the potential of primary Si refinement by Al<sub>2</sub>O<sub>3</sub>, P-doped alumina was prepared by impregnation of ( $\alpha$  or  $\gamma$ ) Al<sub>2</sub>O<sub>3</sub> powder with an aqueous solution of H<sub>3</sub>PO<sub>4</sub> [159]. 5 g of ( $\alpha$  or  $\gamma$ ) Al<sub>2</sub>O<sub>3</sub> powder (0.5  $\mu\text{m}$  in size) was mixed with 50 ml of aqueous solution of phosphoric acid (11 wt% H<sub>3</sub>PO<sub>4</sub>) for 72 h followed by filtration, drying at 120 °C for 12 h and finally calcining at 500 °C for 2 h. The produced dry powder was ground, wrapped in aluminium foil and preheated before use in refinement experiments. After 15-20 min following the addition, samples were taken by using the preheated steel mould which was then water cooled at approximately 15 K/s. The same procedures of preparing P-doped  $\gamma$ -Al<sub>2</sub>O<sub>3</sub> and casting experiments were repeated by using  $\gamma$ -Al<sub>2</sub>O<sub>3</sub> powder, 3  $\mu\text{m}$  in size (supplied by Alfa Aesar Ltd, UK).

### **3.9 A New Solid-Liquid Duplex Casting Process**

The primary Si crystals of hypereutectic Al-Si alloys are reported to be refined by the liquid-liquid duplex casting process [147]. This process, described in detail in section 2.14.3, involves a two-step casting of two molten alloys with different composition; i.e., "the first alloy" with lower liquidus temperature and "the second alloy" with higher liquidus temperature [160]. Although this process has been shown to lead to refined

primary Si, it does not additionally lead to a modified eutectic Si. In order to achieve simultaneous refinement of primary Si and modification of eutectic silicon in the target alloy, a new solid-liquid duplex process is developed.

In the solid-liquid duplex casting process, solid P-treated high silicon content alloy (i.e. pre-refined primary Si) is mixed with molten Sr-treated low silicon content alloy to produce an Al-Si alloy in the Liquid +Primary Si phase field which is then cast. Initial batches of the Al-Si alloys were prepared in an electrical resistance furnace as described in section 3.1. AP1 flux ( $K_2SiF_6$ ) was added to the melt (0.5 wt %) with gentle mixing. The resulting dross was skimmed off prior to casting. AP1 was added to reduce Ca content thus to enhance the refinement of primary Si in the pre-solidified high Si alloy and to enhance the efficiency of Sr modification in the final microstructure.

Figure 3.5 shows an example of the solid-liquid duplex casting process. Where, Al-19Si+P+Sr was prepared by mixing 1:1 (by mass) solid P-treated Al-30Si alloy and molten Sr-treated Al-8Si alloy.

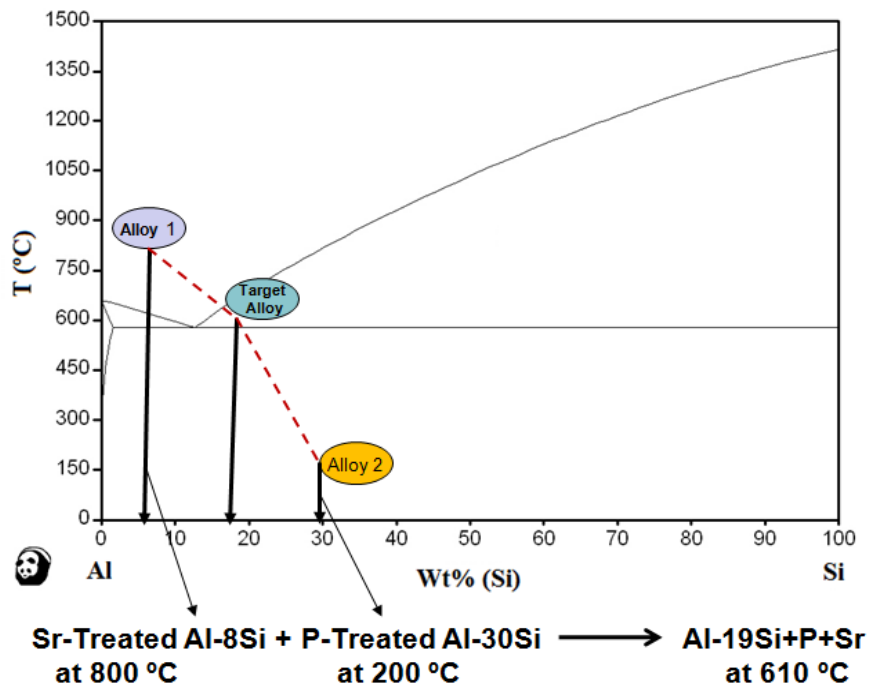


**Figure 3.5** Preparation of Al-19Si (Target Alloy) by mixing the melt of Sr-treated Al-8Si (Alloy 1) with P-treated Al-30Si solid chips (Alloy 2) and casting from 610 °C.

The Al-30Si was melted to 50 °C above its liquidus and then 400 ppm P was added in the form of Cu-P shot (Supplied by Aura Metals Ltd). After 20 min the melt was cast in a water-cooled mould and cut in small solid pieces 5 g in weight each (chips). The Al-8Si alloy was melted at 800 °C and then 400 ppm Sr was added in the form of

Al-10Sr master alloy (supplied by Roba Metals Ltd, UK). After 20 min, chips of the P-treated Al-30Si (preheated to 200 °C) were manually stirred into the Sr-treated Al-8Si alloy melt until the temperature reached 610 °C at which point the melt was sampled using the preheated steel mould which was then water cooled at approximately 15 K/s. Al-19Si alloys with a range of P and Sr content (as shown in Table 3.3) were produced using the solid-liquid duplex casting process in order to optimize the composition of both alloys to achieve simultaneous refinement of primary Si and modification of eutectic silicon in the target alloy. Each experiment was given a code consists from letters SLD and a number, e.g. SLD1.

Experiments were also conducted to find the optimum Si content in Sr-treated Al-Si Alloy by mixing P-treated Al-30Si solid chips with Sr-treated low Si melt (0-15 wt% Si) to produce Al-19Si containing the optimum P and Sr content (as shown in Table 3.4).

Another set of experiments was conducted to study the effect of casting temperature on the morphology of Si phases using the optimum P and Sr content in Al-19Si alloy prepared using the solid-liquid duplex casting process. The castings were carried at 610 °C, 710 °C and 750 °C (as shown in Table 3.4).

For comparison of conventional casting with the solid-liquid duplex casting process, 200 ppm P and 200 ppm Sr were added simultaneously to liquid Al-19Si alloy at 800 °C which was then cast conventionally. Samples were taken by using a preheated steel mould which was then water cooled at approximately 15 K/s. The above experiments (conventional and duplex casting process) were repeated for Al-18Si as the target alloy.

**Table 3.3** Experimental parameters to produce Al-19Si alloy from solid Al-30Si alloy with varying P additions and liquid Al-8Si melt varying Sr additions. The mass ratio of the two alloys was fixed of 1:1 and the casting temperature was fixed at 610 °C.

Exp. No.	Starting Alloy 1 (L) at 800 °C				Starting Alloy 2 (S) at 200 °C				Cast Temp. °C	Final content of P and Sr in target alloy
	Comp.	Mass of Alloy (g)	Mass of Sr (g)	Sr (ppm)	Comp.	Mass of Alloy (g)	Mass of P (g)	P (ppm)		
SLD1	Al-8Si	200	-	-	Al-30Si	200	-	-	610	Al-19Si
SLD2	Al-8Si	200	-	-	Al-30Si	200	0.01	50	610	Al-19Si+25ppm P
SLD3	Al-8Si	200	-	-	Al-30Si	200	0.02	100	610	Al-19Si+50ppm P
SLD4	Al-8Si	200	0.08	400	Al-30Si	200	-	-	610	Al-19Si+200ppm Sr
SLD5	Al-8Si	200	0.08	400	Al-30Si	200	0.01	50	610	Al-19Si+25ppm P+200ppm Sr
SLD6	Al-8Si	200	0.08	400	Al-30Si	200	0.02	100	610	Al-19Si+50ppm P+200ppm Sr

L: Liquid S: Solid

**Table 3.3** continued.

Exp. No.	Starting Alloy 1 (L) at 800 °C				Starting Alloy 2 (S) at 200 °C				Cast Temp. °C	Final content of P and Sr in target alloy
	Comp.	Mass of Alloy (g)	Mass of Sr (g)	Sr (ppm)	Comp.	Mass of Alloy (g)	Mass of P (g)	p (ppm)		
SLD7	AI-8Si	200	0.08	400	AI-30Si	200	0.04	200	610	Al-19Si+100ppm P+200ppm Sr
SLD8	AI-8Si	200	0.08	400	AI-30Si	200	0.06	300	610	Al-19Si+150ppm P+200ppm Sr
SLD9	AI-8Si	200	0.08	400	AI-30Si	200	0.08	400	610	Al-19Si+200ppm P+200ppm Sr
SLD10	AI-8Si	200	0.06	300	AI-30Si	200	0.08	400	610	Al-19Si+200ppm P+150ppm Sr
SLD11	AI-8Si	200	0.04	200	AI-30Si	200	0.08	400	610	Al-19Si+200ppm P+100ppm Sr
SLD12	AI-8Si	200	0.06	300	AI-30Si	200	0.06	300	610	Al-19Si+150ppm P+150ppm Sr

L: Liquid S: Solid

**Table 3.4** Experimental parameters to produce Al-19Si alloy from solid Al-30Si and liquid alloys of different Si content or varying casting temperature.

Exp. No.	Starting Alloy 1 (L) at 800 °C				Starting Alloy 2 (S) at 200 °C				Cast Temp. °C	Final content of P and Sr in target alloy
	Comp.	Mass of Alloy (g)	Mass of Sr (g)	Sr (ppm)	Comp.	Mass of Alloy (g)	Mass of P (g)	p (ppm)		
SLD13	CP Al	148	0.08	540	Al-30Si	252	0.10	400	610	Al-19Si+252ppm P+200ppm Sr
SLD14	AI-12.6Si	252	0.08	317	Al-30Si	148	0.06	400	610	Al-19Si+148ppm P+200ppm Sr
SLD15	AI-15Si	292	0.08	274	Al-30Si	108	0.04	400	610	Al-19Si+108ppm P+200ppm Sr
SLD16	AI-12.6Si	252	0.08	317	Al-30Si	148	0.06	400	710	Al-19Si+148ppm P+200ppm Sr
SLD17	AI-12.6Si	252	0.08	317	Al-30Si	148	0.06	400	750	Al-19Si+148ppm P+200ppm Sr
SLD18	AI-12.6Si	252	0.08	317	Al-30Si	148	0.08	540	610	Al-19Si+200ppm P+200ppm Sr

L: Liquid S: Solid

## **3.10 Characterisation Methods**

### **3.10.1 Preparation of samples**

Each cylindrical cast sample was sectioned longitudinally into two halves. One half for each sample was chemically analysed using optical emission spectroscopy (OES) (see section 3.10.2). The other longitudinal section of each sample was prepared for metallographic analysis using the standard techniques of grinding with SiC abrasive papers with various grit sizes (120, 800, 1200, 2500 and 4000), and polishing with  $1\mu\text{m}$  diamond suspension followed by silica suspension.

### **3.10.2 Chemical composition analysis**

It was essential to measure the chemical composition of the prepared alloys to verify whether their composition was close to that of the target. In this work chemical composition for all alloys was analysed using a “Worldwide Analysis System (WAS) AG, Foundry Master” optical emission spectrometer (OES). A spark is produced on the surface of the sample to energise the surface and to emit photons with element specific wavelengths, which are detected by the optical spectrometer. A detailed explanation of “spark source spectrometry” is given in Gill (1997) [161]. The equipped WASLAB software compares the measured data with standard data and gives the final results in wt% of chemical compositions. To produce flat surfaces for this analysis, samples were polished with 120 grit SiC paper. Several tests were performed on a single sample and an average result was recorded as the final composition.

### **3.10.3 Optical microscopy (OM)**

Microstructure characterization was accomplished using an optical microscope (Carl Zeiss Axioskop 2 MAT) equipped with image analysis software. For each sample, more than 30 micrographs were taken covering the whole section. The average particle size, shape factor and number density of primary Si particles were quantified for more than 500 particles per sample. Primary Si particle size was measured as an equivalent circular diameter with standard error of mean. The shape of the primary Si particles was quantified in terms of a shape factor S:

$$S=4\pi A/P^2$$

where  $A$  and  $P$  are the area and perimeter of each particle on the plane of the polished surface respectively. The shape factor  $S$  has a value of one for perfectly round particles, and increasingly less than one as the particles become more irregular in shape.

### **3.11 Scanning Electron Microscopy (SEM)**

The scanning electron microscopy (SEM) examination was carried out using a Zeiss Supra 35 FEG microscope. The microscope, equipped with an energy dispersive spectroscopy (EDS) facility, operated at an accelerating voltage of 5-20 kV. A scanning electron microscope (SEM) is a microscope with an electron beam scanning back and forth over a sample. Several different signals are produced due to the interaction between the beam and the sample. These signals provide the user with detailed information about the differences of atomic number within the sample, surface structure or information about the elemental content [162]. A signal is measured individually from each point, with the use of advanced detectors, which collects a range of X-rays and electrons from different depths of the surface. The SEM used in this study has primary electron imaging, secondary electron imaging or back scattered electron (BSE) imaging, and energy-dispersive X-ray spectroscopy (EDS) operational modes. The advantage of SEM over optical microscopy is the large depth of field and higher resolution, thus producing high resolution images at high magnification (up to 50,000 times).

### **3.12 Mechanical Property Tests**

Cylindrical bars (2.54 cm diameter x 20 cm length) were prepared by casting similarly prepared Al-Si alloys into a steel mould pre-heated to 200 °C, and cooling in air at a cooling rate of approximately 16 K/s in order to obtain microstructures similar to those obtained by the sampling process. The bars were then machined to produce tensile test samples of 6.4 mm in gauge diameter, 25 mm in gauge length and 12 mm diameter in the grip section. Static tensile tests were carried out using an Instron® 5569 machine at a cross head speed of 2 mm/min (strain rate:  $1.33 \times 10^{-3} \text{ s}^{-1}$ ). The 'Instron® 5569' system was connected to a PC for automated testing and calculation of tensile test results such as yield stress, ultimate tensile strength and elongation to fracture. All samples were tested at room temperature.

# **Chapter 4**

## **Results**

Results gained from each series of experiments are introduced in this chapter. As mentioned in Chapter Three, all experiments were carried out to cover the thesis outlines which include the effect of solidification rate, chemical additions and casting techniques on a wide range of Al-Si alloys. The effects of all above parameters on the morphologies of primary and eutectic Si following solidification of hypereutectic Al-Si alloys were studied. In this chapter figures showing optical micrographs generally consist of pairs of micrographs, one at a lower magnification to illustrate the scale and morphology of primary Si and the other to reveal the nature of the eutectic structure at a higher magnification.

### **4.1 Effect of Solidification Rate on Primary and Eutectic Si**

The effects of superheat temperature and cooling rate on the solidification of hypereutectic Al-15Si alloy were investigated. The microstructure evolution and quantitative analysis of primary Si particles were characterized by optical microscopy. A robust casting and sampling procedure was developed for consistent measurement and evaluation.

#### **4.1.1 Effect of cooling rate**

Standard TP-1 test samples for different melt temperatures illustrated in Figure 3.2 showed that coarse primary Si concentrated in a thick zone at the top of the cast samples. This segregation band became denser and more sharply delineated with increasing superheat temperature. It was clear that primary Si in Al-15Si alloy suffers from macro-segregation to the top of the TP-1 test specimens. The silicon distributions/segregation were studied by chemically analyzing the longitudinal sectioned castings using optical emission spectroscopy (Foundry Master). The silicon content was 22 wt% Si in the segregation zone and about eutectic composition 12.6 wt% Si with only a low volume fraction of primary Si at the core region.

Figure 4.1 shows optical micrographs of Al-15Si alloy cast at 750 °C for different cooling rate in using TP-1 test (with cooling rate of 3.5 K/s at the central region of a cross-section, 38 mm from the base), or by a Boron Nitride coated steel mould cooled either in a water bath with cooling rate of 15 K/s or air cooled with cooling rate of 1 K/s. There was a significant macro-segregation of primary Si to the top of TP-1 test sample

and to the top of air cooled steel mould while in the water cooled steel mould there was a homogenous distribution of primary Si in the whole section. It is clear that at low cooling rate the morphology of primary Si in the segregation zone was a mixture of branched plate-like and coarse polygonal particles dispersed in an acicular eutectic structure. With the increase of cooling rate, the primary Si became mostly polygonal or compact in morphology and dispersed in a refined lamella eutectic structure.

From the above results, we can conclude that there is a tendency for primary Si to segregate to the top of sampling specimens particularly under slow solidifications conditions. High cooling rates produce refined lamellar eutectic structures with fine and compact particles of primary Si. Using the water cooled steel mould with cooling rate in excess of 15 K/s is very efficient at minimising the macro-segregation of primary Si even at high pouring temperature where the solidification time will be longer. All subsequent experiments were carried out using the water cooled steel mould to ensure repeatability.

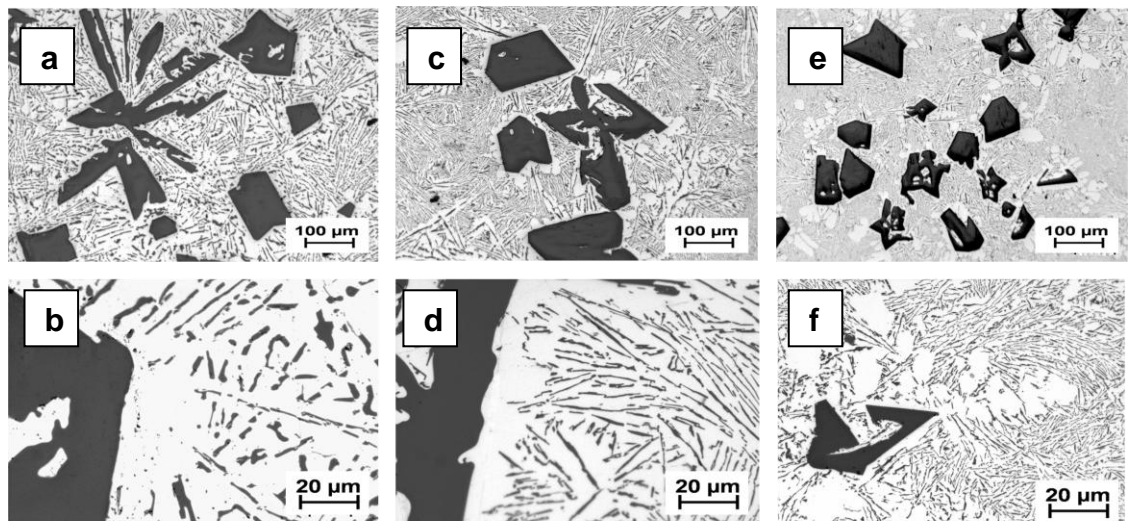


**Figure 4.1** Optical micrographs of Al-15Si alloy to show the morphology of primary Si and the eutectic structure cast at 750 °C for different cooling rates: (a,b) air cooled steel mould (1K/s); (c,d) TP-1 test ( about 3.5 K/s); and (e,f) water cooled steel mould (15 K/s). (a, c, e) low magnification and (b, d, f) high magnification.

#### 4.1.2 Effect of melt superheat

Figures 4.2 and 4.3 show low and high magnification optical micrographs of the longitudinal section of Al-15Si specimens cooled from different melt temperatures. These samples were taken by using the preheated steel mould which was then water cooled at approximately 15 K/s. It is clear from the optical micrographs that the

morphology of primary and eutectic Si changed with increasing melt temperature i.e. the superheat. Figure 4.2 shows that the primary Si become more refined and compact, Figure 4.3 shows that higher superheat produces a finer lamellar eutectic structure.

Figure 4.4 shows the particle size distributions of primary Si in Al-15Si alloy cast from melt temperature and Figure 4.5 presents the effect of superheat temperature on average primary Si particle size, shape factor, particle number density and primary Si volume fraction. It is clear that the average particle size and volume fraction of primary Si decreased approximately linearly up to a casting temperature of 845 °C and then decreased at a lower rate as melt temperature increased further. The shape factor mirrored this trend, where it increased linearly up to 845 °C and then increased at a lower rate. The particle number density of primary Si increased slightly for casting temperatures of less than 845 °C and then significantly increased for casting temperatures above 845 °C.

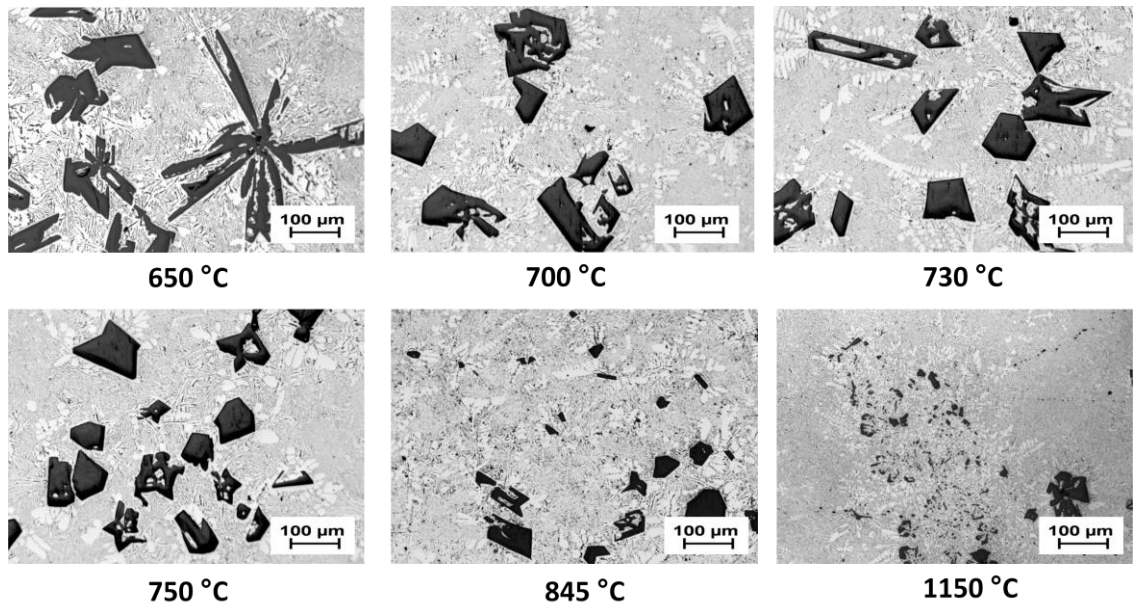


**Figure 4.2** Comparison of primary Si morphologies of Al-15Si alloy cast from different melt temperatures.

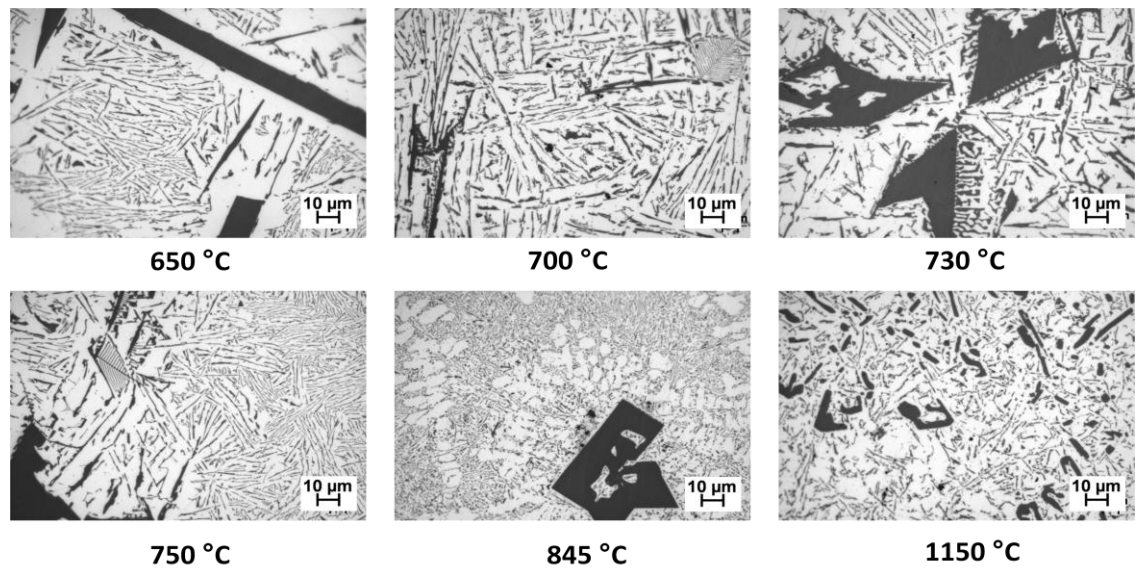


**Figure 4.3** Comparison of eutectic silicon morphologies of Al-15Si alloy cast from different melt temperatures.

According to results described above; the morphologies of primary and eutectic Si change with increasing melt temperature. The high superheat produces refined lamellar eutectic structure with polygonal particles of primary Si having a narrower particle size range as shown in Figure 4.4. The optical micrographs across the whole section of casting specimens showed that the eutectic matrix seemed to become denser with the increase in the melt superheat, along with a decrease in the volume fraction of primary Si in the Al-Si matrix as shown in Figure 4.5d. Generally, the average particle size of primary Si decreases with the increasing melt superheat temperature while the particles became more compact in shape. The particle number density of primary Si in Al-15Si increases significantly in the temperature range from 845 °C to 1150 °C. The combination of decreased particle size and increased number density of primary Si suggests that nucleation of these particles is enhanced at higher melt temperature. From these results, all other experiments in this thesis were carried out at temperature above 800 °C for complete homogenization and then to enhance the refinement and modification processes of the Si phases.

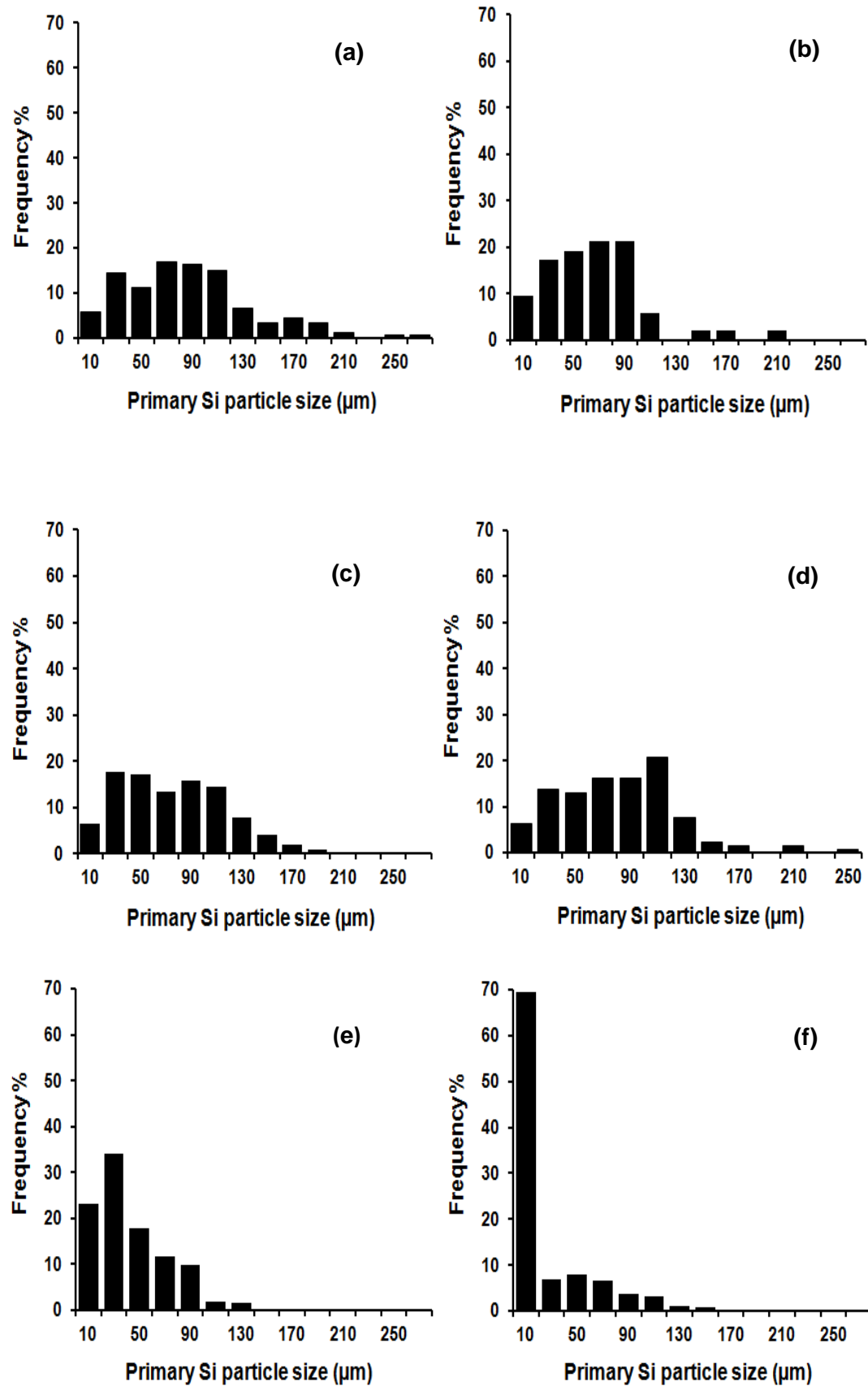


**Figure 4.4** Particle size distribution of primary Si in Al-15Si alloy cast from: (a) 650 °C; (b) 700 °C; (c) 730 °C; (d) 750 °C; (e) 845 °C; and (f) 1150 °C.

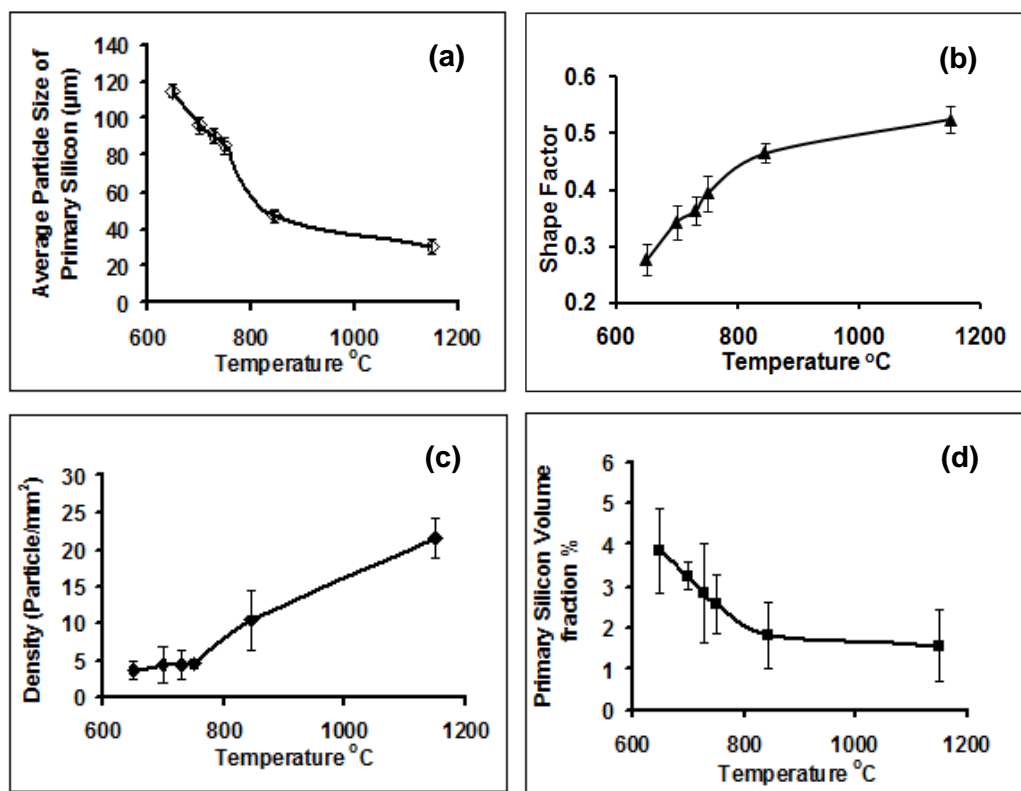


**Figure 4.5** Effect of melt temperature on: (a) primary Si particle size; (b) shape factor, (c) particle number density and (d) primary Si volume fraction of Al-15Si alloy.

## 4.2 Refinement and Modification of a High Purity Hypereutectic Al-Si Alloy

Preliminary studies for this thesis (not included) showed that Ca content affects primary Si particle size for commercial purity Al-Si alloys in addition to modification of the eutectic. The optical emission spectroscopy showed that Ca content was not well controlled leading to unreliable results for the same alloy. The objective of these experiments was to investigate the effect of Ca and P content on solidification of high purity hypereutectic Al-15Si alloy. Experiments were conducted for high purity Al-15Si, Al-15Si with 20 ppm P and Al-15Si with 30 ppm Ca alloys.

### 4.2.1 Unmodified/unrefined high purity Al-15Si alloy

Figure 4.6 shows optical micrographs of unmodified/unrefined high purity and commercial purity Al-15Si alloy. The microstructure of the high purity alloy consisted of irregular coarse primary Si particles, 68 μm in size, and dispersed in a lamellar eutectic structure (Figure 4.6 (a,b)). Figure 4.6 (c,d) shows typical micrographs of commercial purity Al-15Si alloy which consisted of coarse polygonal primary Si with average particle size of approximately 48 μm in a eutectic that had a mostly fibrous morphology.

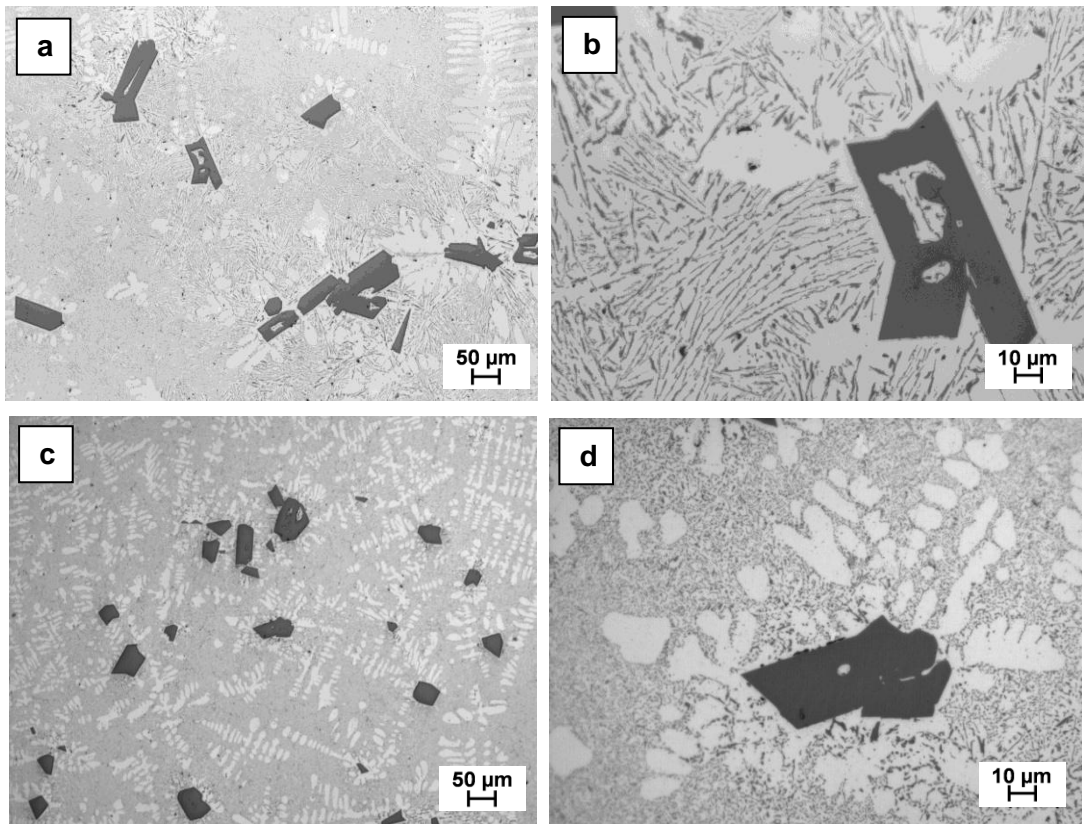


**Figure 4.6** Optical micrographs of Al-15Si alloys solidified from 800°C: (a,b) high purity alloy; (c,d) commercial purity alloy. (a,c) low magnification and (b,d) high magnification.

The chemical composition of the commercial purity Al-15Si alloy analysed by optical emission spectroscopy showed that the Ca content was more than 200 ppm and the P content was less than 20 ppm. Hence, the fibrous structure of eutectic Si in solidified commercial purity Al-15Si alloy is due to the presence of Ca in an amount sufficient to modify the eutectic matrix and restrict the growth of primary Si. It is well established that calcium and phosphorus are among the various trace elements reported to exist in commercial purity Al-Si alloys. The origin of Ca impurity in Al-Si alloys is mainly from the commercial purity Si [163]. The source of phosphorus in Al-Si alloy is its raw materials which include the phosphorus content of painted and inked aluminium scrap and the phosphorus content of metallic silicon [164]. The mechanism for nucleation of primary Si and growth of eutectic Si of unrefined/unmodified high purity Al-15Si alloy will be discussed in the next chapter.

#### 4.2.2 High purity Al-15Si alloy refined with P

The effect of adding P on the morphology of silicon on solidification of high purity alloy was studied. Figure 4.7 shows optical micrographs of P-refined high purity and commercial purity Al-15Si alloys. It is clear from the optical micrographs that adding 20 ppm P was quite enough to refine primary Si and to reduce the average particle size

from 68  $\mu\text{m}$  to 20  $\mu\text{m}$  as shown in Figure 4.7 (a,b). Similarly, adding 20ppm P to commercial purity Al-15Si alloy refined the primary Si and reduced the average particle size from 48  $\mu\text{m}$  to 25  $\mu\text{m}$  as shown in Figure 4.7 (c,d). The eutectic Si structure of the solidified high purity and commercial purity Al-15Si+20ppm P alloys was lamellar in structure.

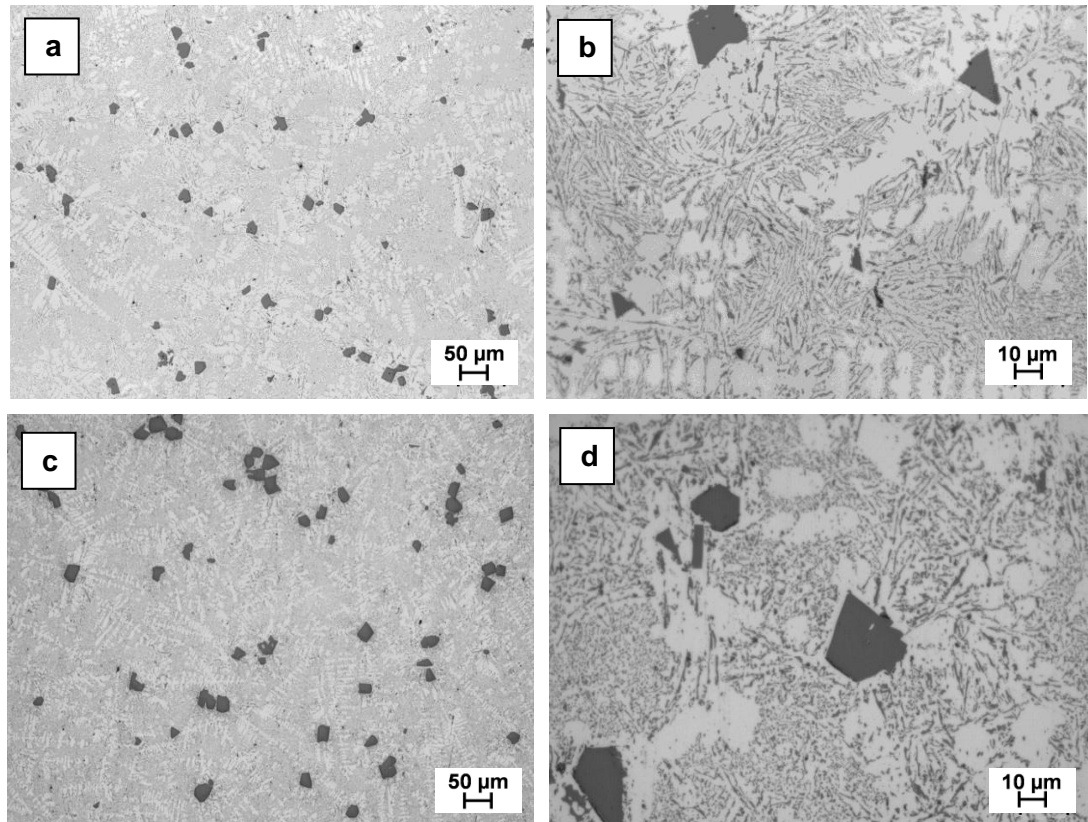


**Figure 4.7** Optical micrographs of Al-15Si+20ppm P alloy solidified from 800  $^{\circ}\text{C}$ : (a,b) high purity alloy; (c,d) commercial purity alloy. (a,c) low magnification and (b,d) high magnification.

#### 4.2.3 High purity Al-15Si alloy modified with Ca

Figure 4.8 shows optical micrographs of high purity Al-15Si alloy modified with Ca. This figure shows that adding 30 ppm of Ca to the high purity Al-15Si has a significant modification effect on the eutectic Si. It is clear that the modified high purity Al-15Si alloy appears to contain no primary Si particles, i.e. there was a shift in the apparent eutectic position with the addition of Ca. The eutectic matrix in commercial purity Al-15Si alloy which contained more than 200ppm Ca, is already modified as shown in Figure 4.6 d.

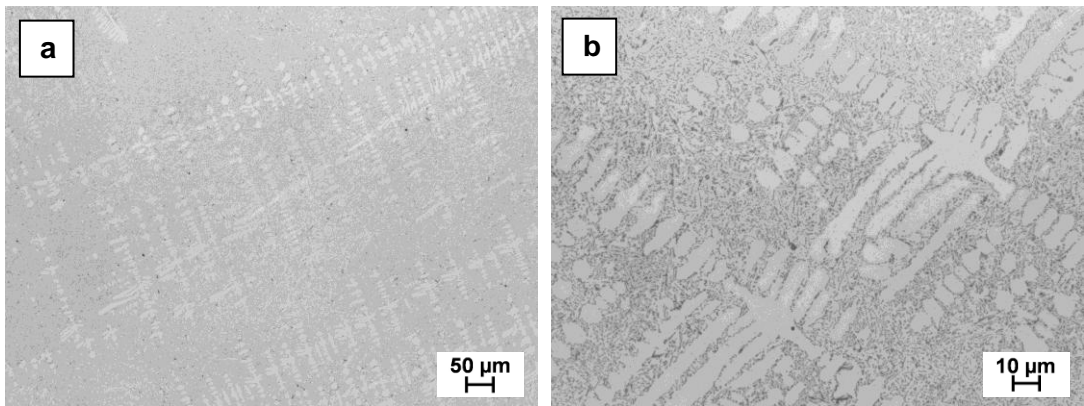


**Figure 4.8** Optical micrographs of high purity Al-15Si+30ppm Ca alloy solidified from 800 °C. (a) low magnification and (b) high magnification.

The typical unmodified Al-Si eutectic is closer to a lamellar structure than to a fibrous one. Trace amounts of Ca can effectively modify the eutectic Si shape, similar to that with sodium or strontium under the same melting and casting conditions. In conclusion, due to the low level of P content in high purity Al-15Si (less than 1 ppm), the modification with 30 ppm Ca was very efficient. The optimum amount of Ca used to modify eutectic Si in commercial purity Al-Si alloy is normally more than 50 ppm [6].

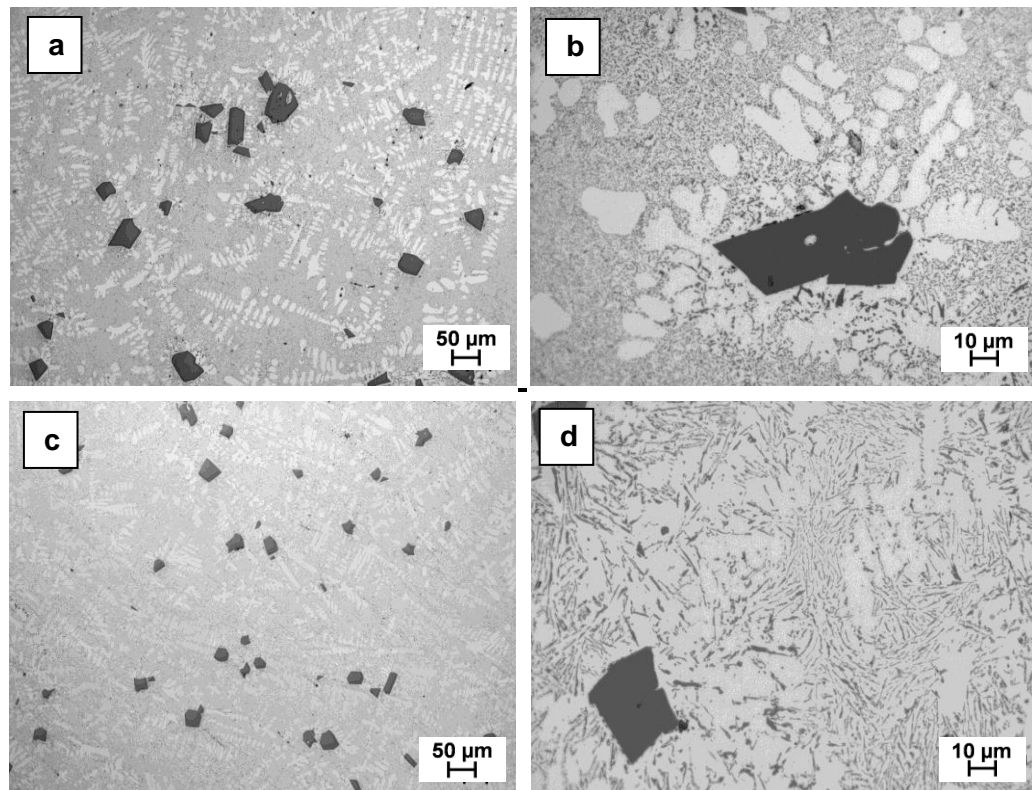
### 4.3 Effect of Ca Level on Primary and Eutectic Si

The effect of Ca level on the morphologies of primary and eutectic Si during solidification of commercial purity hypereutectic Al-Si alloys was investigated. The effect of Ca was studied either by reducing its content by the use of  $K_2SiF_6$  (AP1) flux or increasing its content by adding 0.5 wt% Ca into the melt. Also, the effect of Ca content was studied in the presence of other alloying elements such as Mg and Sb.

#### 4.3.1 Removal of Ca by $K_2SiF_6$ flux

Optical emission spectroscopy analysis of the solidified commercial purity Al-15Si alloy showed that use of the  $K_2SiF_6$  flux reduced the Ca impurity content from approximately 200 ppm to less than 20 ppm. Figure 4.9 shows typical microstructures of Al-15Si alloy without and with the addition of  $K_2SiF_6$  flux cast from 800 °C. As shown in Figure 4.9 (a,b) the untreated Al-15Si alloy contained coarse primary Si with an average particle size of approximately 48 µm and the eutectic Si had a mostly fibrous morphology. It is generally known that a small addition of Ca is effective in the modification of eutectic Si [77]. Hence, the amount of Ca ( $\approx 200$  ppm) in the untreated Al-15Si alloy was sufficient to modify the eutectic Si. Figure 4.9c shows that the use of  $K_2SiF_6$  flux, and the consequential reduction of Ca impurity content, led to refinement of the primary Si

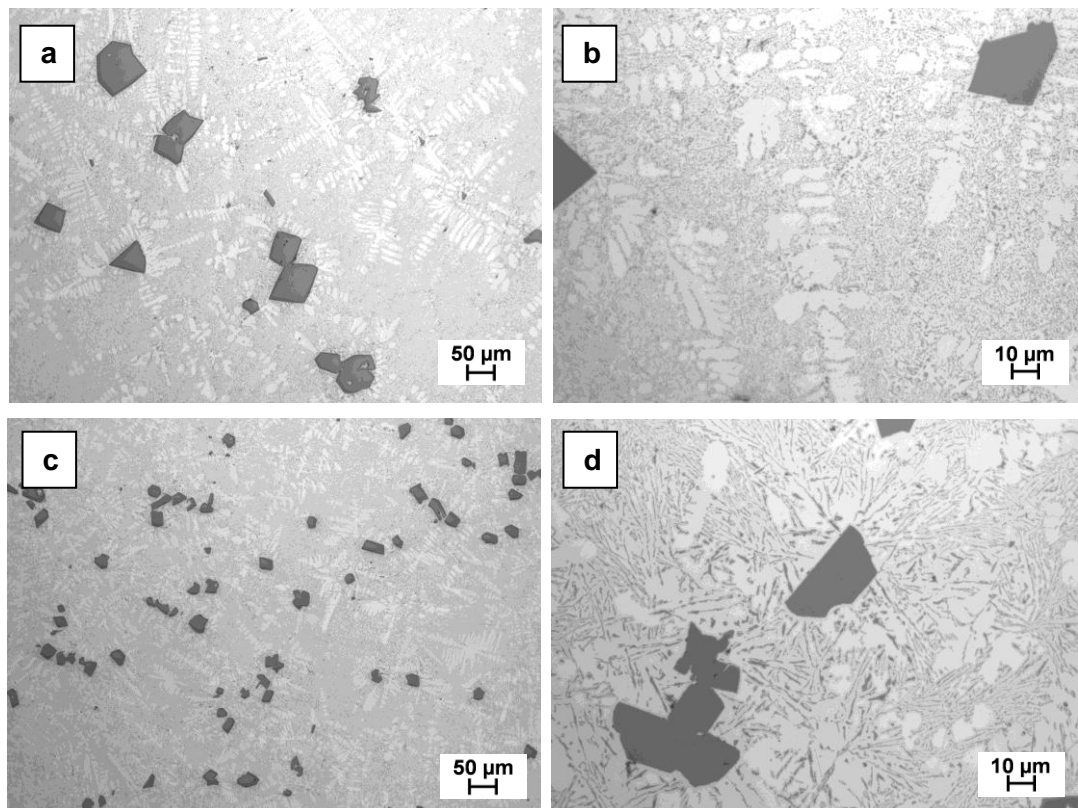
particles which had an average size of 20  $\mu\text{m}$ . The morphology of Si in the eutectic matrix changed from the fibrous structure of the untreated alloy to a short plate-like structure as shown in Figure 4.9d.



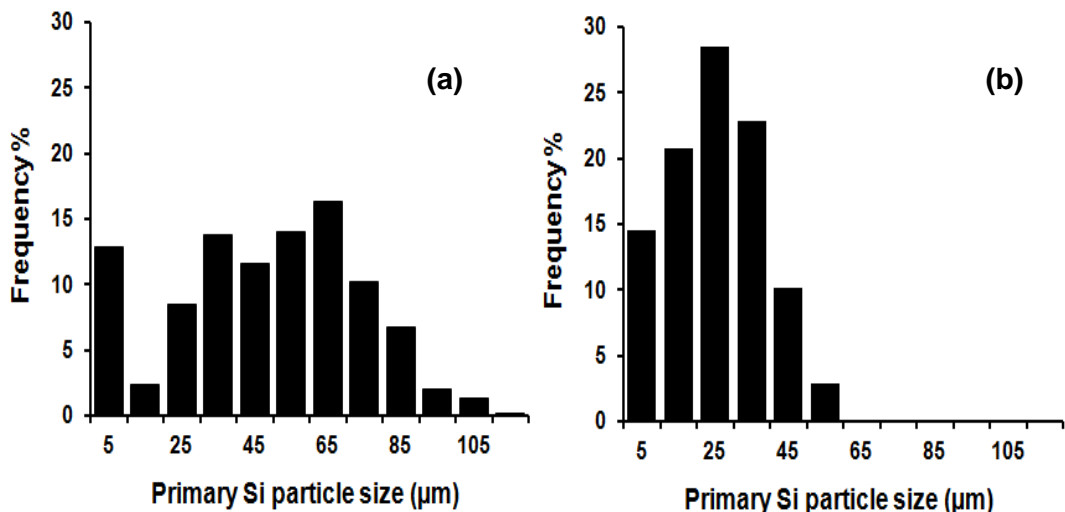
**Figure 4.9** Optical micrographs of Al-15Si alloy solidified from 800 °C: (a,b) without  $\text{K}_2\text{SiF}_6$  flux; (c,d) with 0.5 wt.%  $\text{K}_2\text{SiF}_6$  flux. (a,c) low magnification; (b,d) high magnification.

Figure 4.10 shows typical microstructures of Al-18Si alloy without and with the addition of  $\text{K}_2\text{SiF}_6$  flux cast from 800 °C. This figure shows that the use of  $\text{K}_2\text{SiF}_6$  flux and with the associated reduction of Ca impurity content to less than 20 ppm, the average particle size of primary Si reduced from 52  $\mu\text{m}$  to 23  $\mu\text{m}$  as shown in Figure 4.10c compared with Figure 4.10a. The morphology of Si in the eutectic matrix changed from the fibrous structure of the untreated alloy to a short plate-like structure as shown in Figure 4.10d compared with Figure 4.10b.

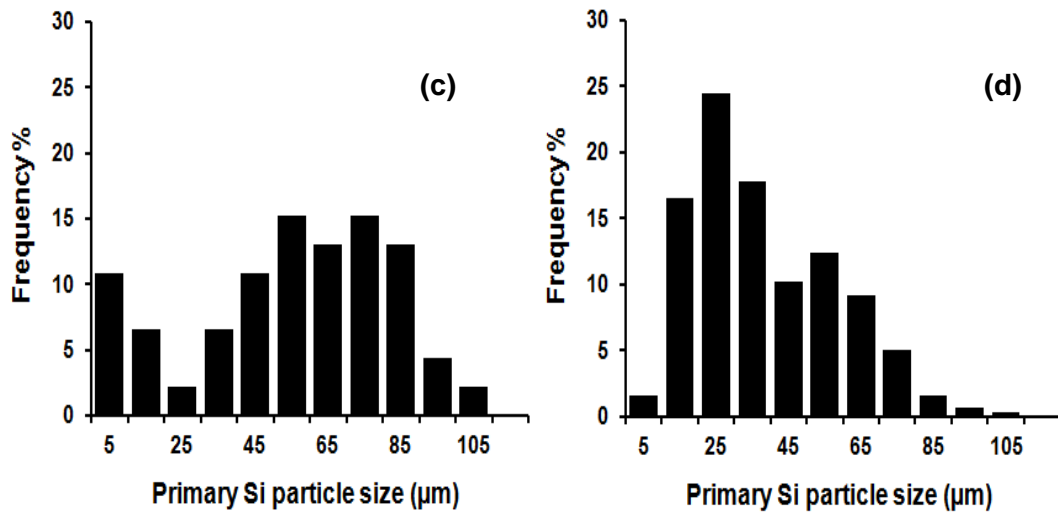
Figure 4.11 shows the particle size distribution of Al-15Si and Al-18Si alloys without and with the addition of  $\text{K}_2\text{SiF}_6$  flux (AP1). It is clear from this figure that refinement of Al-15Si alloy is more efficient than that for Al-18Si alloy. The particle size range for Al-15Si became narrow with a high percentage of particles with size less than 20  $\mu\text{m}$ . While for the Al-18Si alloy the range of particle sizes was the same as in the untreated alloy and the higher percentage of particles size was around 25  $\mu\text{m}$ .



**Figure 4.10** Optical micrographs of Al-18Si alloy solidified from 800 °C: (a,b) without  $K_2SiF_6$  flux; (c,d) with 0.5 wt.%  $K_2SiF_6$  flux. (a,c) low magnification; (b,d) high magnification.



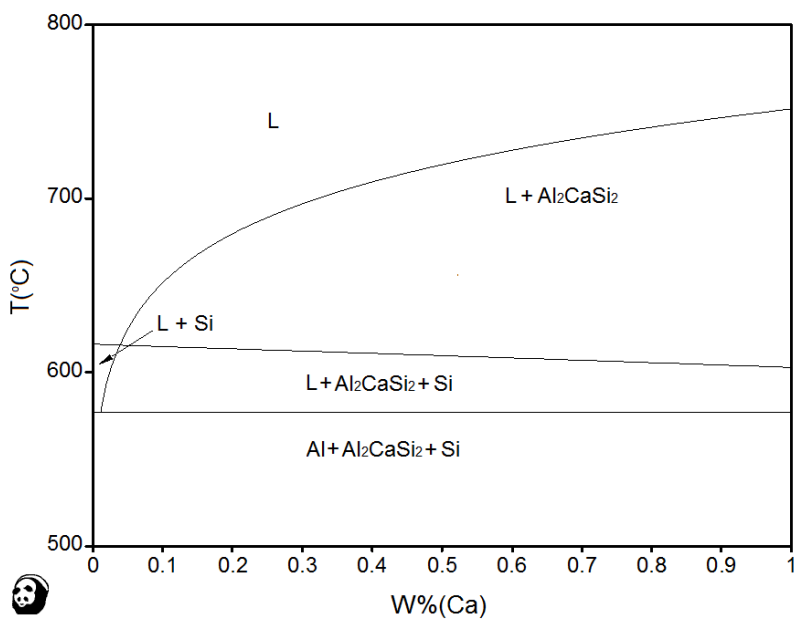
**Figure 4.11** Particle size distribution of primary Si in: (a) Al-15Si Alloy; (b) Al-15Si with 0.5 wt%  $K_2SiF_6$  flux; (c) Al-18Si alloy and (d) Al-18Si with 0.5 wt%  $K_2SiF_6$  flux.



**Figure 4.11** continued.

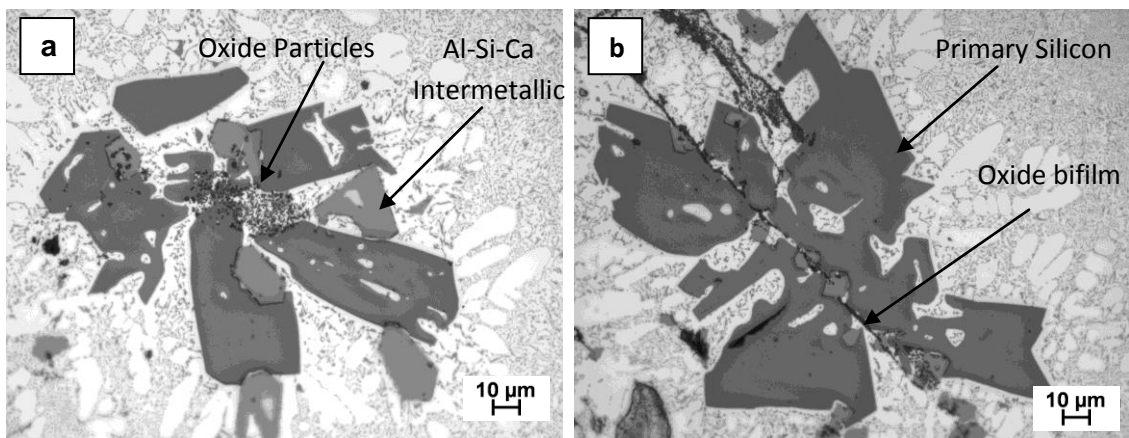
### 4.3.2 High Ca content

Figure 4.12 is a vertical section of the Al-Si-Ca phase diagram for Al-15Si-xCa calculated using the commercial PandaT software with PanAl8 database. It shows that when the Ca content is greater than approximately 400 ppm the first phase to form on solidification is expected to be  $\text{Al}_2\text{CaSi}_2$ .



**Figure 4.12** Vertical section of the Al-Si-Ca phase diagram for Al-15Si-xCa (x=0-1wt%).

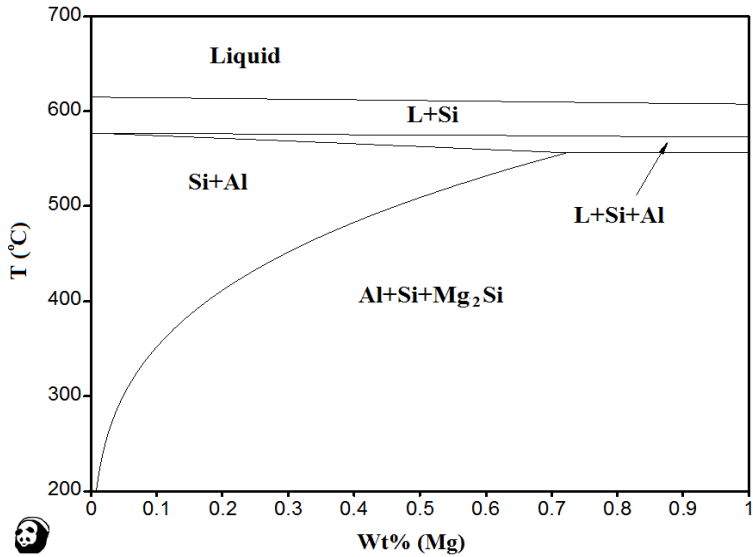
Figure 4.13 comprises optical micrographs showing the typical morphologies of phases in the solidified Al-15Si alloy with 0.5 wt% Ca added. In this case the primary Si (dark phase) was coarse of more than 50  $\mu\text{m}$  in size and had a much more irregular morphology compared with that in the alloy without added Ca or the  $\text{K}_2\text{SiF}_6$  fluxed alloy as shown in Figure 4.13 (a,b). The eutectic Si was fully modified. In addition to  $\alpha$ -Al and Si there was a third phase present in the form of dispersoids (mid-grey) that were intimately associated with primary Si. This third phase was expected to be an intermetallic containing Ca, and Figure 4.12 suggests that these dispersoids are likely to be  $\text{Al}_2\text{CaSi}_2$ . Both the primary Si and the dispersoids were associated with oxide particles (Figure 4.13a) and oxide bifilms (Figure 4.13b).



**Figure 4.13** Optical micrographs of the typical morphology of primary Si and an Al-Si-Ca phase, in the Al-15Si-0.5Ca alloy, formed in association with each other and with oxide particles (a) and bifilms (b).

#### 4.3.3 Effect of Ca in the presence of Mg or Sb

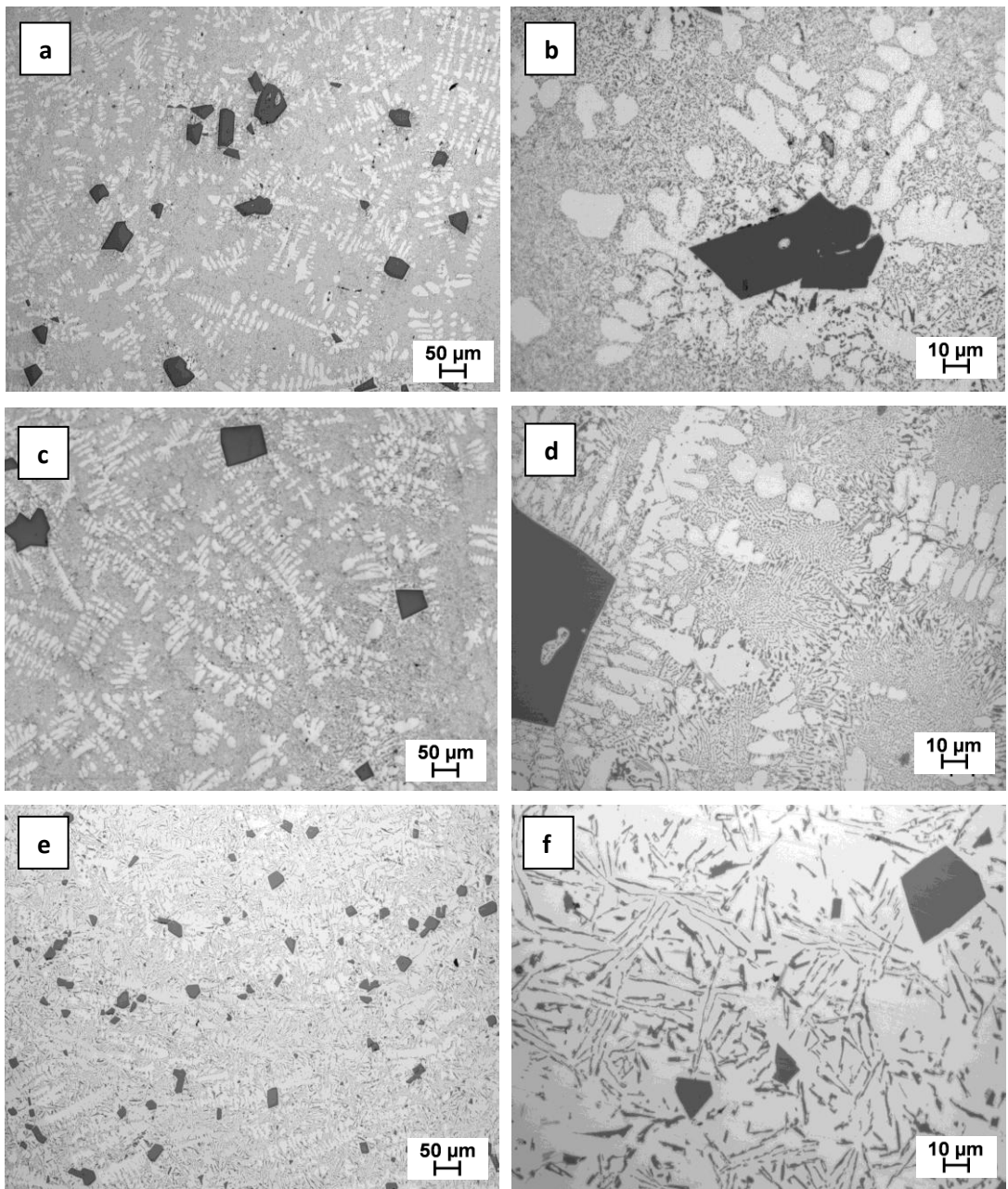
Due to the interaction between Ca and the trace elements in commercial purity Al-Si alloys as described in section 2.5, experiments were conducted to study the effect of Ca content on the morphology of primary and eutectic Si in the presence of Mg or Sb in the Al-15Si alloy. These elements were chosen because Mg has a significant effect on the morphology of primary Si (as will be explained in detail in section 4.4.1) and Sb can modify the eutectic of Si in Al-Si alloys (section 2.2). Figure 4.14 is a vertical section of the Al-Si-Mg phase diagram for Al-15Si-xMg calculated using the commercial PandaT software with PanAl8 database. It shows that when the Mg content is 0.5wt% the eutectic structure contains the  $\text{Mg}_2\text{Si}$  phase.



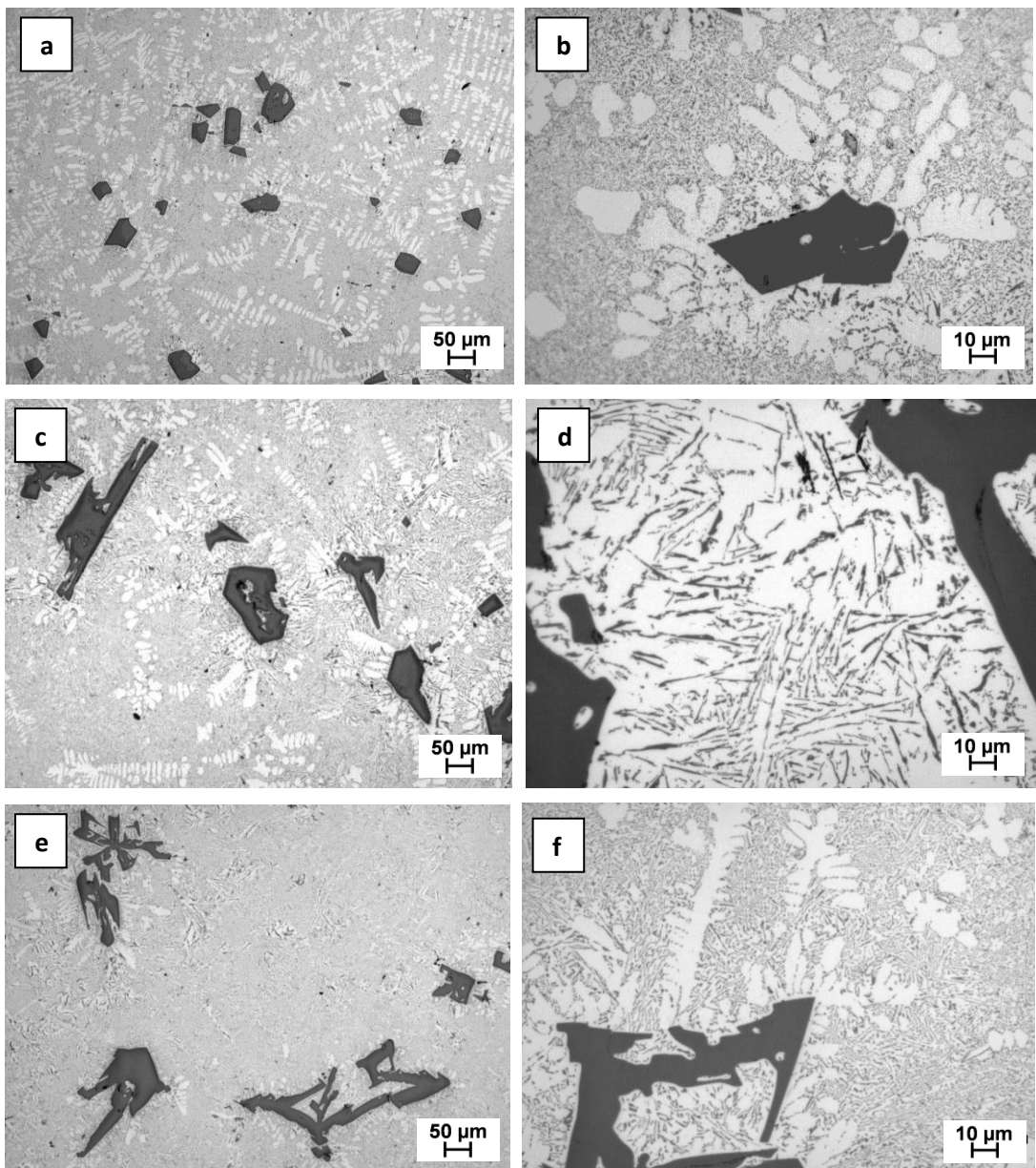
**Figure 4.14** Vertical section of the Al-Si-Mg phase diagram for Al-15Si-xMg ( $x=0\text{-}1\text{wt\%}$ ).

Figure 4.15 comprises optical micrographs showing the effect of Ca content on the morphology of Al-15Si alloys without and with Mg addition. Figure 4.15 (c,d) show that commercial purity Al-15Si+0.5wt%Mg alloy, which contained more than 200 ppm Ca, consisted of coarse primary Si particles of 45  $\mu\text{m}$  in size dispersed in Al+Si+Mg<sub>2</sub>Si eutectic as suggested in Figure 4.14. When the Al-15Si base alloy was fluxed with AP1 prior to the Mg addition, there was a significant refinement in primary Si particles of 30  $\mu\text{m}$  in size dispersed in a coarse plate-like eutectic structure as shown in Figure 4.15 (e,f).

Figure 4.16 comprises optical micrographs showing the effect of Ca content on the morphology of Al-15Si alloy without and with Sb addition. For the interaction between Sb and Ca, Figure 4.16 (c,d) compared with Figure 4.16 (a,b) show that adding 0.5 wt% Sb to the commercial purity Al-15Si alloy, which contained more than 200 ppm Ca, the eutectic Si refined in lamellar structure and the primary Si particles became more irregular in shape with particle size of 65  $\mu\text{m}$ . With reducing Ca content by fluxing prior to adding 0.5wt% Sb to the Al-15Si alloy, irregular particles of primary Si of 70  $\mu\text{m}$  in size dispersed in finer lamellar structure produced as shown in Figure 4.16 (e,f). Hence, removing Ca before adding Sb to Al-Si alloys can improve the modification process.



**Figure 4.15** Optical micrographs of: (a,b) Al-15Si alloy; (c,d) Al-15Si alloy with 0.5 wt% Mg; and (e,f) Al-15Si alloy fluxed with 0.5 wt % AP1 then alloyed with 0.5 wt % Mg cast from 800 °C. (a,c & e) low magnification to show the size and distribution of primary Si and (b,d & f) high magnification to show the eutectic structure.



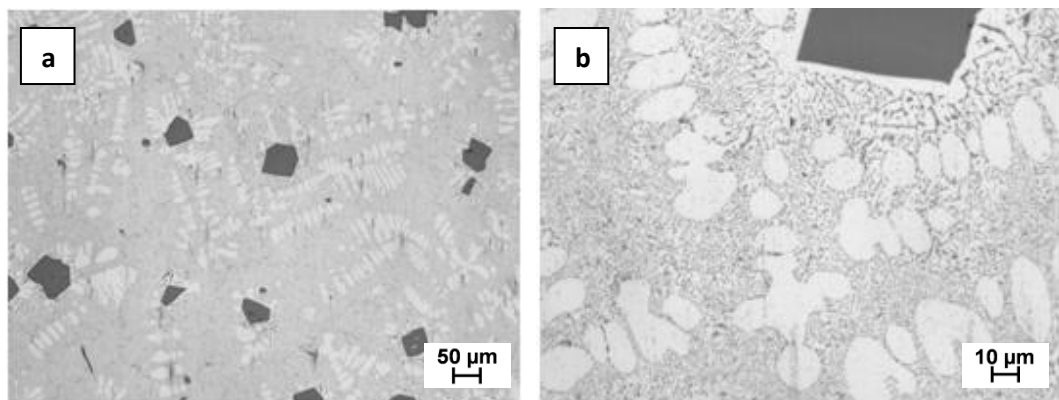
**Figure 4.16** Optical micrographs of: (a,b) Al-15Si alloy; (c,d) with 0.5 wt% Sb; and (e,f) fluxed with 0.5 wt% AP1 then alloyed with 0.5 wt% Sb cast from 800 °C. (a,c & e) low magnification to show the size and distribution of primary Si and (b,d & f) high magnification to show the eutectic structure.

#### 4.4 Effect of Chemical Additions on Primary and Eutectic Si

This section describes the effect on refining primary Si in Al-Si alloy of the addition a variety of inoculants. The various inoculants studied were Mg, oxides ( $\text{Al}_2\text{O}_3$ ,  $\text{MgO}$  and  $\text{CaO}$ ),  $\text{ZnS}$ ,  $\text{Na}_2\text{S}$  and Zn. The effect of adding the above inoculants on the Si morphology will be explained in this section. The effect of  $\text{Al}_2\text{O}_3$  on the morphology of silicon will be discussed in detail in section 4.5.

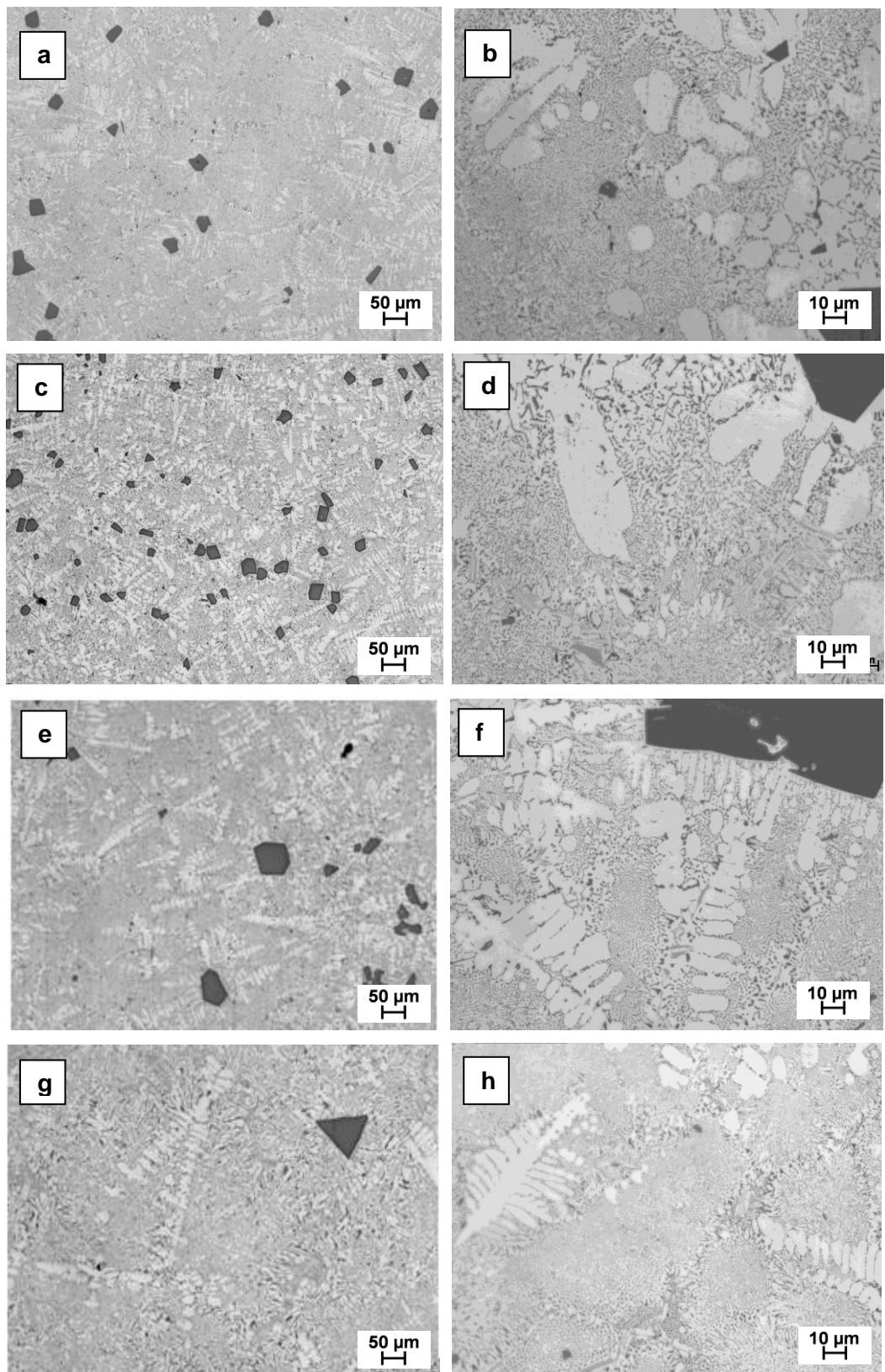
#### 4.4.1 Magnesium (Mg)

Figure 4.17 shows the microstructure obtained during the solidification of a commercial purity Al-15Si alloy cast from 800 °C. The base Al-15Si alloy contains large polygonal primary Si particles 48 µm in size dispersed in a fibrous binary Al-Si eutectic matrix. The modification of the eutectic structure is because of a high Ca content in the commercial purity Al-Si alloy. The Ca level in the Al-15Si was more than 200 ppm.



**Figure 4.17** Optical micrographs of the Al-15Si alloy cast from 800 °C. (a) low magnification and (b) high magnification.

Figure 4.18 shows the microstructures of Al-15Si with Mg addition up to 1.0 wt% in the as-cast condition. With the addition of Mg up to 0.3 wt% to the binary alloy, the size of the primary Si decreased significantly as shown in a comparison of Figure 4.17 (a,b) with Figure 4.18(a,b) and Figure 4.18(c,d). On adding 0.4 wt% Mg, the size of the primary Si increased again, and continued to increase with Mg addition up to 0.75 wt%. The average primary Si particle size changed from 48 µm to 26, 22, 35, 45 and 54.5 µm with the addition of 0.1, 0.3, 0.4, 0.5 and 0.75 wt% Mg respectively as shown in Figure 4.19, which is a plot of primary Si particle size against Mg addition. Figure 4.20 shows the particle size distribution of Al-15Si alloys with 0.1, 0.3, 0.4, 0.5, 0.75 wt% Mg additions. It is clear from Figure 4.20 that there was a significant reduction in particle size range up to 0.3 wt% Mg addition, then the size range increased again with a higher percentage of larger sized primary Si particles. The optical micrographs show that the increase in the size of primary Si particles was associated with a reduced number of primary Si particles. There were no primary Si particles evident in the alloy containing 1.0 wt% Mg. The morphology and size of the eutectic Si particles changed with the addition of Mg to a fine and compact form with a Chinese script like morphology (as shown in Figure 4.18l). A refinement of both primary and eutectic Si particles was only observed for the alloy with Mg content ≤ 0.3% Mg if compared with the binary Al-15Si base alloy. This indicates that Mg can enhance refinement and modification of silicon at this level of Mg concentration.



**Figure 4.18** Optical micrographs of Al-15Si alloy with the addition of (a,b) 0.1 wt% Mg, (c,d) 0.3 wt% Mg, (e,f) 0.4 wt% Mg, (g,h) 0.5 wt% Mg, (i,j) 0.75 wt% Mg and (k,l) 1% wt Mg. (a,c,e,g,I & k) low magnification to show the size and distribution of primary Si; (b,d,f,h,j & I) high magnification to show the eutectic structure. Continued overleaf.

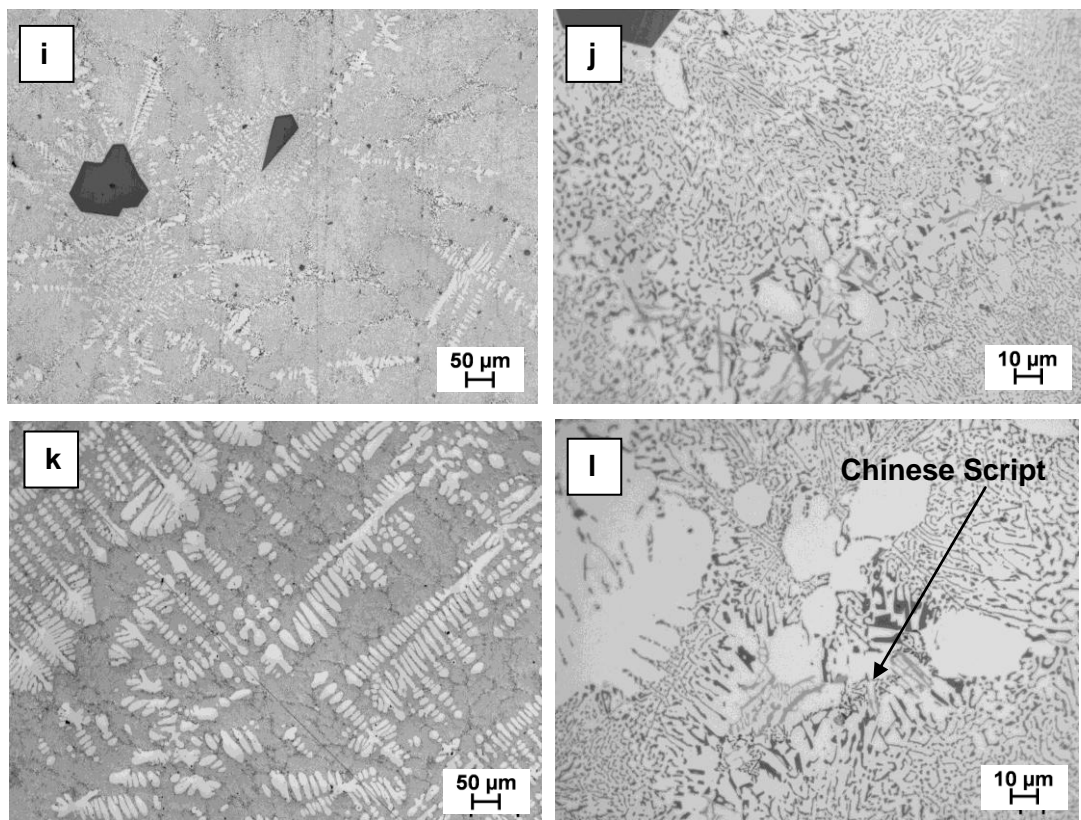


**Figure 4.18** Continued.

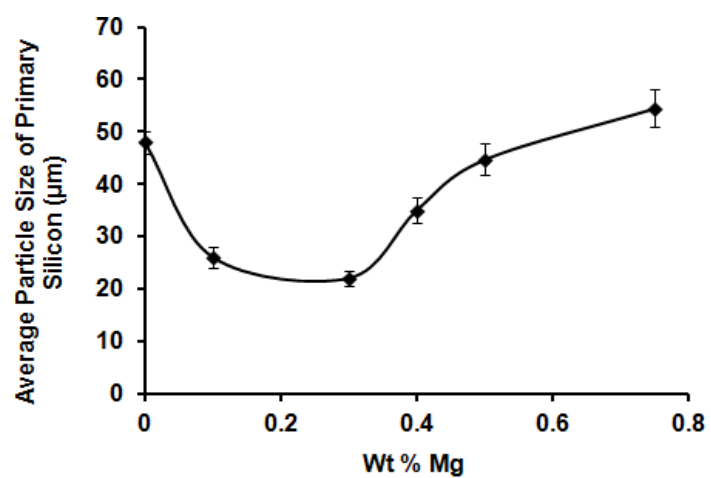


**Figure 4.19** Plot of primary Si particle size as a function of Mg addition (wt%) to commercial purity Al-15Si alloy.

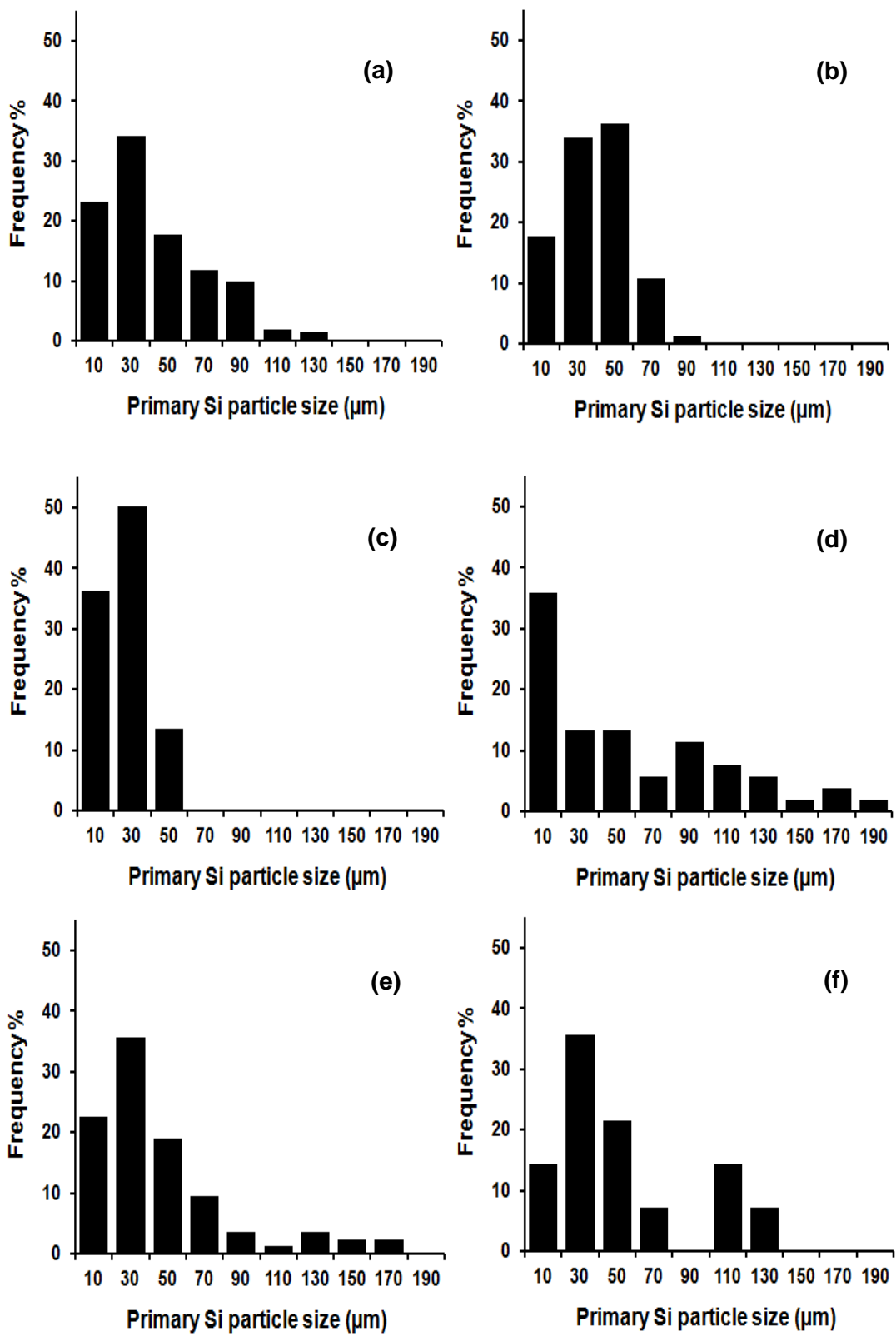


**Figure 4.20** Particle size distribution of primary Si in Al-15Si alloys with: (a) 0.0; (b) 0.1; (c) 0.3; (d) 0.4; (e) 0.5 and (f) 0.75 wt% Mg additions.

#### 4.4.2 Mg and Ca oxides

In order to study the effect of oxides, experiments were carried out by adding MgO and CaO to Al-15Si alloy (see section 3.6). Figure 4.21 shows optical micrographs of Al-15Si alloys without and with the addition of MgO and CaO. As shown in Figure 4.21 (a,b), the commercial purity Al-15Si alloy consists of large polygonal primary Si particles (48 µm in size) dispersed in a fibrous eutectic Si matrix. Adding 0.5 wt% of MgO or CaO to the alloy resulted in polygonal coarse primary Si particles dispersed in a fibrous Si eutectic structure. The average particle size of primary Si increased from 48 µm to 56 µm or 68 µm on adding 0.5 wt% of MgO or CaO respectively to commercial purity Al-15Si alloy.

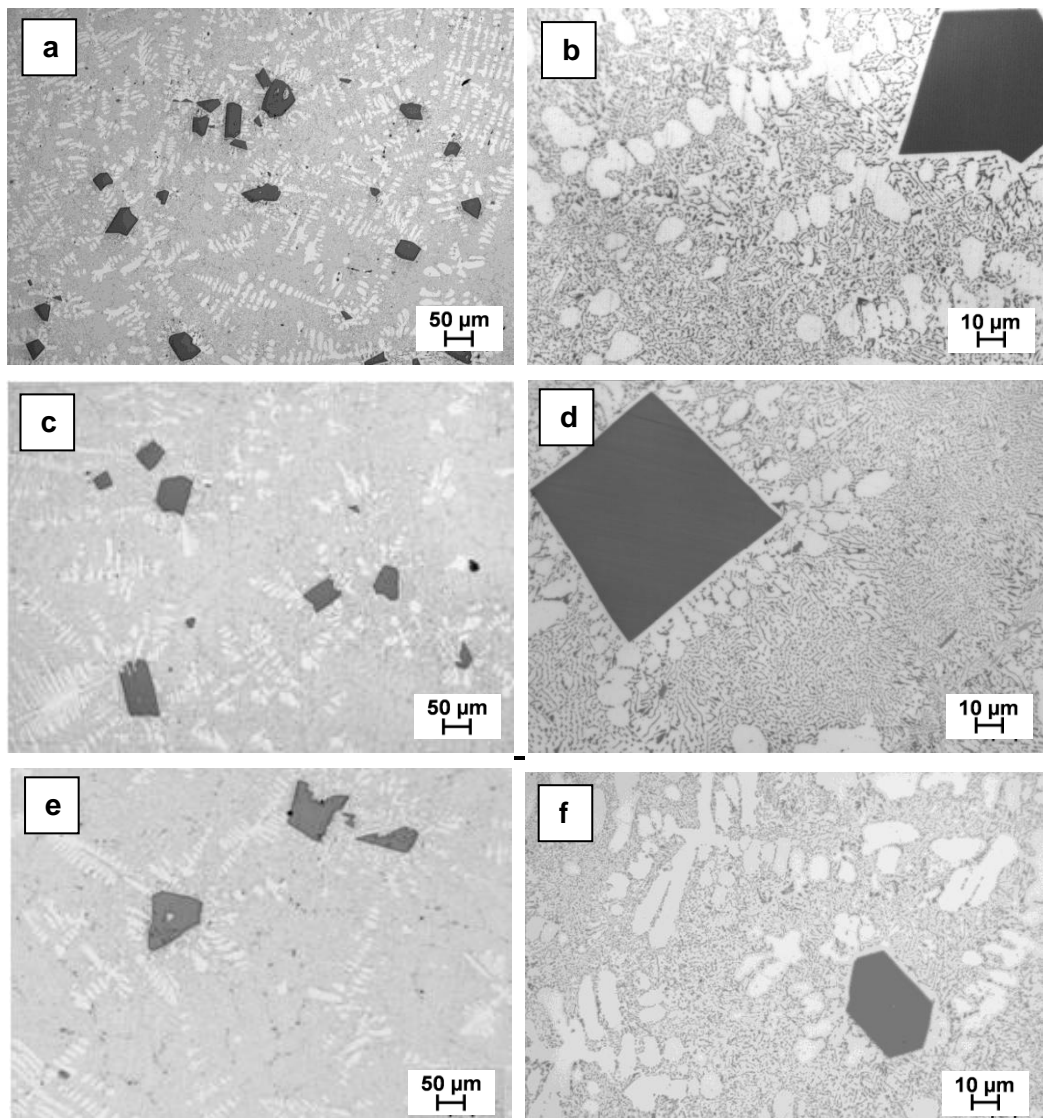


**Figure 4.21** Optical micrographs of Al-15Si alloys cast from 800 °C: (a,b) Al-15Si alloy; (c,d) Al-15Si with 0.5 wt% MgO and (e,f) Al-15Si with 0.5 wt% CaO. (a,c & e) low magnification to show the size and distribution of primary Si and (b,d & f) high magnification to show the eutectic structure.

#### 4.4.3 Zincblende ZnS

Due to the structural similarity of ZnS in its zincblende form, and its similar lattice parameter to those of Si and AlP, its use as an inoculant to refine the primary Si in solidification of hypereutectic Al-Si alloys was examined. Different sizes and sources of ZnS particles were used.

##### 4.4.3.1 ZnS micron scale particles

Experiments were carried out by adding zincblende ZnS powder ( $\leq 44 \mu\text{m}$  in size) to Al-18Si alloy at  $800^\circ\text{C}$ . Figure 4.22 shows typical microstructures of conventionally cast Al-18Si alloy. The untreated Al-18Si (Figure 4.22) contained coarse primary Si with average particle size of approximately  $52 \mu\text{m}$  and the eutectic Si had a mostly fibrous morphology. It is generally known that a small addition of Ca is effective in the modification of eutectic Si, as is sodium and strontium. Hence, the amount of Ca ( $\approx 200 \text{ ppm}$ ) existing in the commercial purity Al-18Si alloy is sufficient to modify the eutectic Si. The origin of Ca impurity in Al-Si alloys is mainly from the commercial purity silicon [163].

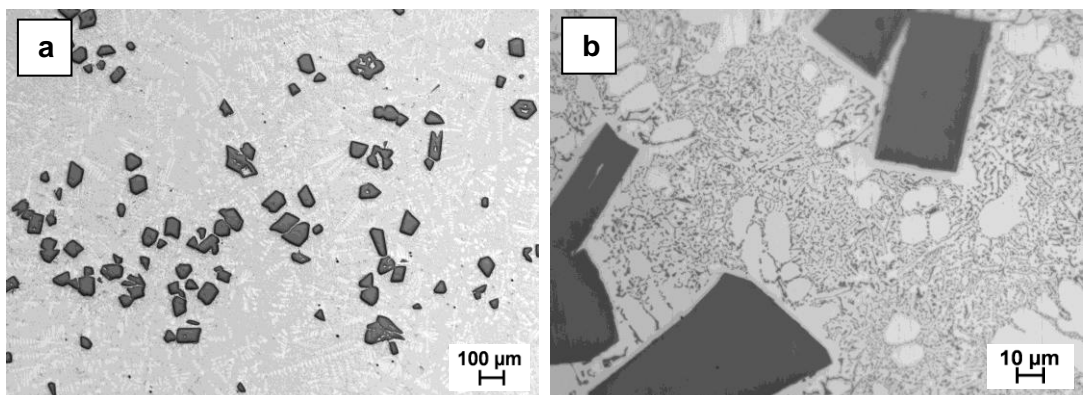


**Figure 4.22** Optical micrographs of Al-18Si alloy: (a) low magnification to show the size and distribution of primary Si and (b) high magnification to show the eutectic structure.

On adding 0.5 wt% of ZnS powder, there was a significant refinement of the primary Si particles to  $44 \mu\text{m}$  without any change in the modification level of the eutectic structure as shown in Figure 4.23 (a,b). Figure 4.23 (c,d) show optical micrographs of Al-18Si with 100 ppm P added. In this case the primary Si particle size was reduced to  $20 \mu\text{m}$  compared with its reduction to  $44 \mu\text{m}$  with the addition of the ZnS powder. Thus, whilst primary Si refinement was evident for ZnS in this form it was less efficient than refinement with P. However the addition of P led to a more plate-like, and thus a loss of modification of eutectic Si. The latter suggest that ZnS does not interact with Ca in the melt unlike AlP. These results suggest that ZnS could be a potent substrate for

nucleation of primary Si, although inefficient in this as-purchased form, whilst allowing simultaneous modification of the eutectic unlike AlP.

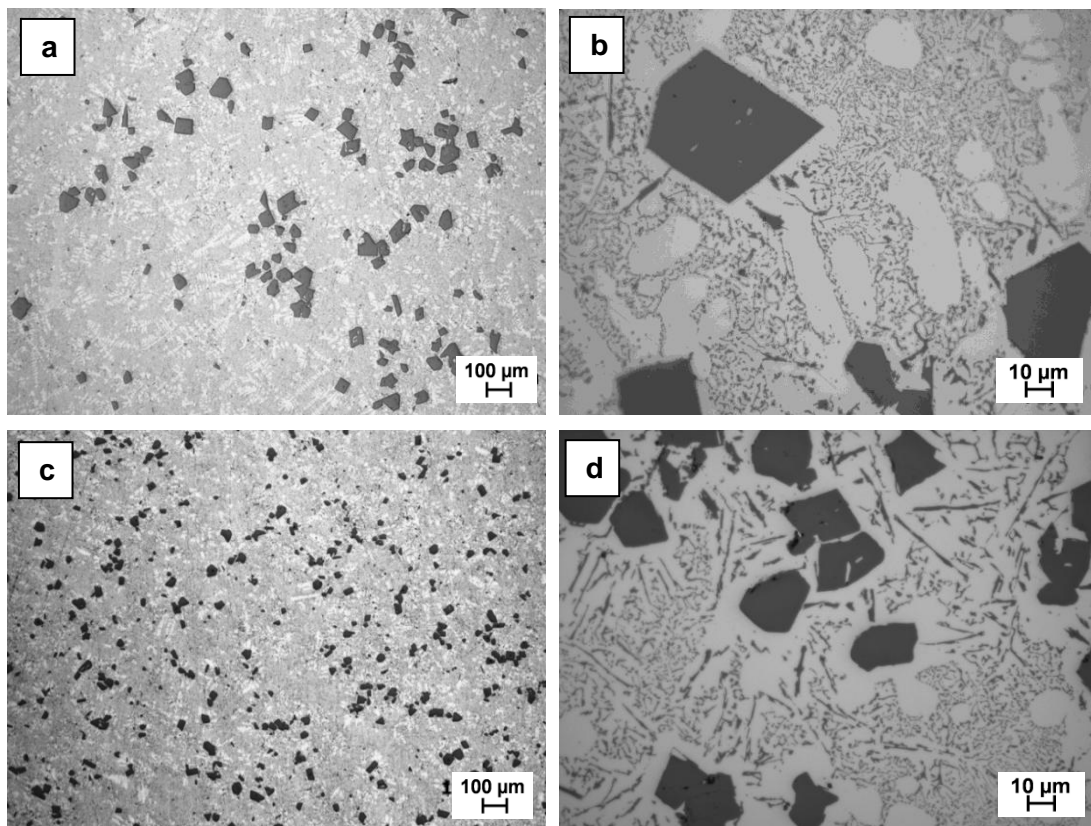


**Figure 4.23** Optical micrographs of: (a, b) Al-18Si with the addition of 0.5 wt% ZnS ( $\leq 44 \mu\text{m}$  in size), (c, d) Al-18Si alloy with the addition of 100 ppm P. (a, c) low magnification and (b, d) high magnification.

#### 4.4.3.2 ZnS nanoparticles

In response to the significant, but inefficient refinement of primary Si using ZnS  $< 44 \mu\text{m}$  particles, experiments were carried out to raise the efficiency by the use of zincblende ZnS nanoparticles. As a cost effective supplier of these nanoparticles could not be found, zincblende ZnS nanoparticles were prepared by solid-liquid chemical reaction [155] (see section 3.7.2). Figure 4.24 comprises optical micrographs showing the morphologies of Si phases in solidified Al-18Si alloy with 0.5 wt% ZnS nanoparticles added. As shown in Figure 4.24; there was some refinement in the primary Si without any change in eutectic structure if compared with commercial purity Al-18Si alloy (with Ca content more than 200 ppm). As shown in Figure 4.24 the efficiency of ZnS nanoparticles in refinement of primary Si in Al-18Si alloy was less than that of P. The average particle size of primary Si reduced from 52  $\mu\text{m}$  to 41  $\mu\text{m}$  on adding 0.5 wt% zincblende ZnS nanoparticles to the commercial purity Al-18Si alloy cast from 800 °C, whereas the average particle size of primary Si of Al-18Si+100 ppm P alloy reduced to

20  $\mu\text{m}$ . This could be due to agglomeration of the ZnS nanoparticles, low wettability of ZnS with the melt or instability of zincblende under the operating conditions. The modification of the eutectic Si was retained when using ZnS nanoparticles whereas it was lost when using P, as shown in Figure 4.24 (d,f).

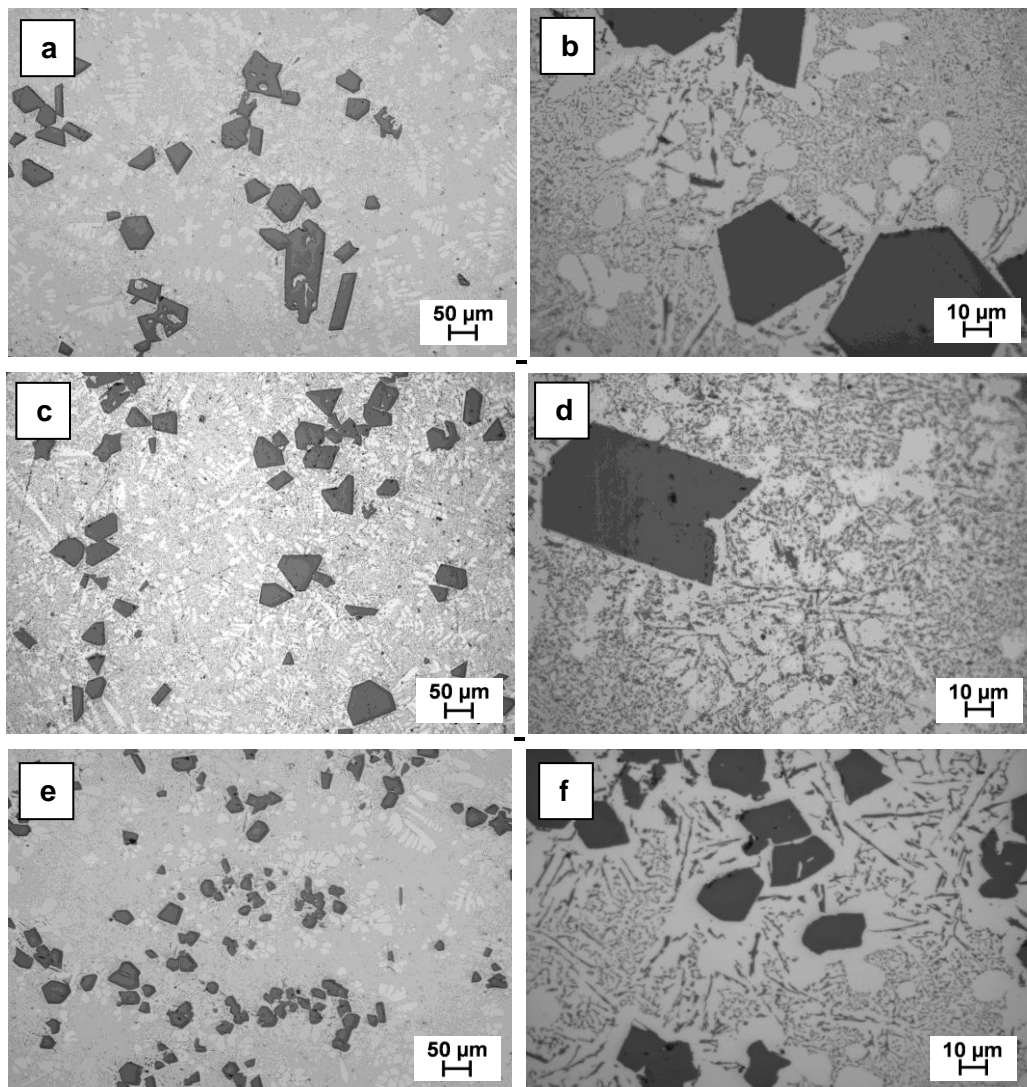


**Figure 4.24** Optical micrographs of as-cast alloys: (a,b) Al-18Si alloy; (c,d) Al-18Si with the addition of 0.5 wt% ZnS nanoparticles, (e,f) Al-18Si alloy with the addition of 100 ppm P. (a,c&e) low magnification to show the size and distribution of primary Si and (b,d&f) high magnification to show the eutectic structure.

The point of this experiment was to improve the refinement efficiency of ZnS nanoparticles instead of <44  $\mu\text{m}$  powder. Figure 4.25 shows the particle size distribution of primary Si in Al-18Si with no addition, with the addition of P and the two different forms of ZnS. It is clear from Figure 4.25 that the ZnS nanoparticles were no more efficient than the ZnS powder and adding ZnS in any form can refine the primary Si. But still the efficiency of adding ZnS is less than that with adding P.

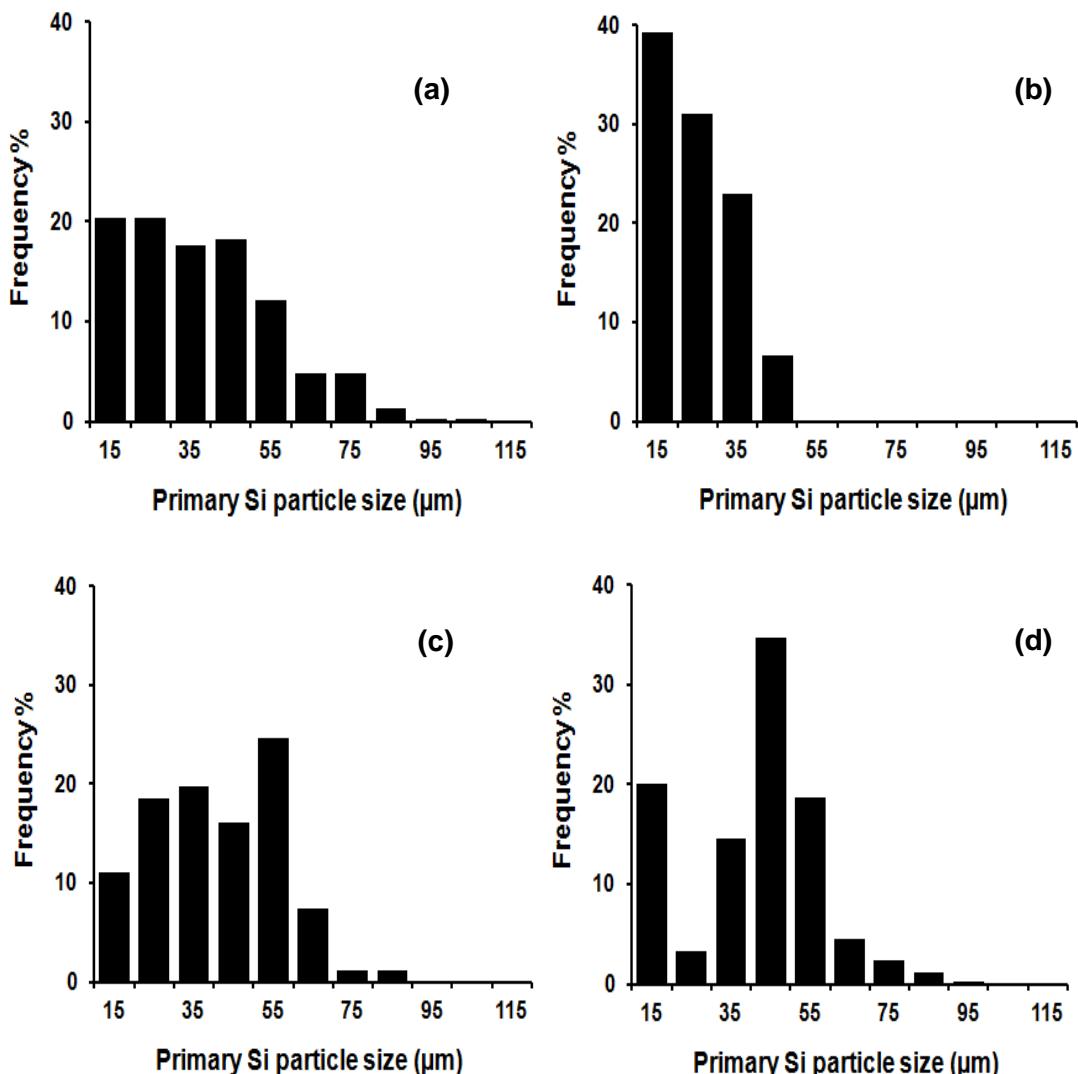


**Figure 4.25** Particle size distribution of primary Si in Al-18Si alloys: (a) with no additions; (b) with 100 ppm P; (c) with 0.5 wt% ZnS  $<44\text{ }\mu\text{m}$  and (d) with 0.5 wt% ZnS nanoparticles.

#### 4.4.3.3 *In situ* prepared ZnS

As an alternative route to increase the refinement efficiency of ZnS, experiments were designed to create ZnS *in situ* by adding Zn and excess amount of Na<sub>2</sub>S to Al-18Si melt at 800 °C (see section 3.7.3). In this case we may get fine and wettable particles of zincblende ZnS particles. Figure 4.26 comprises optical micrographs showing the morphologies of primary and eutectic Si in solidified Al-18Si alloy with ZnS formed *in situ*. As shown in Figure 4.26; there was a good refinement of the primary Si which was reduced from 52 μm to 22 μm in size. In comparison the average particle size of primary Si of Al-18Si+100 ppm P alloy reduced to 20 μm. The modification of the eutectic Si matrix by the Ca impurity in the alloy remained. Figure 4.27 shows the particle size distributions of primary Si in Al-18Si without and with ZnS prepared *in situ*

and that of Al-18Si with 100 ppm P. This figure shows the strong improvement of refinement efficiency in using *in situ* prepared ZnS zincblende and how narrow the particles size range is in comparison with the base alloy and with some similarity with the case of adding 100 ppm P to Al-18Si alloy.

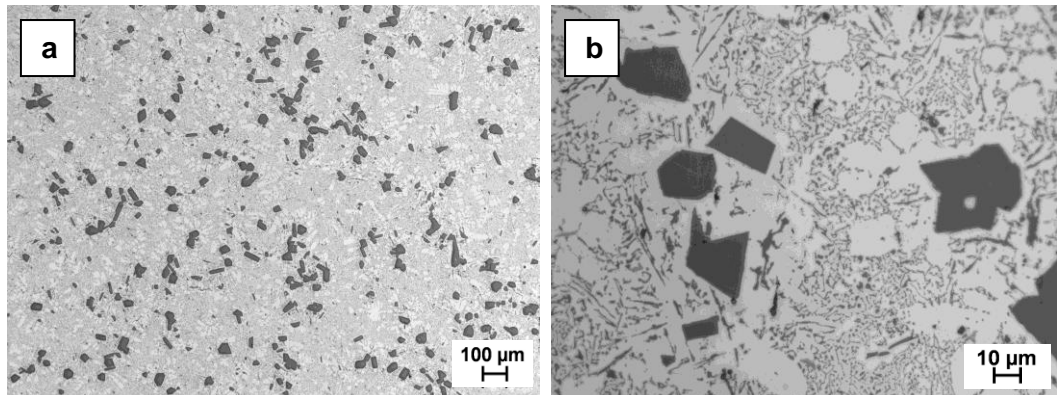


**Figure 4.26** Optical micrographs of Al-18Si with nominally 0.27 wt% ZnS formed *in situ*. (a) low magnification, and (b) high magnification.

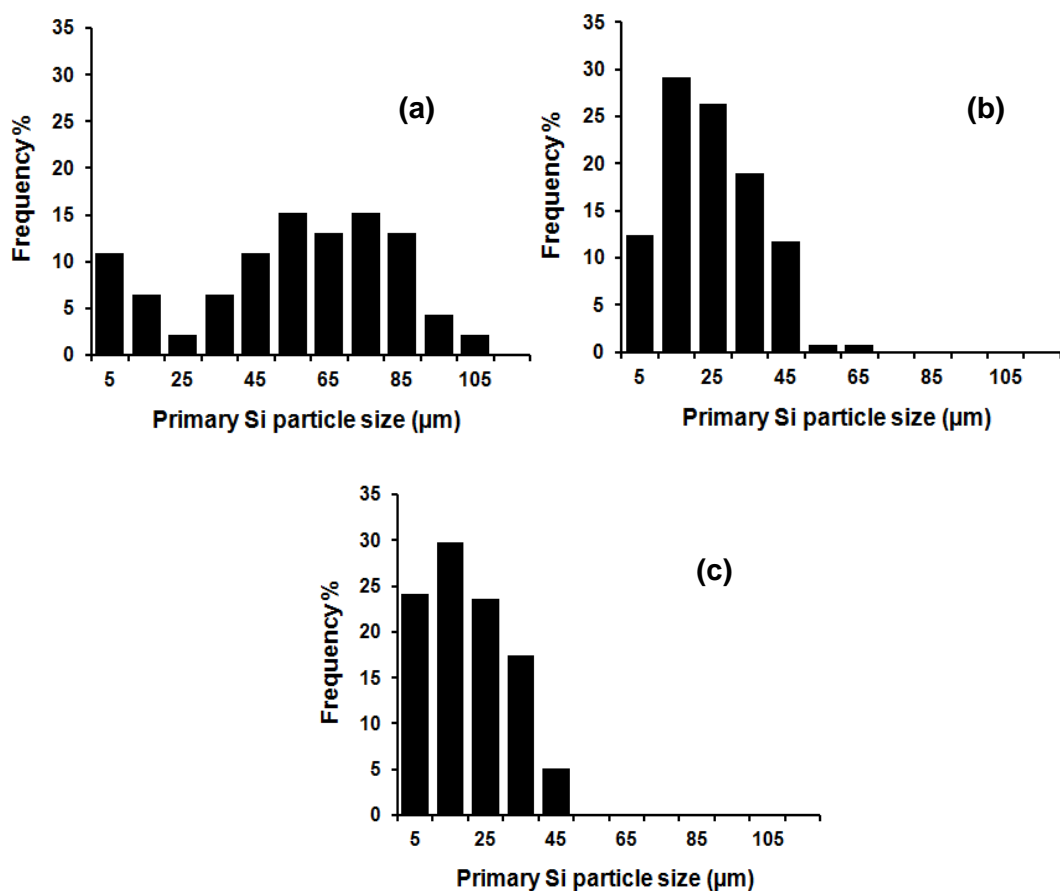


**Figure 4.27** Particle size distribution of primary Si in: (a) Al-18Si alloy; (b) Al-18Si with the addition of 0.27 wt% ZnS zincblende; and (c) Al-18Si with the addition of 100 ppm P.

Optical emission spectroscopy (OES) analysis of Zn in the solidified Al-18Si+ZnS alloy showed that the produced alloy contains 0.27% ZnS (if we assume that all Zn was converted to ZnS). The results from these experiments leave no doubt that the zincblende ZnS particles prepared *in situ* are potent substrates to refine the primary Si crystals. Furthermore this refinement does not come at the expense of eutectic modification.

#### 4.4.3.4 Characterisation of an Al-ZnS master alloy

Because of the exciting results described in the previous section, an Al-ZnS master alloy was prepared by adding Zn followed by adding an excess amount of Na<sub>2</sub>S to high purity aluminium at 800 °C. Figure 4.28 illustrates SEM micrographs and an EDS spectrum showing the formation of precipitated ZnS particles in the prepared Al-ZnS master alloy. Figure 4.28 confirmed the formation of ZnS particles in the master alloy. The high Al content that appeared in analysis of ZnS particles can be attributed to the small size of the ZnS particle and the large beam size used for EDS measurement and the Ca content can be attributed to its presence in the Na<sub>2</sub>S and Zn.

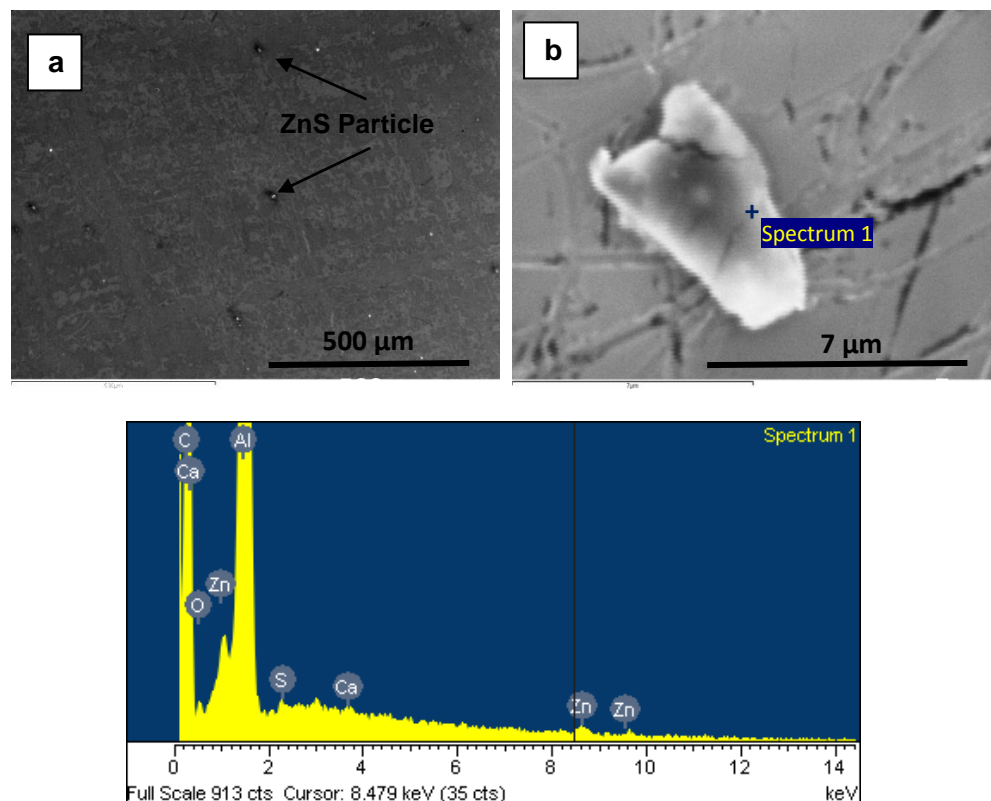


**Figure 4.28** SEM micrographs and EDS spectrum showing the formation of precipitated ZnS particles. (a) low magnification to show the size and distribution of ZnS particles, and (b) high magnification to show the morphology of ZnS particles.

It is clear that ZnS particles can be precipitated in the melt, and their formation is according to the following chemical equation;



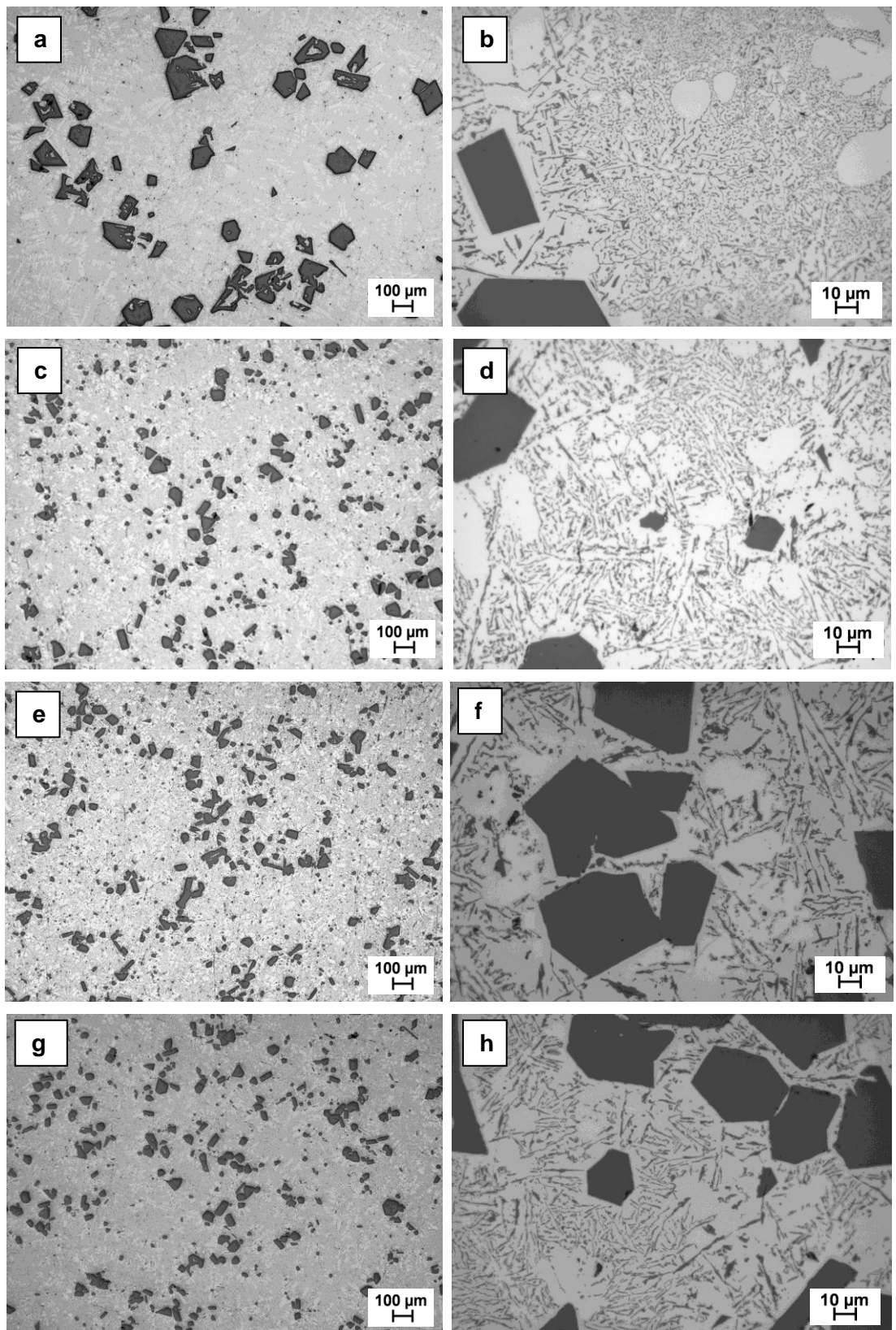
The same principle is used to remove Zn from wastewater or etching solution in the form of ZnS by adding Na<sub>2</sub>S [156]. ZnS crystallizes with the cubic zincblende structure below 1020 °C and with the hexagonal wurtzite structure above this phase transition temperature [154]. Since, the master alloy was prepared at 800 °C; the precipitated particles are zincblende ZnS. From the chemical analysis of the master alloy, and according to the chemical equation, the nominal composition of the master alloy is Al-1.5wt%ZnS. Separation of these ZnS particles for full characterisation and optimization of the master alloy composition will be the subject of further work.

#### 4.4.3.5 Effect of the Al-ZnS Master Alloy

Initial results of the use of ZnS encouraged the use of this master alloy to examine its refinement performance in solidification of hypereutectic Al-Si alloys. Figure 4.29 comprises optical micrographs showing the morphologies of primary and eutectic Si in solidified Al-22Si alloy with the addition of different amount of ZnS. The untreated Al-22Si alloy, shown in Figure 4.29 (a,b), contained coarse irregular primary Si with average particle size of approximately 74 µm and because of the high Ca content in commercial purity alloy (> 200 ppm) the eutectic Si had a mostly fibrous morphology.

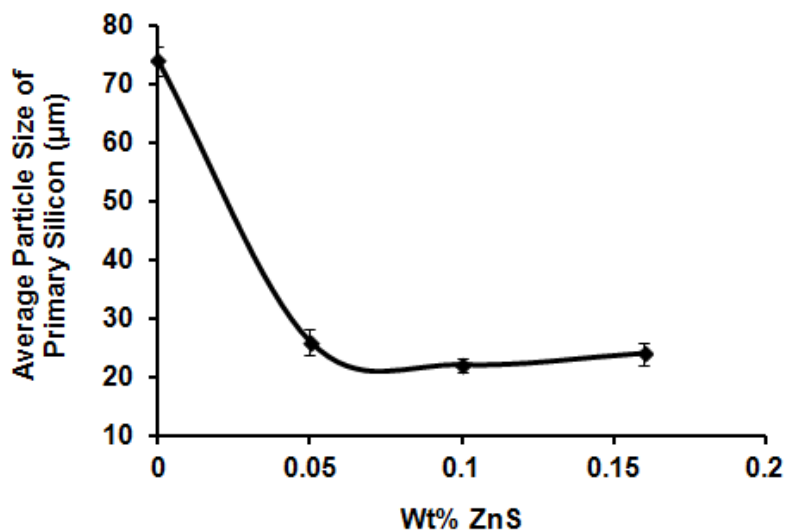
Refinement with Al-1.5ZnS master alloy resulted in primary Si particle size being reduced to 26, 22 and 24 µm with 0.05, 0.1 and 0.16 wt% addition of ZnS respectively and 20 min holding time prior to casting as shown in Figure 4.30, which is a plot of primary Si particle size against ZnS addition. The morphologies of primary Si crystals on solidification of Al-22Si alloy are changed from irregular morphologies to compact morphologies with some loss in the modification of the eutectic Si matrix. It was clear that with the increase of ZnS content up to 0.1wt% the average particle size of the primary Si decreased. Above 0.1wt% ZnS addition the size of primary Si no longer decreased.

Figure 4.31 shows the particle size distributions of Al-22Si with addition of different amount of ZnS. This figure shows how efficient Al-ZnS master alloy is of refining the primary Si and how narrow the particle size range is when compared with the commercial purity Al-22Si alloy.



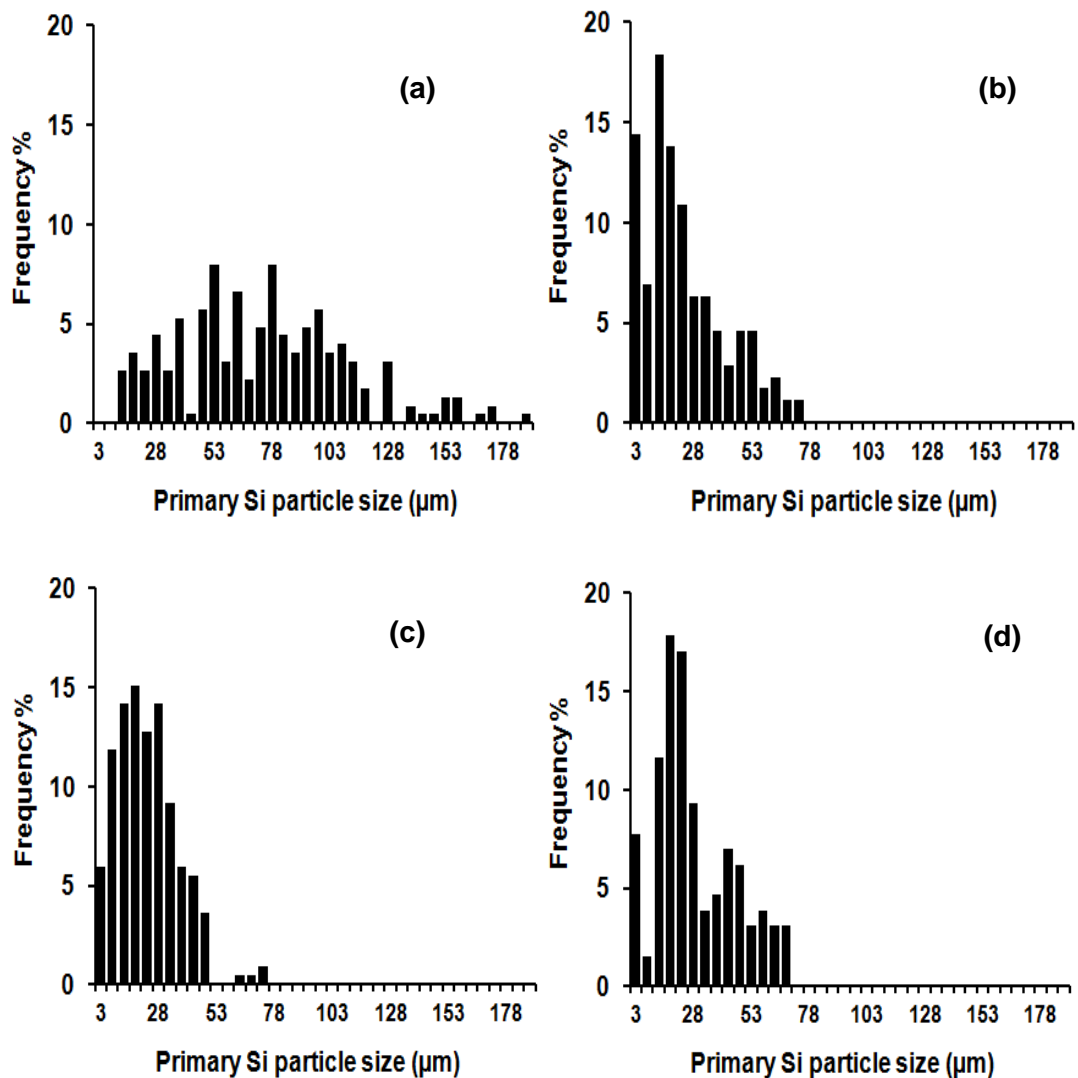
**Figure 4.29** Optical micrographs of (a, b) Al-22Si alloy; (c, d) Al-22Si with the addition of 0.05 wt% ZnS cast after 20 min; (e,f) Al-22Si with the addition of 0.1 wt% ZnS cast after 20 min; (g,h) Al-22Si with the addition of 0.16 wt% ZnS cast after 20 min; (a,c,e & g) low magnification and (b,d,f & h) high magnification. ZnS was added in the form of the Al-ZnS master alloy.

Figure 4.32 comprises optical micrographs showing the morphologies of primary and eutectic Si in solidified Al-22Si alloy with the addition of 0.1 wt% ZnS and 1.5 hr holding time prior to casting. With an increase in the holding time prior to casting up to 1.5 hr, the average particle size of primary Si was 33  $\mu\text{m}$  by adding 0.1 wt% of ZnS in solidification of Al-22Si, compared with 22  $\mu\text{m}$  achieved with the shorter holding time of 20 min. This reduction in the efficiency of the refinement of primary Si at high holding time could be due to the agglomeration of ZnS particles or could be due to its sedimentation to the bottom of the melt. Furthermore, the high holding time leads to continuous removal of the Ca by oxidation, and thus the eutectic Si matrix loses its modification.



**Figure 4.30** Plot of primary Si particle size as a function of ZnS addition (wt%), in the form of Al-ZnS master alloy, to commercial purity Al-22Si alloy.

The chemical composition analysed by optical emission spectroscopy (OES) of Al-22Si alloy after adding the master alloy (0.1 wt% ZnS) showed that the Si composition had reduced to around 20%Si because of dilution. Hence, to compare with P refinement, an experiment was conducted by adding 200 ppm of P to Al-20Si alloy. The average particle size of primary Si was reduced to 20  $\mu\text{m}$ , as shown in Figure 4.33.



**Figure 4.31** Particle size distribution of primary Si in Al-22Si alloys: (a) with no addition, (b) with 0.05 wt% ZnS, (c) with 0.1 wt% ZnS and (d) 0.16 wt% ZnS addition.

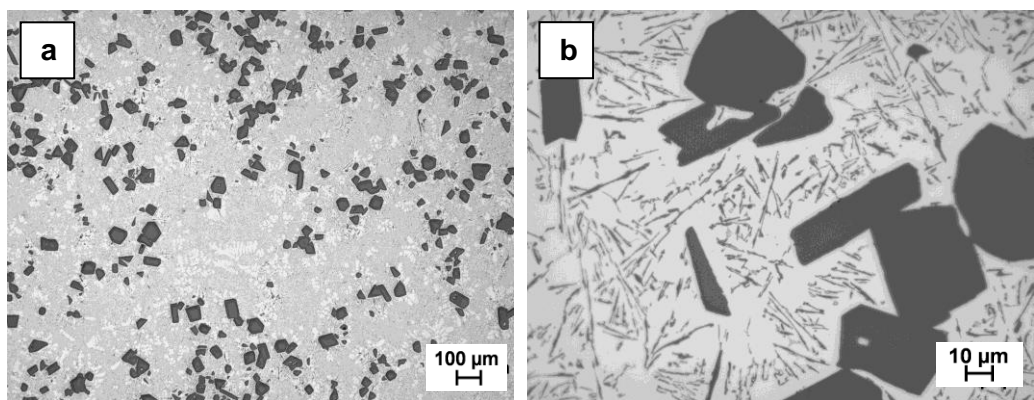


**Figure 4.32** Optical micrographs of Al-22Si with the addition of 0.1 wt% ZnS cast after 1.5 hr holding time prior to casting. (a) low magnification and (b) high magnification.

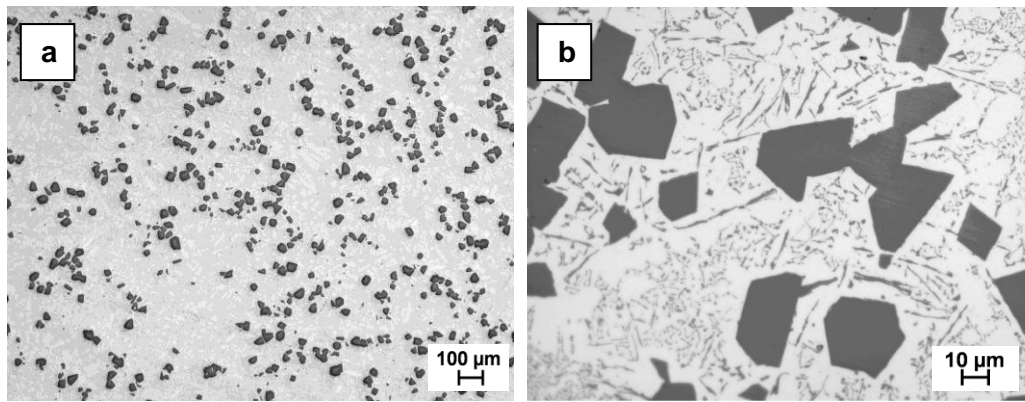


**Figure 4.33** Optical micrographs of Al-20Si alloy with the addition of 200 ppm P. (a) low magnification and (b) high magnification.

In using P for refinement of primary Si in hypereutectic Al-Si alloy, AIP particles will form *in situ* which has a zincblende crystal structure with a lattice constant of 5.431 Å. These particles are suspended in the melt and act as potent sites for epitaxial nucleation of primary Si [165]. And, due to the interaction between P and Ca the modification level of the eutectic Si will drop. Figure 4.34 shows the particle size distributions of primary Si in Al-22Si+0.1 wt% ZnS (20 min holding time prior to casting) and Al-20Si+200 ppm P alloys. It is very clear that the *in situ* prepared zincblende ZnS had a similar efficiency to that of P for the refinement of primary Si and is likely to follow the same refinement mechanism.

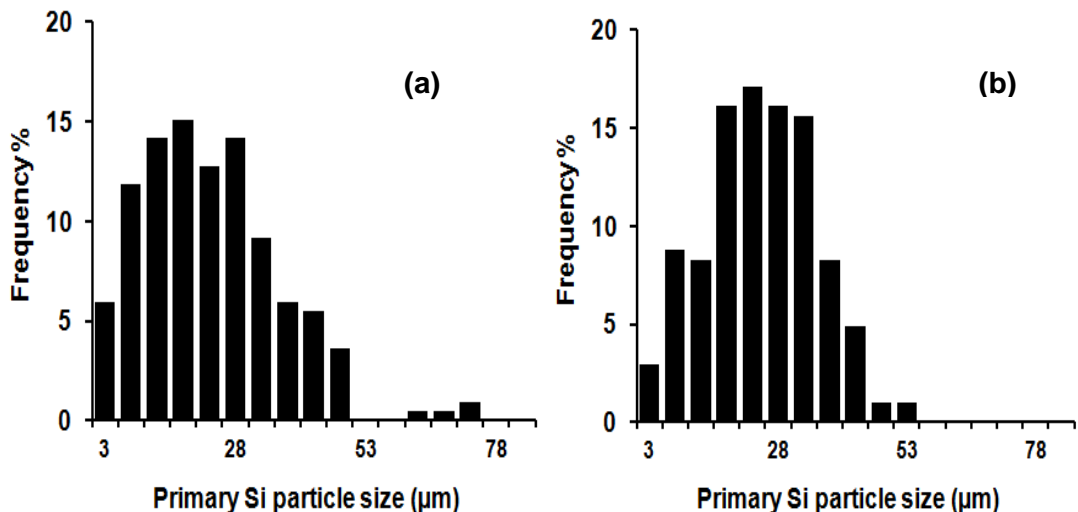


**Figure 4.34** Particle size distribution of primary Si in: (a) Al-22Si alloys with 0.1 wt% ZnS (20 min holding time prior to casting), (b) Al-20Si with 200 ppm P.

#### 4.4.4 Sodium Sulphide ( $\text{Na}_2\text{S}$ )

Experiments were conducted to investigate the effect of  $\text{Na}_2\text{S}$  on the size and morphology of primary Si in Al-Si alloys.  $\text{Na}_2\text{S}$  was chosen because it was used in preparing ZnS and is likely to exist with ZnS as an impurity. These experiments were to check whether or not  $\text{Na}_2\text{S}$  was behind or contributed to the refinement of primary Si by ZnS addition. Figure 4.35 illustrates optical micrographs of Al-18Si alloy with the addition of 0.5 wt%  $\text{Na}_2\text{S}$ . As shown in Figure 4.35,  $\text{Na}_2\text{S}$  had just a modification effect on the eutectic Si in Al-18Si. This action could be due to the decomposition of  $\text{Na}_2\text{S}$  to produce Na that modifies the eutectic matrix and interacts with the existing P. It is clear that the eutectic Si is over modified and the primary Si became coarse and more irregular if compared with the base Al-18Si (Figure 4.24 (a,b)). The average particle size of primary Si increased from 52 to 65  $\mu\text{m}$ .

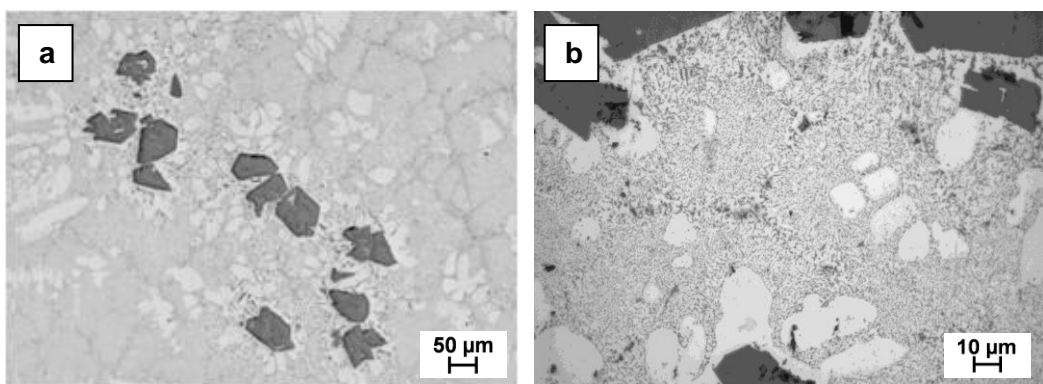


**Figure 4.35** Optical micrographs of Al-18Si with the addition of 0.5 wt%  $\text{Na}_2\text{S}$ . (a) low magnification to show the size and distribution of primary Si and (b) high magnification to show the eutectic structure.

#### 4.4.5 Zinc (Zn)

Experiments were conducted to investigate the effect of Zn on primary Si in Al-Si alloys. Zn was chosen because it was used in preparing ZnS *in situ* and it could be exist with ZnS particles as an impurity. These experiments were to check whether Zn was behind or contributed to the refinement of primary Si by ZnS particle addition. Figure 4.36 illustrates the optical micrographs of Al-22Si alloy without and with the addition of 0.5 wt% Zn. As shown in Figure 4.36, Zn had no refinement effect on the primary Si in solidification of the Al-22Si alloy. Also, there was no effect on the modification level of the eutectic silicon matrix.

The conclusions for the effect of chemical additions on the microstructure of hypereutectic Al-Si alloys are: Mg and ZnS refined primary Si whereas MgO, CaO,  $\text{Na}_2\text{S}$  coarsened the primary Si together with a modification effect on the eutectic Si. Adding Zn had no effect on morphology of Si phases.

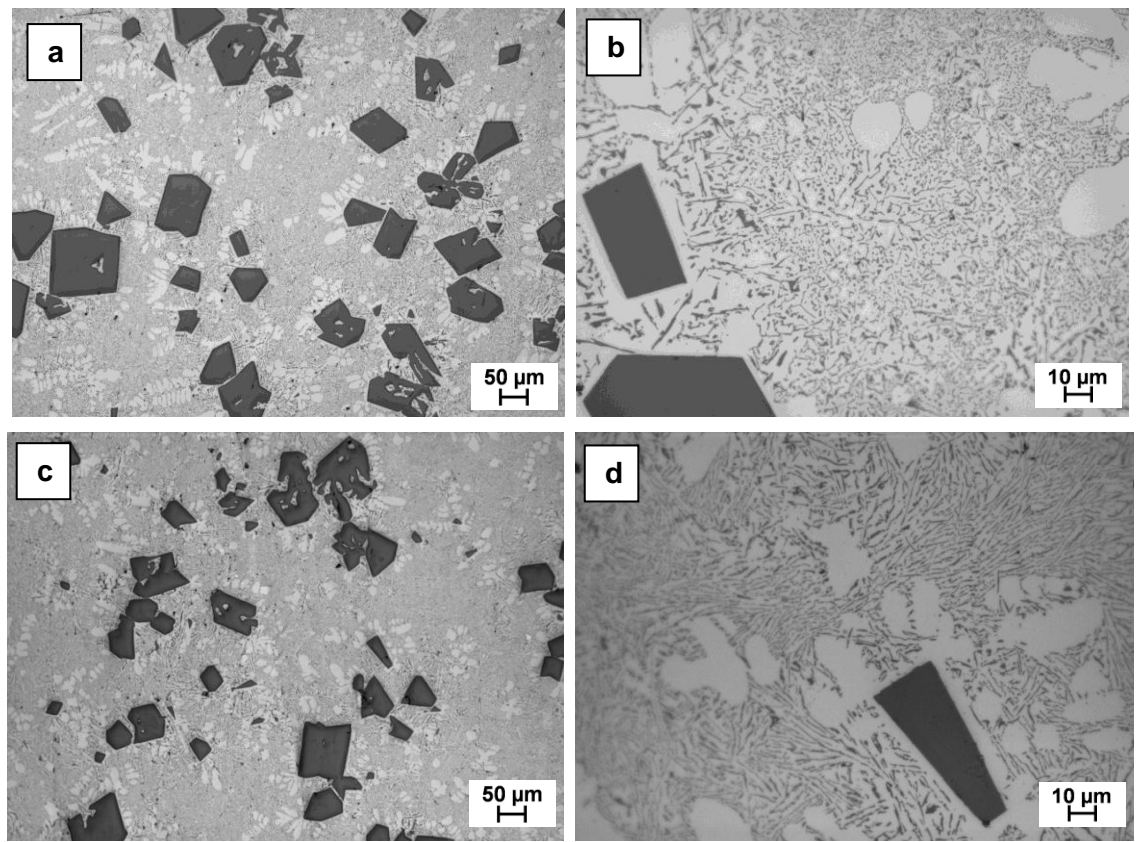


**Figure 4.36** Optical micrographs of as-cast alloys: (a,b) Al-22Si alloy, (c,d) Al-22Si with the addition of 0.5 wt% Zn. (a,c) low magnification to show the size and distribution of primary Si and (b,d) high magnification to show the eutectic structure.

#### 4.5 Nucleation and Growth of Primary Si on $\text{Al}_2\text{O}_3$

In some experimental results it was noticed that primary Si particles were intimately associated with invisible or visible oxide bifilm. Examples of which primary Si nucleated with visible oxide bifilm are shown in Figure 4.37.

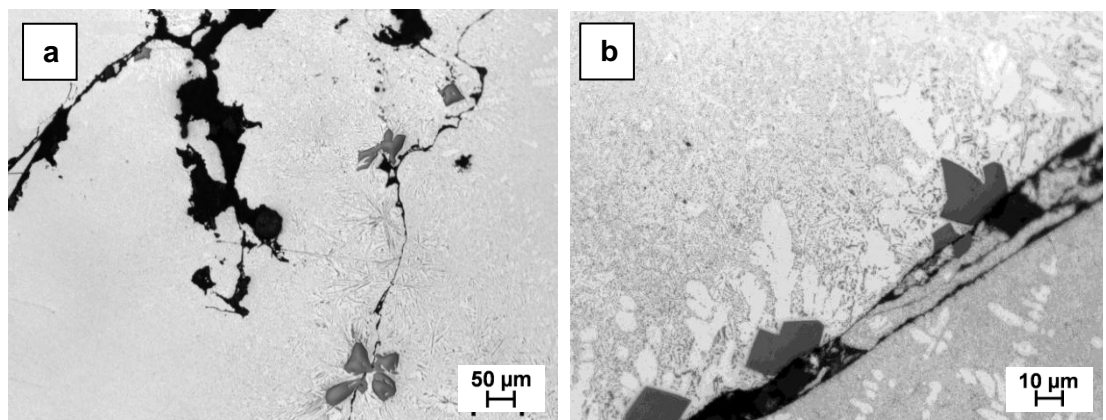


**Figure 4.37** Optical micrographs showing example of the association of primary Si with oxide bifilms in Al-18Si alloy cast from 800 °C. (a) low magnification and (b) high magnification.

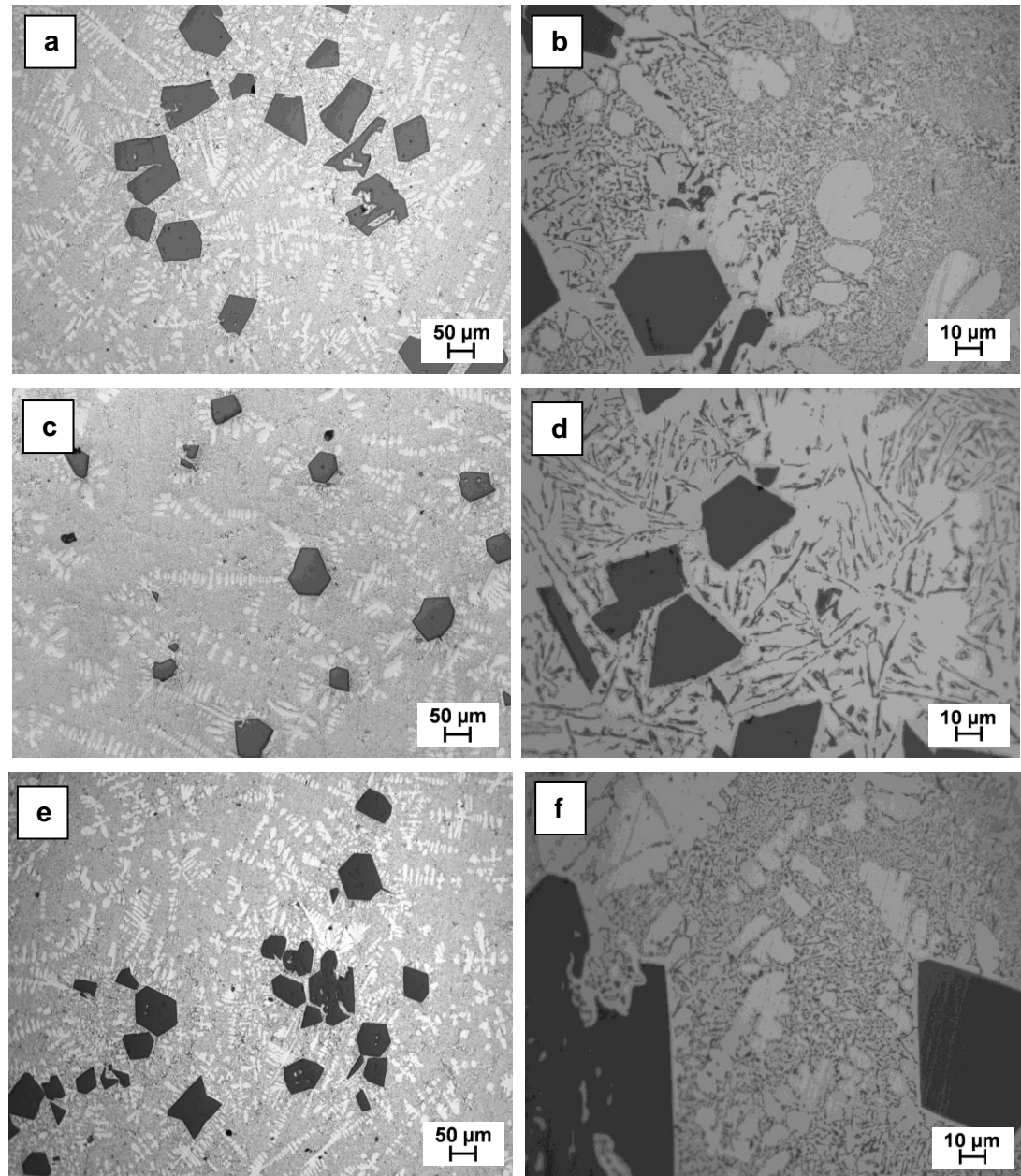
In view of this, experiments were carried out by adding  $\alpha$ -Al<sub>2</sub>O<sub>3</sub>,  $\gamma$ -Al<sub>2</sub>O<sub>3</sub>, P-doped  $\alpha$ -Al<sub>2</sub>O<sub>3</sub> and P-doped  $\gamma$ -Al<sub>2</sub>O<sub>3</sub> to commercial purity Al-18Si alloys. The latter experiments were to examine the possibility of supporting P on aluminium oxide to refine the primary Si in solidification of hypereutectic Al-Si alloys. Figure 4.38 illustrates optical micrographs of Al-18Si alloy without and with the addition of 0.5 wt% of  $\alpha$ -Al<sub>2</sub>O<sub>3</sub> and 0.5 wt% of  $\gamma$ -Al<sub>2</sub>O<sub>3</sub>. As shown in Figure 4.38, adding 0.5 wt% of  $\alpha$ -Al<sub>2</sub>O<sub>3</sub> (0.5  $\mu\text{m}$  in size) there was no change in the size and morphology of primary Si but the eutectic Si lost its modification. While, in adding 0.5 wt% of  $\gamma$ -Al<sub>2</sub>O<sub>3</sub> (0.5  $\mu\text{m}$  in size) the average particle size of primary Si reduced slightly from 52  $\mu\text{m}$  to 48  $\mu\text{m}$  with no change in modification level of eutectic Si.

Figure 4.39 shows optical micrographs of commercial purity Al-18Si alloys without and with the addition of 0.5 wt% of P-doped  $\alpha$ -Al<sub>2</sub>O<sub>3</sub> and 0.5wt% of P-doped  $\gamma$ -Al<sub>2</sub>O<sub>3</sub> (0.5  $\mu\text{m}$  in size). The average particle size of primary Si decreased from 52  $\mu\text{m}$  to 25  $\mu\text{m}$  and 22  $\mu\text{m}$  in adding P-doped  $\alpha$ -Al<sub>2</sub>O<sub>3</sub> and P-doped  $\gamma$ -Al<sub>2</sub>O<sub>3</sub> respectively. Although the addition of P-doped  $\alpha$ -Al<sub>2</sub>O<sub>3</sub> led to refinement of primary Si the eutectic did not retain its modified structure (Figure 4.39d). However, it is clear that P-doped  $\gamma$ -Al<sub>2</sub>O<sub>3</sub> led to good refinement of primary Si and the modification effect on eutectic Si was retained in solidification of commercial purity Al-18Si alloy (Figure 4.39f).

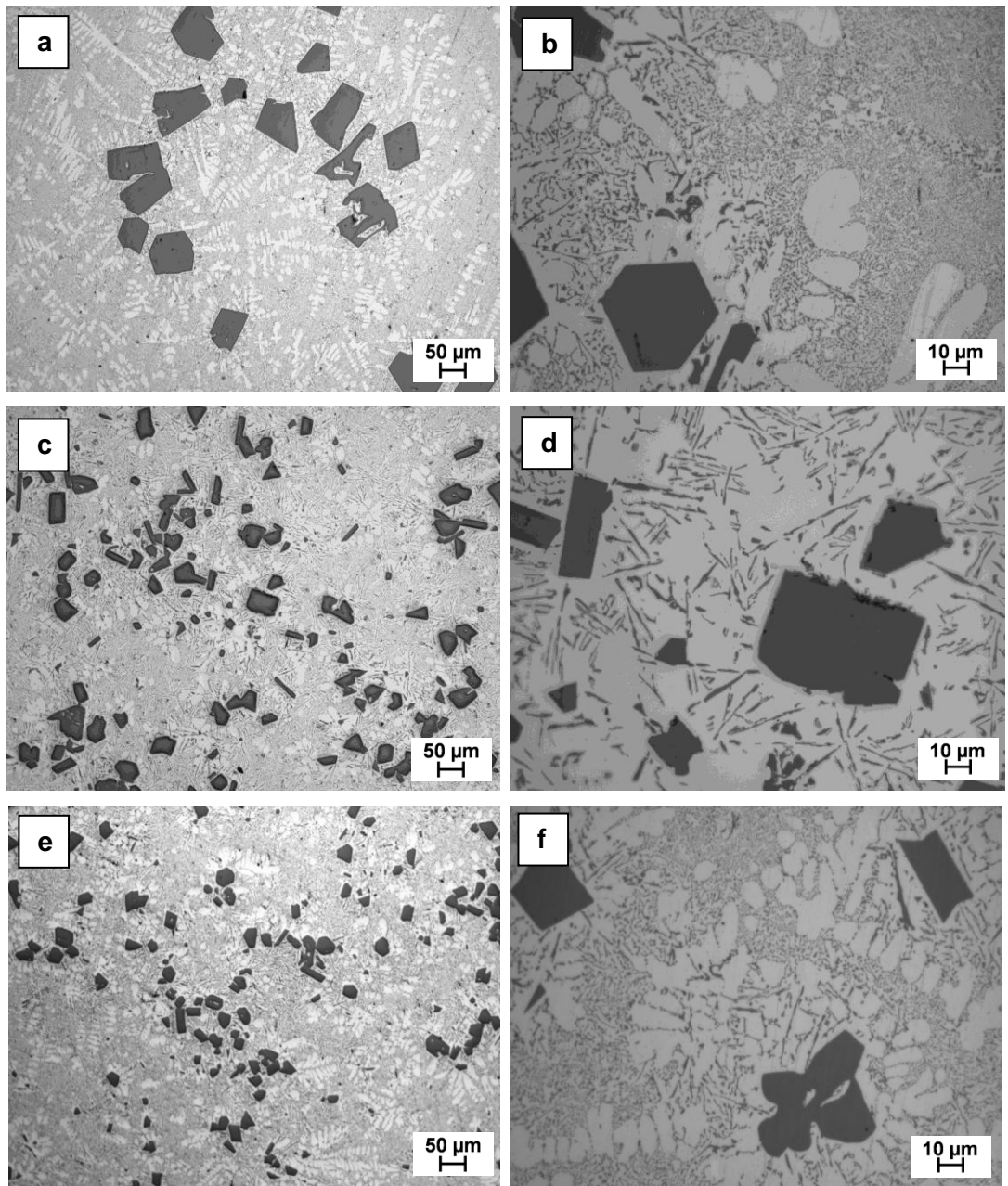
Another set of experiments were conducted by adding 0.5 wt% P-doped  $\gamma$ -Al<sub>2</sub>O<sub>3</sub> with average particle size 3  $\mu\text{m}$ , i.e. coarser particles, to the commercial purity Al-18Si alloy. Figure 4.40 shows optical micrographs of commercial purity Al-18Si alloy without and with the addition of 0.5wt % of P-doped  $\gamma$ -Al<sub>2</sub>O<sub>3</sub> (3  $\mu\text{m}$  in size) and 100 ppm P for comparison. In the case of the 0.5wt % of P-doped 3  $\mu\text{m}$  particles the average particle size of primary Si was about 25  $\mu\text{m}$ , compared with 52  $\mu\text{m}$  for Al-18Si without addition and 22  $\mu\text{m}$  for the addition of 0.5wt% of 0.5  $\mu\text{m}$  P-doped  $\gamma$ -Al<sub>2</sub>O<sub>3</sub> particles with good modification in eutectic matrix as shown in Figure 4.40 (c,d). These results compared well with the refinement of primary Si by adding 100 ppm P, as shown in Figure 4.40 (e,f), for which the average particle size of primary Si was 20  $\mu\text{m}$  and the eutectic Si morphology changed from a fibrous to a plate-like structure. Table 4.1 summarizes the effect of different form and size of Al<sub>2</sub>O<sub>3</sub> particles without and with P on the average particles size of primary Si and compared with P addition.

Figure 4.41 compares the particle size distributions of Al-18Si alloy with Al-18Si with 0.5 wt% P-doped  $\gamma$ -Al<sub>2</sub>O<sub>3</sub> (0.5  $\mu\text{m}$  in size), Al-18Si with 0.5wt% P-doped  $\gamma$ - Al<sub>2</sub>O<sub>3</sub> (3  $\mu\text{m}$  in size), and Al-18Si+100ppm P additions. Adding P-doped  $\gamma$ - Al<sub>2</sub>O<sub>3</sub> give a good primary Si refinement to Al-18Si alloy if compared with the addition of P and using finer  $\gamma$ - Al<sub>2</sub>O<sub>3</sub> powder give narrower particle size range similar to that of adding P.

Further work should be done in the future to detect the presence of phosphorus at the interface between oxides, whether added or present as bifilms, and the nucleated primary Si particles.



**Figure 4.38** Optical micrographs of as-cast alloys: (a,b) Al-18Si alloy; (c,d) Al-18Si with the addition of 0.5wt%  $\alpha$ -Al<sub>2</sub>O<sub>3</sub> (0.5  $\mu$ m); (e,f) Al-18Si with the addition of 0.5wt%  $\gamma$ -Al<sub>2</sub>O<sub>3</sub> (0.5  $\mu$ m). (a,c & e) low magnification to show the size and distribution of primary Si and (b,d & f) high magnification to show the eutectic structure.



**Figure 4.39** Optical micrographs of as-cast alloys: (a,b) Al-18Si alloy; (c,d) Al-18Si with the addition of 0.5wt% P-doped  $\alpha$ - $\text{Al}_2\text{O}_3$  (0.5  $\mu\text{m}$  in size); (e,f) Al-18Si with the addition of 0.5wt% P-doped  $\gamma$ - $\text{Al}_2\text{O}_3$  (0.5  $\mu\text{m}$  in size). (a,c & e) low magnification to show the size and distribution of primary Si and (b,d & f) high magnification to show the eutectic structure.

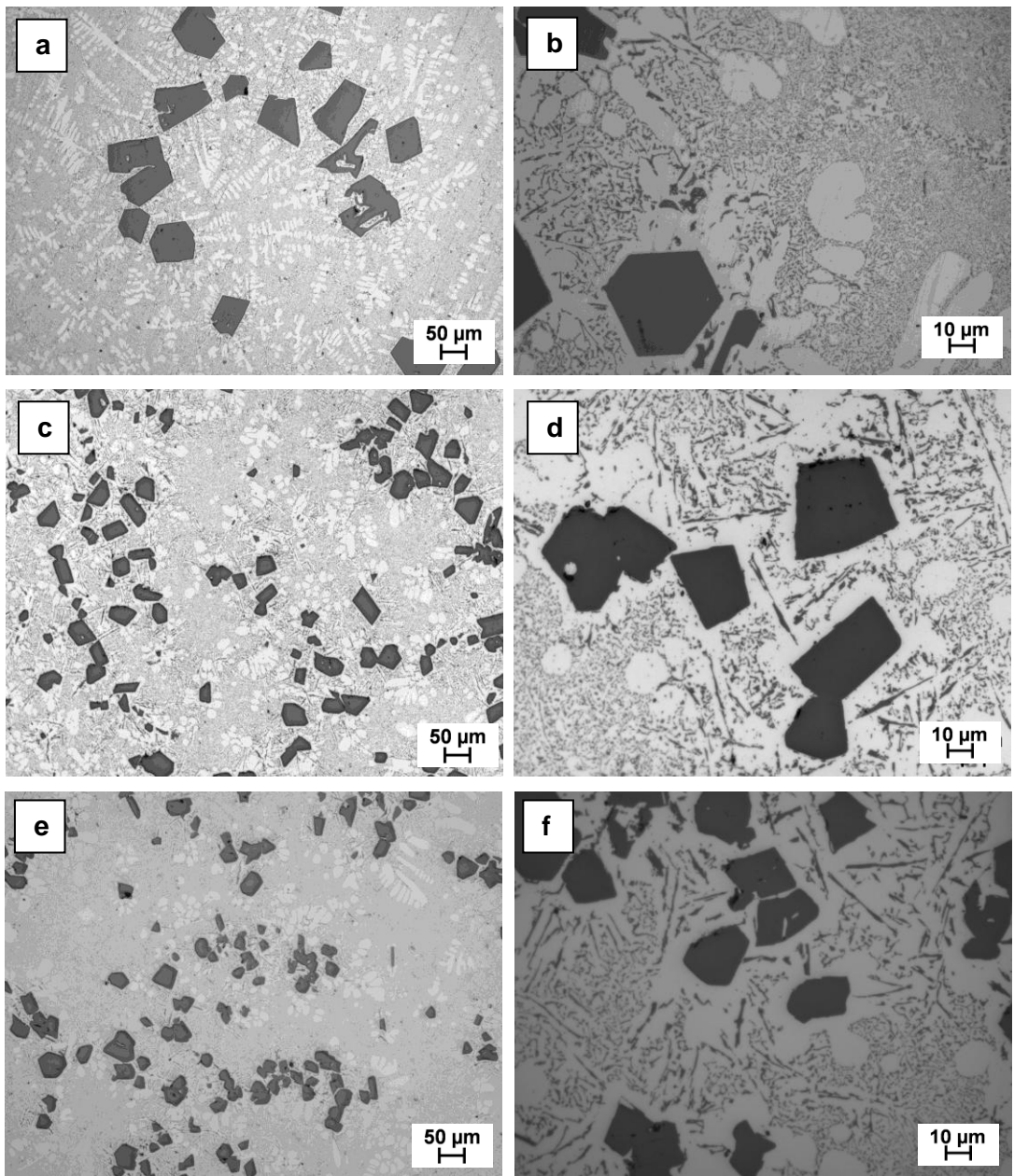


**Figure 4.40** Optical micrographs of as-cast alloys: (a,b) Al-18Si alloy; (c,d) Al-18Si with the addition of 0.5wt% P-doped  $\gamma$ -Al<sub>2</sub>O<sub>3</sub> (3  $\mu\text{m}$ ); (e,f) Al-18Si with the addition of 100 ppm P. (a,c & e) low magnification to show the size and distribution of primary Si and (b,d & f) high magnification to show the eutectic structure.

**Table 4.1** Effect of different form and size of  $\text{Al}_2\text{O}_3$  without and with P on the average particles size of primary Si ( $\mu\text{m}$ ) and compared with P addition.

Alloy	Al-18Si	Al-18Si + $\alpha$ - $\text{Al}_2\text{O}_3$ (0.5 $\mu\text{m}$ )	Al-18Si + $\gamma$ - $\text{Al}_2\text{O}_3$ (0.5 $\mu\text{m}$ )	Al-18Si +P-doped $\alpha$ - $\text{Al}_2\text{O}_3$ (0.5 $\mu\text{m}$ )	Al-18Si +P-doped $\gamma$ - $\text{Al}_2\text{O}_3$ (0.5 $\mu\text{m}$ )	Al-18Si +P-doped $\gamma$ - $\text{Al}_2\text{O}_3$ (3 $\mu\text{m}$ )	Al-18Si +100 ppm P
<b>Size of primary Si (<math>\mu\text{m}</math>)</b>	52±4.3	52±2.5	48±5.6	25±2.9	22±1.7	25±2.8	20±2.2

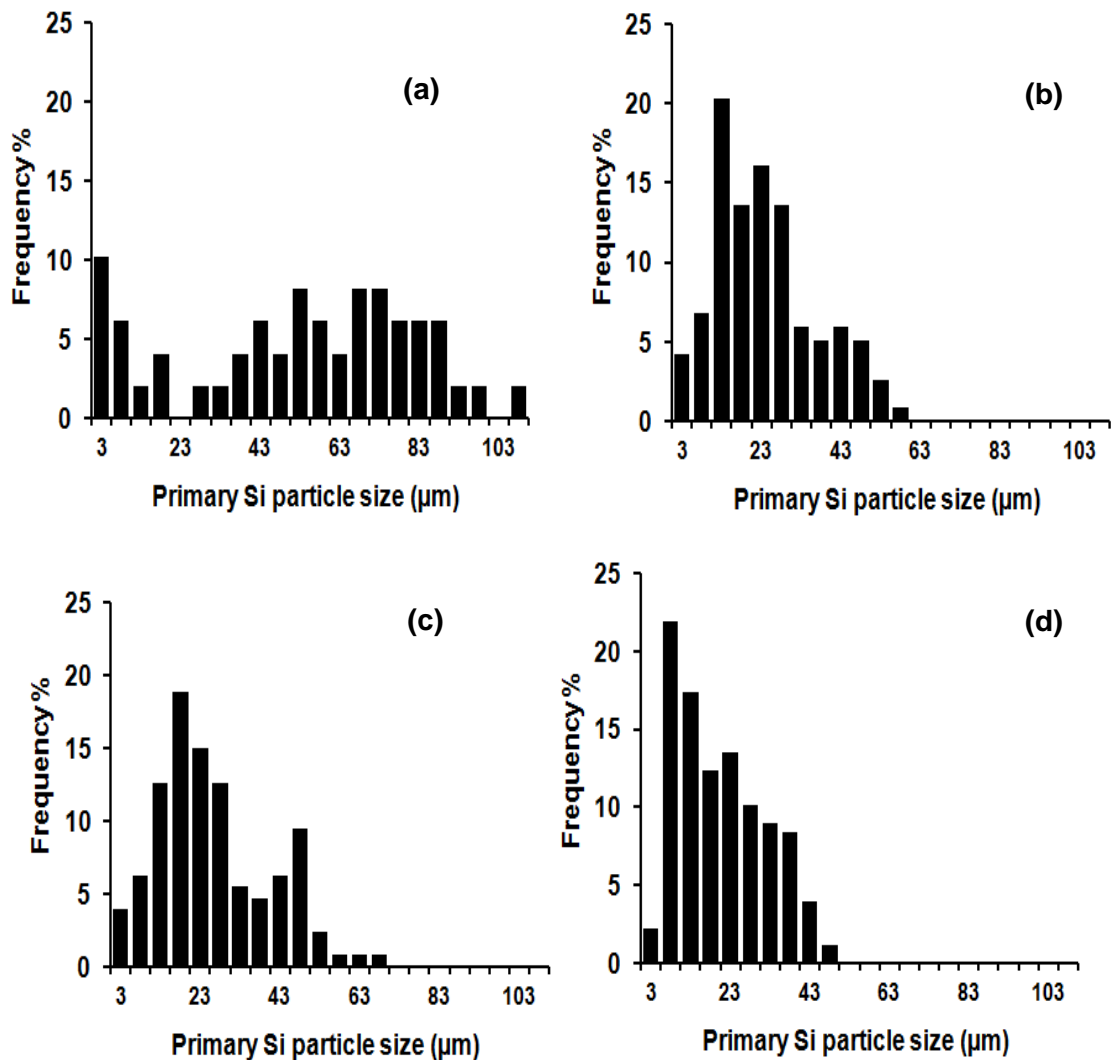


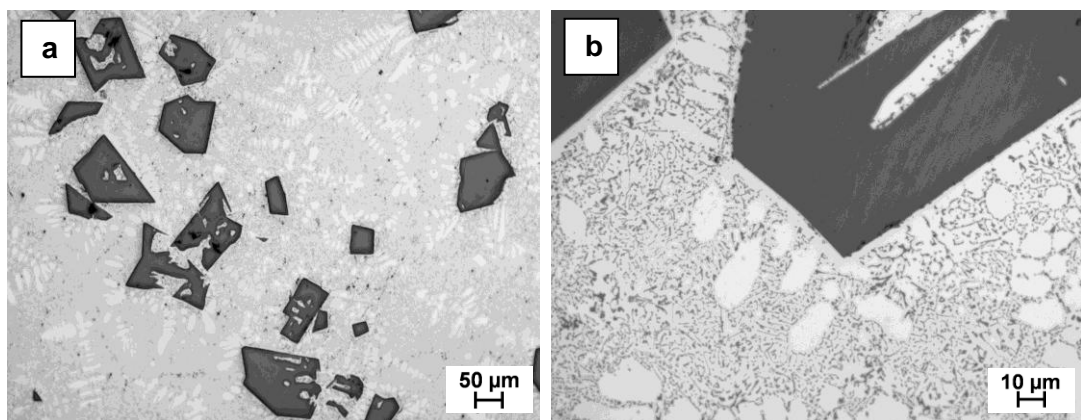
**Figure 4.41** Particle size distribution of primary Si in: (a) Al-18Si alloys; (b) with 0.5wt% P-doped  $\gamma$ - $\text{Al}_2\text{O}_3$  (0.5  $\mu\text{m}$  in size); (c) with 0.5wt% P-doped  $\gamma$ - $\text{Al}_2\text{O}_3$  (3  $\mu\text{m}$  in size) addition; and (d) with 100ppm P.

## 4.6 The New Solid-Liquid Duplex Casting Process

This section describes the results of a new solid-liquid duplex casting process to control morphology of both primary and eutectic Si on solidification of hypereutectic Al-Si alloys. For comparison and evaluation of the process, the same alloys were produced by conventional casting as well as by the new casting process.

### 4.6.1 Conventional casting

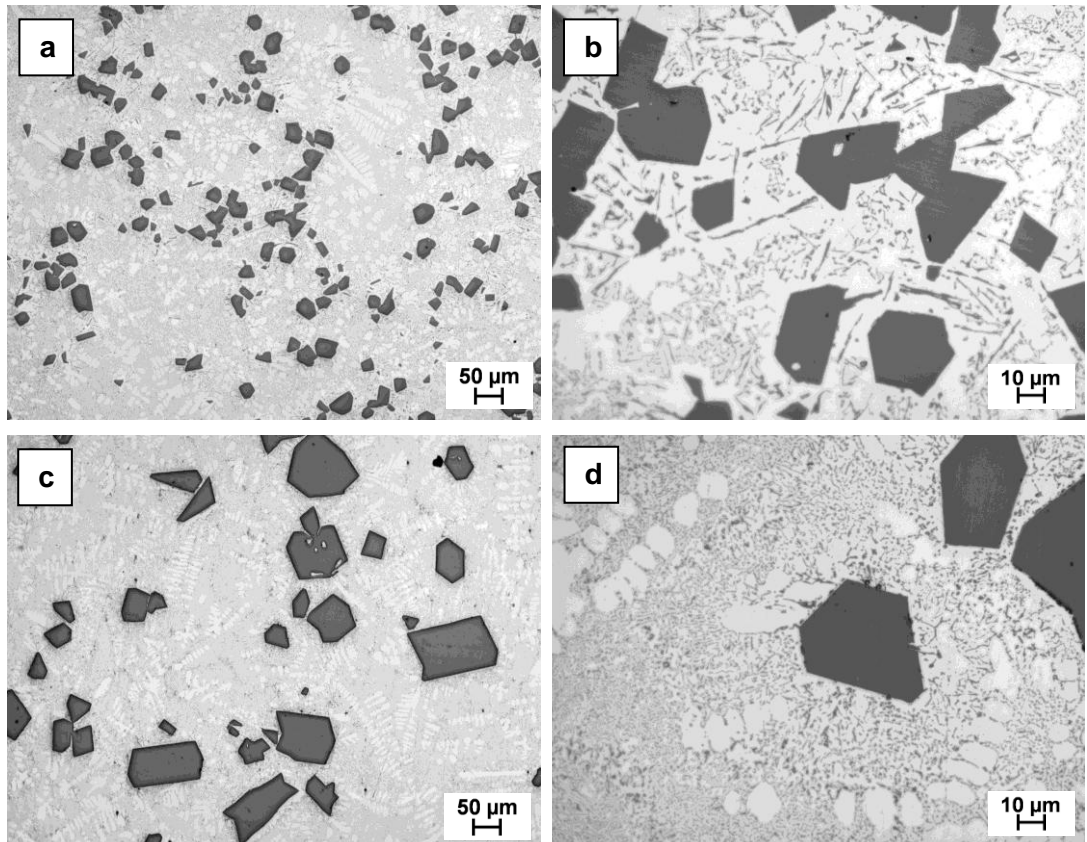
Figure 4.42 shows typical microstructures of conventionally cast untreated Al-19Si produced by using commercial purity aluminium and silicon. The untreated Al-19Si contained coarse primary Si with average particle size of approximately 74 µm (Figure 4.42a) and the eutectic Si had a mostly fibrous morphology due to an inherent Ca content of more than 200 ppm as shown in Figure 4.42b. Figure 4.43 comprises optical micrographs showing the morphologies of primary and eutectic Si in Al-19Si alloy with 200 ppm P and 200 ppm Sr conventionally cast from 800 °C. The conventionally cast Al-19Si treated with 200ppm P contained refined primary Si particles with average particle size of 26 µm dispersed in mixture of plate-like and fibrous Al-Si eutectic matrix, as shown in Figure 4.43 (a,b), while the conventionally cast Al-19Si alloy treated with 200ppm Sr contained large primary Si particles with average particle size of 65 µm dispersed in a fibrous structure typical of a fully modified eutectic as shown in Figure 4.43 (c,d).



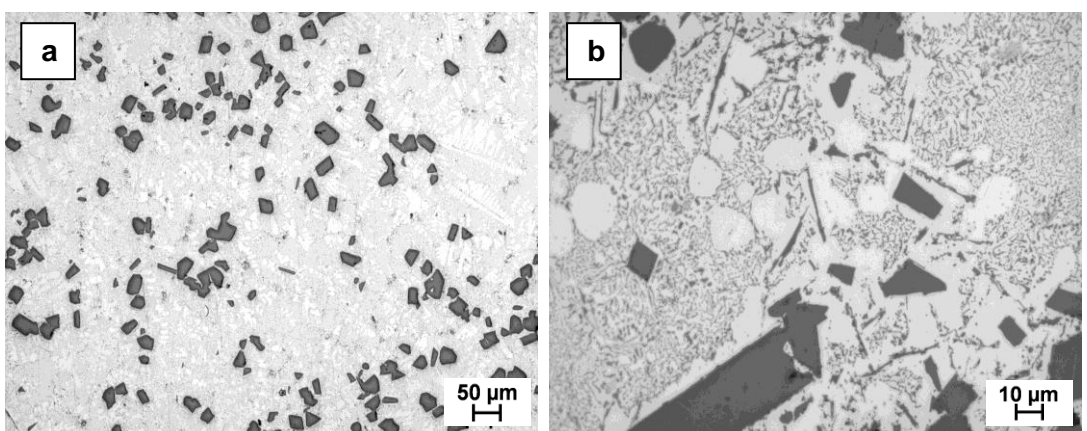
**Figure 4.42** Optical micrographs of conventionally cast Al-19Si alloy without P or Sr addition at (a) low magnification to show the size and distribution of primary Si and (b) high magnification to show the eutectic structure.

Figure 4.44 illustrates the optical micrographs showing typical morphologies of primary and eutectic Si in conventionally cast of Al-19Si alloy with simultaneous additions of P and Sr. The conventionally cast Al-19Si treated with both 200ppm P and

200ppm Sr contained refined polygonal primary Si particles with average particle size of 26  $\mu\text{m}$  dispersed in a partially modified Al-Si eutectic matrix, as shown in Figure 4.44.



**Figure 4.43** Optical micrographs of conventionally cast Al-19Si alloy: (a,b) Al-19Si+200ppm P and (c,d) Al-19Si+200ppm Sr at (a,c) low magnification to show the size and distribution of primary Si and (b,d) high magnification to show the eutectic structure.



**Figure 4.44** Optical micrographs of conventionally cast Al-19Si+200ppm P+200ppm Sr at (a) low magnification and (b) high magnification.

#### 4.6.2 The solid-liquid duplex casting process

A solid-liquid duplex casting process was applied to achieve simultaneous refinement and modification of primary and eutectic Si respectively in hypereutectic Al-Si alloys. Experiments were conducted to find the optimum P and Sr content in the two alloys to be mixed to prepare the target Al-19Si alloy with simultaneous refinement of primary Si and modification of eutectic silicon. Also, experiments were carried out to optimize the Si content in Sr-treated Al-Si alloy and the casting temperature. Solid-liquid duplex casting process was tested to achieve simultaneous refinement of primary Si modification of eutectic silicon in hypereutectic Al-18Si alloy with checking the improvement in mechanical properties.

##### 4.6.2.1 Optimum P and Sr for P-treated and Sr-treated alloys

For the solid-liquid duplex process, experiments were done to optimize the amount of P and Sr to be added to the Al-30Si (solid) and Al-8Si (liquid) starting alloys respectively, in order to get simultaneous refinement of primary Si and modification of eutectic Si in the target alloy. Figure 4.45 shows the microstructure of the untreated Al-8Si alloy prepared to carry out the initial set of experiments. The unmodified Al-8Si alloy consists of plate-like structure of eutectic Si.

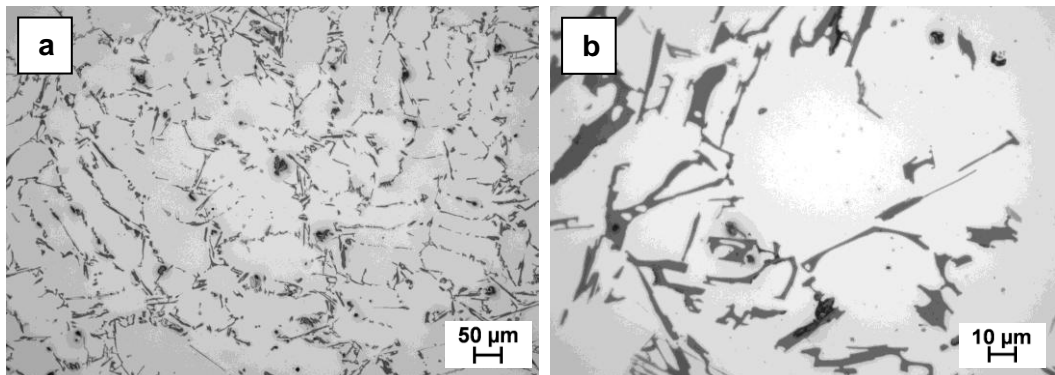


**Figure 4.45** Optical micrographs of Al-8Si alloy cast from 800 °C, at: (a) low magnification and (b) high magnification.

A range of P additions was made to Al-30Si alloy in order to prepare the P-treated solid starting alloy with very fine particles of primary Si. Figure 4.46 shows the size and morphology of primary Si in Al-30Si without and with P additions. As shown in Figure 4.46, the size and morphology of primary Si changed with the added amount of P. The primary Si particles became refined and more compact in shape with increasing addition of P. The alloy with no P addition and the alloy with 50ppm P (Figure 4.46 (a,b)) had primary Si that was generally coarse and irregular in shape. The alloy with 100 ppm P added P (Figure 4.46c) had a mixture of coarse irregular and finer compact

primary Si. The alloys with 200 ppm, 300 ppm and 400 ppm added P were generally refined. Figure 4.47 shows the particle size distributions of primary Si in Al-30Si alloy with different amount of P added. It is clear in this figure that with the increase of P content the particle size range decreases with a higher percentage of smaller particle size. The mean particle size of primary Si for the Al-30Si alloy without P addition was 158  $\mu\text{m}$ . On adding 50, 100, 200, 300 and 400 ppm P the mean particle size of primary Si decreased to 56, 44, 40, 38 and 37  $\mu\text{m}$  respectively as shown in Figure 4.48 which is a plot of average primary Si particle size against the amount of added P.

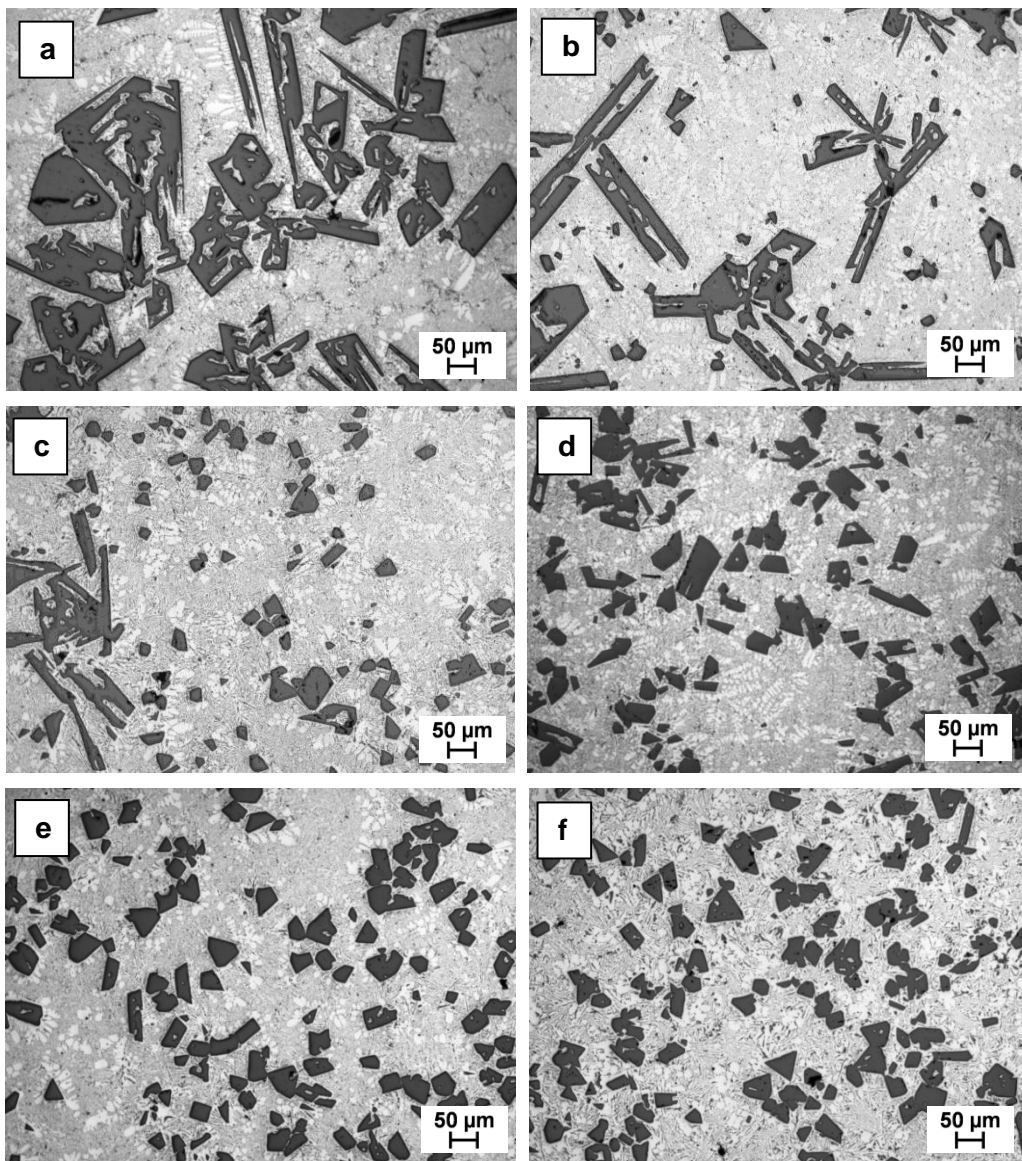


**Figure 4.46** Optical micrographs of Al-30Si: (a) without added P; (b) with 50 ppm added P; (c) with 100 ppm added P; (d) with 200 ppm added P; (e) with 300 ppm added P and (f) with 400 ppm added P.

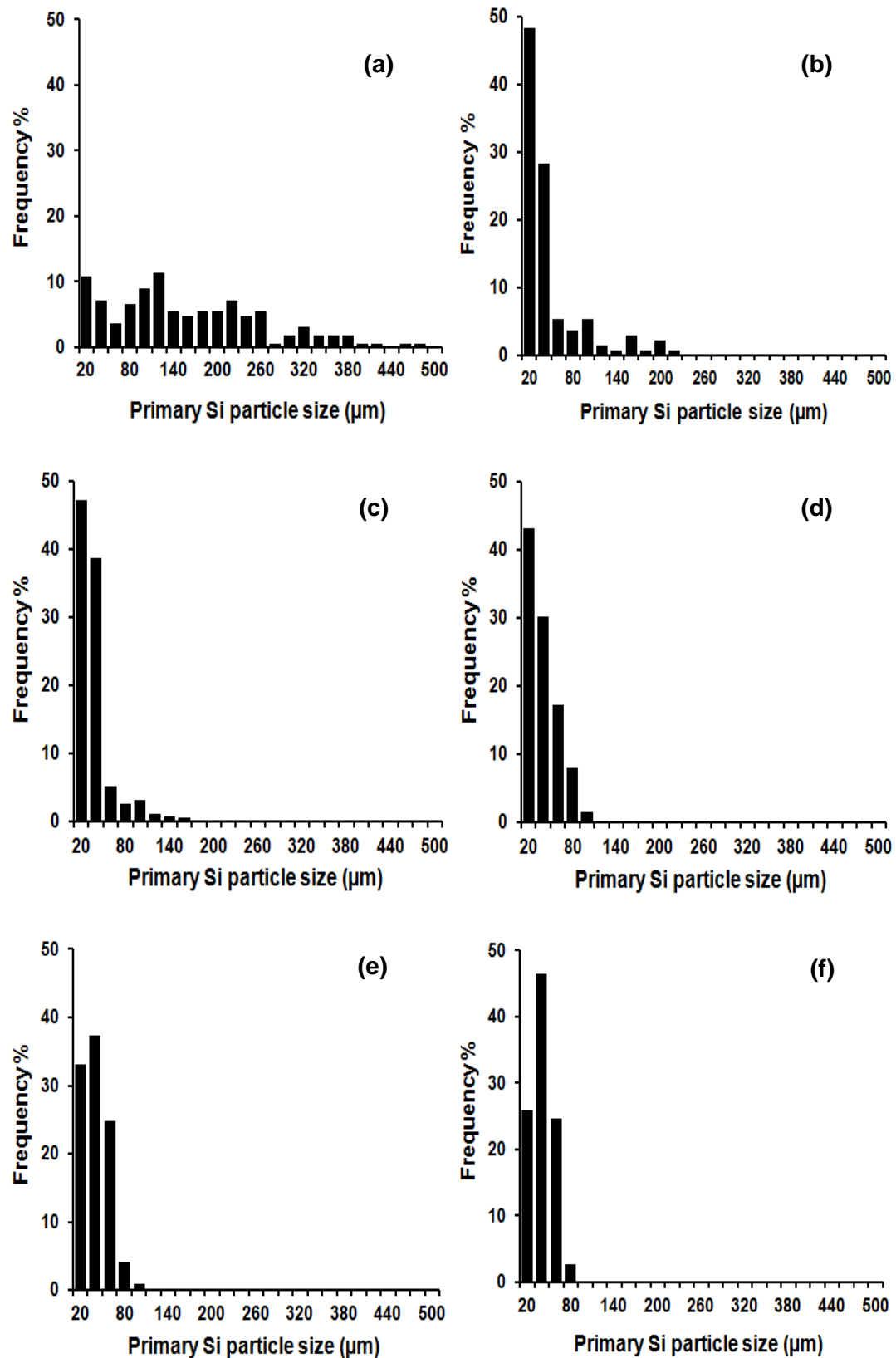


**Figure 4.47** Particle size distribution of primary Si in Al-30Si alloys: (a) with no addition; (b) with 50 ppm P; (c) with 100 ppm P; (d) with 200 ppm P; (e) 300 ppm P and (f) 400 ppm P addition.

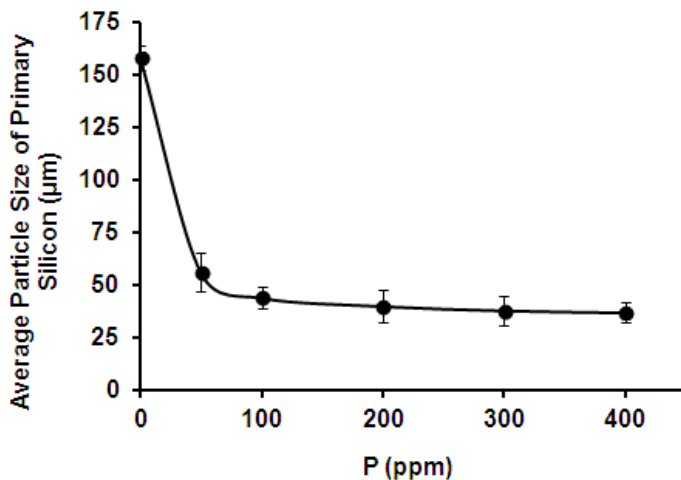


**Figure 4.48** Plot of particle size of primary Si against the amount of P added to commercial purity Al-30Si Alloy.

The first set of solid-liquid duplex process experiments were conducted to produce Al-19Si alloy by mixing liquid Al-8Si alloy with solid Al-30Si alloy treated with different amount of P cast from 610 °C. Each solid-liquid duplex casting experiment with different alloy and process parameters was given a code consisting of the letters SLD and a number, e.g. SLD1. Micrographs in Figure 4.49 show the morphologies of primary Si (a,c & e) and eutectic Si (b,d & f) in the target Al-19Si alloy with no added P (SLD1) and with 50ppm (SLD2) and 100ppm (SLD3) added P, and no added Sr. It is clear that without any addition of P and Sr (SLD1) (Figure 4.49 (a,b)) there was some refinement of the primary Si without any modification of the eutectic. The mean particle size of primary Si was 78 μm, although there were some very coarse irregular particles, without any P addition in using solid-liquid duplex process, while the size of primary Si was 158 μm in the untreated Al-30Si alloy. As the amount of P increased (Figure 4.49 (c,e)) in the P-treated Al-30Si alloy there was a good improvement in refinement of primary Si in the target alloy. When mixing Al-8Si with Al-30Si+50 ppm P alloy (SLD2) and with Al-30Si+100ppm P alloy (SLD3), the mean particle size of primary Si in the target Al-19Si was 36 and 34 μm respectively. In comparison, the size of primary Si in Al-30Si+50ppm P and Al-30Si+100ppm P alloy was 56 and 44 μm respectively. Figure 4.50 shows the particle size distribution of primary Si in the Al-19Si target alloy produced by mixing liquid Al-8Si with Al-30Si (SLD1), Al-30Si+50ppm P (SLD2) and Al-30Si+100ppm P (SLD3) cast from 610 °C. This figure shows a significant reduction in the primary Si particle size range. Details of each experiment using a fixed liquid alloy:solid alloy ratio of 1:1 (by mass) are provided in Table 4.2. Although the solid-liquid duplex process for mixing untreated liquid Al-8Si with solid P-treated Al-30Si led to refined primary Si, the eutectic was unmodified.

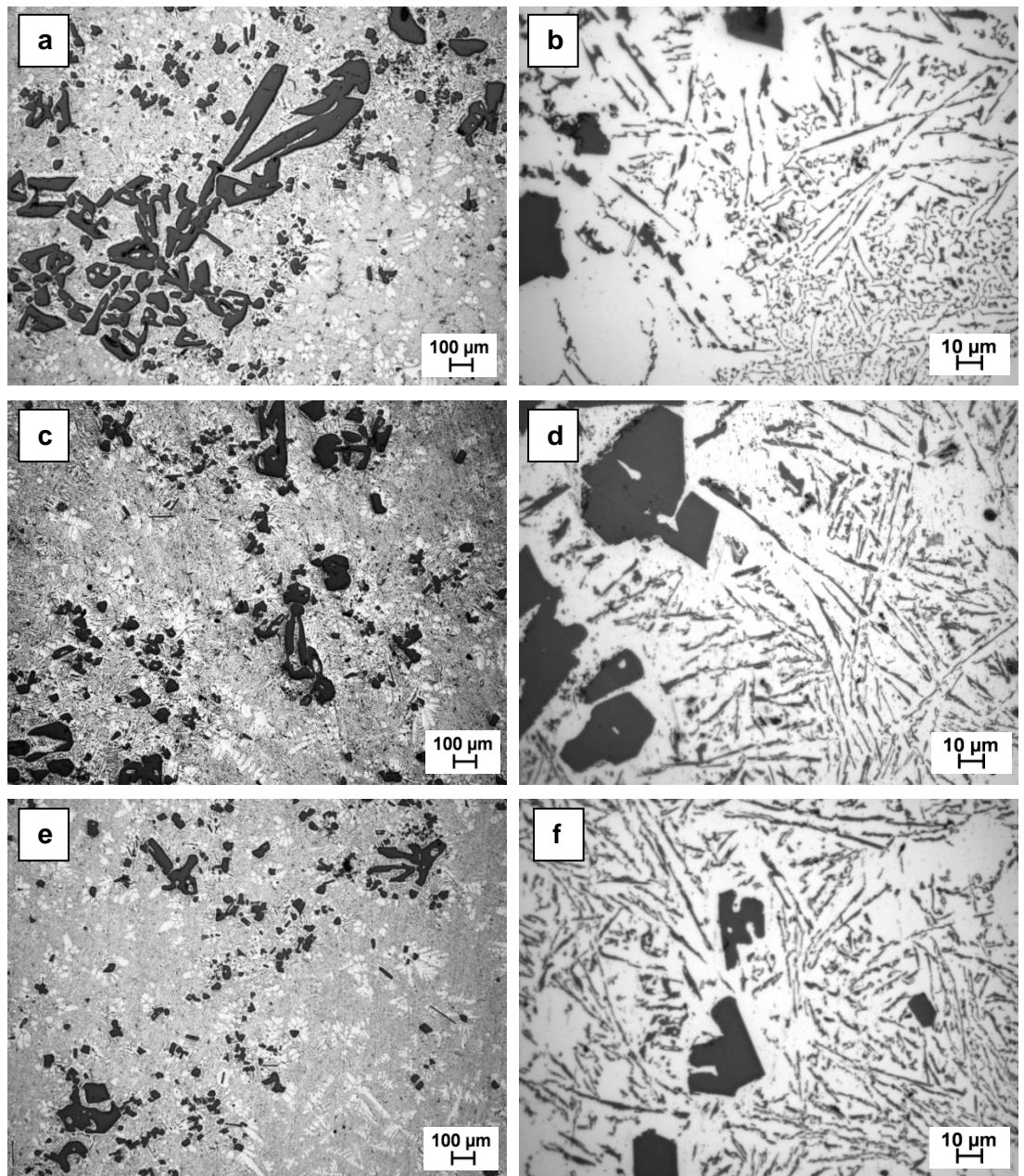


**Figure 4.49** Optical micrographs of Al-19Si+P produced by mixing Al-8Si with: (a,b) Al-30Si alloy (SLD1), (c,d) Al-30Si+50ppm P alloy (SLD2) and (e,f) Al-30Si+100ppm P (SLD3). (a,c & e) low magnification and (b,d & f) high magnification.

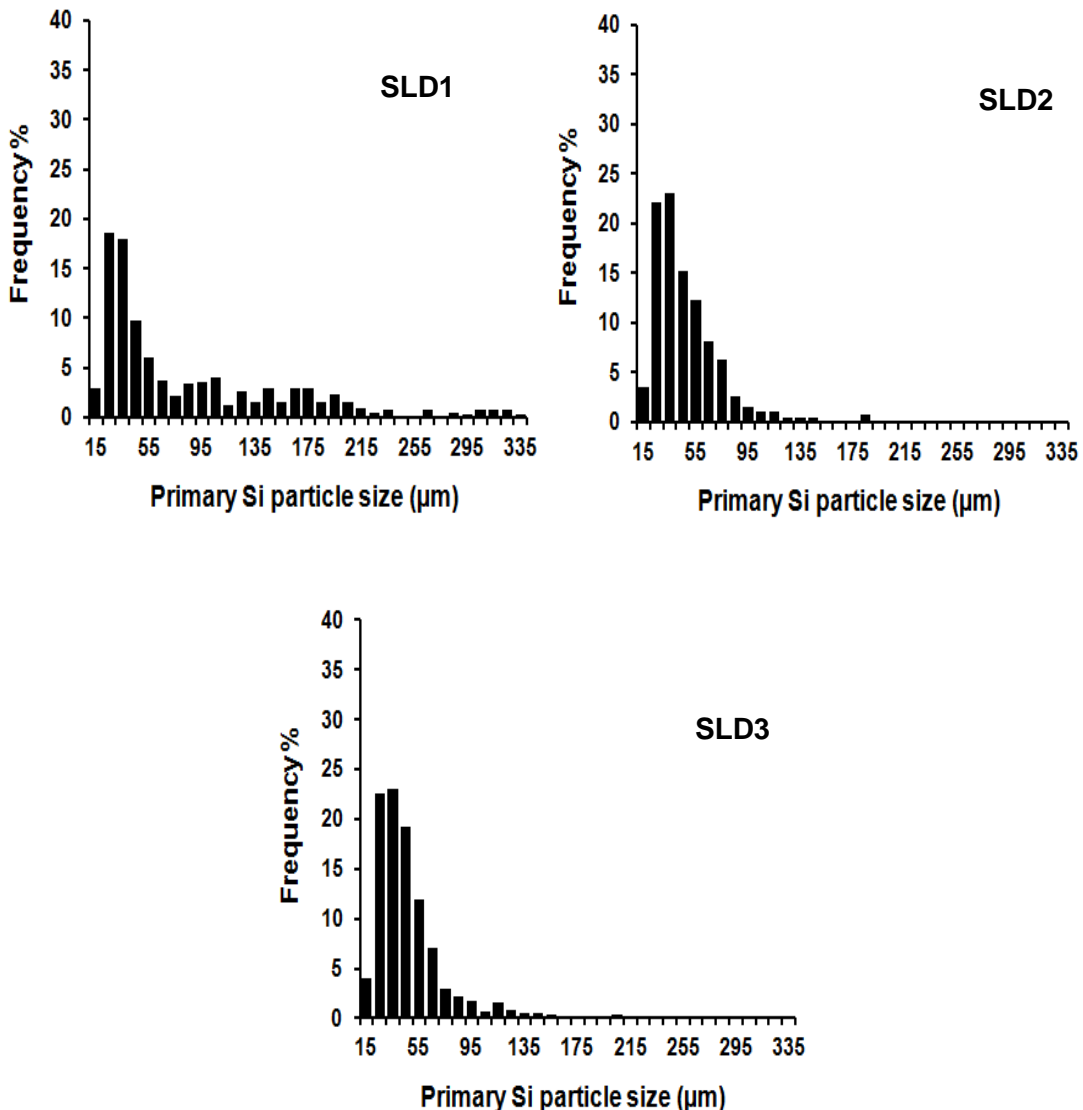


**Figure 4.50** Particle size distribution of primary Si in Al-19Si+P produced by mixing Al-8Si liquid alloy with solid (SLD1) Al-30Si alloy; (SLD2) Al-30Si+50ppm P alloy and (SLD3) Al-30Si+100ppm P.

For the modification of eutectic Al-Si matrix, 400 ppm Sr was added to liquid Al-8Si starting alloy. Figure 4.51 shows optical micrographs of fully modified Al-8Si alloy by the addition of 400ppm Sr addition. Initially, liquid Al-8Si+400 ppm Sr alloy was mixed with solid Al-30Si alloy. Figure 4.52 shows the optical micrographs of Al-19Si+200ppm Sr cast from 610 °C by mixing 1:1 liquid Al-8Si+400ppm Sr and solid Al-30Si alloys (SLD4). There was good modification of the eutectic matrix: the eutectic Si morphology changed from a plate-like to a fibrous structure as shown in Figure 4.52. However, the primary Si was unrefined and with an irregular morphology, with an average particle size of 48.8  $\mu\text{m}$ .

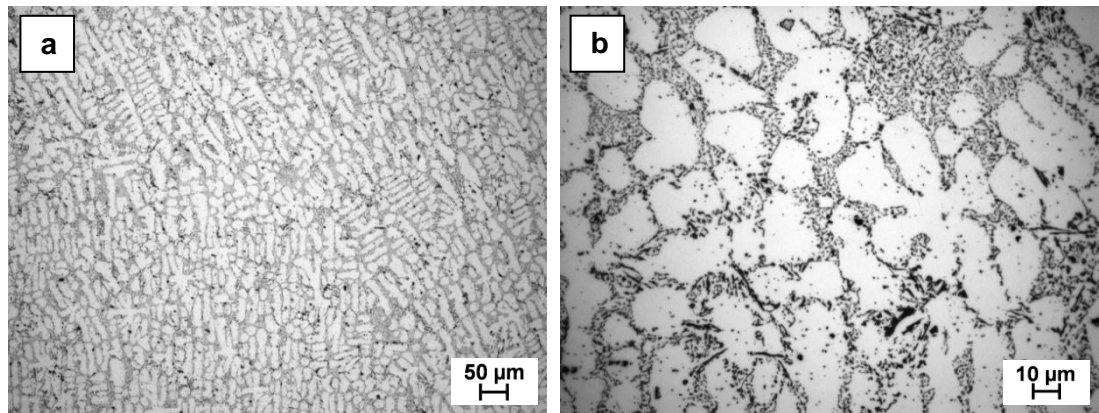


**Figure 4.51** Optical micrographs of Al-8Si+400ppm Sr alloy cast from 800 °C, at (a) low magnification and (b) high magnification.

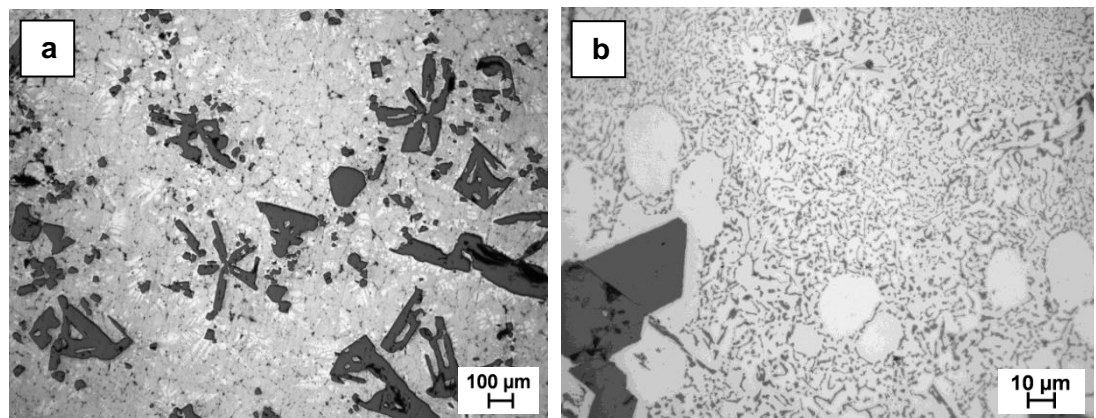


**Figure 4.52** Optical micrographs of Al-19Si+200ppm Sr alloy produced by mixing liquid Al-8Si+400ppm Sr and solid Al-30Si alloys (SLD4), cast from 610 °C, at (a) low magnification and (b) high magnification.

A set of experiments was conducted by mixing liquid Al-8Si+400ppm Sr alloy with solid Al-30Si treated with 50-400 ppm P (SLD5-SLD9). Figure 4.53 shows the optical micrographs of Al-19Si+200ppm Sr+P produced by mixing liquid Al-8Si+400ppm Sr and P-treated Al-30Si solid with different P addition and cast from 610 °C. As shown in Figure 4.53, there was a significant simultaneous refinement of primary Si and modification of eutectic Si. For the same Sr content in the liquid Al-8Si alloy, as the P content increased in the solid Al-30Si starting alloy the mean particle size of primary Si in the target alloy decreased. The average particle size of primary Si was 35, 33, 31, 30 and 29 µm for the Al-30Si starting alloy with 50 (SLD5), 100 (SLD6), 200 (SLD7), 300 (SLD8) and 400 ppm (SLD9) added P respectively, as shown in Figure 4.54. Figure 4.55 shows the particle size distributions of primary Si in Al-19Si+200ppm Sr+P alloy produced by mixing liquid Al-8Si+400ppm Sr and P-treated Al-30Si solid with different

added P and cast from 610 °C (SLD5-SLD9). It is clear that mixing liquid Al-8Si+400ppm Sr with Al-30Si+400ppm P solid (SLD9) using the solid-liquid duplex casting process gave the narrowest particle size range. It is very clear from micrographs in Figure 4.53 that mixing 1:1 (by mass) liquid Al-8Si+400ppm Sr with Al-30Si+400ppm P solid chips (SLD9) using the solid-liquid duplex casting process, allowed for the simultaneous action of P and Sr. The target alloy produced was Al-19Si+200ppm P+200ppm Sr with mean primary Si particle size of 29 µm dispersed in a fully modified Al-Si eutectic matrix, as shown in Figure 4.53 (i,j).

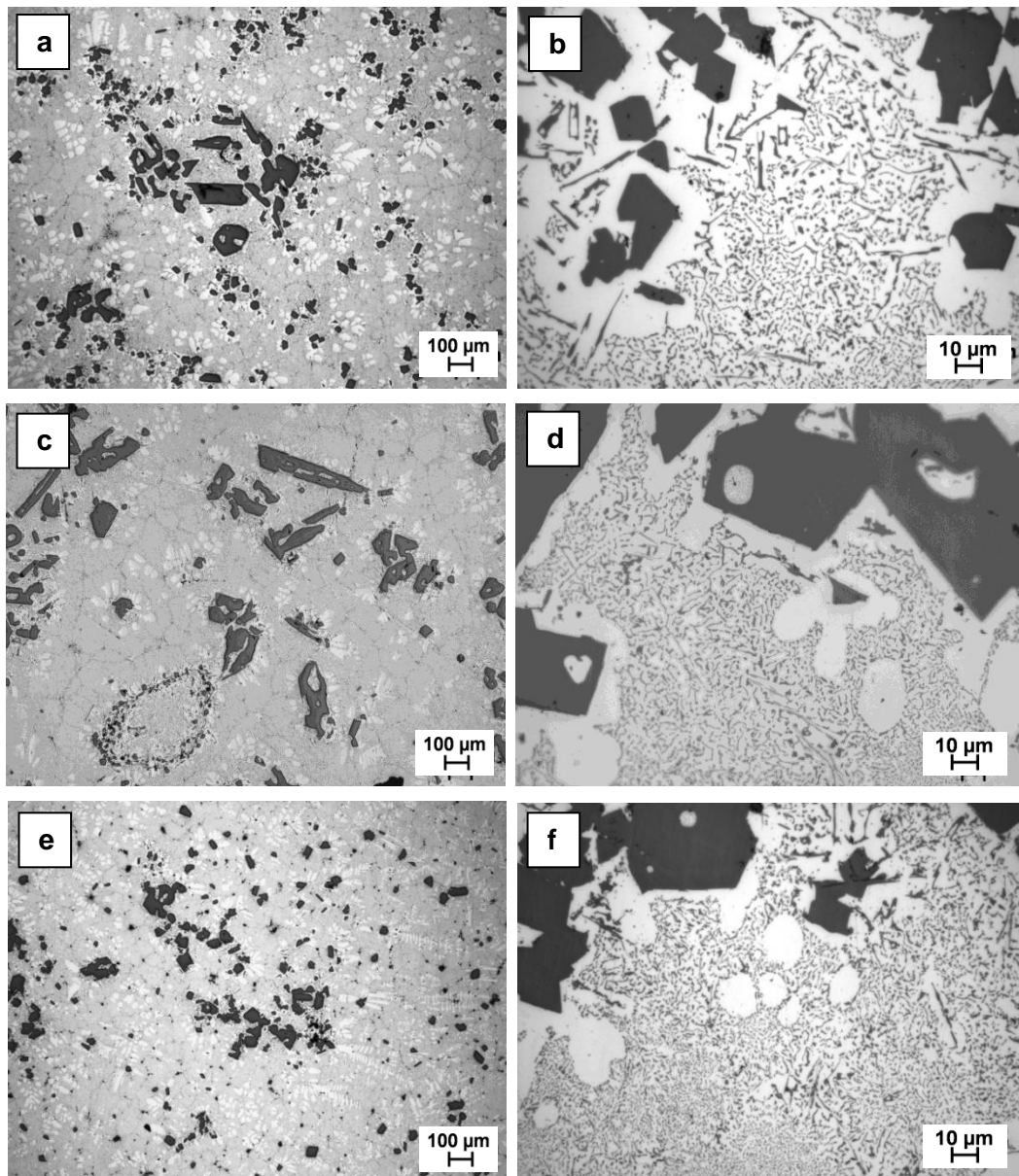


**Figure 4.53** Optical micrographs of Al-19Si+200ppm Sr+P produced by mixing liquid Al-8Si+400ppm Sr with solid (a,b) Al-30Si+50ppm P (SLD5); (c,d) Al-30Si+100ppm P (SLD6); (e,f) Al-30Si+200ppm P (SLD7); (g,h) Al-30Si+300 ppm P (SLD8) and (I,j) Al-30Si+400ppm P (SLD9). (a,c,e,g&i) low magnification and (b,d,f,h&j) high magnification. Continued overleaf.

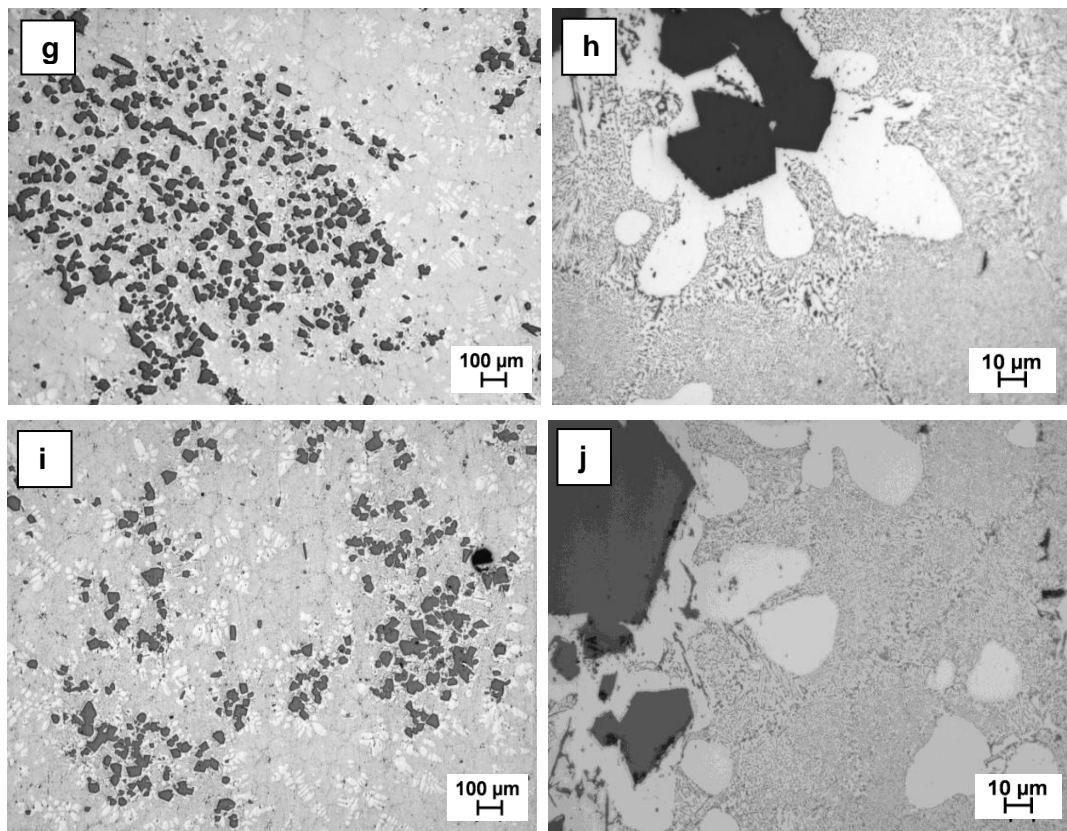


**Figure 4.53** continued

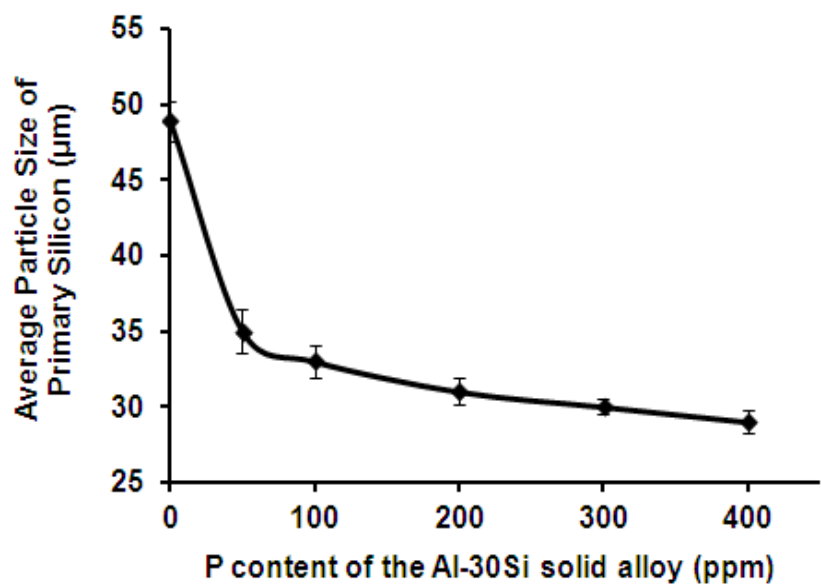


**Figure 4.54** Plot of primary Si particle size in the target alloy against P content of the Al-30Si solid starting alloy when mixed with Al-8Si+400ppm Sr alloy and cast from 610 °C (SLD5-SLD9).

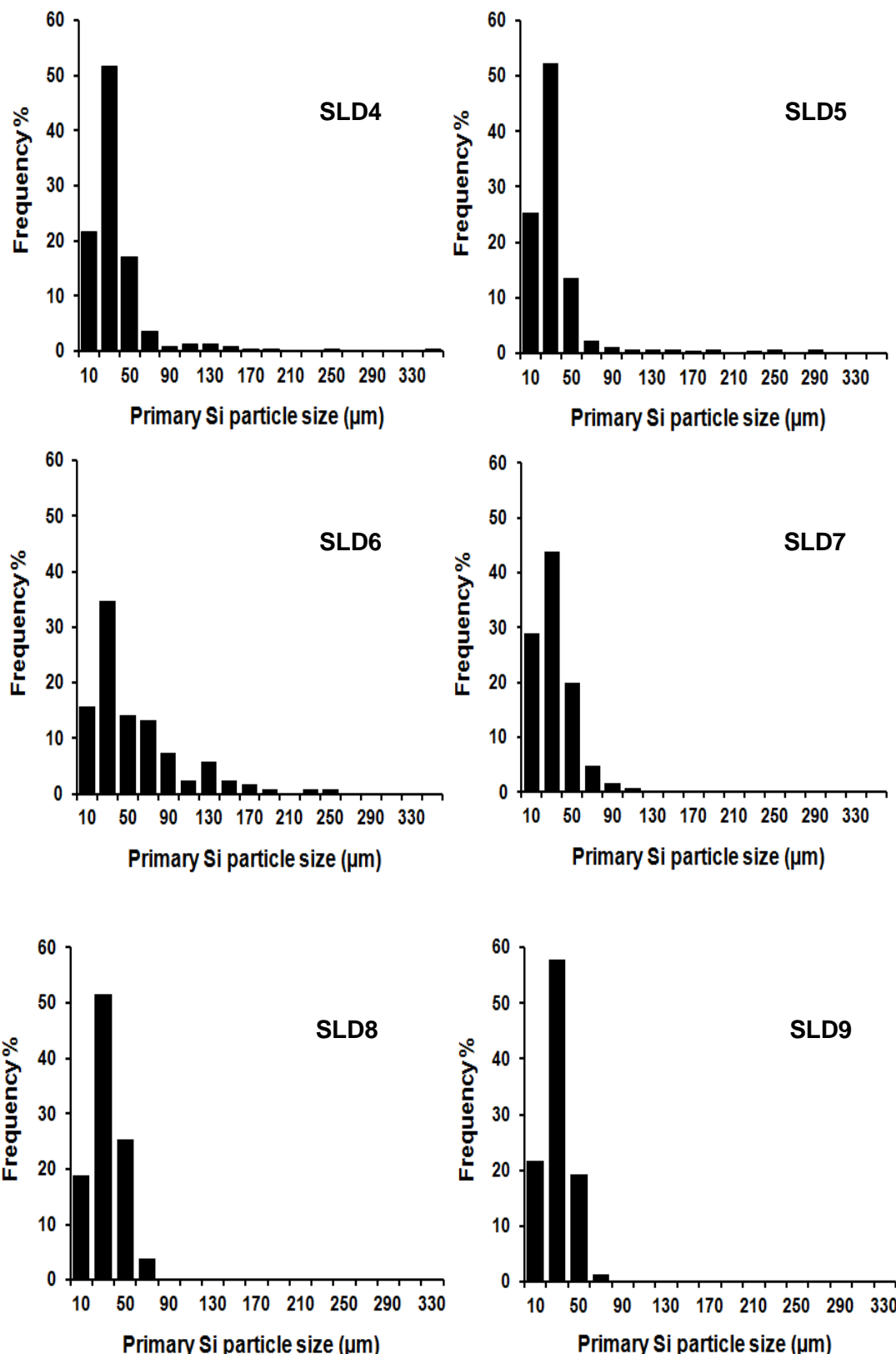


**Figure 4.55** Particle size distribution of primary Si in Al-19Si+200ppm Sr+P produced by mixing liquid Al-8Si+400ppm Sr with solid: (SLD4) Al-30Si; (SLD5)Al-30Si+50ppm P; (SLD6) Al-30Si+100ppm P; (SLD7) Al-30Si+200ppm P; (SLD8) Al-30Si+300ppm P and (SLD9) Al-30Si+400ppm P.

To study the effect of Sr content, another set of experiments was carried out. Figure 4.56 shows optical micrographs of Al-19Si+Sr+200ppm P alloy produced by mixing solid Al-30Si+400ppm P with liquid Al-8Si+300ppm Sr (SLD10) and liquid Al-8Si+200ppm Sr (SLD11) cast from 610 °C.

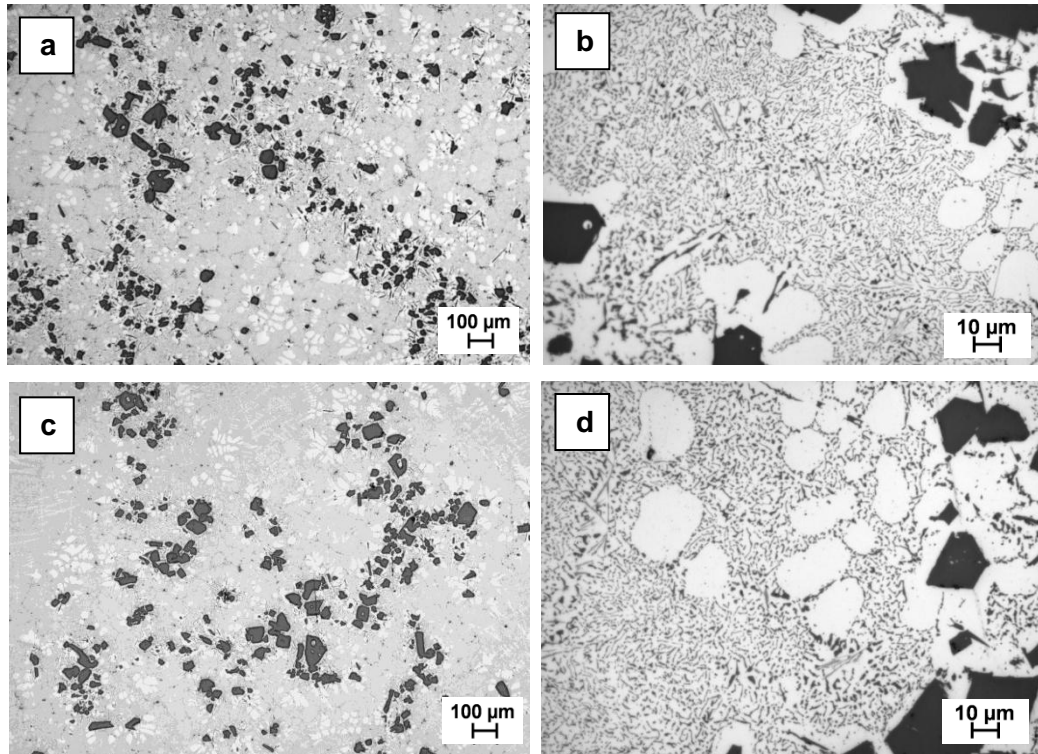


**Figure 4.56** Optical micrographs of Al-19Si+Sr+200ppm P alloy produced by mixing solid Al-30Si+400ppm P with liquid (a,b) Al-8Si+300ppm Sr (SLD10); (c,d) Al-8Si+200ppm Sr (SLD11). (a,c) low magnification and (b,d) high magnification.

As shown in Figure 4.56 with the decrease of Sr less than 400 ppm, there will be only partial modification of the eutectic matrix with an increase in particle size of primary Si. For mixing solid Al-30Si+400ppm P alloy and liquid Al-8Si treated with 300 (SLD10) and 200 ppm Sr (SLD11), the average particle size of primary Si was 29 and 34  $\mu\text{m}$  respectively.

Figure 4.57 shows the morphologies of primary and eutectic Si in the target alloy produced by mixing solid Al-30Si+300ppm P with liquid Al-8Si+300ppm Sr (SLD12) and cast from 610 °C. In the case of mixing solid Al-30Si+300ppm P with liquid Al-8Si+300ppm Sr (SLD12), the resulting alloy was Al-19Si+150ppm Sr+150ppm P and the average particle size of primary Si was 35  $\mu\text{m}$  dispersed in a partially modified Al-Si eutectic as shown in Figure 4.57. Hence with the decrease of Sr and P content there will be an increase in particle size of primary Si and the particle size distribution plots illustrated in Figure 4.58 and Figure 4.59 support this finding.

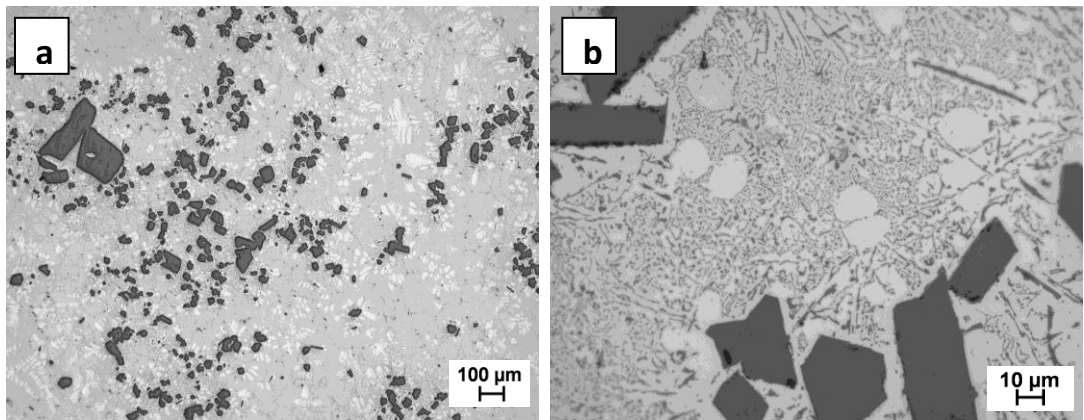


**Figure 4.57** Optical micrographs of Al-19Si+150ppm Sr+150ppm P alloy produced by mixing solid Al-30Si+300ppm P and liquid Al-8Si+300ppm Sr (SLD12) at (a) low magnification and (b) high magnification.

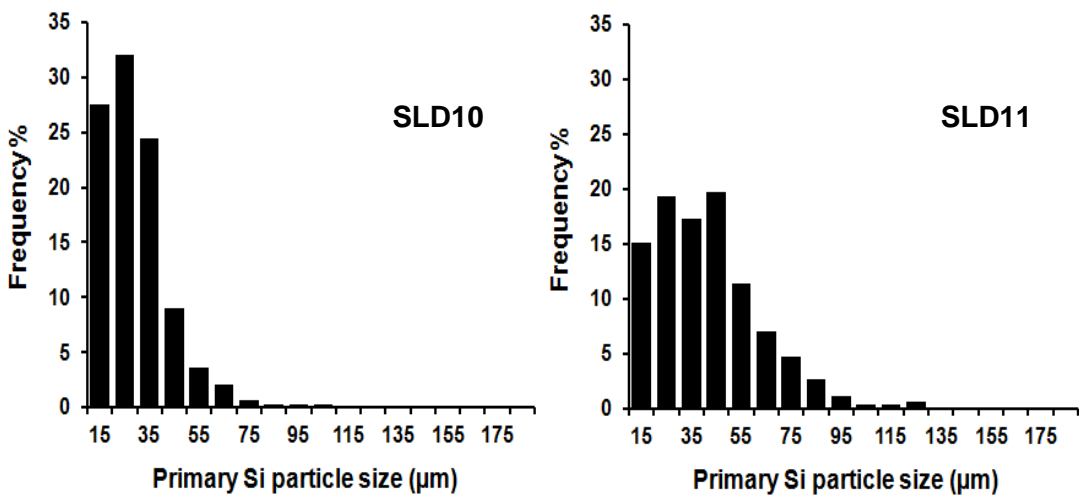


**Figure 4.58** Particle size distributions of primary Si in Al-19Si+Sr+200ppm P alloy produced by mixing solid Al-30Si+400ppm P with liquid: (SLD10) Al-8Si+300ppm Sr and (SLD11) Al-8Si+200ppm Sr.

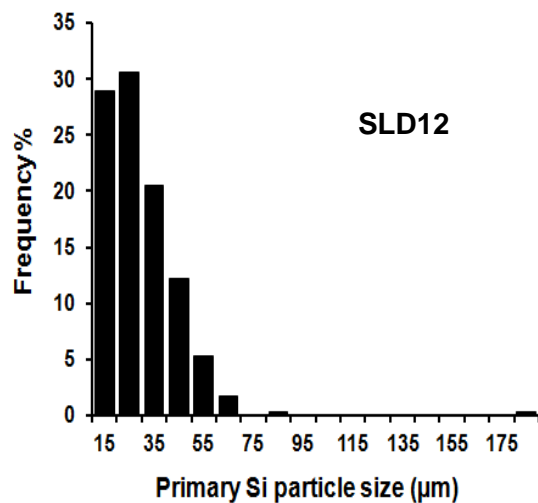


**Figure 4.59** Particle size distribution of primary Si in Al-19Si+150ppm Sr+150ppm P alloy produced by mixing solid Al-30Si+300ppm P and liquid Al-8Si+300ppm Sr (SLD12).

A summary of all above results related to the solid-liquid duplex casting process are summarized in Table (4.2). From all of these results, the optimum amount of P in the solid Al-30Si alloy is 400 ppm and optimum amount of Sr in the target alloy is 200 ppm. These optimum values will allow for simultaneous refinement of primary Si and modification of eutectic Si in the Al-19Si alloy with a good distribution of primary Si particles.

**Table 4.2** Alloying parameters and key microstructural results for solid-liquid duplex casting of a target Al-19Si alloy cast from 610 °C using fixed solid : liquid alloy ratio of 1:1 (by mass). Continued overleaf.

Exp. No.	Starting Alloy 1 (L) at 800 °C				Starting Alloy 2 (S) at 200 °C					Cast Temp. °C	Primary Si size in target alloy (μm)	Al-Si eutectic modification degree
	Comp.	Mass (g)	Mass of Sr (g)	Sr (ppm)	Comp.	Mass (g)	Mass of P (g)	P (ppm)	Primary Si size (μm)			
SLD1	Al-8Si	200	-	-	Al-30Si	200	-	-	158±6.1	610	78±7.4	PL
SLD2	Al-8Si	200	-	-	Al-30Si	200	0.01	50	56±9.2	610	36±4.4	PL
SLD3	Al-8Si	200	-	-	Al-30Si	200	0.02	100	44±5.3	610	34±3.2	PL
SLD4	Al-8Si	200	0.08	400	Al-30Si	200	-	-	158±6.1	610	48.8±1.3	F
SLD5	Al-8Si	200	0.08	400	Al-30Si	200	0.01	50	56±9.2	610	35±1.4	F
SLD6	Al-8Si	200	0.08	400	Al-30Si	200	0.02	100	44±5.3	610	33±1.1	F

L: Liquid      S: Solid      F: Fibrous      PL: Plate-Like

**Table 4.2** Continued

Exp. No.	Starting Alloy 1 (L) at 800 °C				Starting Alloy 2 (S) at 200 °C					Cast Temp. °C	Primary Si size in target alloy (μm)	Al-Si eutectic modification degree
	Comp.	Mass (g)	Mass of Sr (g)	Sr (ppm)	Comp.	Mass (g)	Mass of P (g)	P (ppm)	Primary Si size (μm)			
<b>SLD7</b>	<b>AI-8Si</b>	200	0.08	400	<b>AI-30Si</b>	200	0.04	200	40±8.2	610	31±0.9	F
<b>SLD8</b>	<b>AI-8Si</b>	200	0.08	400	<b>AI-30Si</b>	200	0.06	300	38±7.1	610	30±0.5	F
<b>SLD9</b>	<b>AI-8Si</b>	200	0.08	400	<b>AI-30Si</b>	200	0.08	400	37±5.4	610	29±1.1	F
<b>SLD10</b>	<b>AI-8Si</b>	200	0.06	300	<b>AI-30Si</b>	200	0.08	400	37±5.4	610	29±1.2	F+PL
<b>SLD11</b>	<b>AI-8Si</b>	200	0.04	200	<b>AI-30Si</b>	200	0.08	400	37±5.4	610	34±2.3	F+PL
<b>SLD12</b>	<b>AI-8Si</b>	200	0.06	300	<b>AI-30Si</b>	200	0.06	300	38±7.1	610	35±1.8	F+PL

**L:** Liquid      **S:** Solid      **F:** Fibrous      **PL:** Plate-Like

#### 4.6.2.2 Optimum Si content in Sr-treated Al-Si alloy

Experiments were carried out to optimize the Si content in the Sr-treated liquid Al-Si alloy to be mixed with the solid Al-30Si+400ppm P alloy, and the relative masses of the two starting alloys, cast at 610 °C to produce Al-19Si+P+200ppm Sr alloy. The alloying parameters and experiments codes are provided in Table 4.3.

Figures 4.60-4.63 show morphology of Si phases in the target alloy produced by mixing solid Al-30Si+400ppm P with liquid: commercial purity (CP) Al+540ppm Sr (SLD13), Al-8Si+400ppm Sr (SLD9), Al-12.6Si+317ppm Sr (SLD14) and Al-15Si+274ppm Sr (SLD15) respectively. As shown in Figures 4.60-4.63, in using commercial purity aluminium alloy CPAI+540ppm Sr, Al-8Si+400ppm Sr, Al-12.6Si+317ppm Sr and Al-15Si+274ppm Sr the mean particle size of primary Si in the resulting Al-19Si alloy were 36.2 µm (SLD13), 29 µm (SLD9), 21 µm (SLD14) and 33.9 µm(SLD15) respectively. Furthermore, in the latter case (SLD15) there were occasional very coarse irregular primary Si particles. Accordingly the optimum Si content in Sr-treated melt for the solid-liquid duplex casting process is the eutectic composition i.e. Al-12.6Si, to produce Al-19Si+148ppm P+200ppm Sr as shown in Figure 4.64 which is a plot of average primary Si particle size against Si content of the liquid starting alloy. The particle size distribution of primary Si for this set of experiments is shown in Figure 4.65. It is clear that eutectic composition of the Sr-treated liquid alloy (SLD14) gave the narrowest range of primary Si particle size. A summary of all the above results related to optimum Si content in Sr-treated liquid Al-Si alloy for the solid-liquid duplex casting process is provided in Table 4.3. The optimum Si content in Sr-treated melt for the solid-liquid duplex casting process is the eutectic composition, i.e. Al-12.6Si. This optimum value will allow for simultaneous refinement of primary Si and modification of eutectic Si in the Al-19Si alloy.

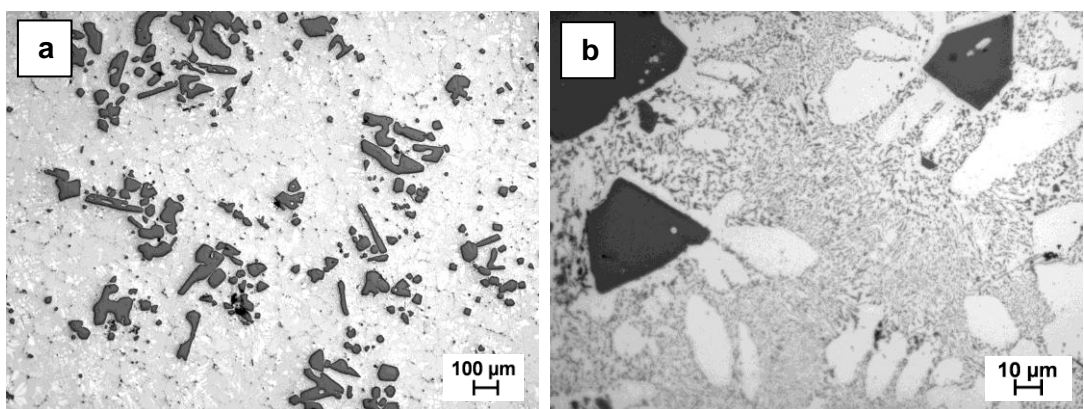


**Figure 4.60** Optical micrographs of Al-19Si+252ppm P+200ppm Sr alloy produced by mixing solid Al-30Si+400ppm P alloy with liquid CP Al+540ppm Sr alloy cast from 610 °C (SLD13) (a) low magnification and (b) high magnification.

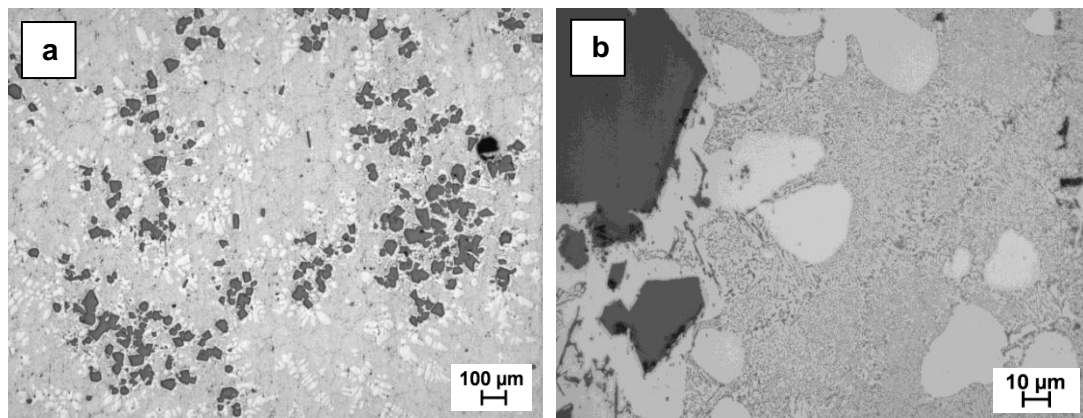


**Figure 4.61** Optical micrographs of Al-19Si+200ppm P+200ppm Sr alloy produced by mixing solid Al-30Si+400ppm P alloy with liquid Al-8Si+400ppm Sr alloy cast from 610 °C (SLD9) (a) low magnification and (b) high magnification.

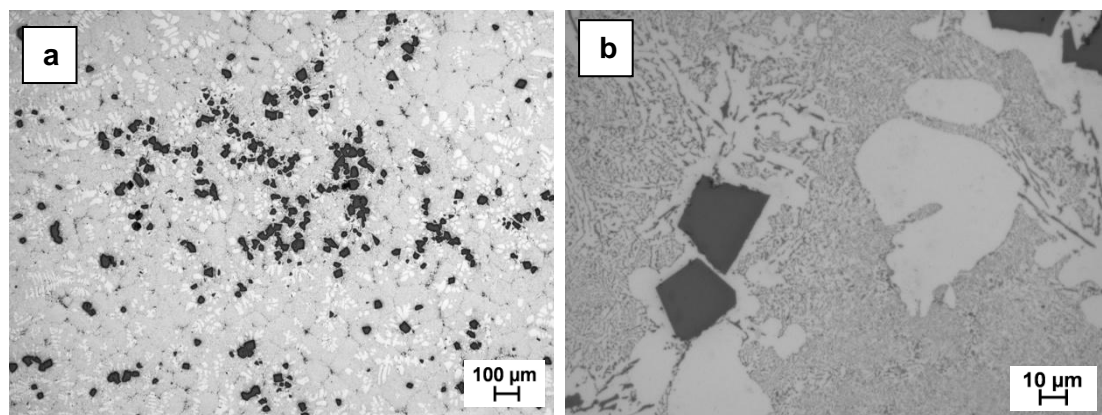


**Figure 4.62** Optical micrographs of Al-19Si+148ppm P+200ppm Sr alloy produced by mixing solid Al-30Si+400ppm P alloy with liquid Al-12.6Si+317ppm Sr alloy cast from 610 °C (SLD14) (a) low magnification and (b) high magnification.

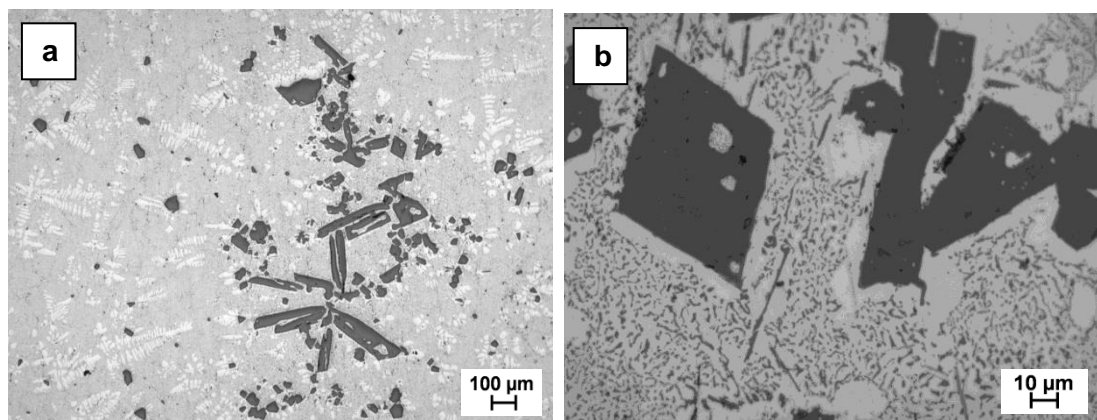


**Figure 4.63** Optical micrographs of Al-19Si+108ppm P+200ppm Sr alloy produced by mixing solid Al-30Si+400ppm P alloy with liquid Al-15Si+274ppm Sr alloy cast from 610 °C (SLD15) (a) low magnification and (b) high magnification.

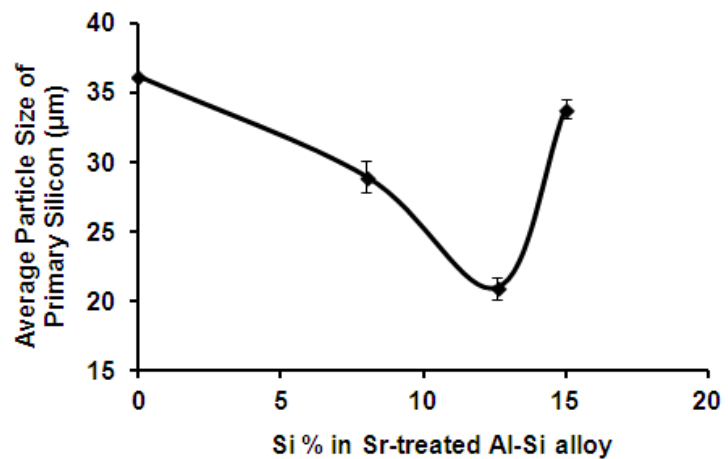


**Figure 4.64** Plot of average primary Si particle size in the Al-19Si target alloy against Si content of the liquid Sr-treated Al-Si starting alloy (SLD13, 9, 14, 15).

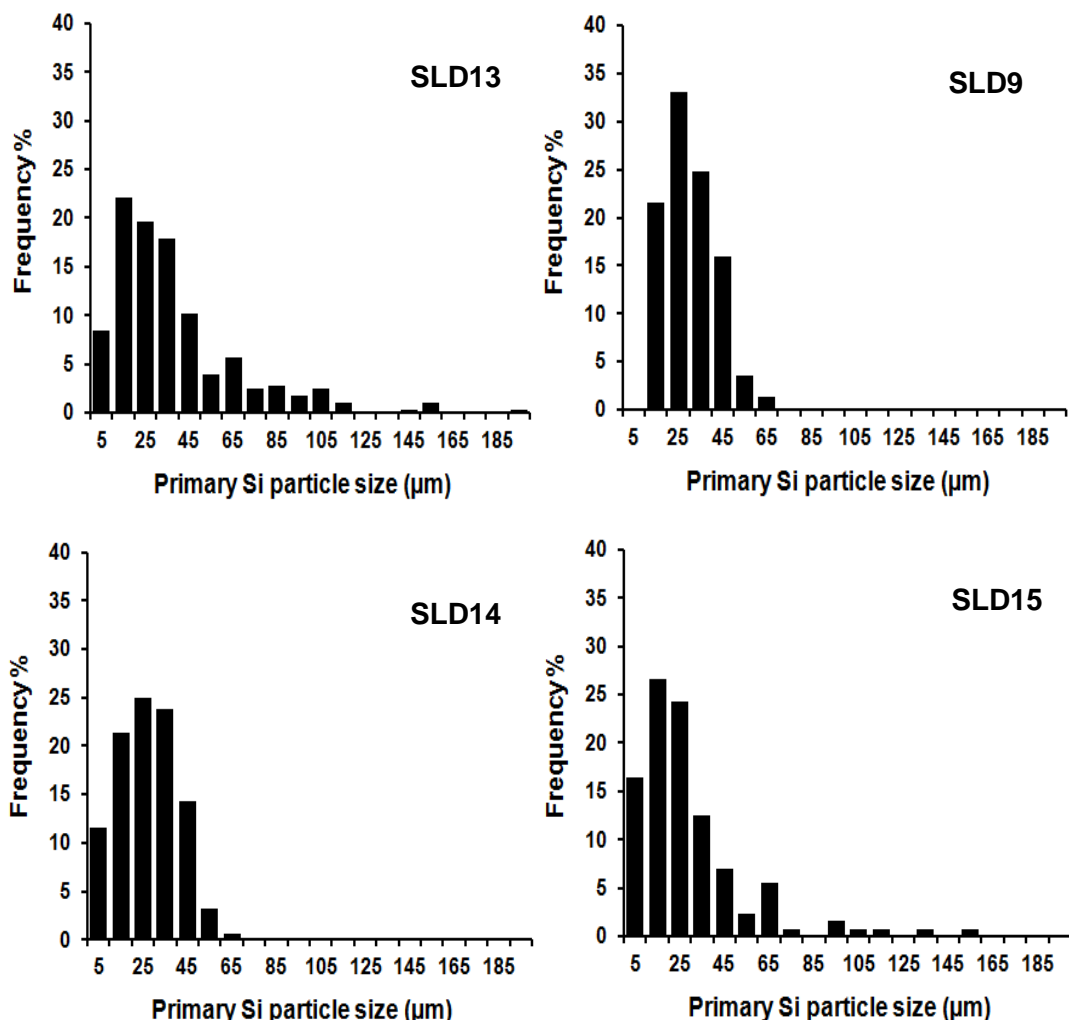


**Figure 4.65** Particle size distribution of primary Si in Al-19Si+P+Sr alloy cast from 610 °C produced by mixing: (SLD13) solid Al-30Si+400ppm P alloy with liquid CPAI+540ppm Sr alloy; (SLD9) solid Al-30Si+400ppm P alloy with liquid Al-8Si+400ppm Sr alloy; (SLD14) solid Al-30Si+400ppm P alloy with liquid Al-12.6Si+317ppm Sr alloy and (SLD15) solid Al-30Si+400ppm P alloy with liquid Al-15Si+274ppm Sr alloy.

**Table 4.3** Alloying parameters and key microstructural results for solid-liquid duplex casting of a target Al-19Si alloy cast from 610 °C varying Si content of the low Si liquid alloy and the associated solid alloy : liquid alloy mass ratio.

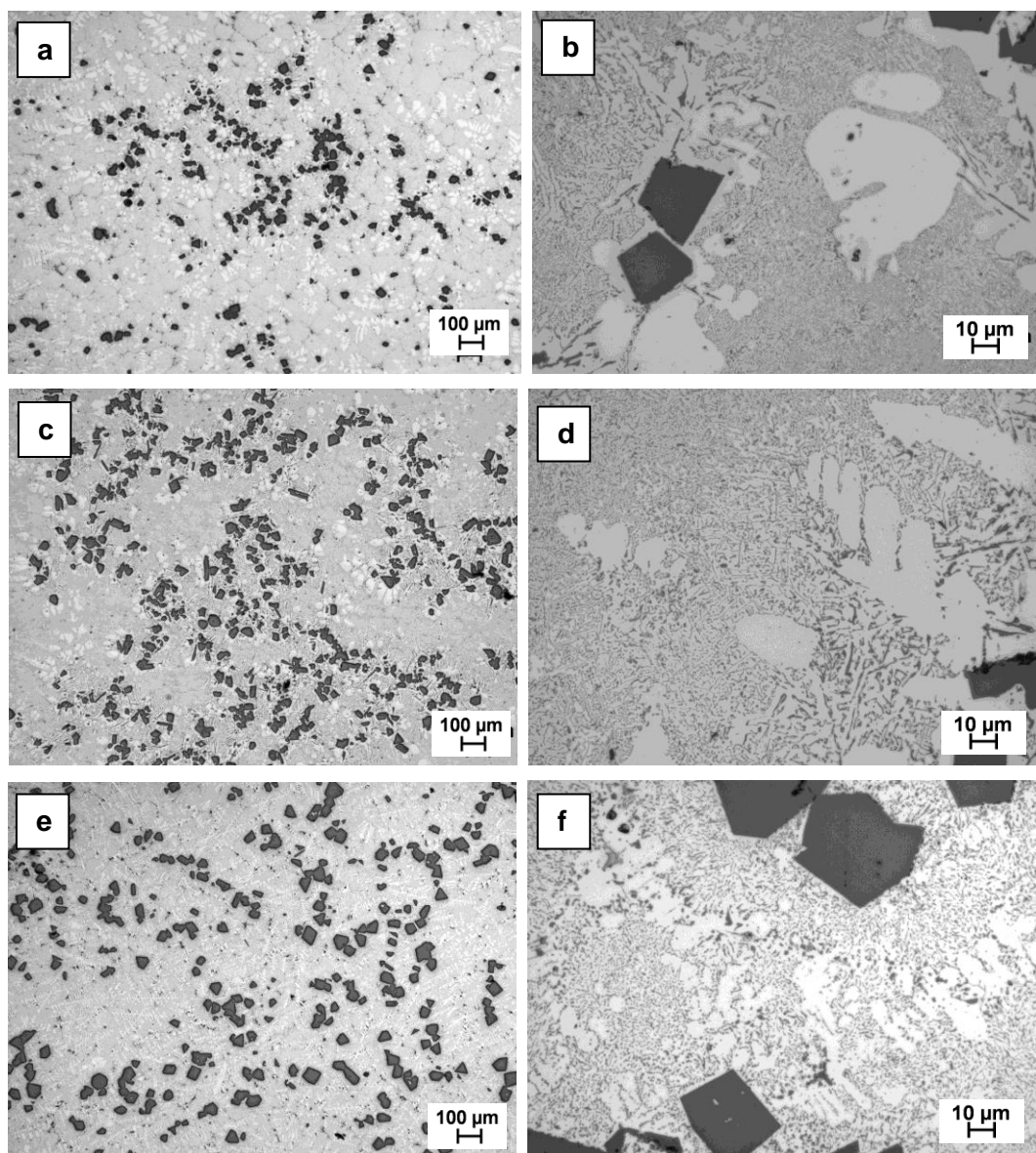
Exp. No.	Starting Alloy 1 (L) at 800 °C				Starting Alloy 2 (S) at 200 °C				Cast Temp. °C	Final content of P and Sr ( Al-Si eutectic modification degree )	Primary Si size in target alloy ( $\mu\text{m}$ )
	Comp.	Mass (g)	Mass of Sr (g)	Sr (ppm)	Comp.	Mass (g)	Mass of P (g)	p (ppm)			
SLD13	CP Al	148	0.08	540	Al-30Si	252	0.10	400	610	252ppm P+200ppm Sr ( Fibrous )	36.2±0.1
SLD9	Al-8Si	200	0.08	400	Al-30Si	200	0.08	400	610	200ppm P+200ppm Sr ( Fibrous )	29±1.1
SLD14	Al-12.6Si	252	0.08	317	Al-30Si	148	0.06	400	610	148ppm P+200ppm Sr ( Fibrous )	21±0.8
SLD15	Al-15Si	292	0.08	274	Al-30Si	108	0.04	400	610	108ppm P+200ppm Sr ( Fibrous )	33.9±0.7

L: Liquid      S: Solid

#### 4.6.2.3 Effect of casting temperature

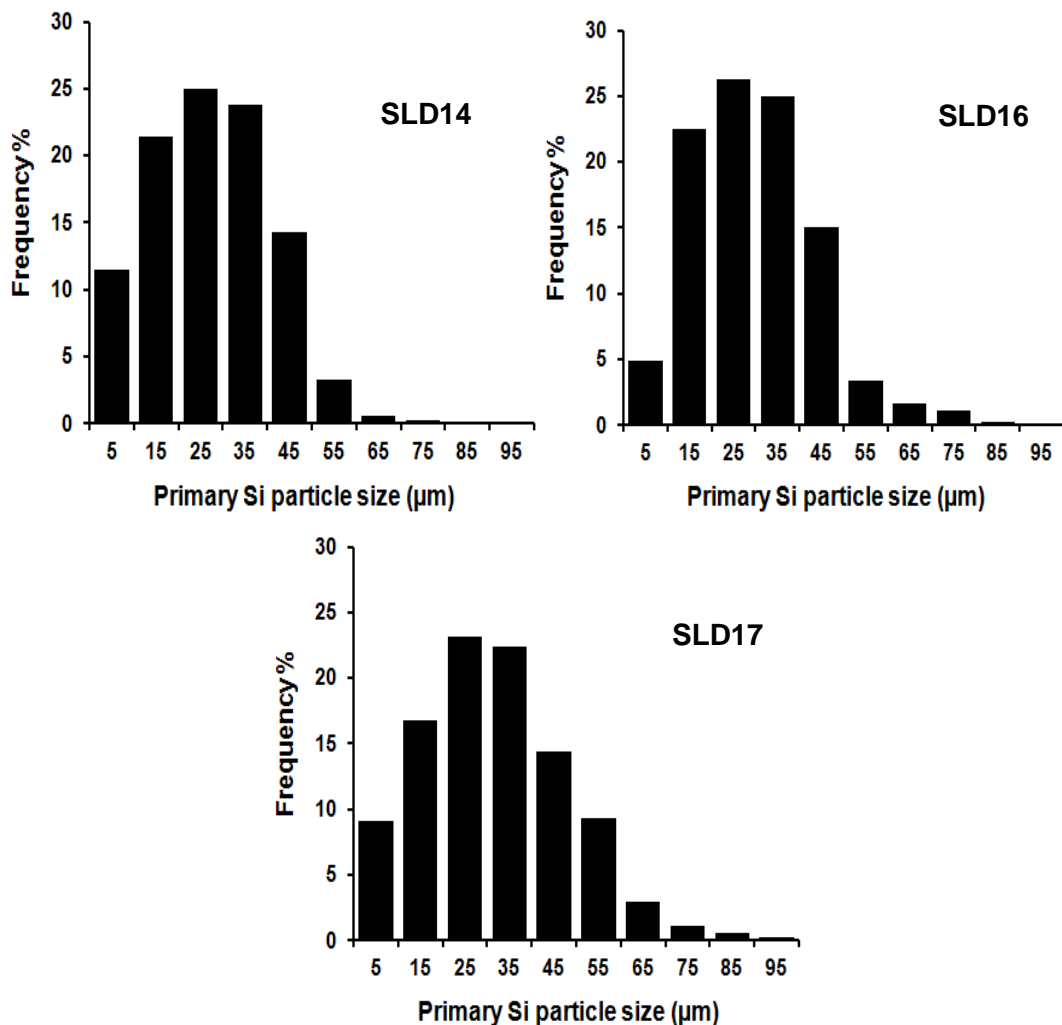
In the previously described experiments for solid-liquid duplex process, the casting temperature was 610 °C i.e. in a semi-solid condition. In order to study the effect of casting temperature, experiments were conducted in the duplex process by mixing solid Al-30Si+400ppm P alloy with liquid Al-12.6Si+317ppm Sr melt to produce the target alloy Al-19Si+148ppm P+200ppm Sr. The casting temperatures were 610 °C, 710 °C and 750 °C. The experimental details and results are provided in Table 4.4.

Figure 4.66 shows the morphologies of primary and eutectic Si of the Al-19Si target alloy produced by mixing solid Al-30Si+400ppm P with liquid Al-12.6Si+317ppm Sr cast from 610 °C (SLD14), 710 °C (SLD16) and 750 °C (SLD17).



**Figure 4.66** Optical micrographs of Al-19Si+148ppm P+200 ppm Sr alloy produced by mixing solid Al-30Si+400ppm P with liquid Al-12.6Si+317ppm Sr cast from: (a,b) 610 °C (SLD14); (c,d) 710 °C (SLD16) and (e,f) 750 °C (SLD17). (a,c & e) low magnification and (b,d & f) high magnification.

As shown in Figure 4.66 with the increase of casting temperature, the size of primary Si particles increased and they were uniformly distributed in a modified eutectic Si matrix. Figure 4.67 shows the particle size distributions of primary Si in Al-19Si +148ppm P+200ppm Sr alloy produced by solid-liquid duplex casting process at different casting temperatures. The range of particle size of primary Si increased with the increase of casting temperature as shown in Figure 4.67. The measured average particle size of primary Si in the target alloy was 21, 25 and 29  $\mu\text{m}$  for casting temperatures of 610 °C (SLD14), 710 °C (SLD16) and 750 °C (SLD17) respectively as shown in Figure 4.68 which is a plot of average primary Si particle size against casting temperature of Al-19Si+148ppm P+200ppm Sr alloy produced by the solid-liquid duplex casting process. A summary of all above results related to the effect of casting temperature for the solid-liquid duplex casting process is provided in Table 4.4.



**Figure 4.67** Particle size distribution of primary Si in Al-19Si+148ppm P+200ppm Sr alloy produced by mixing solid Al-30Si+400ppm P with liquid Al-12.6Si+317ppm Sr cast from: (SLD14) 610 °C; (SLD16) 710 °C and (SLD17) 750 °C.

**Table 4.4** Alloying parameters and key microstructural results for solid-liquid duplex casting of a target Al-19Si alloy produced by mixing solid Al-30Si+400ppm P with liquid Al-12.6Si+317ppm Sr cast from different casting temperatures. In addition to SLD18 in which Al-19Si+200ppm P+200ppm Sr alloy produced by solid-liquid duplex process, cast from 610 °C.

Exp. No.	Starting Alloy 1 (L) at 800 °C				Starting Alloy 2 (S) at 200 °C				Cast Temp. °C	Final content of P and Sr ( Al-Si eutectic modification degree )	Primary Si size in target alloy (µm)
	Comp.	Mass (g)	Mass of Sr (g)	Sr (ppm)	Comp.	Mass (g)	Mass of P (g)	p (ppm)			
SLD14	Al-12.6Si	252	0.08	317	Al-30Si	148	0.06	400	610	148ppm P+200ppm Sr ( Fibrous )	21±0.8
SLD16	Al-12.6Si	252	0.08	317	Al-30Si	148	0.06	400	710	148ppm P+200ppm Sr ( Fibrous )	26±0.3
SLD17	Al-12.6Si	252	0.08	317	Al-30Si	148	0.06	400	750	148ppm P+200ppm Sr ( Fibrous )	29±0.6
SLD18	Al-12.6Si	252	0.08	317	Al-30Si	148	0.08	540	610	200ppm P+200ppm Sr ( Fibrous )	21±1.1

L: Liquid      S: Solid

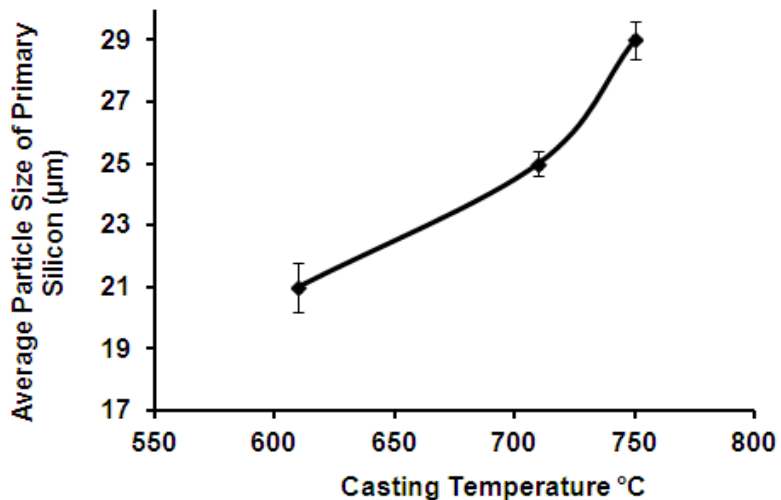


**Figure 4.68** Plot of average primary Si particle size in Al-19Si+148ppm P+200ppm Sr alloy produced by solid-liquid duplex casting process against casting temperature (SLD14, 16, 17).

Since in the case of SLD16 & SLD17 the casting was above the liquidus temperature, it is effectively no longer solid-liquid duplex casting and the pre-refined primary Si should have melted. The above results show that casting at higher temperature in the solid-liquid duplex process can give a refined primary Si with a good distribution in a modified Al-Si eutectic matrix. This indicates that the AIP particles are remain isolated from the Sr modifier in the Sr-treated Al-Si starting alloy so there was no loss in modification. To check this hypothesis, another experiment was conducted by adding 200 ppm P to Al-19Si alloy melted at 800 °C. After 20 min this alloy was cooled downed to about 700 °C and 200 ppm Sr was added to the melt with gentle stirring and cast from 610 °C. Figure 4.69 shows the morphologies of Si of the Al-19Si+200ppm P+200ppm Sr produced by adding 200ppm Sr to Al-19Si+200ppm P at 700 °C then cast from 610 °C after 20 min. As shown in Figure 4.69 (a,b) the mean particle size of primary Si was refined to 22 μm and the eutectic Si had a fibrous structure. Figure 4.70 shows the particle size distribution of primary Si in the Al-Si eutectic matrix. Figure 4.70 confirms the improved refinement of primary Si using the latter process.

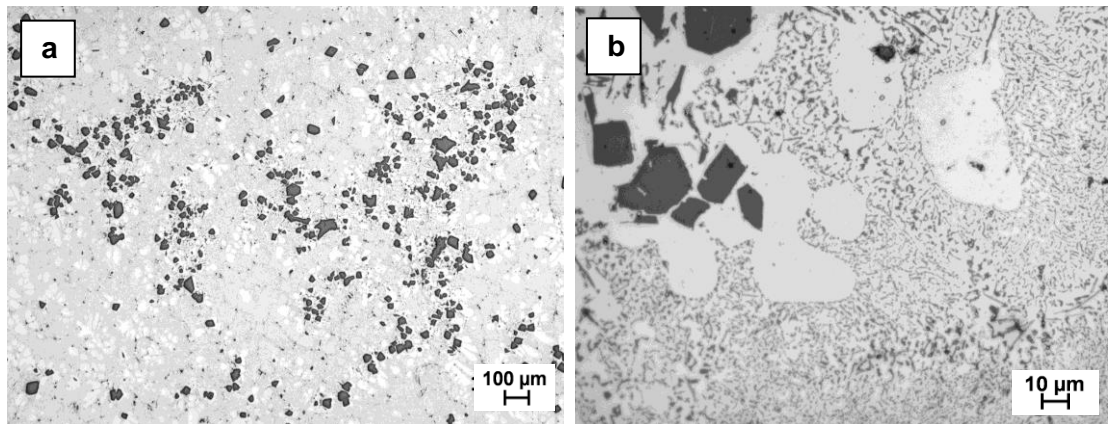


**Figure 4.69** Optical micrographs of Al-19Si+200ppm P+200ppm Sr alloy produced by: conventional casting process of Al-19Si+200ppm P cooled down from 800 °C to 700 °C then adding 200 ppm Sr, cast from 610 °C. (a) low magnification and (b) high magnification.

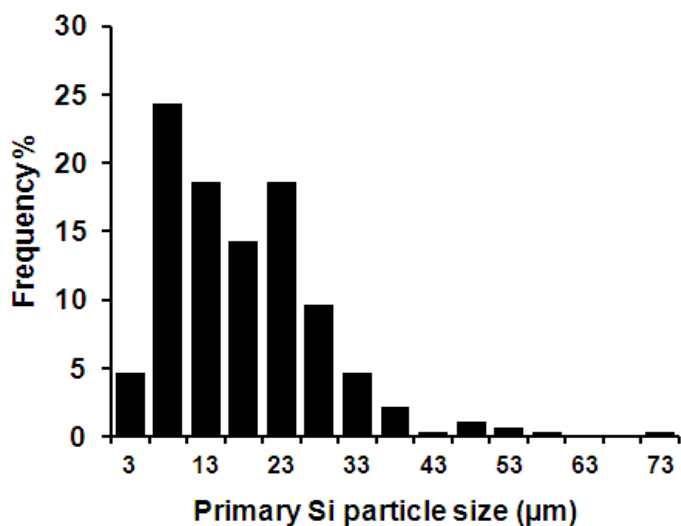


**Figure 4.70** Particle size distribution of primary Si in Al-19Si+200ppm P+200 ppm Sr produced by conventional casting process of Al-19Si+200ppm P cooled down from 800 °C to 700 °C then adding 200ppm Sr, cast from 610 °C.

#### 4.6.2.4 Comparison between the solid-liquid duplex and conventional casting processes

In order to evaluate the solid-liquid duplex casting process, Al-19Si+200ppm P +200ppm Sr alloy was produced by both conventional and duplex casting processes. The optical micrographs in Figure 4.71 show the morphologies of primary and eutectic Si in the Al-19Si+200ppm P+200ppm Sr target alloy produced by conventional casting process by adding 200ppm P and 200ppm Sr and casting from 800 °C and by the solid-liquid duplex casting process by mixing solid Al-30Si+540ppm P with liquid

Al-12.6Si+317ppm Sr cast from 610 °C (SLD18 in Table 4.4). As shown in Figure 4.71 (c,d) the mean particle size of primary Si was refined to less than 21 µm and the eutectic Si had a fibrous structure. In using the conventional casting process as discussed in section 4.6.1, the mean particle size of primary Si was 26 µm dispersed in a partially modified Al-Si eutectic matrix, as shown in Figure 4.71 (a,b). Figure 4.72 compares the primary Si particle size distribution of Al-19Si alloy treated with 200ppm P and 200ppm Sr cast conventionally and produced by using solid-liquid duplex casting approach. Figure 4.72 confirms the further refinement of primary Si using the solid-liquid duplex casting process.

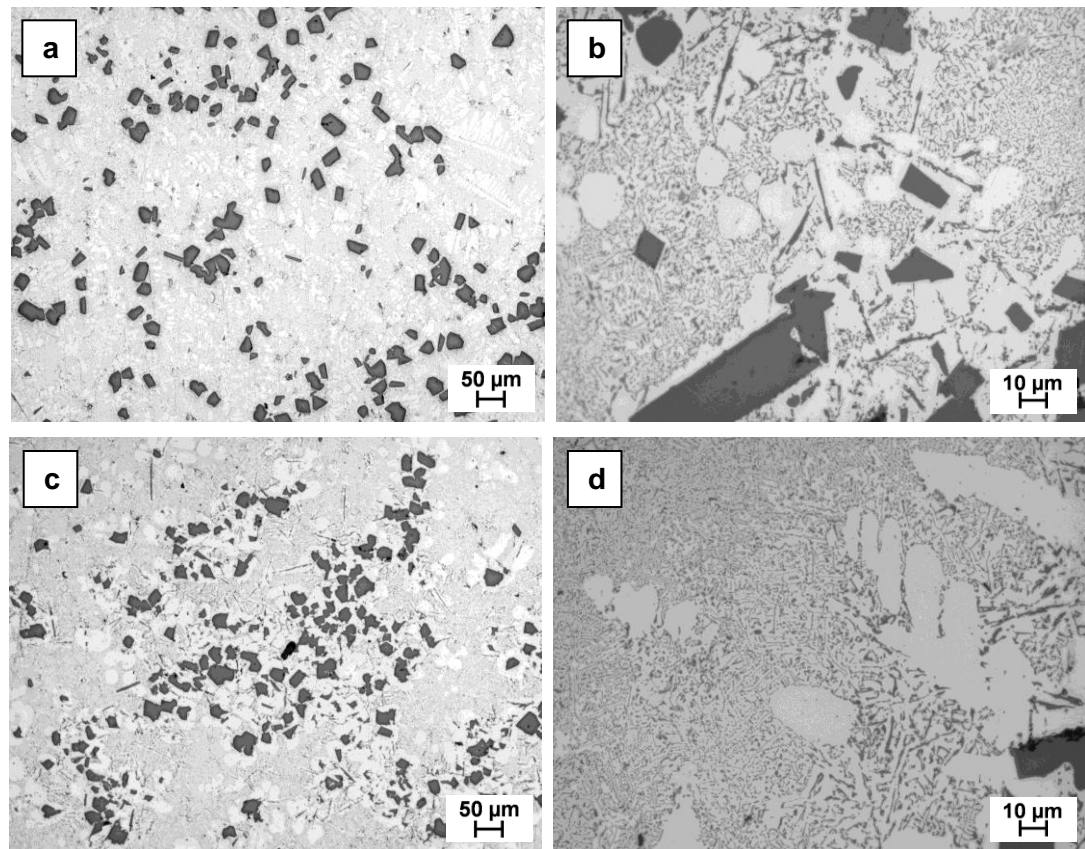


**Figure 4.71** Optical micrographs of Al-19Si+200ppm P+200ppm Sr alloy produced by: (a,b) conventional casting process at 800 °C, (c,d) solid-liquid duplex casting process 610 °C (SLD18). (a,c) low magnification and (b,d) high magnification.

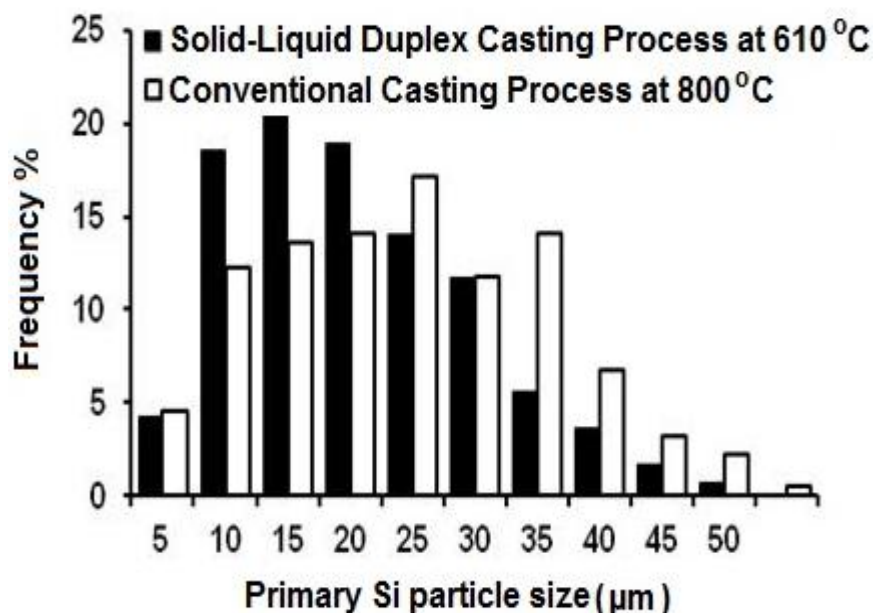
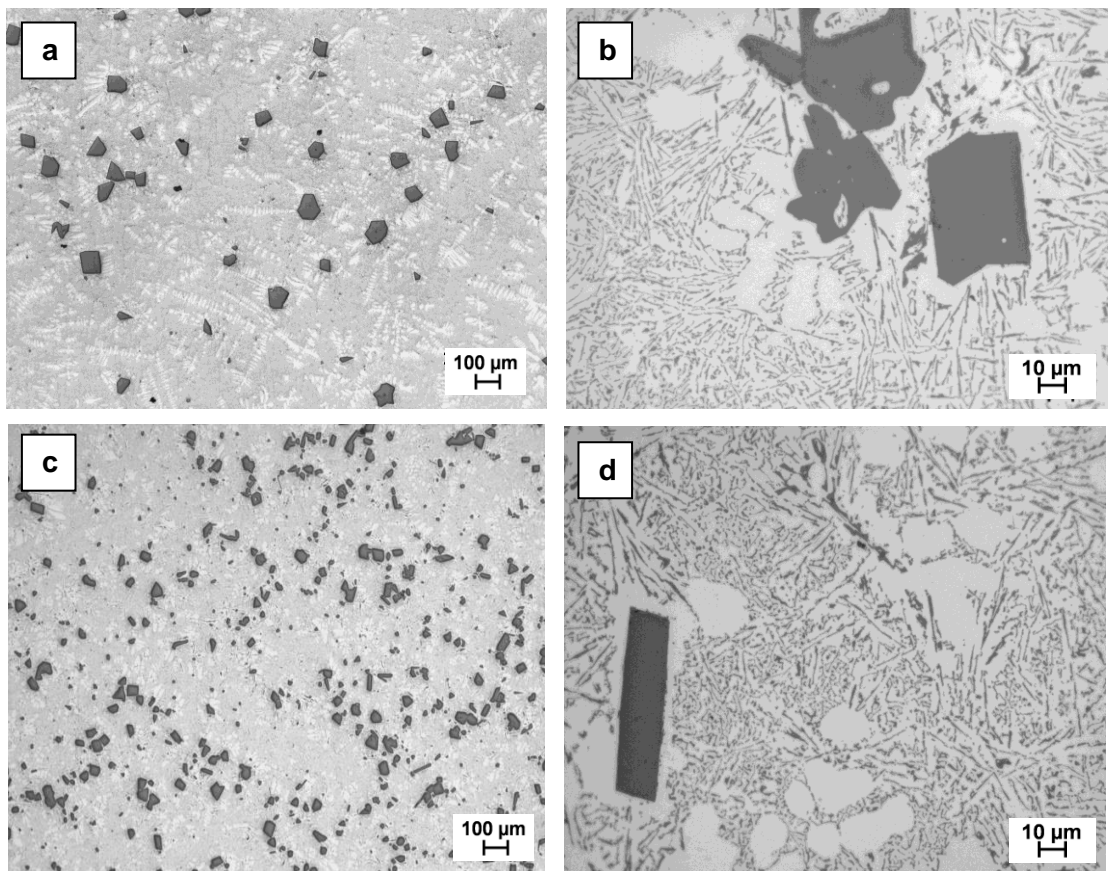


**Figure 4.72** Particle size distribution of primary Si in Al-19Si+200ppm P+200ppm Sr produced by the solid-liquid duplex (SLD18) and conventional casting processes.

#### 4.6.2.5 Application of the solid-liquid duplex process for producing Al-18Si alloy

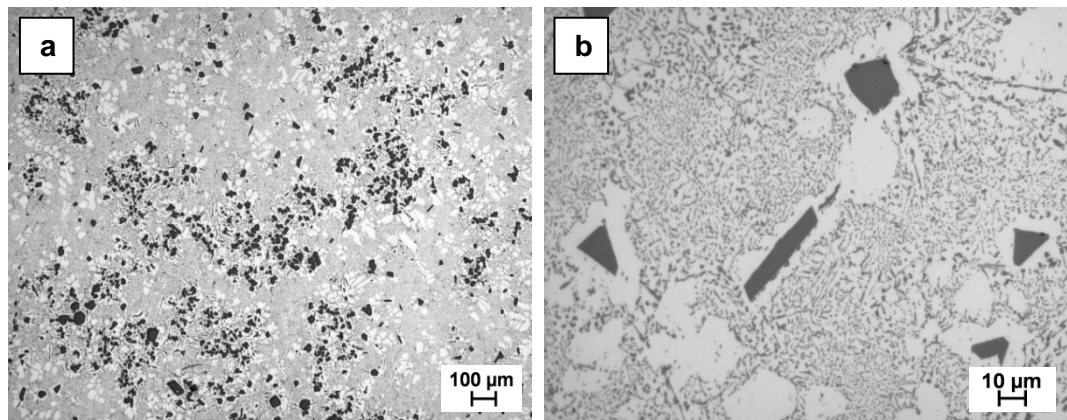
For the production of another target alloy such as Al-18Si with simultaneous refinement of primary Si and modification of eutectic Si, a further experiment was carried out by applying the solid-liquid duplex casting process. In this experiment P-treated Al-24Si with 100ppm P solid alloy was mixed with Sr-treated Al-12.6Si+400ppm Sr molten alloy to provide an Al-18Si alloy in the Liquid + Primary Si phase field and then cast from 610 °C. The resultant alloy was Al-18Si+50ppm P+200ppm Sr.

Figure 4.73 shows typical microstructures of conventionally cast Al-18Si without and with addition of Sr and P. The untreated Al-18Si (Figure 4.73 (a,b)) contained coarse primary Si with average particle size of approximately 50  $\mu\text{m}$  and the eutectic Si had a mostly plate-like morphology as shown in Figure 4.73b. The conventionally cast Al-18Si treated with both P and Sr contained refined primary Si particles with average particle size of 20  $\mu\text{m}$  dispersed in a partially modified Al-Si eutectic matrix, as shown in Figure 4.73 (c,d).



**Figure 4.73** Optical micrographs of conventionally cast Al-18Si alloy: (a,b) Al-18Si without P and Sr and (c,d) Al-18Si+50ppm P+200ppm Sr. (a,c) low magnification to show the size and distribution of primary Si, (b,d) high magnification to show the eutectic structure.

Typical microstructures of Al-18Si treated with P and Sr using the solid-liquid duplex casting process are provided in Figure 4.74. The mean particle size of primary Si was duly more refined than the conventionally cast alloy to less than 15  $\mu\text{m}$  and the eutectic Si had a fibrous structure typical of a fully modified eutectic.



**Figure 4.74** Optical micrographs of Al-18Si+50ppm P+200ppm Sr produced by the solid-liquid duplex casting process cast at 610  $^{\circ}\text{C}$ . (a) low magnification and (b) high magnification.

Figure 4.75 compares the primary Si particle size distribution of Al-18Si treated with 50ppm P and 200ppm Sr cast conventionally and using the solid-liquid duplex casting approach. Figure 4.75 confirms the improved refinement of primary Si using the latter process.

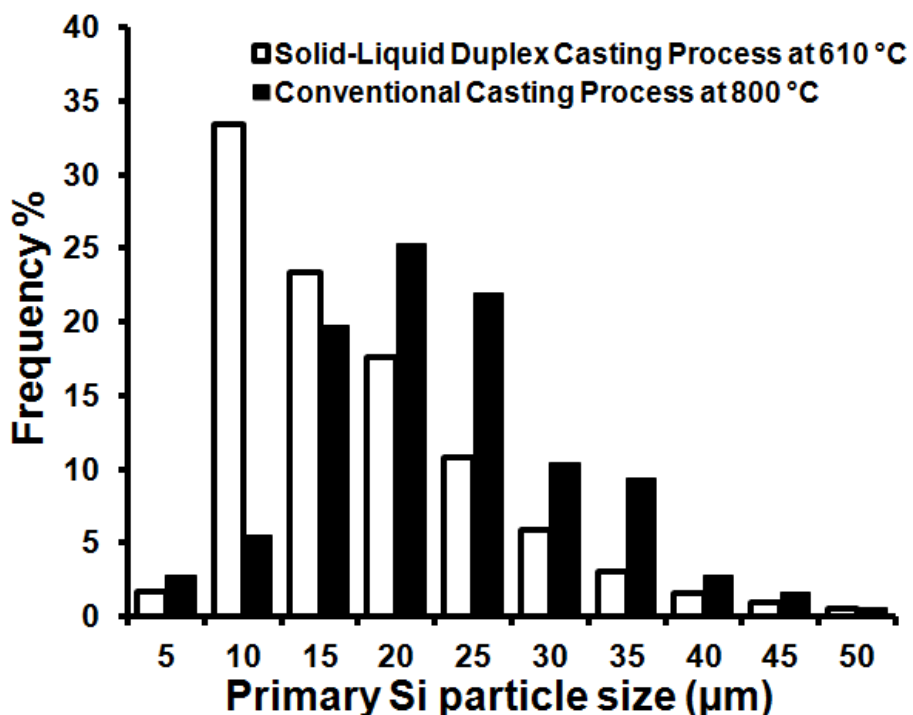


**Figure 4.75** Particle size distribution of primary Si in Al-18Si+50ppm P+200ppm Sr produced by the solid-liquid duplex and conventional casting processes.

#### 4.6.3 Mechanical properties

In order to evaluate the new solid-liquid duplex casting process in comparison with the conventional casting process, the mechanical properties (ultimate tensile stress and elongation) of Al-18Si alloy produced by each casting process such as solid-liquid duplex and conventional casting processes were measured. Figure 4.76 shows the ultimate tensile stress and elongation of Al-18Si alloy produced either by solid-liquid duplex casting process (SLD at 610 °C) or by conventional casting process (at 800 °C) without and with P and Sr additions. As shown in Figure 4.76, the ultimate tensile strength (UTS) of Al-18Si alloy increased by approximately 9.4, 10, 12 and 14% from 153.5 MPa for the conventionally cast untreated alloy to 168, 169, 172 and 175.1 MPa for the Sr, P, P+Sr treated alloy and for the solid-liquid duplex casting process respectively. Similarly the elongation was more than doubled from 1.64% for untreated Al-Si alloy to 3.76% for Al-18Si alloy produced by solid-liquid duplex casting process.

There was also a small improvement in UTS and elongation in comparison to conventionally cast Al-18Si treated with P and/or Sr.

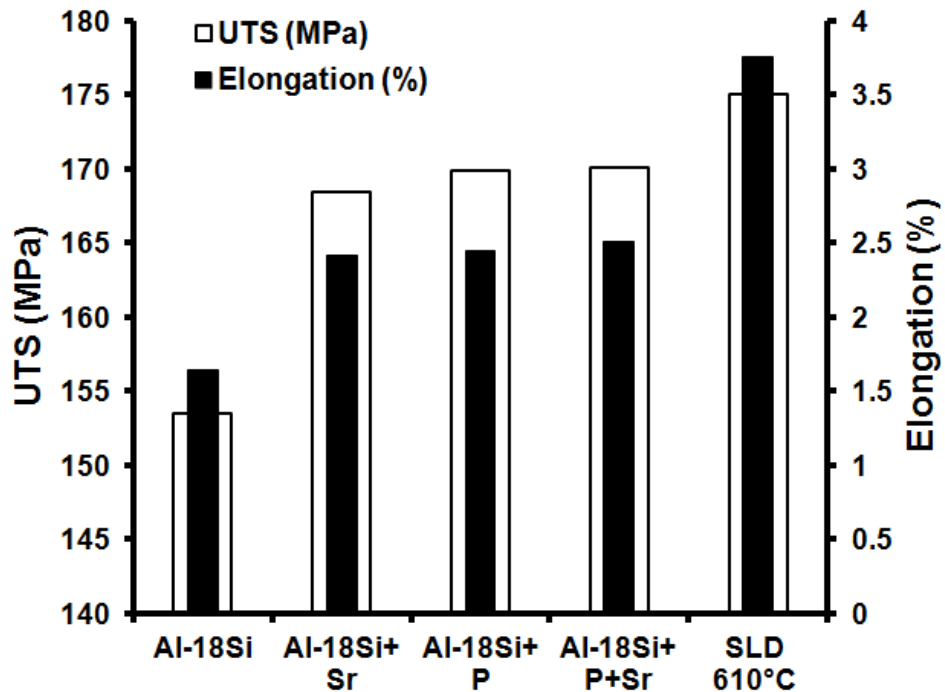


**Figure 4.76** Ultimate tensile strength and elongation of Al-18Si produced by the solid-liquid duplex (SLD) and conventional casting processes (without and with 50 ppm P and 200 ppm Sr addition cast from 800 °C).

In summary the solid-liquid duplex casting process is a promising technique for producing hypereutectic Al-Si alloys. It allows for simultaneous refinement of primary Si and modification of eutectic Si with significant improvement in the mechanical properties if compared with the conventional casting process.

Further work is required to optimize this casting process for industrial application and check the improvement in mechanical properties if compared with the conventional casting process cast at 610 °C.

# Chapter 5

## Discussion

In the previous chapter a significant improvement in refinement of primary Si and modification of eutectic Si were shown to be achieved under different casting conditions. The most significant results were:

- The tendency for primary Si to segregate to the top of a sampled specimen particularly under slow solidifications conditions and the direct effect of solidification rate (cooling rate and superheat) on the macro-segregation of primary Si and on the morphologies of primary and eutectic Si.
- The significant effect of Ca content on the morphologies of primary and eutectic Si and thus on the refinement and modification processes.
- Using a promising Al-ZnS master alloy shows that zincblende ZnS particles prepared *in situ* are potent substrates to refine the primary Si crystals without loss of eutectic modification.
- P-doped  $\gamma\text{-Al}_2\text{O}_3$  is a potent substrate to nucleate primary Si retaining good modification of the eutectic matrix in solidification of hypereutectic Al-Si alloys.
- The morphologies of primary and eutectic Si can be controlled by using a new solid-liquid duplex casting process.

The explanation and discussion of these results will be covered in detail in this chapter.

### 5.1 Effect of Solidification Rate on Primary and Eutectic Si

According to the literature, the morphologies of primary and eutectic Si in hypereutectic Al-Si alloys are a strong function of the solidification conditions such as cooling rate and melt temperature [13]. The effect of solidification rate on macro-segregation and morphologies of Si in solidification of Al-15Si alloy will be discussed in this section.

#### 5.1.1 Effect of cooling rate

In slowly cooled castings of hypereutectic Al-Si alloys, it is reported that the primary Si segregates to the upper parts of the casting. This phenomenon is assumed to be caused by gravity segregation, i.e. less dense silicon particles float in the aluminium melt during solidification [29]. Thus, for accurate microstructure analysis and evaluation of different refinement solidification conditions and methods in this study; a robust casting and sampling procedure was developed.

It is clear from the results described in section 4.1.1 that primary Si in Al-15Si alloy suffers from macro-segregation to the top of the test specimens, particularly under slow directional solidifications conditions i.e. at low cooling rate or at high pouring temperature. This was particularly evident under the low cooling rate in a standard TP-1 test sample with cooling rate equal to 3.5 K/s at the central region of a cross-section, 38 mm from the base of the TP-1 sample. This low cooling rate increases the solidification time which allows more time for the segregation and floatation of primary Si particles. Liang [128] has suggested that localized growth of primary Si (involving diffusive transport of silicon atoms in the melt) as well as floatation of primary Si particles (buoyancy driven convection) are operative at low cooling rates. Because time was available for both processes, the nucleation and growth as well as floatation of primary Si were to be expected under low cooling rate. The same phenomena were noticed for samples using the air cooled steel mould with cooling rate equal to 1K/s.

Macro-segregation of primary Si was restricted in the case of using the water cooled steel mould even at high pouring temperature. Thus, the high cooling rate (in excess of 15 K/s) decreases the solidification time and there will be less time for the segregation and floatation of primary Si. The results from the experiments leave no doubt that gravity segregation of the primary Si occurs at cooling rates below 15 K/s.

It is clear that at low cooling rate the morphology of primary Si in the segregation zone was a mixture of branched plate-like and polyhedral particles dispersed in an acicular eutectic structure. With the increase of cooling rate, the primary Si became mostly polyhedral and dispersed in a refined lamellar eutectic structure.

Generally, primary Si grows by attachment of Si atoms to the atomic planes of primary Si particles. Accordingly, the diffusion of Si atoms will play an important role during the growth of primary Si. With increasing cooling rate the diffusion of Si atoms in the liquid metal will become more difficult, and thus the growth of primary Si will be restricted. Therefore, the primary Si size is significantly decreased with the increasing cooling rate which is evident from the microstructures seen in Figure 4.1.

From the above discussion, we can conclude that there is a tendency for primary Si to segregate to the top of sampled specimens particularly under slow solidifications conditions. High cooling rates produce refined lamellar eutectic structures with good distribution of fine and compact particles of primary Si. Using the water cooled steel mould with cooling rate in excess of 15 K/s is very efficient at minimising the macro-segregation of primary Si even at high pouring temperature.

### 5.1.2 Effect of melt superheat

The optical micrographs illustrated in Figures 4.2 and 4.3 show that the morphology of primary and eutectic Si changed with increasing melt temperature. Higher superheat produces a refined lamellar eutectic structure with a good distribution of refined polyhedral particles of primary Si. With increasing melt superheat temperature, some Si-Si bonds in the Si-Si clusters are destroyed and silicon atoms diffuse from Si-Si clusters into the Al bulk melt. Therefore, the higher melt superheat, the smaller the size of Si-Si clusters due to the destruction of Si-Si bonds. Furthermore, structural studies have shown that superheat changes the melt structure [166-168]. Some researchers have suggested that the nucleation of star-like primary Si results from the formation of tetrahedral groups of silicon atoms in the liquid melt. Generally, Si-Si clusters of larger size should generate more silicon tetrahedra than those of smaller size. Therefore, in the present study, it can be safe to deduce that Si-Si clusters of larger size should be beneficial for the formation of the nucleus of star-like and other irregular primary Si and Si-Si clusters of smaller size should be beneficial for the formation of the nuclei of octahedral or polygonal primary Si [13].

Inci *et al.* [22] suggested that breaking of the Si-Si bonds happens in the melt with increasing temperature and that Si atoms diffuse into the Al bulk melt. Where, during the diffusion process, some original Si-Si bonds are destroyed whilst at the same time some new Al-Si bonds are formed. From this fact, it can be deduced that the Si atoms occupied the positions of Al atoms in the bulk melt after leaving the Si-Si clusters. The melt structure seems to become more homogeneous with the increase in melt superheat, leading to a decrease in the volume fraction of primary Si in the Al-Si matrix as shown in Figure 4.5. Calvo-Dahlborg *et al.* [169] investigated the effect of superheat on the microstructure of Al-Si alloys of hyper, hypo and eutectic compositions by Small Angle Neutron Scattering (SANS) during thermal cycles above the liquidus temperature. They proved that for all compositions, the melt is more homogeneous at the maximum temperature after heating.

Bian and Wang [11] investigated the structures of the melt of Al-13Si alloy heated in the temperature range from 625 °C to 1250 °C. The high temperature X-ray diffractometer showed that with increasing the temperature up to 775 °C, the atomic density and the coordination number of the alloy increase slowly, then a sudden change in those parameters occurs in the temperature range from 775 °C to 875 °C. These results suggest that the liquid structure changed, which is caused by dissolving of Si-Si clusters into the Al bulk melt. This finding supports our results that there was a significant change in silicon morphology at melt temperature above 750 °C as shown in Figure 4.5.

### **5.1.3 Summary**

From above results, we can conclude that:

1. There is a tendency for primary Si to segregate to the top of sampled specimens particularly under slow solidifications conditions.
2. With increasing cooling rate, the primary Si became mostly polyhedral and dispersed in a refined lamellar eutectic structure.
3. Using the water cooled steel mould provided a cooling rate in excess of 15 K/s which is very efficient in preventing the macro-segregation of primary Si even at high pouring temperature.
4. The morphologies of primary and eutectic Si change with increasing melt superheat. High superheat produces refined lamellar eutectic structure with a good distribution of polyhedral particles of primary Si.
5. The melt structure becomes more homogeneous with increasing melt superheat. This leads to a decrease in the average particle size of primary Si with increasing melt superheat while the particles became more compact in shape. The particle number density of primary Si in Al-15Si significantly increased in the melt temperature range from 845 °C to 1150 °C suggesting enhanced nucleation.
6. Any future experiments, e.g. in order to study the effect of parameters other than melt superheat, need to be carried at temperatures of around 800 °C for Al-15Si alloy and samples should be taken by using a technique with a cooling rate of no less than 15 K/s to overcome the macro-segregation of primary Si and eliminate the effect of superheat.

## **5.2 Refinement and Modification in a High Purity Hypereutectic Al-Si Alloy**

### **5.2.1 Unmodified/unrefined high purity Al-15Si alloy**

The optical micrographs in Figure 4.6 show that unmodified/unrefined high purity Al-15Si alloy consists of irregular coarse primary Si particles with average particle size of 68 µm dispersed in a lamellar eutectic structure. However, typical micrographs of commercial purity Al-15Si alloy show that it consists of coarse polygonal primary Si with average particle size of approximately 48 µm with eutectic Si having a mostly fibrous morphology. In solidification of unrefined and unmodified Al-15Si alloy, the mechanism for nucleation and growth of primary and eutectic Si are as follows:

### (1) Homogeneous nucleation and growth mechanism of primary Si in unrefined hypereutectic Al-Si alloys

Before solidification of unrefined hypereutectic Al-Si alloys, Si atoms will arrange themselves in the form of tetrahedra when close to their freezing point. Then, the Si nucleates on embryos that form by the coalescence of these tetrahedra. The optimum shape of these embryos is determined by surface energy considerations. An embryo bound by low energy facets of {111} planes is the most thermodynamically stable. Thus, the most stable Si nucleus is a decahedron bound by {111} facets. This formed nucleus grows at locations with multiple twins by the Twin Plane Re-entrant Edge (TPRE) mechanism. Hence, primary Si nucleates on equiaxed, twinned embryos and grows into different morphologies [170]. The most commonly observed primary Si morphologies are massive primary Si, which is also known as polygonal Si (compact surface), and star-like primary Si which is highly irregular in shape [39].

Xu *et al.* [171] suggested different sequences of crystal growth of octahedral primary Si in inoculated hypereutectic Al-Si alloys as shown in Figure 5.1. According to the vector relationship for a Si crystal, illustrated in Figure 5.2, they suggested that at the initial stage, a primary Si crystal will grow rapidly along [100] directions to form stable initial branches (see the second step in Figure 5.1). As a result, growth is suppressed in all directions except the high-mobility [100] direction due to the strong faceting tendency of the growing primary Si crystal. They found that:

- The primary Si crystal will grow as a perfect octahedron when  $V_{[100]}/V_{[111]}= 1.5$  as observed in most examples of solidification of commercial purity Al-Si alloys in this thesis and shown in Figure 4.6.
- If  $V_{[100]}/V_{[111]} < 1.5$ , the primary Si crystal will grow as other irregular morphologies which occurs in solidification of Al-Si alloys at low cooling rate or solidification of high Si content unrefined Al-Si alloy as illustrated in Figures 4.2 & 4.46a.

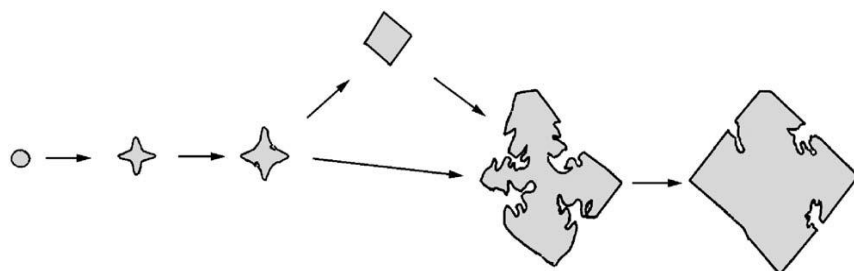


**Figure 5.1** A schematic diagram illustrating the different growth sequences of octahedral primary Si in unmodified Al-Si alloys [171].

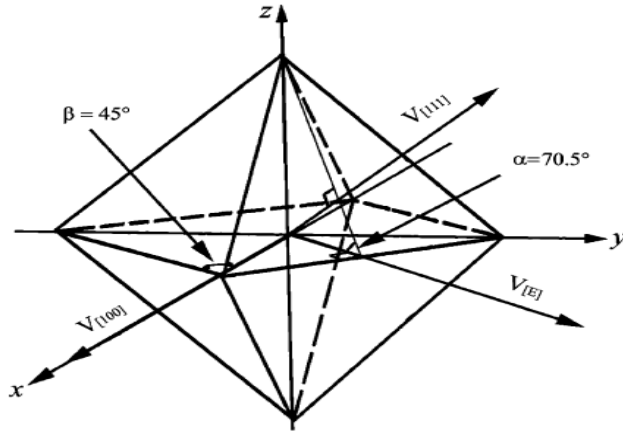


**Figure 5.2** A schematic diagram illustrating the vector relationship between the growth rate  $V_{[100]}$  normal to the [100] growth direction, growth rate  $V_{[E]}$  normal to the edges and the growth rate  $V_{[111]}$  normal to the {111} facets [171].

Some investigations have been made to study the octahedral morphologies of primary Si in unrefined hypereutectic Al-Si alloys. Wang *et al.* [172] have investigated the relationships between the morphologies and growth mechanisms of primary Si and believed that octahedral primary Si can be formed primarily by layer growth, which is the generation of repeated parallel {111} planes on {111} facets. At the same time, they derived a general equation for stable faceted growth of the Si, and indicated that no evidence of the Twin Plane Re-entrant Edge (TPRE) growth mechanism was found in the growth of the octahedral-type crystals. However, they also suggested that the dislocation mechanism provided a major source for layer growth of the primary Si crystal by the observation of dislocation spirals on {111} facets [173].

## (2) Growth of unmodified eutectic Si in Al-Si alloy

In the Al-Si system, Si is a non-metal with directional covalent bonds. It tends to grow anisotropically into faceted crystals and hence it requires more undercooling for its growth than the isotropic aluminium phase. Therefore, the coupled region in the Al-Si system is asymmetric [174]. Coupled regions represent fields within the phase diagram where the two phases of the eutectic are organized in the solid in such a way as to allow diffusion in the liquid to occur effectively at a duplex solid/liquid front as shown in Figure 5.3 [39]. The morphology of unmodified eutectic Si is typically coarse and flaky and is usually observed in slowly cooled foundry alloys and when no chemical modifiers are added.

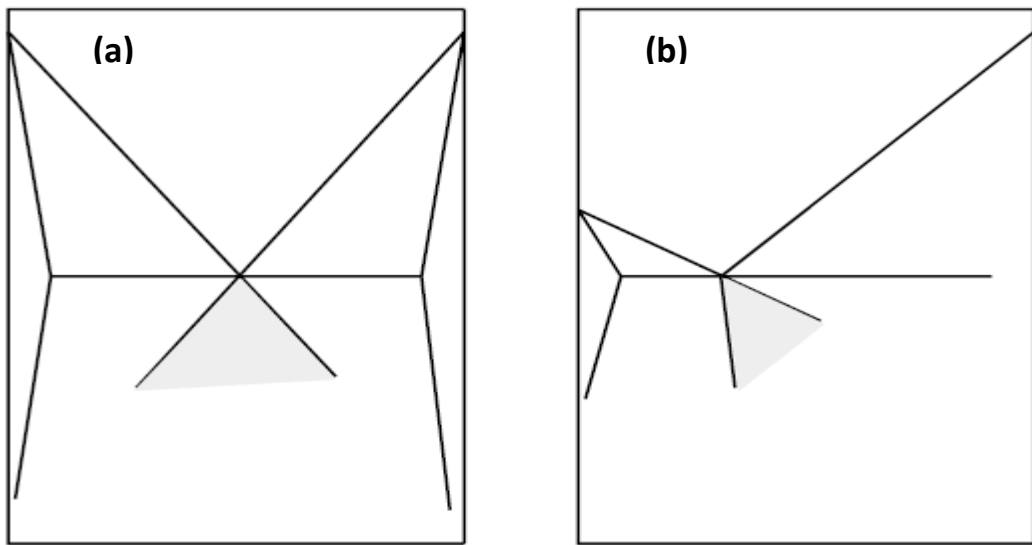


**Figure 5.3** Coupled zones in (a) symmetrical and (b) asymmetrical phase diagrams. The Al-Si system has a typical asymmetrical phase diagram [39].

Wagner [175] proposed a Twin Plane Re-entrant Edge (TPRE) growth mechanism of the eutectic Si in un-modified Al-Si alloys. The unmodified plate-like form of Si can grow easily only in the  $\langle 112 \rangle$  crystallographic direction, and when the crystal structure of Si is taken into account, this implies that the large flat faces of the crystal are  $\{111\}$  planes. A very important feature of Si crystallization is that twins are easily formed and hence unmodified Si occurs basically in an unbranched, flat-plate morphology.

Crosley and Mondolfo [176] suggested that the needle-like Si particles observed in unmodified alloys must be flakes or sheets. Now, with the availability of electron microscopy, it is confirmed that Si in unmodified Al-Si eutectics has the flake-like structure.

### 5.2.2 High purity Al-15Si alloy refined with P

Optical micrographs in Figure 4.7 for solidification of Al-Si alloys show that adding 20 ppm P is quite enough to refine primary Si in the high purity alloy and to reduce the average particle size from 68  $\mu\text{m}$  to 20  $\mu\text{m}$ , while adding 20 ppm P to commercial purity Al-15Si alloy refine the primary Si and reduce the average particle size from 48  $\mu\text{m}$  to 25  $\mu\text{m}$ .

In heterogeneous nucleation of primary Si, the added phosphorus combines with molten aluminium to form tiny, insoluble AlP particles. These particles are suspended in the melt and act as potent sites for epitaxial nucleation and growth of primary Si. At the same time these AlP particles are responsible for the nucleation of Si in the eutectic matrix [65]. In using commercial purity Al-15Si alloy, the amount of P required to refine

primary Si to less 20  $\mu\text{m}$  should be more than 50 ppm [68]. It has been proven that high Ca content can lead to P refinement inefficiency. This phenomenon is due to the formation of  $\text{Ca}_x\text{P}_y$  compounds, which are more stable than AIP in the Al-Si melt [163] or the rapid and continuous oxidation of Ca leads to transformation of AIP to non potent  $\text{AlPO}_4$  particles. The estimated free enthalpy of formation of  $\text{Ca}_3\text{P}_2$  (-506 kJ mol<sup>-1</sup>) is much less than that of the AIP phase (-111.66 kJ mol<sup>-1</sup>) [177]. Hence, in the presence of elements with more negative enthalpy of phosphide formation, the AIP will become depleted. It is important to point out that the lack of AIP phase results in an increased primary Si particle size. The eutectic Si structure in solidification of both high purity and commercial purity Al-15Si+20ppm P alloys was lamellar.

### 5.2.3 High purity Al-15Si alloy modified with Ca

Optical micrographs in Figure 4.8 show that adding 30 ppm of Ca has a significant effect on modification of high purity Al-15Si alloy. The Ca modified high purity Al-15Si alloy contains no primary Si particles, i.e. there was a shift in the apparent eutectic position with the addition of Ca.

It is well established in the literature that alloys within a few percent of the usual eutectic composition of 12.6 wt% Si are sensitive to the presence of a refiner such as phosphorus or a modifier such as sodium or strontium: Alloys containing 11 or 12 wt% Si easily develop numerous primary Si particles in the presence of phosphorus, and alloys containing 13 or 14 wt% Si will contain no primary Si in the presence of sufficient sodium or strontium [30] as shown in Figure 5.3. Jenkinson *et al.* [178] investigated the effect of adding Sr to high purity Al-Si alloys and they found that in the presence of 0.02 wt% Sr no primary Si appears in any alloy containing up to 17 wt% Si. They concluded that the apparent shift of the eutectic point can be attributed to the shape of the coupled region boundary, and the suppression of primary Si.

The typical unmodified Al-Si eutectic is closer to a lamellar structure than to a fibrous one. This structure is usually attributed to the strong anisotropy of growth of Si and to the relatively low interfacial energy between Si and aluminium [39]. Trace amounts of Ca can effectively modify the eutectic Si shape, similar to that with sodium or strontium under the same melting and casting conditions. Knuutinen *et al.* [87] reported that Ca can cause a depression of the eutectic arrest and result in fibrous eutectic Si. Due to the low level of P content in high purity Al-15Si (less than 1 ppm), the modification with 30 ppm Ca was very efficient. The optimum amount of Ca used to modify eutectic Si in commercial purity Al-Si alloy should be more than 40 ppm [6].

### **5.2.4 Summary**

The conclusions from the above results are:

1. High purity Al-15Si alloy, cast in the steel mould with a cooling rate of 15K/s, consists of irregular coarse primary Si particles, 68 µm in size, dispersed in a lamellar eutectic structure. On the other hand, commercial purity Al-15Si alloy consists of a coarse octahedral primary Si with average particle size of approximately 48 µm and the eutectic Si had a mostly fibrous morphology.
2. Adding 20 ppm P was quite enough to refine primary Si in high purity Al-15Si alloy and to reduce the average particle size from 68 µm to 20 µm. The same amount of P also refined primary Si in commercial purity Al-15Si alloy and reduced the average particle size from 48 µm to 25 µm.
3. Adding 30 ppm of Ca to the high purity Al-15Si can modify the eutectic matrix to a fibrous structure and suppress formation of primary Si, i.e. the apparent eutectic position is shifted.

## **5.3 Effect of Ca Level on Primary and Eutectic Si**

The effect of Ca on the formation of primary and eutectic Si during solidification of commercial purity Al-15Si alloy was studied through both the reduction of Ca impurity level by the addition of  $K_2SiF_6$  flux and by raising the Ca level by adding 0.5 wt % Ca. In addition, the effect of Ca level on Si morphologies in the presence of Mg and Sb will be discussed.

### **5.3.1 Removal of Ca by $K_2SiF_6$ flux**

Results in section 4.3.1 show that the use of  $K_2SiF_6$  flux, and the consequential reduction of Ca impurity content, led to refinement of the primary Si particles to an average size of 20 µm. The morphology of Si in the eutectic matrix changed from the fibrous structure of the untreated alloy to a plate-like structure.

Liu *et al.* (2005) [78] studied the effect of Ca content in A390 alloy on the efficiency of P as a refiner of primary Si. They found that the efficiency of P could be recovered by adding  $C_2Cl_6$  to remove Ca, and explained that the inefficiency of P as a refiner for primary Si in the presence of Ca is due to the formation of Ca-Si-P phases reducing the amount of potent AlP available for enhancing the nucleation of primary Si [177].

The free energies of formation of  $SiP$ ,  $AlP$  and  $Ca_3P_2$  are  $-50.85\text{ kJmol}^{-1}$ ,  $-128.74\text{ kJmol}^{-1}$  and  $-522.48\text{ kJmol}^{-1}$  respectively [177, 179]. Hence  $Ca_3P_2$  is significantly more stable than AlP. When an Al-Si alloy contains both Ca and P they will interact, and if there is an excess of Ca then the eutectic Si will be modified and the

primary Si unrefined, and if there is an excess of P then the primary Si will be refined and the eutectic Si unmodified.

### 5.3.2 High Ca content

The Al-15Si alloy with 0.5 wt% Ca added contained a far greater quantity of entrained oxide bifilms than the alloy with only impurity levels of Ca as shown in Figure 4.13 and Figure 5.4 suggesting the presence of a weak oxide film on the surface of the melt.

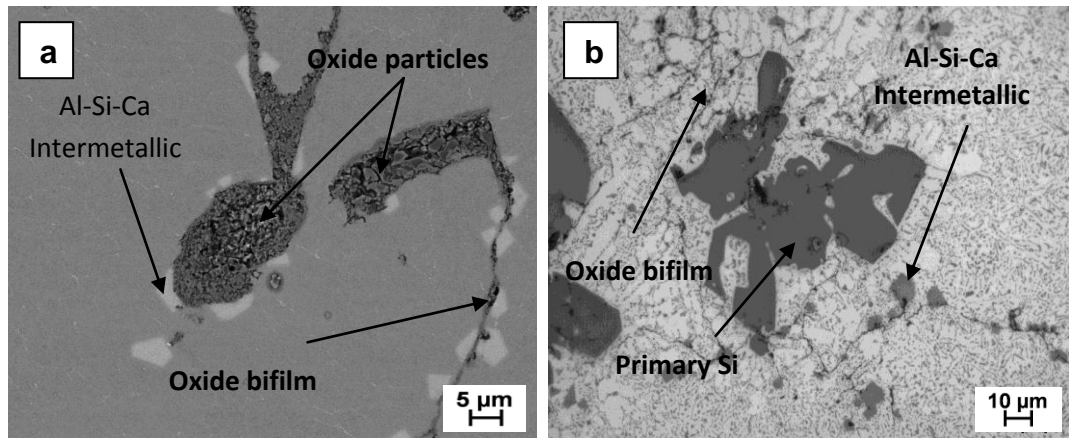


**Figure 5.4** back scattered SEM and optical micrographs of the typical morphology of primary Si and the Al-Si-Ca phase, in the Al-15Si-0.5Ca alloy. (a) Entrained oxide bifilm and (b) primary Si and Al-Si-Ca phase formed in association with each other and with oxide bifilms.

Such a weak oxide film may break up in turbulent flow or even under the action of gentle mixing and become incorporated in the bulk of the casting in the form of entrained inclusions and bifilms [6]. Figure 5.5a is an SEM image showing an example of the high concentration of bifilms. Figure 5.5a also shows that the bifilms were decorated by dispersoids. Figure 5.5b is an EDS point analysis of the dispersoids attached to the oxide bifilms which confirmed that the dispersoids contained Al, Si and Ca. The vertical section of the Al-Si-Ca phase diagram shown in Figure 4.12 indicates that the first phase to form in solidification of Al-15Si-0.5Ca alloy should be  $\text{Al}_2\text{CaSi}_2$ . Together the EDS analysis and the phase diagram indicate that the dispersoids decorating the oxide bifilms were  $\text{Al}_2\text{CaSi}_2$ .

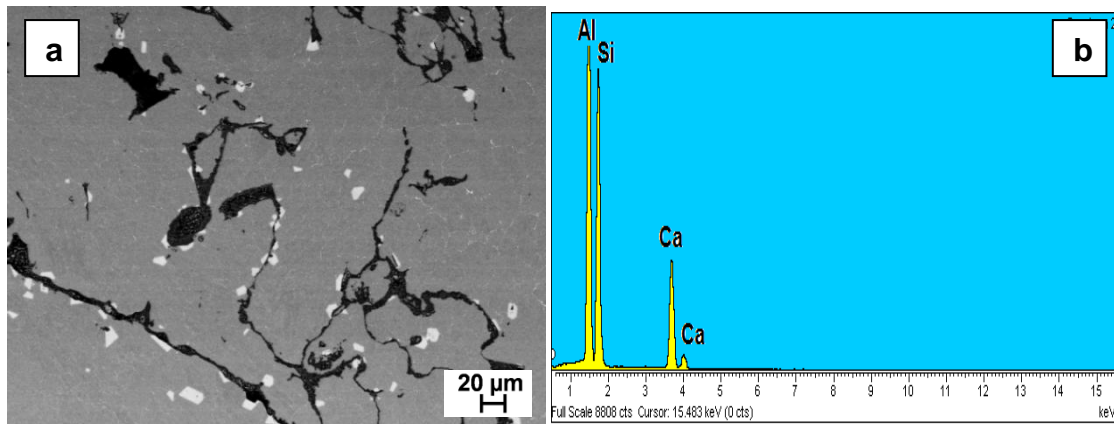


**Figure 5.5** (a) Back scattered SEM micrograph showing the high level of entrained oxide in the Al-15Si-0.5Ca alloy, and the association of Al-Si-Ca dispersoids with the oxide bifilms; and (b) typical EDS point analysis spectrum from the Al-Si-Ca dispersoids.

Figure 4.13 & 5.4 show that primary Si and the  $\text{Al}_2\text{CaSi}_2$  phase formed in intimate association with each other and in association with the oxide inclusions. There has been some previous experimental evidence to suggest that Si particles may nucleate and grow on oxide bifilms during solidification of hypereutectic Al-Si alloys [65]. The nucleation of primary Si on oxide bifilms may be due to one of the following hypotheses:

1. AIP particles first nucleate on oxide films and serve as nucleation sites for Si. This is because of the high tendency for P to be adsorbed to the surface of  $\text{Al}_2\text{O}_3$  [159]. Work by Pennors *et al.* [157] supports this hypothesis. They presented clear microstructures in which AIP particles are seen aligning along oxide bifilms. However, no evidence was found in the present study that revealed AIP particles on the entrained oxide bifilms.
2. The oxide film contains a potent substrate for heterogeneous nucleation of primary Si. Table 5.1 provides crystallographic data, potential orientation relationships and associated calculated lattice misfits between Si and AIP,  $\text{Al}_2\text{CaSi}_2$  and relevant oxides. The misfit between Si and AIP is very close to zero, leading to the extremely high potency for AIP to nucleate Si. The misfits between Si and the two common forms of  $\text{Al}_2\text{O}_3$  are too high for the oxides to act as heterogeneous nucleants for Si. Choi *et al.* [18] investigated how  $\gamma\text{-Al}_2\text{O}_3$  nanoparticles can be used for simultaneous refinement and modification of Si in hypereutectic Al-Si-Cu alloy melts. In this case, the  $\gamma\text{-Al}_2\text{O}_3$  nanoparticles were incorporated in the melt during ultrasonic processing. Zhang *et al.* [25] found ultrasonic vibrations to be effective for refinement and modification of the Si phases in hypereutectic Al-Si alloys, and so the refinement and modification of

Si in the results of Choi *et al.* [18] may have been due to their method of incorporating the  $\gamma$ -Al<sub>2</sub>O<sub>3</sub> nanoparticles rather than the nanoparticles themselves.

The evidence for the nucleation of primary Si on oxide inclusions is not strong. However, Table 5.1 shows that the misfit between Si and Al<sub>2</sub>CaSi<sub>2</sub> is less than 8%, suggesting that Al<sub>2</sub>CaSi<sub>2</sub> could be an effective heterogeneous nucleant for primary Si.

**Table 5.1** Calculated lattice misfit  $f$  between Si and some substrates.\*

Interface	Crystal structure & lattice parameters {nm} [60, 177, 180]	OR: (hkl)[uvw] <sub>Si</sub> // (h'k'l')[u'v'w'] <sub>S</sub>	d[uvw] <sub>Si</sub> {nm}	d [u'v'w'] <sub>S</sub> {nm}	f {%)
Si /AlP	Si: cubic, a=0.5421, AlP: cubic, a=0.5431	(111)[110]//(111)[110]	0.3833	0.3840	-0.18
Si/ Al <sub>2</sub> CaSi <sub>2</sub>	Si: cubic, a=0.5421, Al <sub>2</sub> CaSi <sub>2</sub> : hexagonal, a=0.4130, c=0.7145	OR I:(111)[110]//(0001)[11-20], OR II:(111)[110]//(0001)[10-10]	0.3833 2x0.3833	0.4130 0.7153	7.7 6.7
Si/ $\alpha$ -Al <sub>2</sub> O <sub>3</sub>	Si: cubic, a=0.5421, $\alpha$ -Al <sub>2</sub> O <sub>3</sub> : rhomb. a=0.4782; c=1.3057	(111)[110]//(0001)[11-20]	0.3833	0.4782	-24.8
Si/ $\gamma$ -Al <sub>2</sub> O <sub>3</sub>	Si: cubic, a=0.5421, $\gamma$ -Al <sub>2</sub> O <sub>3</sub> : cubic, a=0.7963	(111)[110]//(111)[110]	0.3833	0.5631	-46.9

\* Subscript S=substrate. OR=orientation relationship which is according to the match of most densely packed planes and directions. The misfit  $f$  is defined as  $(d[u\ v\ w]_{Si} - d[u'\ v'\ w']_S) / d[u\ v\ w]_{Si}$  [126].

Table 5.2 provides crystallographic data, potential orientation relationships and associated calculated lattice misfits between Al<sub>2</sub>CaSi<sub>2</sub> and relevant oxides. The data shows that neither of the oxides has a sufficiently small misfit with Al<sub>2</sub>CaSi<sub>2</sub> for them to act as potent substrates for nucleation of this phase over a single lattice spacing. However Al<sub>2</sub>CaSi<sub>2</sub> has an orientation relationship with  $\alpha$ -Al<sub>2</sub>O<sub>3</sub> (OR II) that has a misfit of only -0.28% over two lattice spacings of Al<sub>2</sub>CaSi<sub>2</sub>. Moreover Al<sub>2</sub>CaSi<sub>2</sub> has an orientation relationship with  $\gamma$ -Al<sub>2</sub>O<sub>3</sub> (OR II) over two lattice spacings of the intermetallic, with a misfit less than 5%.

Taking into account the microstructural evidence and the crystallographic data provided in this section it is proposed that in the Al-15Si alloy with 0.5 wt% Ca added: (i) Al<sub>2</sub>CaSi<sub>2</sub> is the first phase to form during solidification and it nucleates and grows on the entrained oxide inclusions and bifilms, then (ii) primary Si forms by nucleation and growth on the Al<sub>2</sub>CaSi<sub>2</sub> particles [181].

**Table 5.2** Calculated lattice misfit  $f$  between  $\text{Al}_2\text{CaSi}_2$  and some substrates.\*

Interface	Crystal structure & lattice parameters {nm} [60, 180]	OR: $(hkl)[uvw]_{\text{Al}_2\text{CaSi}_2} // (h'k'l')[u'v'w']_S$	$d[uvw]_{\text{Al}_2\text{CaSi}_2}$ {nm}	$d[u'v'w']_S$ {nm}	$f$ {%
$\text{Al}_2\text{CaSi}_2 / \alpha\text{-Al}_2\text{O}_3$	$\text{Al}_2\text{CaSi}_2$ : hexagon al, $a=0.4130$ , $c=0.7145$ , $\alpha\text{-Al}_2\text{O}_3$ : rhomb. $a=0.4782$ ; $c=1.3057$	OR I: $(0001)[11\cdot20] // (0001)[11\cdot20]$ OR II: $(0001)[11\cdot20] // (0001)[10\cdot10]$	0.4130 $2\times 0.4130$	0.4782 0.8283	-15.8 -0.28
$\text{Al}_2\text{CaSi}_2 / \gamma\text{-Al}_2\text{O}_3$	$\text{Al}_2\text{CaSi}_2$ : hexagon al, $a=0.4130$ , $c=0.7145$ , $\gamma\text{-Al}_2\text{O}_3$ : cubic, $a=0.7963$	OR I: $(0001)[11\cdot20] // (111)[110]$ OR II: $(0001)[11\cdot20] // (100)[001]$	0.4130 $2\times 0.4130$	0.5631 0.7963	-36.3 3.59

\* Subscript S=substrate. OR=orientation relationship which is according to the match of most densely packed planes and directions. The misfit  $f$  is defined as  $(d[uvw]_{\text{Al}_2\text{CaSi}_2} - d[u'v'w']_S) / d[uvw]_{\text{Al}_2\text{CaSi}_2}$  [126].

### 5.3.3 Effect of Ca in the presence of Mg or Sb

Experiments were conducted to study the effect of Ca content on morphology of primary and eutectic silicon in the presence of Mg or Sb in Al-15Si alloy. These elements were chosen because Mg has a significant effect on the morphology of primary Si and Sb can modify the eutectic Si in Al-Si alloys (see section 2.2). The results of these experiments were shown in section 4.3.3.

On adding 0.5 wt% Mg to commercial purity Al-15Si alloy, which contained more than 200 ppm Ca, the primary Si particles were coarse of 45  $\mu\text{m}$  in size dispersed in  $\text{Al}+\text{Si}+\text{Mg}_2\text{Si}$  eutectic as illustrated in Figure 4.15 (c,d). When Al-15Si base alloy was fluxed with AP1 flux prior to the Mg addition, there was a significant refinement of the primary Si particles and they were dispersed in a plate-like eutectic structure. The chemical analysis using optical emission spectroscopy showed that the Mg content decreased as the initial nominal Ca content increased. This is because of the rapid and continuous oxidation of Ca and then Mg which is removed with the dross. Hence, as Ca content is reduced by AP1 flux the refining effect of Mg on primary Si will be more significant. In addition, with the removal of Ca the number of AIP particle will increase and the P refinement efficiency can be recovered.

Usually, adding Sb to commercial purity Al-15Si alloy, with more than 200 ppm Ca, the eutectic Si is modified to a lamellar structure [92]. On reducing the Ca content by fluxing, a finer lamellar eutectic structure was produced when adding 0.5 wt% Sb to fluxed Al-15Si alloy. The chemical analysis using optical emission spectroscopy showed that the Sb content decreased as the initial Ca content increased. It is believed

that an insoluble intermetallic compound can form between Sb and Ca, which separates out and combines with the aluminium oxide surface dross. Hence, removing Ca before adding Sb to Al-Si alloys improves the modification process.

Daniels and Bonsignore [182] have found that additions of either Ca or Sr could scavenge Sb from aluminium alloys. Sb content could be reduced from 2800 ppm to 50 ppm by treating the melt with 1500 ppm Ca. The optimum amount of Sb used as a eutectic Si modifier in Al-Si alloy is 0.1-0.15 wt% [6].

### 5.3.4 Summary

The conclusions for the effect of Ca content on solidification of hypereutectic Al-Si alloys in this study are:

1. The commercial purity alloy contained 200 ppm Ca which was sufficient to lead to a modified Al-Si eutectic.
2. After the addition of  $K_2SiF_6$  flux the Ca impurity level was 20 ppm which was too little to modify the eutectic Si, but primary Si was refined. This suggests fluxing with  $K_2SiF_6$  can remove Ca effectively such that the trace level of P (~20 ppm) in commercial purity hypereutectic Al-Si alloys is sufficient to refine the primary Si without any deliberate addition of P.
3. In the case of adding 0.5 wt.% Ca to the Al-15Si alloy, the eutectic Si was highly modified and the primary Si was coarse and irregular in morphology (unrefined). The addition of such a high level of Ca led to enhanced quantities of entrained oxide inclusions/bifilms.
4. For the Al-15Si-0.5Ca alloy, the first phase to solidify was  $Al_2CaSi_2$  which nucleated and grew on the oxide bifilms. Primary Si then formed by nucleation and growth on the  $Al_2CaSi_2$  particles.
5. On fluxing with AP1 prior to a Mg addition, the refinement in primary Si particles was significant. The fine primary Si particles were dispersed in a plate-like eutectic structure. The reason is that the removal of Ca led to an increase in the amount of P available to form AIP particles for the nucleation of primary Si with an associated reduction in the modification of the eutectic.
6. On reducing the Ca content by fluxing, a finer lamellar eutectic structure was produced when adding 0.5 wt% Sb to Al-15Si alloy when compared with the un-fluxed alloy.

## 5.4 Effect of Chemical Additions on Primary and Eutectic Si

Various inoculants - Mg, oxides (MgO and CaO), ZnS, Na<sub>2</sub>S and Zn - were studied. Microstructural analysis in section 4.4 showed that Mg and ZnS refined primary Si whereas MgO, CaO and Na<sub>2</sub>S coarsened the primary Si together with a modification effect on the eutectic Si. Adding Zn had no effect on the morphology of either primary or eutectic Si.

### 5.4.1 Magnesium (Mg)

Microstructures of Al-15Si with different Mg concentrations in section 4.4.1 show that with increasing addition of Mg up to 0.3 wt% to the binary alloy, the size of the primary Si decreases significantly. On adding more than 0.3 wt% up to 0.75 wt% of Mg, the size of the primary Si increased again to a size larger than that in the base alloy. The increase in the size of primary Si particles was associated with a reduced number of primary Si particles. On adding 1.0 wt% Mg there was no primary Si at all. The morphology and size of the eutectic Si particles change with the addition of Mg to a fine and compact form with a Chinese script like morphology of the eutectic matrix as shown in Figure 4.18l.

Eutectic Mg<sub>2</sub>Si particles were observed in the eutectic network of the alloys with Chinese script morphology. This is due to the occurrence of the ternary eutectic reaction at non-equilibrium solidification. Owing to the change of the eutectic formation reaction from the binary (Liquid → Al+Si) to the ternary (Liquid → Al+Si+ Mg<sub>2</sub>Si) as calculated by using the commercial PandaT software with PanAl8 database and shown in Figure 4.14, the eutectic formation temperature of the matrix will reduce. This change affects the size and morphology of the eutectic Si phase in the matrix [183].

Both refinement of primary Si and modification of eutectic Si was only observed for the alloys with Mg content ≤ 0.3% Mg when compared with the binary Al-15Si base alloy. This indicates that the presence of Mg can enhance refinement and modification of Si at this level of concentration. The refinement of primary Si could be due to the formation of MgAl<sub>2</sub>O<sub>4</sub>. Magnesium-alumina spinel (MgAl<sub>2</sub>O<sub>4</sub>) is one of the common compounds in a family of mixed oxide spinels having a cubic structure with a lattice parameter of 8.08 Å [184]. MgAl<sub>2</sub>O<sub>4</sub> has an orientation relationship with Si: (001)[100]Si//(111)[110] MgAl<sub>2</sub>O<sub>4</sub> with a misfit less than 5%.

The spinel's lattice parameter depends on the stability of oxides, i.e. whether α-Al<sub>2</sub>O<sub>3</sub> or γ-Al<sub>2</sub>O<sub>3</sub> is present in the spinel [185]. So, for this case up to 0.3 wt% Mg content might be sufficient to form the MgAl<sub>2</sub>O<sub>4</sub> and then to act as a nucleation substrate to refine primary Si.

Such change in morphology of the eutectic matrix has been shown to result in the increase of the overall hardness of high Mg alloys even though the hardness of the primary  $Mg_2Si$  particles is lower than that of the primary Si particles [183]. Mg has been found to be the most effective element to increase the hardness of Al-Si Alloys [186].

### 5.4.2 Mg and Ca oxides

As mentioned in section 2.4, elements with Pilling-Bedworth (PB) ratios (oxide density to metal density) less than one form discontinuous and non-protective oxides, while those with PB ratios  $> 1$  form continuous and protective oxides. PB ratios of BeO, ZnO,  $ZrO_2$ ,  $\gamma-Al_2O_3$ ,  $\alpha-Al_2O_3$ , MgO and CaO, are 1.70, 1.58, 1.56, 1.31, 1.28, 0.80 and 0.64 respectively [61]. The Ellingham diagram shown in Figure 5.6 shows also that CaO is more stable than MgO and  $Al_2O_3$ , thus, a melt containing Ca and Mg cannot maintain its continuous protective  $Al_2O_3$  skin even when the melt is quiescent. Instead, it will be subjected to a rapid and continuous trapping of oxygen leading to formation of more oxide. Optical micrographs illustrated in Figure 4.21 show that there was significant coarsening of the primary Si with modification of the eutectic structure on adding MgO and CaO. The reason for the coarse size of primary Si could be due to the decrease of nucleation particles such as AIP. As shown in Figure 5.7, Ca is more effectively oxidized than Mg for less than 20 hr operation [6]. Hence, the melt will be subjected to rapid and continuous oxidation leading to formation of greater quantities of oxides. Accordingly, AIP could oxidize to form  $AlPO_4$  which has a Hexagonal crystal structure with lattice parameter,  $a_o = 0.439$  nm,  $c_o = 1.094$  nm and the mismatch between Si and  $AlPO_4$  is more than 20% and thus  $AlPO_4$  is not a potent substrate for nucleation of Si. Thus the depletion of AIP particles by oxidation cause the size of primary Si to be bigger and more irregular [28].

In conclusion, the reason behind the coarsening of primary Si is the depletion of P either by interaction with the inclusions or oxidation and conversion to non potent  $AlPO_4$  particles. Also, due to the high chemical affinity of Ca for oxidation in comparison to Mg [57], the probability of P depletion is higher and hence the primary Si particles are coarser.

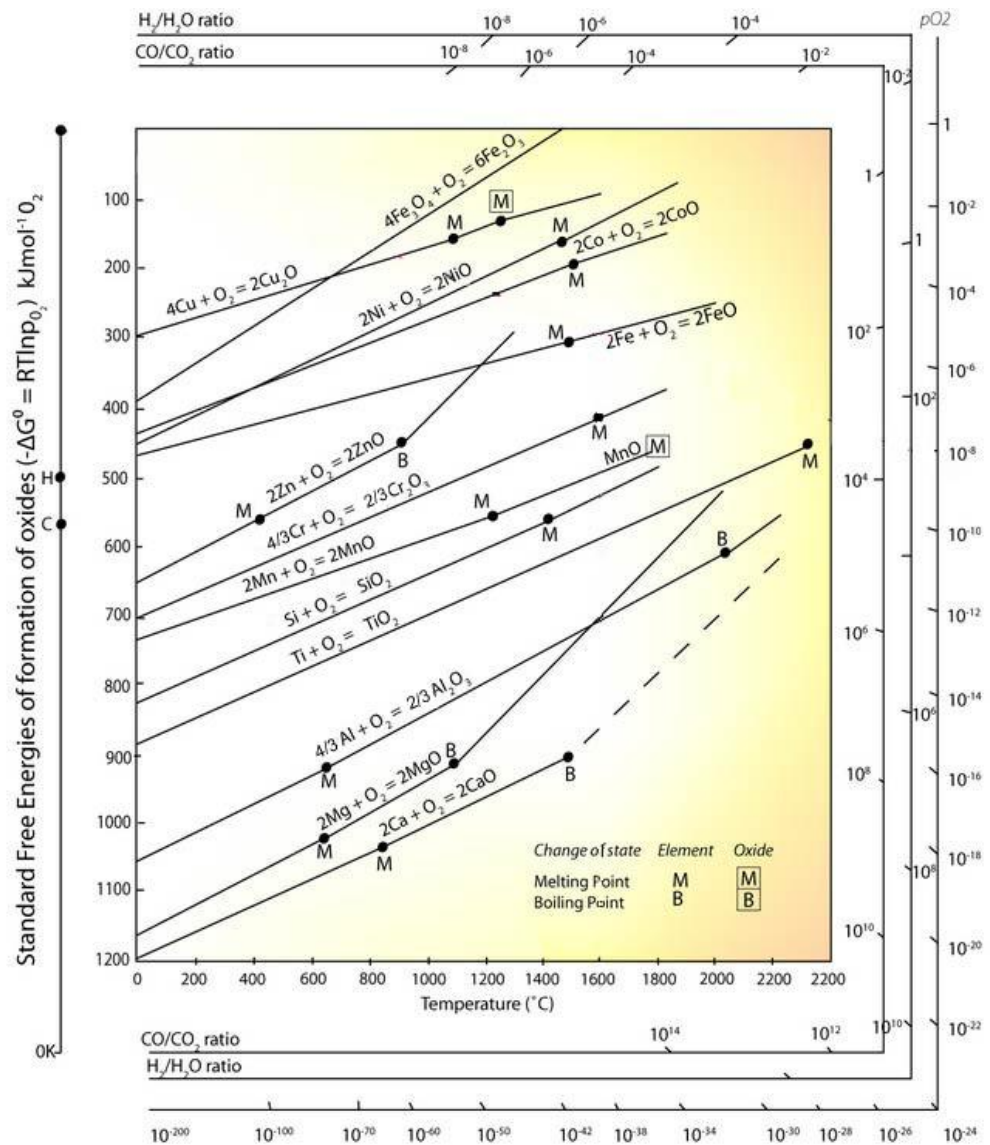


**Figure 5.6** Ellingham diagram plots showing the standard free energy of a reaction as a function of temperature.

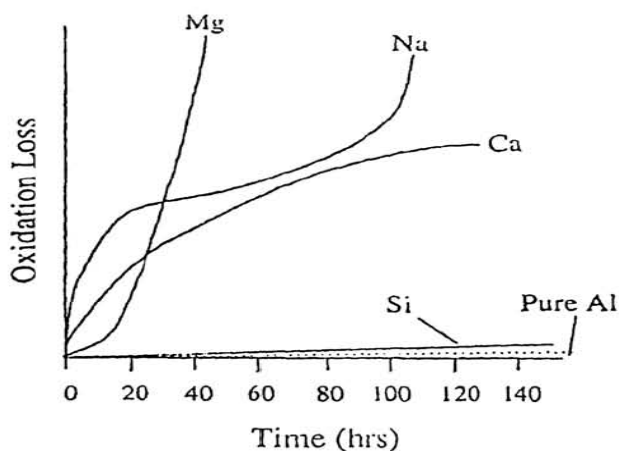


**Figure 5.7** Comparative oxidation losses caused by the addition of various elements to aluminium melt [6].

### **5.4.3 Refinement of primary Silicon crystals by zincblende ZnS**

ZnS occurs in two common polytypes, zincblende (also called sphalerite: cubic with lattice parameter  $a_0 = 5.41 \text{ \AA}$ ) and wurtzite (hexagonal with lattice parameters  $a_0 = 3.2495 \text{ \AA}$ ,  $c_0 = 5.2069 \text{ \AA}$ ). ZnS crystallizes with the cubic zincblende structure below 1020 °C and with the hexagonal wurtzite structure above this phase transition temperature [154]. On adding 0.5 wt% of zincblende ZnS powder to Al-18Si alloy, there was a significant refinement of the primary Si particles without any change in the modification level for the eutectic structure when compared with the commercial purity binary alloy. Micrographs in Figures 4.23 and 4.24 show that in using the prepared ZnS nanoparticles there was also good refinement of the primary Si without any change in eutectic. According to heterogeneous nucleation theory, ZnS particles can act as potent substrate for nucleation of primary Si. AIP has a similar cubic crystal structure and lattice parameter to those of Si and it is well known that AIP is a potent substrate for nucleation of primary Si. Zincblende ZnS is isostructural with AIP and has almost identical lattice parameter to those of AIP and Si, and so we might expect zincblende ZnS to also be a potent substrate for nucleation of primary Si. Optical micrographs and particle size distribution in Figures 4.23-4.25 show that in the present experiments the efficiency of ZnS which was added as micro or nano particles on refinement of primary Si in Al-18Si alloy is less than that of AIP by the addition of P.

Generally, a potent and efficient nucleus should provide the following [28];

- Crystallographic similarities.
- Less surface tension with the phase that is nucleating.
- Present as a solid at the appropriate temperature and composition of the liquid.
- Suitable size distribution.
- Capable of being wetted by the liquid.
- Should not be consumed or enveloped by reactions that have occurred earlier in solidification.

The reason for the lower efficiency of ZnS nano size powder prepared in the present experiments could be due to agglomeration of the ZnS particles, low wettability of ZnS with the melt, inappropriate particle size distribution or instability of zincblende under the operating condition. Despite the relative inefficiency of ZnS added in this form, the microstructure had a more strongly modified eutectic Si than that with P added. Loss of modification in the addition of P is due to the interaction of the added P with Ca existing in the melt which is mainly responsible for eutectic modification. It seems that there is no interaction between ZnS and the Ca existing in the melt and hence there was no loss of modification of the eutectic Si in Al-18Si alloy.

A new Al-ZnS master alloy has been successfully formed by an *in situ* reaction of Zn and Na<sub>2</sub>S in high purity aluminium melt as illustrated in section 4.4.3.4. This master alloy was used to refine primary Si crystals in solidification of hypereutectic Al-Si alloys. The SEM work shown in Figure 4.28 confirmed that there are many pre-formed ZnS particles contained in the master alloy.

The optical micrographs in section 4.4.3.5 show that the morphologies of primary Si crystals on solidification of Al-22Si alloy with the addition of the Al-ZnS master alloy are drastically changed from irregular coarse morphologies to fine regular particles. The primary Si crystals are refined from 74 µm to 26, 22, 24 µm by adding 0.05, 0.1, 0.15 wt% ZnS respectively with holding time of 20 min as shown in Figure 4.30. In comparison the average particle size of primary Si refined by 200 ppm P was 20 µm. It was clear that with the increase of ZnS content up to 0.1 wt% the average particle size of the primary Si decreases. Above 0.1 wt% ZnS the size of primary Si increases again slightly, this could be due to the agglomeration of ZnS particles in the melt.

With an increase of holding time after Al-ZnS master alloy addition up to 1.5 hr the primary Si size increased up to 33 µm for the addition of 0.1 wt% ZnS, which is larger than the primary Si particle size for the holding time of 20min. This inefficiency in the refinement of primary Si at higher holding time could be due to the agglomeration of ZnS particles or could be due to their sedimentation to the bottom of the crucible where the density of ZnS is 4.1 g/cm<sup>3</sup>. Also, the high holding time leads to continuous removal of the Ca by oxidation, and then the eutectic Si matrix loses its modification.

To be sure that zincblende ZnS was behind the refinement of primary Si and not the reactant materials; we examined the refinement effect of adding Na<sub>2</sub>S and Zn on solidification of hypereutectic Al-Si alloys was examined.

Sodium sulphide Na<sub>2</sub>S is an anhydrous crystalline solid with a density of 1.856 g/cm<sup>3</sup> at 20 °C. Its structure is a fluorite-type ionic cubic lattice with a lattice parameter of 6.504 Å [187]. Optical micrographs in Figure 4.35 show that adding Na<sub>2</sub>S had a strong modification effect on the eutectic Si in Al-15Si alloy. This action could be due to the decomposition of Na<sub>2</sub>S to produce Na that modifies the eutectic matrix. Na is specified as an optional modifier for Al-Si alloys. The optimum amount of Na used as modifier for eutectic Si in Al-Si alloys is 100 ppm [6]. It is clear from the micrographs that the eutectic Si is over modified and the primary Si became coarse and more irregular in shape when compared with the base Al-15Si alloy. The conclusion from these results is that Na<sub>2</sub>S cannot be behind the refinement of primary Si in the presence of ZnS particles produced from Zn and Na<sub>2</sub>S.

On adding Zn there was no change in the microstructure of commercial purity Al-Si alloy. Since, Na<sub>2</sub>S and Zn have no refinement effect we can conclude that neither is

responsible for the refinement of primary Si in the presence of ZnS particles produced *in situ* from Zn and Na<sub>2</sub>S. Since neither of the reactants used to form ZnS lead to refinement of primary Si, it can be concluded that the refinement of primary Si in the presence of ZnS must be due to potent nucleation on the zincblende ZnS particles.

#### 5.4.4 Summary

The conclusions from the above results are:

1. Both refinement of primary Si and modification of eutectic Si were only observed for the Al-15Si alloys with Mg content ≤ 0.3 wt% Mg when compared to the binary Al-15Si base alloy. This indicates that up to 0.3 wt% Mg content, MgAl<sub>2</sub>O<sub>4</sub> might form and then act as a nucleation substrate to refine primary Si. The average particle size of primary Si in Al-15Si alloy changed from 48 µm to 26, 22, 45 and 54.5 µm with the addition of 0.1, 0.3, 0.5 and 0.75 wt% Mg respectively. On addition of 1 wt% Mg there was no primary Si at all owing to the change in the eutectic formation reaction from the binary (Liquid → Al + Si) to the ternary (Liquid → Al + Si + Mg<sub>2</sub>Si)
2. There was significant coarsening of the primary Si and modification of the eutectic structure on adding 0.5 wt% MgO or CaO to Al-15Si alloy. This could be because of a lack of nucleation sites such as AIP particles, which have been removed by continuous oxidation of the melt or interaction with the inclusion.
3. On adding 0.5 wt% of ZnS powder of nanoparticles, there was a significant refinement of the primary Si particles without any loss of the modification level of the eutectic structure.
4. According to heterogeneous nucleation theory, ZnS particles can act as potent substrate for nucleation of primary Si. AIP has a similar cubic crystal structure and lattice parameter to those of Si and it is well known that AIP is a potent substrate for nucleation of primary Si. Zincblende ZnS is isostructural with AIP and has almost identical lattice parameter to those of AIP and Si; so we might expect zincblende ZnS to be a potent substrate for nucleation of primary Si.
5. The results from this study show that the novel Al-ZnS master alloy is a promising refiner in solidification of hypereutectic Al-Si alloys. It has the same efficiency as adding P in the form of Cu-P master alloy in the refinement of primary Si and follows the same refinement mechanism. It seems that there is no interaction between ZnS and Ca that exists in the

melt and hence there was no loss in modification of the eutectic Si in commercial purity Al-Si alloy.

6. Adding  $\text{Na}_2\text{S}$  has a modification effect on the eutectic Si in Al-15Si. This action could be due to the decomposition of  $\text{Na}_2\text{S}$  to produce Na that modifies the eutectic matrix.  $\text{Na}_2\text{S}$  also led to coarser primary Si. Adding Zn has no refinement effect on the primary Si in solidification of hypereutectic Al-Si alloys. The refinement of primary Si in the presence of  $\text{ZnS}$  produced *in situ* from Zn and  $\text{Na}_2\text{S}$  must be due to the  $\text{ZnS}$  particles.

## 5.5 Nucleation and Growth of Primary Silicon on $\text{Al}_2\text{O}_3$

There is much experimental evidence to conclude that some primary Si particles nucleate and grow on aluminium oxide bifilms during the solidification of hypereutectic Al-Si alloys as mentioned in section 5.3.

In the case of unalloyed aluminium, the oxide film is initially  $\gamma\text{-Al}_2\text{O}_3$ . As mentioned previously in section 2.4,  $\gamma\text{-Al}_2\text{O}_3$  is one of a number of metastable polytypes of  $\text{Al}_2\text{O}_3$  and is used extensively as a catalytic support material because of its high porosity and large specific surface area. At temperatures in the range 1000-1200°C,  $\gamma\text{-Al}_2\text{O}_3$  transforms rapidly into the thermodynamically stable  $\alpha\text{-Al}_2\text{O}_3$  phase (corundum), significantly reducing the surface area and thus suppressing the catalytic activity of the system. The phase transformation can be shifted to higher temperatures by doping  $\gamma\text{-Al}_2\text{O}_3$  with one of many elements such as La, Ba, or P [63].

It is well established that due to the high tendency of phosphorus to be adsorbed on the surface of  $\text{Al}_2\text{O}_3$ , a mono layer of phosphorus will form during the adsorption process [159]. According to the literature, the adsorption capacity of P on an  $\text{Al}_2\text{O}_3$  surface ranged between 15 and 30 mg/g for alumina having an average particle size between 1mm and 400nm respectively [188-189]. This may explain why P-doped  $\gamma\text{-Al}_2\text{O}_3$  is more efficient than P-doped  $\alpha\text{-Al}_2\text{O}_3$  but this needs further characterisation to be done.

Because of the high tendency of phosphorus to be adsorbed on the surface of  $\text{Al}_2\text{O}_3$  [159], AIP particles may first nucleate on  $\gamma\text{-Al}_2\text{O}_3$  and serve as nucleation sites for Si. Work by Pennors *et al.* [157] supported this hypothesis, they presented clear microstructures in which AIP particles are seen aligning along oxide bifilms and serve as nucleation sites for Si and subsequently spread across the oxide substrate.

The micrographs in Figure 4.39 show that P-doped  $\gamma\text{-Al}_2\text{O}_3$  is a potent substrate for nucleation of primary Si in solidification of hypereutectic Al-Si alloys and it is more efficient than P-doped  $\alpha\text{-Al}_2\text{O}_3$  or undoped  $\text{Al}_2\text{O}_3$ .

The conclusion from the above results is that phosphorus could be supported on alumina particles to be used as a refiner for primary Si in the solidification of hypereutectic Al-Si alloys. P is currently most effectively added to melt in the form of Cu-P, Al-Cu-P or Al-Fe-P master alloys, potentially leading to incorporation of impurities. Hence, using P-doped  $\gamma$ -Al<sub>2</sub>O<sub>3</sub> could be a perfect source of P without additional impurities. Also, the above result supports the hypothesis that nucleation of Si around oxide bifilms could be due to phosphorus adsorbed on the oxide film in aluminium alloys during processing cycles.

For future work, we need to determine the adsorption isotherm to find out the exact adsorption capacity of P on  $\gamma$ -Al<sub>2</sub>O<sub>3</sub> powder. Then, a deep study is required examining the stability of P-doped  $\gamma$ -Al<sub>2</sub>O<sub>3</sub> at casting conditions.

### 5.5.1 Summary

From above results, we can conclude that:

1. P-doped  $\gamma$ -Al<sub>2</sub>O<sub>3</sub> is a potent substrate to nucleate primary Si with good modification in the eutectic matrix in solidification of hypereutectic Al-Si alloys.
2. The high efficiency of  $\gamma$ -Al<sub>2</sub>O<sub>3</sub> may be because of its high porosity and large surface area which increase the adsorption capacity of P on the surface.

## 5.6 The New Solid-Liquid Duplex Casting

It has long been considered that the best mechanical properties of hypereutectic Al-Si alloys would be obtained from a microstructure that is both refined and modified. Due to the interaction between P and the modification chemicals such as Sr, Na and Ca, it is not possible to achieve both refinement of primary Si and modification of eutectic Si simultaneously in hypereutectic alloys [18]. This has become a goal for researchers and practising foundrymen [29].

The solid-liquid duplex casting process was devised to achieve simultaneous refinement and modification of Si phases in hypereutectic Al-Si alloys with improvement in mechanical properties. Unlike the existing liquid-liquid duplex casting process described in section 2.14.3, the solid-liquid duplex casting process offers the opportunity to retain pre-refined primary Si particles in a high Si P-treated solid alloy mixed with a Sr-treated melt to provide a modified eutectic matrix surrounding the pre-refined primary Si particles.

Optimizing the composition of the P-treated solid chips and Sr-treated melt with the casting temperature is very important for reasons of economics and efficient simultaneous refinement and modification of Si phases in the target alloy.

### **5.6.1 Optimum P and Sr content for P-treated and Sr-treated alloys**

The optical micrographs in Figure 4.46 show that with increasing P content in the P-treated high Si alloy, the particle size of primary Si decreased due to enhanced nucleation on potent AIP substrates to refine the primary Si. The primary Si size decreased sharply with 50ppm P then decreased more slowly with further additions. For the highest levels of P there was no further change in the size of primary Si as shown in Figure 4.48, but there was a good particle size distribution as shown in Figure 5.47. The P level of the P-treated high Si solid chips was fixed at 400 ppm. Accordingly, with the increase of P content up to 400ppm P in the P-treated solid alloy there was a significant decrease of the primary Si size in the target alloy as shown in Figures 4.49 and 4.53 with a good particle size distribution as shown in Figure 4.55.

With the increase of Sr in the target alloy, the eutectic Si matrix will be fully modified but there is a limitation to the amount of modifier addition to avoid porosity formation which then affects the mechanical properties of alloy obtained [84, 190]. The normal accepted limit of Sr is 200 ppm [6]. Thus this limit for the target alloy was set. With Sr over-modification, coarsening and reversion of fine fibrous Si structure to an interconnected plate form will take place [84], however, no over modification was observed throughout the present research confirming that the set limit was not too high.

According to the restricted nucleation theory of modification, Sr neutralizes the heterogeneous nucleation on AIP. This neutralization suppresses the undercooling in the melt before eutectic solidification and modification of the eutectic takes place [106]. Since in the solid-liquid duplex casting process there is no or only limited interaction between P and Sr, this theory is not valid. Alternatively, according to the restricted growth theories of modification, Sr is adsorbed on twin re-entrant grooves or growing surfaces of the Si phase, thus the growth of eutectic Si is inhibited and modification takes place. Generally, in the modification process, the number of twins increases in comparison with the unmodified eutectic Si which has few or no twins [84].

The results show that adding Sr to the low Si liquid starting alloy modifies the eutectic and restricts the growth of primary Si in the target alloy when compared with the case of mixing low Si liquid alloy without Sr with P-treated solid chips. It is well known that Sr is adsorbed onto growing surfaces of the Si phase, thus the growth of primary Si and eutectic Si is inhibited and modification takes place [84].

### 5.6.2 Optimum Si content in Sr-treated Al-Si alloy

The results described in section 4.6.2.2 and Table 4.3 show that the optimum Si content in Sr-treated melt for solid-liquid duplex casting process is the eutectic composition i.e. Al-12.6Si alloy. This alloy gave the minimum average particle size of primary Si in the target alloy when mixed with P-treated high Si alloy with a good particle size distribution as shown in Figure 4.65. Jones *et al.* [191] have measured the viscosity of liquid Al-Si alloys as a function of Si content. They found that the eutectic alloy has the lowest viscosity among the binary Al-Si alloys as shown in Figure 5.8. Hence, the mobility of pre-existing refined primary Si particles in eutectic alloy will be very easy without agglomeration and the average particle size will be reduced if compared with other Si alloys. Also, there will be less excess unrefined primary Si in the eutectic matrix and no need for more refinement.

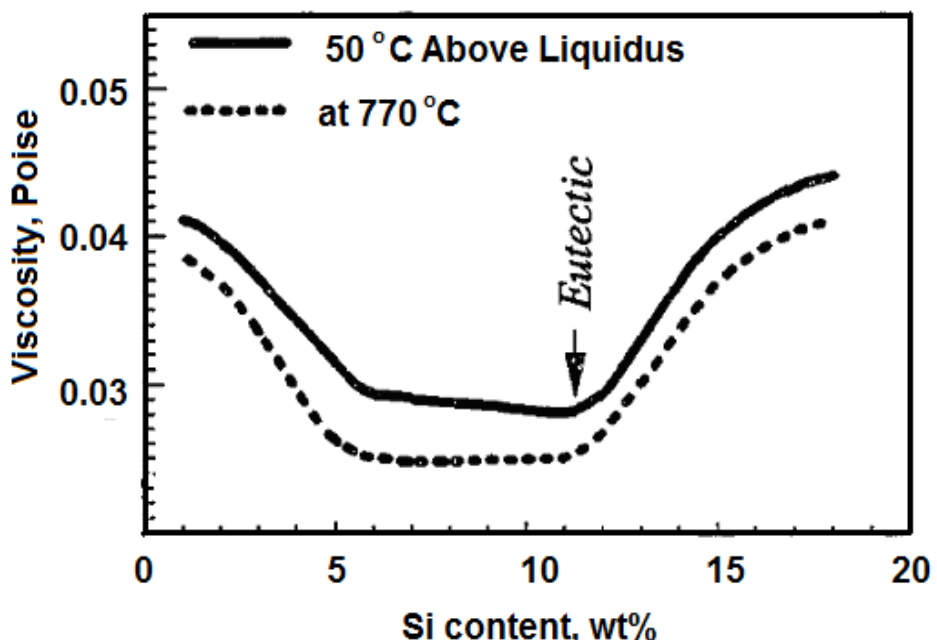


Figure 5.8: Viscosity of Al-Si alloys as a function of Si content [191].

### 5.6.3 Effect of casting temperature

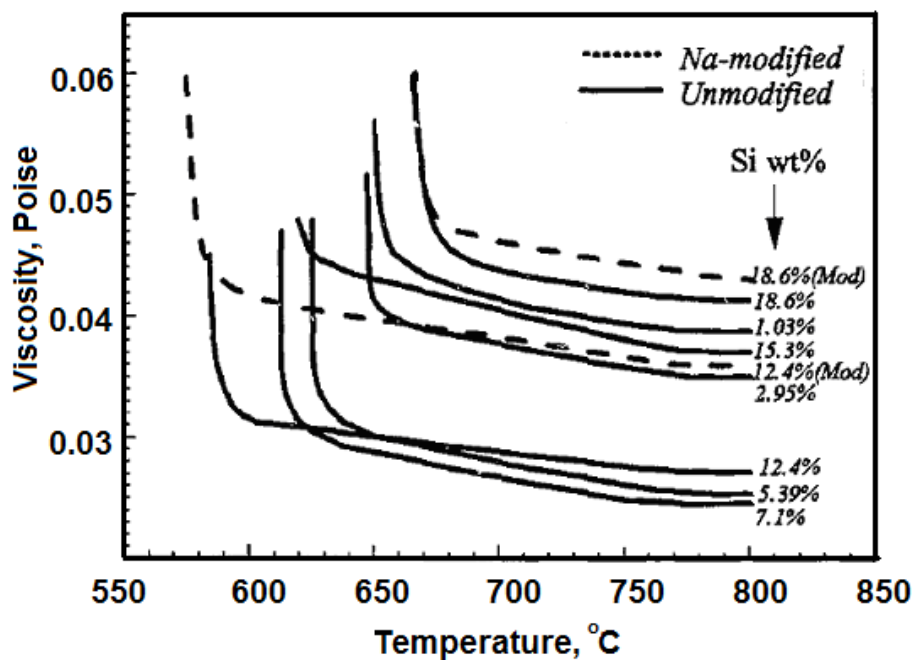
With the increase of casting temperature the size of primary Si particles increases and they are uniformly distributed in mixed modified eutectic Si matrix. With the increase of casting temperature, the solidification time will increase. Hence, there will be enough time for the growth of Si on the pre-existing refined primary Si particles. It is well established that the viscosity of liquid metals is sensitive to temperature. Jones *et al.* [191] have measured the viscosity of liquid Al-Si alloys as a function of temperature. They found that viscosity increases by decreasing the temperature, as shown in

Figure 5.9. Accordingly, increasing casting temperature will enhance the distribution of primary Si particles within the matrix and there will be a long time for the growth of primary Si. Working around 600 °C for Na-modified or unmodified eutectic alloy is quiet enough to reduce the viscosity as shown in Figure 5.9 which support our results. The only data available on the effect of modifiers on viscosity is for sodium as shown in Figure 5.9.

As mentioned in section 4.6.2.3 the higher temperature castings in this set of experiment was from above liquidus temperature so it is effectively no longer solid-liquid duplex casting and the pre-refined primary Si particles should be melted. The results gained from adding 200ppm P to Al-19Si alloy melted at 800 °C, cooled down to about 700 °C and then adding 200 ppm Sr to be cast from 610 °C, illustrated in Figure 4.69 prove the following hypothesis:

Most of the AlP particles in the P-treated hypereutectic Al-30Si alloy are tied up in the pre-existing primary Si particles and after melting to above the liquidus temperature there will be a thin layer of Si atoms adsorbed onto AlP surfaces, so there will be no direct contact between AlP and Sr. Accordingly the produced alloy consists of refined primary Si dispersed in a modified eutectic Al-Si matrix i.e. no loss in the modification.

Dai *et al.* [192] investigated the interface between AlP and Si crystals using pseudopotential-based density functional theory (DFT). They predicted the atomic structure, bonding type and ideal work of adhesion of the interface formed between AlP(100)/Si(100), AlP(110)/Si(110) and AlP(111)/Si(111). The results show that the main bonding between AlP and Si is covalent P-Si or Al-Si bonds, accompanied by some ionic characteristic. In all, the zigzag shape interfaces have larger adhesion energies. Moreover, the P-Si interfacial energy is larger than the Al-Si interfacial energy on the same crystallographic plane interface. As a result, Si atoms are not on the top of Al or P atoms, but on the bridge sites between Al and P atoms. This study supports our above hypothesis and proves the potency of AlP particles to nucleate and refine primary Si in hypereutectic Al-Si alloys. In addition, the pre-refined primary Si particles are stable when melted again and can control the morphology of primary and eutectic Si and then to achieve simultaneous refinement of primary Si and modification of eutectic Si.



**Figure 5.9:** Viscosity of Al-Si alloys as a function of temperature [191].

#### 5.6.4 The mechanism of refinement and modification in Solid-Liquid Duplex casting process

In mixing the hypereutectic P-treated Al-30Si solid chips with Sr-treated eutectic Al-12.6Si liquid alloy, there is a large difference between their solute content, in addition to the difference in their temperatures. Hence, thermal diffusion will occur simultaneously with solute diffusion during the mixing and casting process. The following heat and mass transfer processes will occur during the casting process:

- Absorption of the superheat of the eutectic Al-12.6Si liquid metal by the solid Al-30Si alloy. The driving force for thermal diffusion is the temperature difference between the two mixing alloys.
- Dissolution of Al-Si eutectic and some primary Si from the solid Al-30Si alloy and diffusion into the liquid.
- The dispersal of primary Si particles from the Al-30Si alloy within the liquid.
- Diffusion of Sr within the liquid to allow modification throughout the alloy on final solidification. The driving force for diffusion is the concentration difference between the solute rich Sr-treated Al-12.6Si alloy and newly melted grains the solute (Sr) free P-treated Al-30Si alloy.
- Nucleation and growth of the remaining primary Si on any available residual AlP particles.
- Eutectic solidification.

Due to the low casting temperature and the short solidification time in the solid-liquid duplex process, the pre-existing refined primary Si particles will be supplemented by very fine primary Si particles. The particle size distribution of primary Si in the target alloy illustrated in Figures 4.72 and 4.75 support this finding.

In the solid-liquid duplex casting process the pre-solidified Si-rich hypereutectic alloy (Al-30Si) contains refined primary Si particles due to enhanced nucleation of primary Si on AlP particles present because of the addition of 400 ppm P. This alloy partially remelts on its addition to the hotter liquid eutectic alloy, but a large proportion of the pre-refined primary Si particles are retained. Most of the P in the resulting intermediate hypereutectic alloy (Al-19Si) is tied up in the AlP particles within the pre-existing primary Si particles. As a result, interaction between Sr and P in the liquid is limited and there is an excess of Sr. Thus the Al-Si eutectic will be fully modified.

In conclusion, in the conventional casting process, simultaneous addition of excess P and Sr tends to produce refined primary Si particles dispersed in an only partially modified eutectic Al-Si matrix due to the interaction between P and Sr. On the other hand, refined primary Si crystals dispersed in a fully modified eutectic are observed in the ingots obtained by combined use of the solid-liquid duplex casting process and additions of P and Sr. This finding is more practical and acceptable if compared with that obtained by combined use of liquid-liquid duplex process and addition of Na and P, where the average particle size of primary Si was 40  $\mu\text{m}$  dispersed in a partial modified eutectic [148].

In addition to the simultaneous refinement of primary and modification of eutectic Si phases, the solid-liquid duplex process shows that the tensile strength (UTS) increased by approximately 14% and the elongation more than doubled compared with conventionally cast process. The probability of crack initiation by premature fracture of Si decreases with the refinement and modification of Si phases [17, 134]. The improvement of mechanical properties is therefore attributed to the combination of refined primary Si and to the fibrous structure of the modified Al-Si eutectic matrix.

### 5.6.5 Summary

The conclusions to Solid-Liquid Duplex casting process are:

1. The solid-liquid duplex casting process is a promising technique for producing hypereutectic Al-Si alloys with refined primary Si distributed in a modified Al-Si eutectic matrix. The solid-liquid duplex casting process allows the simultaneous action of P and Sr that is not possible in conventional casting.
2. P added to the high-Si hypereutectic component provides pre-refined primary Si particles. Since most of the P is tied up in AlP particles within the pre-existing

primary Si, the Sr added to the low Si liquid component cannot be neutralized and is available for effective modification during eutectic solidification.

3. The optimum P content in the P-treated solid chips should be enough to produce fine pre-existing refined primary Si particles. The optimum Sr in the Sr-treated liquid alloy should be enough to produce a target alloy with 200 ppm Sr.
4. The casting temperature should be low enough to provide the target alloy in the Liquid + Primary Si phase field before casting.
5. The optimum Si content in the Sr-treated melt alloy is 12.6 wt% i.e. Sr-treated Al-12.6Si gives the minimum primary Si particle size in the target alloy.
6. The static mechanical properties of Al-Si produced by the solid-liquid duplex casting process are significantly better than conventionally cast untreated Al-Si and slightly better than conventionally cast Al-Si treated with P and/or Sr.

# Chapter 6

## Conclusions

The overall goal of the thesis was to develop one or more methods of refining primary Si in cast hypereutectic Al-Si alloys to compete with the conventional process of adding phosphorous and to achieve the secondary goal of simultaneous modification of silicon in the Al-Si eutectic. The conclusions drawn from this investigation are summarised as follows:

### 6.1 Effect of Solidification Rate on Primary and Eutectic Si

The morphologies and homogeneity of distribution of primary and eutectic Si in solidified hypereutectic Al-Si alloys are a strong function of the solidification conditions such as cooling rate and melt superheat. The conclusions are:

- At low cooling rate, i.e. less than 15 K/s, the morphology of primary Si was mixture of branched plate-like and polyhedral particles dispersed in an acicular eutectic structure. With the increase of cooling rate, the primary Si became mostly polyhedral and dispersed in a refined lamellar eutectic structure.
- There is a tendency for primary Si to segregate to the top of sampled specimens particularly those solidified under slow cooling conditions. A water cooled steel mould with cooling rate in excess of 15 K/s was very efficient in preventing the macro-segregation of primary Si even at a high pouring temperature. The high cooling rate of the water cooled steel mould generally produced a good distribution of compact primary Si particles in a refined lamellar eutectic matrix.
- The morphology of Si changes with increasing melt temperature. A high melt superheat produces a good distribution of polyhedral primary Si particles in a refined lamellar eutectic matrix.
- The eutectic Al-Si structure seems to become more homogeneous with increasing in the melt superheat.
- The average particle sizes and volume fraction of primary Si decrease approximately linearly up to a casting temperature of 845 °C and then decrease at a lower rate as temperature increases further. The shape factor increase linearly up to 845 °C and then increases at a lower rate. The particle number density of primary Si increases slightly with increasing casting temperature up to

845 °C and then significantly increased with further increasing casting temperature beyond 845 °C.

## 6.2 Refinement and Modification in High Purity Hypereutectic Al-Si Alloy

Due to the interaction between P and Ca the simultaneous refinement and modification of Si phases can not be achieved during conventional casting of hypereutectic Al-Si alloys. Experiments were conducted to investigate the refinement of primary Si and modification of eutectic Si during solidification of high purity hypereutectic Al-Si alloy. The conclusions from this study were:

- High purity Al-15Si alloy, cast in the steel mould with cooling rate 15K/s, consists of irregular coarse primary Si particles, 68 µm in size, dispersed in a lamellar eutectic structure. On the other hand, commercial purity Al-15Si alloy consists of a compact polyhedral primary Si with an average particle size of approximately 48 µm in a mostly fibrous (modified) eutectic.
- Adding 20 ppm P to high purity Al-15Si alloy was quite enough to refine primary Si from an average particle size of 68 µm to 20 µm. The same amount of P added to commercial purity Al-15Si refined the primary Si from an average particle size of 48 µm to 25 µm.
- Adding 30 ppm of Ca to the high purity Al-15Si can transform the eutectic matrix to a modified fibrous structure, and no primary Si is evident, i.e. the apparent eutectic position is shifted.

## 6.3 Effect of Ca Level on Primary and Eutectic Si

The effect of Ca content on Si morphology and its interaction with other alloying elements were studied either by reducing its content by the use of  $K_2SiF_6$  (AP1) flux or increasing its content by adding 0.5 wt% Ca into the melt. The conclusions from this study were:

- The commercial purity Al-15Si alloy contained 200 ppm Ca which was sufficient to lead to a modified Al-Si eutectic.
- After the addition of  $K_2SiF_6$  flux the Ca impurity level was 20 ppm which was too little to modify the eutectic Si, but primary Si was refined. This suggests fluxing with  $K_2SiF_6$  can remove Ca effectively such that the trace level of P (~ 20 ppm) in commercial purity hypereutectic Al-Si alloys is sufficient to refine the primary Si without any deliberate addition of P.
- In the case of adding 0.5 wt% Ca to the Al-15Si alloy, the eutectic Si was highly modified and the primary Si was coarse and irregular in morphology (unrefined).

- The addition of such a high level of Ca led to enhanced quantities of entrained oxide inclusions/bifilms. During the solidification of the Al-15Si-0.5Ca alloy, the first phase to solidify was  $\text{Al}_2\text{CaSi}_2$  which nucleated on the oxide bifilms. Crystallographic misfit calculations showed that low order orientation relationships exist between  $\text{Al}_2\text{CaSi}_2$  and  $\alpha\text{-Al}_2\text{O}_3$  or  $\gamma\text{-Al}_2\text{O}_3$  with low misfit over two unit cells, indicating that either of these two oxides could be an effective substrate for nucleation of  $\text{Al}_2\text{CaSi}_2$ . Primary Si then formed by nucleation and growth on the  $\text{Al}_2\text{CaSi}_2$  particles.
- For hypereutectic Al-Si alloys, fluxing with  $\text{K}_2\text{SiF}_6$  prior to making alloying additions of Mg led to significant refinement of primary Si particles. The fine primary Si particles were dispersed in a plate-like eutectic structure. The removal of Ca led to an increase in the number of available AIP particles for the nucleation of primary Si along with a reduction in the modification effect.
- For the interaction between Sb and Ca, on adding 0.5 wt% Sb to the commercial purity Al-15Si alloy, which contained more than 200 ppm Ca, the eutectic Si was refined in lamellar structure and the primary Si particles became more irregular in shape with particle size of 65  $\mu\text{m}$ . With reducing Ca content by fluxing, irregular particles of primary Si 70  $\mu\text{m}$  in size dispersed in a finer lamellar eutectic structure produced in adding 0.5% Sb to Al-15Si alloy. Hence, removing Ca before adding Sb to Al-Si alloys can improve the modification process due to Sb.

#### **6.4 Effect of Chemical Additions on Primary and Eutectic Si**

The effect of adding various inoculants on the Si morphology can be concluded as follows:

- Refinement of Si was observed for the Al-15Si alloy with Mg content  $\leq 0.3$  wt%. The refinement of primary Si could be due to the formation of  $\text{MgAl}_2\text{O}_4$ . So, for this case up to 0.3 wt% Mg content might be sufficient to form the  $\text{MgAl}_2\text{O}_4$  which then acts as a nucleation substrate to refine primary Si. For an addition of 1 wt% Mg, primary Si was completely absent. This is owing to the change of the eutectic formation reaction from the binary to the ternary and associated shifts in eutectic composition and temperature.
- There was significant coarsening of the primary Si with modification of the eutectic structure on adding 0.5%  $\text{MgO}$  or  $\text{CaO}$ . This could be because of a lack of nucleation sites such as AIP particles, which have been removed by continuous oxidation of the melt or interaction with the inclusions.

- On adding 0.5 wt% of  $\leq 44 \mu\text{m}$  ZnS (zincblende) powder to Al-18Si, there was a significant refinement of the primary Si particles without any change in the modification level of the eutectic structure. However the refinement was not as effective as the conventional process of adding P via Cu-P.
- Synthesised ZnS nanoparticles led to primary Si particles with slightly greater refinement than those produced by adding the micron scale ZnS powder, although the refinement was still less effective than the standard technique of adding P via Cu-P.
- A novel Al-ZnS master alloy was developed by *in situ* reaction of Zn and Na<sub>2</sub>S in the Al melt. It refines primary Si to the same extent as that achieved by adding P via Cu-P following the same refinement mechanism. Furthermore, the use of ZnS retains a modified eutectic structure. It seems that there is no interaction between ZnS and the Ca that exists in the melt and hence there was no loss of modification of the eutectic Si in commercial purity Al-Si alloy.
- Adding Na<sub>2</sub>S or Zn has no effect on the size of primary Si particles, but Na<sub>2</sub>S has a modification effect on the eutectic Si in Al-15Si. This action could be due to the decomposition of Na<sub>2</sub>S to produce Na that modifies the eutectic matrix. These results confirm that the refinement effect of primary Si is due to ZnS and not to the residual reactants in the melt.

## 6.5 Nucleation and Growth of Primary Si on Al<sub>2</sub>O<sub>3</sub>

Given the presence of some evidence in the literature, experiments were conducted to examine the possibility of nucleation and growth of Si on Al<sub>2</sub>O<sub>3</sub> or P-doped Al<sub>2</sub>O<sub>3</sub> particles. The results show that:

- P-doped  $\gamma$ -Al<sub>2</sub>O<sub>3</sub> is a potent substrate to nucleate primary Si whilst good modification of the eutectic matrix is retained during solidification of hypereutectic Al-Si alloys.
- The high efficiency of  $\gamma$ -Al<sub>2</sub>O<sub>3</sub> to refine primary Si is because of its high porosity and large surface area which increase the adsorption capacity of P on the surface.
- Using P-doped  $\gamma$ -Al<sub>2</sub>O<sub>3</sub> could be a perfect source of P without additional incorporation impurities associated with artificial Cu-P, Al-Cu-P or Al-Fe-P master alloys.

## **6.6 The New Solid-Liquid Duplex Casting Process**

Due to the interaction between P and the modifying elements such as Sr, Na and Ca, it is not normally possible to achieve both refinement of primary Si and modification of eutectic Si simultaneously in hypereutectic alloys. The new solid-liquid duplex casting process was devised to achieve simultaneous refinement of primary Si and modification of eutectic Si in hypereutectic Al-Si. The conclusions of applying this process are as follow:

- P added to the high Si hypereutectic alloy provides pre-refined primary Si particles. Since most of the P is tied up in AlP particles within the pre-existing primary Si, the Sr added to the low Si liquid component cannot be neutralized and is available for effective modification during eutectic solidification. On combining the solid and liquid alloys the temperature should be within the appropriate window to provide the target alloy in the Liquid + Primary Si phase field before casting.
- The optimum P content in the P-treated solid chips should be enough to produce fine pre-existing refined primary Si particles. The optimum Sr in the Sr-treated liquid alloy should be enough to produce a target alloy with 200 ppm Sr.
- The optimum Si content in the Sr-treated melt alloy is 12.6 wt% (eutectic composition) which gives the minimum primary Si particle size in the target alloy.
- The static mechanical properties of Al-Si produced by the solid-liquid duplex casting process are significantly better than those of conventionally cast untreated Al-Si and slightly better than those of conventionally cast Al-Si treated with P and/or Sr.

# Chapter 7

## Recommendations for further work

### 7.1 Refinement of Primary Si Crystals by Zincblende ZnS

- Further work is required to optimize the operating conditions such as casting temperature with different holding time prior to casting in order to increase the efficiency of the refinement process by using ZnS zincblende.
- It could be useful to study the possibility of producing an Al-ZnS master alloy with higher concentration of ZnS particles to minimize the dilution of the treated alloy by the aluminium in the master alloy.
- A deepest analysis of the morphology and particle size distribution of ZnS zincblende prepared *in situ* or in the Al-ZnS master alloy is required.

### 7.2 Nucleation and Growth of Primary Si on $\text{Al}_2\text{O}_3$

- Work is required to detect the phosphorus at the interface between oxide bifilm and the nucleated primary Si particle. This extra research is to support the hypothesis that P can be adsorbed on the oxide bifilm and then nucleate the primary Si particles.
- Optimization of the doping conditions of  $\gamma\text{-Al}_2\text{O}_3$  with P for the refinement of primary Si in hypereutectic Al-Si alloys is required to produce more stable and higher efficiency P-doped  $\gamma\text{-Al}_2\text{O}_3$ .

### 7.3 The New Solid-Liquid Duplex Casting Process

- Further work is required to optimize the solid-liquid duplex process. For instance the size of P-treated Al-Si alloy chips could be minimized in order to improve the distribution of primary Si particles in the target alloy and to make the process more practical by mixing fine shot of P-treated Al-Si alloy with liquid Sr-treated Al-Si.
- Additional characterisation and investigation of application of the solid-liquid duplex process to commercial compositions is required.

## References

1. Harun, M., Talib, I. A. and Daud, A. R., *Effect of Element Additions on Wear Property of Eutectic Aluminium-Silicon Alloys*. Wear, 1996. **194**(1-2): p. 54-59.
2. Nagarajan, S., Dutta, B. and Surappa, M. K., *The Effect of SiC Particles on the Size and Morphology of Eutectic Silicon in Cast A356/SiC<sub>p</sub> Composites*. Compos. Sci. Technol., 1999. **59**(6): p. 897-902.
3. Zeren, M., Karakulak, E., *Influence of Ti Addition on the Microstructure and Hardness Properties of Near-Eutectic Al-Si Alloys*. J. Alloys Compd., 2008. **450**(1-2): p. 255-259.
4. Kudoh, M., Ohmi, T. and Matsuura, K., *Step Casting (Chapter 14)*: p. 348 in; Cantor, B. and O'Reilly, K. (Ed.), *Solidification and Casting* 2003, UK: IOP publishing Ltd.
5. Utigard, T.A., Friesen, K., Roy, R.R., Lim, J., Silny, A. and Dupuis, C., *The Properties and Uses of Fluxes in Molten Aluminum Processing*. J. Minerals, Met. Mater. Soc., 1998. **50**(11): p. 38-43.
6. Kumari, S.S.S., Pillai, R. M. and Pai, B. C., *Role of Calcium in Aluminium Based Alloys and Composites*. Int. Mater. Rev., 2005. **50**(4): p. 216-238.
7. Ye, H., *An Overview of the Development of Al-Si Alloy Based Material for Engine Applications*. J. Mater. Eng. Perf., 2003. **12**(3): p. 288-297.
8. Boss, S.K., Kumar, R., *Structure of Rapidly Solidified Aluminium-Silicon Alloys*. J. Mater. Sci., 1973. **8**(12): p. 1795-1799.
9. Kyffin, W.J., Rainforth, W. M. and Jones, H., *Effect of Phosphorus Additions on the Spacing between Primary Silicon Particles in a Bridgman Solidified Hypereutectic Al-Si Alloy*. J. Mater. Sci., 2001. **36**(11): p. 2667-2672.
10. Xu, C.L., Wang, H. Y., Qiu, F., Yang, Y. F. and Jiang, Q. C., *Cooling Rate and Microstructure of Rapidly Solidified Al-20wt.% Si Alloy*. J. Mater. Sci. Eng. A 2006. **417**(1-2): p. 275-280.
11. Bian, X., Wang, W., *Thermal-Rate Treatment and Structure Transformation of Al-13 wt.% Si Alloy Melt*. Mater. Lett., 2000. **44**(1): p. 54-58.
12. Li, P., Nikitin, V. I., Kandalova, E. G. and Nikitin, K. V., *Effect of Melt Overheating, Cooling and Solidification Rates on Al-16wt.%Si Alloy Structure*. J. Mater. Sci. Eng. A, 2002. **332**(1-2): p. 371-374.
13. Xu, C.L., Jiang, Q. C., *Morphologies of Primary Silicon in Hypereutectic Al-Si Alloys with Melt Overheating Temperature and Cooling Rate*. J. Mater. Sci. Eng. A, 2006. **437**(2): p. 451-455.

14. Liu, X., Wu, Y. and Bian, X., *The Nucleation Sites of Primary Si in Al-Si Alloys After Addition of Boron and Phosphorus*. J. Alloys Compd., 2005. **391**(1-2): p. 90-94.
15. Yilmaz, F., Atasoy, O. A. and Elliott, R., *Growth Structures in Aluminium-Silicon Alloys II. The Influence of Strontium*. J. Cryst. Growth, 1992. **118**(3-4): p. 377-384.
16. Chang, J., Moon, I. and Choi, C., *Refinement of Cast Microstructure of Hypereutectic Al-Si Alloys Through the Addition of Rare Earth Metals*. J. Mater. Sci., 1998. **33**(20): p. 5015-5023.
17. Kilicaslan, M.F., Lee, W., Lee, T., Sohn, Y. and Hong, S., *Effect of Sc Addition on the Microstructure and Mechanical Properties of As-Atomized and Extruded Al-20Si Alloys*. J. Mater. Lett., 2012. **71**(15 March): p. 164-167.
18. Choi, H., Li, X. , *Refinement of Primary Si and Modification of Eutectic Si for Enhanced Ductility of Hypereutectic Al-20Si-4.5Cu Alloy with Addition of Al<sub>2</sub>O<sub>3</sub> Nanoparticles*. J. Mater. Sci, 2012. **47**(7): p. 3096-3102.
19. Choi, H., Konishi, H. and Li, X., *Al<sub>2</sub>O<sub>3</sub> Nanoparticles Induced Simultaneous Refinement and Modification of Primary and Eutectic Si Particles in Hypereutectic Al-20Si Alloy*. J. Mater. Sci. Eng. A, 2012. **541**(15 April): p. 159-165.
20. Wang, Q., Wang, C., Liu, T., Wang, K. and He, J., *Control of Solidified Structures in Aluminum-Silicon Alloys by High Magnetic Fields*. J. Mater. Sci., 2007. **42**(24): p. 10000-10006.
21. Wang, W.M., Liu, J. M., Bian, X. F., Chen, X. Y. and Liu, Z. G., *Formation of Block-Like Eutectic Silicon under Direct Current in Eutectic Al-Si Alloy*. J. Mater. Sci. Lett., 2002. **21**(8): p. 613-615.
22. Inci, L., Tavoosfard, S. and Stoilov, V., *Microstructure Evolution of AlSi Nano-Composite under Shear Load*. Int. J. Mech. Mater. Des., 2008. **4**(2): p. 197-203.
23. Barekar, N.S., Babu, N. H., Dhindaw, B. K. and Fan, Z., *Effect of Intensive Shearing on Morphology of Primary Silicon and Properties of Hypereutectic Al-Si Alloy*. Mater. Sci. Technol., 2010. **26**(8): p. 975-980.
24. Lu, D., Jiang, Y., Guan, G., Zhou, R., Li, Z. and Zhou, R., *Refinement of Primary Si in Hypereutectic Al-Si Alloy by Electromagnetic Stirring*. J. Mater. Proc. Techn., 2007. **189**(1-3): p. 13-18.
25. Zhang, L., Eskin, D.G., Miroux, A. and Katgerman, L., *Formation of Microstructure in Al-Si Alloys under Ultrasonic Melt Treatment*, in *TMS (The Minerals, Metals & Materials Society)*. 2012, Light Metals. p. 999-1004.

26. Campbell, J., *Effects of Vibration during Solidification*. Int. Mater. Rev., 1981. **26**(1): p. 71-108.
27. Abu-Dheir, N., Khraisheh, M. , Saito, K. and Male, A., *Silicon Morphology Modification in the Eutectic Al-Si Alloy Using Mechanical Mold Vibration*. J. Mater. Sci. Eng. A, 2005. **393**(1-2): p. 109-117.
28. Nogita, K., McDonald, S. D., Tsujimoto, K., Yasuda, K. and Dahle, A. K., *Aluminium Phosphide as a Eutectic Grain Nucleus in Hypoeutectic Al-Si Alloys*. J. Electron Microscopy, 2004. **53**(4): p. 361-369.
29. Tenekeedjiev, N., *Strontium Treatment of Aluminum-17% Silicon Casting Alloys (Ph.D. Thesis)*. 1989, Department of Mining and Metallurgical Engineering, McGill University, Montreal, Quebec.
30. Jorstad, J., Apelian, D., *Hypereutectic Al-Si Alloys: Practical Casting Considerations*. Int. J. Met. cast., 2009. **3**(3): p. 13-36.
31. Fan, Z., *Semisolid Metal Processing*. Int. Mater. Rev., 2002. **47**(2): p. 49-85.
32. Cantor, B., O'Reilly, K., *Solidification and Casting* 2003, UK: IOP publishing Ltd.
33. Ward, P.J., Atkinson, H. V., Anderson, P. R. G., Elias, L. G., Garcia, B., Kahlen, L. and Rodriguez-ibabe, J. M., *Semi-Solid Processing of Novel MMCs Based on Hypereutectic Aluminium-Silicon Alloys*. Acta Metall. Mater., 1996. **44**(5): p. 1717-1727.
34. Taylor, J.A., *Metal Related Castability Effects in Aluminium Foundry Alloys*. Cast Metals, 1995. **8**(4): p. 225-252.
35. Murray, J.L., McAlister, A. J., *The Al-Si (Aluminum-Silicon) System*. Bull. Alloy Phase Diagrams, 1984. **5**(1): p. 74-84.
36. Davis, J.R., *Aluminum and Aluminum Alloys*. ASM International. 1993, Ohio.
37. Elliott, R., *Eutectic Solidification Processing*. 1984, London: Butterworths & Co.
38. Polmear, I.J., *Light Alloys*. 3<sup>rd</sup> ed. 1995, Oxford: Butterworth-Heinemann.
39. Makhlouf, M.M., Guthy, H. V., *The Aluminum-Silicon Eutectic Reaction: Mechanisms and Crystallography*. J. Light Metals, 2001. **1**(4): p. 199-218.
40. Wislei, R.O., Noé, C., Leandro, C. P. and Amauri, G., *Corrosion Resistance and Mechanical Properties of an Al 9wt%Si Alloy Treated by Laser Surface Remelting*. Int. J. Electrochem. Sci., 2009. **4**(6): p. 820-831.
41. Kaufman, J.G., Rooy , E. L., *Aluminum Alloy Castings: Properties, Processes, and Applications*. 2004: ASM International.
42. Jayakumar, E., Rajan, T. P. D. and Pai, B. C., *Effect of Mg on Solidification Microstructures of Homogenous and Functionally Graded A390 Aluminum Alloys*. Trans. Indian Inst. Metals, 2012. **65**(6): p. 677-681.

43. Street, A.C., *The Diecasting Book*. 2<sup>nd</sup> ed. 1986: Portcullis Press Ltd. , Surry, England.
44. Emadi, D., Whiting, L. V. , Sahoo, M. , Sokolowski , J. H., Burke , P. and Hart, M., *Optimal Heat Treatment of A356.2 Alloy*. Light Metals, TMS (The Minerals, Metals & Materials Society), 2003: p. 983-989.
45. Mondolfo, L.F., *Aluminium Alloys: Structure and Properties*. 1976, London: Butterworths.
46. Fang, X., Shao, G., Liu, Y. Q. and Fan, Z., *Effects of Intensive Forced Melt Convection on the Mechanical Properties of Fe-Containing Al-Si Based Alloys*. J. Mater. Sci. Eng. A, 2007. **445-446**(15 February): p. 65-72.
47. Yan, F., Ji, S. and Fan, Z., *Effect of Excess Mg on the Microstructure and Mechanical Properties of Al-Mg<sub>2</sub>Si High Pressure Die Casting Alloys*. Mater. Sci. Forum, 2013. **765**: p. 64-68.
48. Yang, Y., Li, Y., Wu, W., Zhao, D. and Liu, X., *Effect of Existing Form of Alloying Elements on the Microhardness of Al-Si-Cu-Ni-Mg Piston Alloy*. Mater. Sci. Eng. A, 2011. **528**(18): p. 5723-5728.
49. Abdollahi, A., *Effeet of Ca as a Modifier in Hypoeutectic Al-Si Alloys (M.Sc. Thesis)*. 1998, Department of Mining and Metallurgical Engineering, McGill University, Montreal, Canada.
50. Chikezie, W.O., Boniface, A. O., Simeon, I. N. and Camillus, S. O., *Structural Modification of Sand Cast Eutectic Al-Si Alloys with Sulfur/Sodium and Its Effect on Mechanical Properties*. World J. Eng. Technol., 2013. **1**: p. 9-16.
51. Lu, S.Z., Hellawell, A., *The Mechanism of Silicon Modification in Aluminum-Silicon Alloys: Impurity Induced Twinning*. Metall. Mater. Trans. A, 1987. **18**(10): p. 1721-1733.
52. <http://www.nortal.com>
53. <http://www.kspg.com/en/products/cylinder-blocks/low-pressure-die-cast-cylinder/brochures/>
54. <http://www.matweb.com/search/datasheet.aspx>
55. <http://www.nasasolutions.com/technology/TOP31294-Aluminum-Alloy.php>
56. [http://www.us.mahle.com/MAHLE\\_North\\_America/EN/Products/Piston-Systems/Aluminium-pistons-for-diesel-engines](http://www.us.mahle.com/MAHLE_North_America/EN/Products/Piston-Systems/Aluminium-pistons-for-diesel-engines) .
57. Khalifa, W., Samuel, F. and Gruzleski, J., *Nucleation of Solid Aluminum on Inclusion Particles Injected into Al-Si-Fe Alloys*. Metall. Mater. Trans. A, 2004. **35**(10): p. 3233-3250.
58. Kim, J.K., Rohatgi, P. K. , *Nucleation on Ceramic Particles in Cast Metal-Matrix Composites*. Metall. Mater. Trans. A, 2000. **31**(4): p. 1295-1304.

59. Kurz, W., Fisher, D.J., *Fundamentals of Solidification*. 1984, Switzerland: Trans Tech Publications Ltd.
60. Wang, Y., Li, H. T. and Fan, Z., *Oxidation of Aluminium Alloy Melts and Inoculation by Oxide Particles*. Trans. Indian Inst. Metals, 2012. **65**(6): p. 653-661.
61. Davis, J.R., *Heat-Resistant Materials*. 1997, ASM International.
62. Wang, Y., Suryanarayana, C. and An, L., *Phase Transformation in Nanometer-Sized  $\gamma$ -Alumina by Mechanical Milling*. J. Am. Ceram. Soc., 2005. **88**(3): p. 780-783.
63. Borisevich, A.Y., Pennycook, S. J., Rashkeev, S. N. and Pantelides, S. T., *Studies of Single Dopant Atoms on Nanocrystalline  $\gamma$ -Alumina Supports by Aberration-Corrected Z-Contrast STEM and First Principles Calculations*. Microsc. Microanal., 2003. **9**(2): p. 398-399.
64. McKay, B., *Heterogeneous Nucleation in Al-Si Alloys (Ph.D. Thesis)*. 2002, University of Oxford, UK.
65. Campbell, J., Tiryakioglu, M., *Review of Effect of P and Sr on Modification and Porosity Development in Al-Si Alloys*. J. Mater. Sci. Technol., 2010. **26**(3): p. 262-268.
66. Cao, X., Campbell, J., *The Nucleation of Fe-Rich Phases on Oxide Films in Al-11.5Si-0.4Mg Cast Alloys*. Metall. Mater. Trans. A, 2003. **34**(7): p. 1409-1420.
67. Campbell, J., *An Overview of the Effects of Bifilms on the Structure and Properties of Cast Alloys*. Metall. Mater. Trans. B, 2006. **37**(6): p. 857-863.
68. Zhang, Z., Li, H-T, Stone, I. C. and Fan, Z., *Refinement of Primary Si in Hypereutectic Al-Si Alloys by Intensive Melt Shearing*. J. Mater. Sci. Eng., 2011. **27**: p. 1-6.
69. Nogita, K., Drennan, J. and Dahle, A. K., *Evaluation of Silicon Twinning in Hypo-Eutectic Al-Si Alloys*. Mater. Trans. , 2003. **44**(4): p. 625-628.
70. Kumari, S.S.S., Pillai, R. M. and Pai, B. C. , *Structure and Properties of Calcium and Strontium Treated Al-7Si-0.3Mg Alloy: A Comparison*. J. Alloys Compd., 2008. **460**(1-2): p. 472-477.
71. Kumari, S.S.S., *Influence of Alloying Additions on the Structure and Properties of Al-7Si-0.3Mg Alloy (Ph.D. Thesis)*. 2006, Materials and Minerals Division, Cochin University of Science and Technology, India.
72. Suzuki, T., Oshiro, N., *US Pat. No. 6, 336, 955*. 2002.
73. Nakae, H., Kanamoro, H. and Song, K. K. in *Proc. 3rd Asian Foundry Congress*. 1995. Kyongju, South Korea.

74. El-Hadad, S., Samuel, A.M., Samuel, F.H., Doty, H.W. and Valtierra, S., *Effects of Bi and Ca Addition on the Characteristics of Eutectic Si Particles in Sr Modified 319 Alloys*. Int. J. Cast Met. Res., 2003 **15**(5): p. 551-564.
75. Kwon, I.S., Kim, J. H., Kim, K. M. and Yoon, E. P., *Effect of Ca and P on Sr Modification Treatment in Al-7wt%Si-0.3wt%Mg Alloy*. J. Korean Inst. Met. Mater., 1998. **36**(9): p. 1444-1450.
76. Kobayashi, T., Kim, H. J. and Niinomi, M., *Effect of Calcium on Mechanical Properties of Recycled Aluminium Casting Alloys* J. Mater. Sci. Technol., 1997. **13**(6): p. 497-502.
77. Kim, H.J., *Effect of Calcium on Primary Silicon Particle Size in Hypereutectic Al-Si Alloys*. J. Mater. Sci. Technol., 2003. **19**(7): p. 915-918.
78. Liu, X., Qiao, J., Wu, Y. and Bian, X., *EPMA Analysis of Calcium-Rich Compounds in Near Eutectic Al-Si Alloys*. J. Alloys Compd., 2005. **388**(1): p. 83-90.
79. Gallo, R., *Development, Evaluation and Application of Granular and Powder Fluxes in Transfer Ladles, Crucible and Reverberatory Furnaces*. 2002, Foseco. p. 8-16.
80. Dispinar, D., *Determination of Metal Quality of Aluminium and Its Alloys (Ph.D. Thesis)*. 2005, School of Metallurgy and Materials, The University of Birmingham, UK.
81. Pacz, A., *US Patent No. 1387900*. 1921.
82. Jeffries, Z., *Aluminum-Silicon Alloys*. J. Chem. Met. Eng. , 1922. **26**: p. 750-754.
83. Sintef, N. *Roadmap from Europe and North America/ Workshop on Aluminium Recycling*.  
[http://www.sintef.no/upload/Materialer\\_kjemi/dokumenter/roadmap-aluminium-recycling-web.pdf](http://www.sintef.no/upload/Materialer_kjemi/dokumenter/roadmap-aluminium-recycling-web.pdf)
84. Hegde, S., Prabhu, K. N., *Modification of Eutectic Silicon in Al-Si Alloys*. J. Mater. Sci., 2008. **43**(9): p. 3009-3027.
85. Heusler, L., Schneider, W., *Influence of Alloying Elements on the Thermal Analysis Results of Al-Si Cast Alloys*. J. Light Metals, 2002. **2**(1): p. 17-26.
86. Zalenas, D., *Aluminum Casting Technology*. 2<sup>nd</sup> ed. 1993: The American Foundrymen's Society, Inc.
87. Knuutinen, A., Nogita, K., McDonald, S. D. and Dahle, A. K., *Modification of Al-Si Alloys with Ba, Ca, Y and Yb*. J. Light Metals, 2001. **1**(4): p. 229-240.
88. Rao, P.A.K., Das, K., Murty, B. S. and Chakraborty, M., *On the Modification and Segregation Behavior of Sb in Al-7Si Alloy during Solidification*. J. Mater. Lett. , 2008. **62**(12-13): p. 2013-2016.

89. Ho, C.R., Cantor, B., *Modification of Hypoeutectic Al-Si Alloys*. J. Mater. Sci., 1995. **30**(8): p. 1912-1920.
90. Dahle, A.K., Nogita, K., Zindel, J. W., McDonald, S. D. and Hogan, L. M., *Eutectic Nucleation and Growth in Hypoeutectic Al-Si Alloys at Different Strontium Levels*. Metall. Mater. Trans. A, 2001. **32A**(4): p. 949-960.
91. Qiyang, L., Qingchun, L. and Qiful, L. , *Modification of Al-Si Alloys with Sodium*. Acta Metall. Mater., 1991. **39**(11): p. 2497-2502.
92. Dahle, A.K., Nogita, K., McDonald, S. D., Dinnis, C. and Lu, L., *Eutectic Modification and Microstructure Development in Al-Si Alloys*. J. Mater. Sci. Eng. A, 2005. **413-414**(15 December): p. 243-248.
93. Zhao, H.X., Cai, J. , *Inoculating an Al-Si Alloy with Phosphorus, Rare Earths, Sulfur*. J. Mater., 1994. **46**(11): p. 42.
94. Ullah, M.W., Carlberg, T., *Silicon Crystal Morphologies during Solidification Refining from Al-Si Melts*. The 16th International Conference on Crystal Growth (ICCG16)/The 14th International Conference on Vapor Growth and Epitaxy (ICVGE14), 2011. **318**(1): p. 212-218.
95. Atasoy, O.A., Yilmaz, F. and Elliott, R., *Growth Structures in Aluminium-Silicon Alloys I. The Coupled Zone*. J. Cryst. Growth, 1984. **66**(1): p. 137-146.
96. Bayraktar, Y., Liang, D. and Jones, H., *The Effect of Growth Velocity and Temperature Gradient on Growth Characteristics of Matrix Eutectic in a Hypereutectic Aluminium-Silicon Alloy*. J. Mater. Sci., 1995. **30**(23): p. 5939-5943.
97. Li, D., Zuo, M., Zhang, Q. and Liu, X., *The Investigation of Continuous Nucleation and Refinement of Primary Si in Al-30Si Mushy Zone*. J. Alloys Compd., 2010. **502**(2): p. 304-309.
98. Zhang, Q., Liu, X. and Dai, H., *Re-Formation of AlP Compound in Al-Si Melt*. J. Alloys Compd., 2009. **480**(2): p. 376-381.
99. Saha, D., Apelian, D. and Gupta, D. R. , *Inoculants for the Control of Primary Silicon Size and Distribution in Hypereutectic Alloys*, in *8th International Conference on Semi solid Processing of Metals and Alloys*. 2004: Limassol, Cyprus.
100. Xing, P., Gao, B., Zhuang, Y. and Liu, K. , *On the Modification of Hypereutectic Al-Si Alloys using Rare Earth Er*. Acta Metall. Sin.(Engl. Lett.), 2010. **23**(5): p. 327-333.
101. Youn, J.I., Kang, B. I., Ko, D. G. and Kim, Y. J., *Effects of Sonoprocessing on Microstructure and Mechanical Properties of A390 Aluminium Alloy*. Int. J. Cast Met. Res., 2008. **21**(1-2): p. 135-138.

102. Das, A., Kotadia, H. R., *Effect of High-Intensity Ultrasonic Irradiation on the Modification of Solidification Microstructure in a Si-Rich Hypoeutectic Al-Si Alloy*. Mater. Chem. Phys., 2011. **125**(3): p. 853-859.
103. Feng, H.K., Yu, S. R., Li, Y. L. and Gong, L. Y., *Effect of Ultrasonic Treatment on Microstructures of Hypereutectic Al-Si Alloy*. J. Mater. Proc. Technol., 2008. **208**(1-3): p. 330-335.
104. Zuo, Y.B., Fan, Z., Zhu, Q.F., Lei, L. and Cu, J.Z., *Modification of a Hypereutectic Aluminium Silicon Alloy under the Influence of Intensive Melt Shearing*. Mater. Sci. Forum, 2013. **765**: p. 140-144.
105. Hogg, S.C., Atkinson, H. V., *Inhibited Coarsening of a Spray-Formed and Extruded Hypereutectic Aluminum-Silicon Alloy in the Semi-Solid State*. Metallurgical and Materials Transactions A, 2005. **36**(1): p. 149-159.
106. Zarif, M., Mckay, B. and Schumacher, P., *Study of Heterogeneous Nucleation of Eutectic Si in High-Purity Al-Si Alloys with Sr Addition*. Metall. Mater. Trans. A, 2011. **42**(6): p. 1684-1691.
107. Yi, H., Zhang, D., *Morphologies of Si Phase and La-Rich Phase in As-Cast Hypereutectic Al-Si-xLa Alloys*. Mater. Lett., 2003. **57**(16-17): p. 2523-2529.
108. Yi, H., Zhang, D., Sakatab, T. and Morib, H., *Microstructures and La-Rich Compounds in a Cu-containing Hypereutectic Al-Si Alloy*. J. Alloys Compd., 2003. **354**(1-2): p. 159-164.
109. Mahanti, R.K., Lal, K., Sinha, A. N. and Sivaramakrishnan, C. S., *A Novel Technique for Hyper Eutectic Aluminium-Silicon Alloy Melt Treatment*. Mater. Trans., 1993. **34**(12): p. 1207-1211.
110. Iqbal, N., *Solidification: Real-Time Investigation of Grain Nucleation and Growth during Liquid to Solid Phase Transformation of Aluminum Alloys (Ph.D. Thesis)*. 2005, Faculty of Applied Sciences, Delft University of Technology, Netherlands.
111. Volmer, M., Weber, A., Phys. Chem., 1925. **119**: p. 277.
112. Becker, R., Doring, W., *Treatment of the Kinetics of Nucleation in Supersaturated Vapors*. Ann. Phys., 1935. **24**: p. 719-752.
113. Turnbull, D., *Formation of Crystal Nuclei in Liquid Metals*. J. Appl. Phys., 1950. **21**: p. 1022-1028.
114. Qian, M., *Heterogeneous Nucleation on Potent Spherical Substrates during Solidification*. Acta Metall. Mater., 2007. **55**(3): p. 943-953.
115. Yang, L., Birchenall, C. E., Pound, G. M. and Simnad, M.T., *Some Observations on Heterogeneous Nucleation of Sodium Crystals from Atomic Beams*. Acta Metall. Mater., 1954. **2**(3): p. 462-469.
116. Walton, D., *Nucleation of Vapor Deposits*. J. Chem. Phys., 1962. **37**: p. 2182.

117. Sundquist, B.E., *On “Nucleation Catalysis in Supercooled Liquid Tin”*. Acta Metall. Mater., 1963. **11**(6): p. 630–632.
118. Chalmers, B., *Principles of Solidification*. 1964, New York: John Wiley.
119. Bunn, A.M., Schumacher, P., Kearns, M. A., Boothroyd, C. B. and Greer, A. L., *Grain Refinement by Al-Ti-B Alloys in Aluminium Melts: A Study of the Mechanisms of Poisoning by Zirconium*. J. Mater. Sci. Technol., 1999. **15**(10): p. 1115-1123.
120. Talanquer, V., Oxtoby, D. W., *Heterogeneous Nucleation of Molecular and Dipolar Fluids*. Physica A: Statistical Mechanics and its Applications, 1995. **220**(1-2): p. 74-84.
121. Müller, M., *Interplay between Wetting and Miscibility in Thin Binary Polymer Films*. Comput. Phys. Commun., 2002. **147**(1-2): p. 292-297.
122. Kelton, K.F., Greer, A.L., Herlach, D. M. and Holland-Moritz, D., *The Influence of Order on the Nucleation Barrier*. Mater. Res. Bull. , 2004. **29**(12): p. 940-944.
123. Kim, W.T., Cantor, B. , *An Adsorption Model of the Heterogeneous Nucleation of Solidification*. Acta Metall. Mater., 1994. **42**(9): p. 3115-3127.
124. Ho, C.R., Cantor, B., *Heterogeneous Nucleation of Solidification of Si in Al-Si and Al-Si-P Alloys*. Acta Metall. Mater., 1995. **43**(8): p. 3231-3246.
125. Cantor, B., *Heterogeneous Nucleation and Adsorption*. Philos. Trans. Roy. Soc. A 2003. **361**(15 March): p. 409-417.
126. Fan, Z., *An Epitaxial Model for Heterogeneous Nucleation on Potent Substrates*. Metall. Mater. Trans. A, 2013. **44A**(March): p. 1409-1418.
127. Coudurier, L., Eustathopoulos, N., Desre, P. and Passerone, A., *Atomic Roughness and Chemical Adsorption to Solid-Liquid Interfaces of Binary Metal Systems*. Acta Metall. Mater., 1978. **26**: p. 465-475.
128. Liang, D., Bayraktar, Y., Moir, S. A., Barkhudarov, M. and Jones, H., *Primary Silicon Segregation during Isothermal Holding of Hypereutectic Al-18.3 wt%Si Alloy in the Freezing Range*. Scripta Mater., 1994. **31**(4): p. 363-367.
129. Manchang, G., Jun, J., Qingchun, L. and Wenquan, G., *Influences of Trace Additions of Strontium and Phosphorus on Electrical Resistivity and Viscosity of Liquid Al-Si Alloys* Trans. Nonferrous Metals Soc. China, 1997. **7**(4): p. 67-71.
130. Fareg, S.M., *Effect of Material Structure Machining Characteistics of Hypereutectic Al-Si Alloy (Ph.D. Thesis)*. 2007, Universiti Teknologi Malaysia.
131. Clarke, J., Sarkar, A. D., *Wear Characteristics of As-Cast Binary Aluminium-Silicon Alloys*. Wear, 1979. **54**(1): p. 7-16.
132. Dey, S.K., Perry, T. A. and Alpas, A. T., *Micromechanisms of Low Load Wear in an Al-18.5% Si Alloy*. Wear, 2009. **267**(1-4): p. 515-524.

133. Torabian, H., Pathak, J. P. and Tiwari, S. N., *Wear Characteristics of Al-Si Alloys*. Wear, 1994. **172**(1): p. 49-58.
134. Shi, W., Gao, B., Tu, G., Li, S., Hao, Y. and Yu, F., *Effect of Neodymium on Primary Silicon and Mechanical Properties of Hypereutectic Al-15%Si Alloy*. J. Rare Earths, 2010. **28**(1): p. 367-370.
135. Hong, S.J., Suryanarayana, C., *Mechanical Properties and Fracture Behavior of an Ultrafine-Grained Al-20 Wt % Si Alloy*. Metall. Mater. Trans. A, 2005. **36A**(13): p. 715-723.
136. Kotadia, H.R., *Solidification of Al-Sn-Cu Immiscible Alloys and Al-Si Cast Alloys Processed under Intensive Shearing (Ph.D. Thesis)*. 2010, BCAST, Brunel University, UK.
137. Saha, D., *Novel Processing Methods and Mechanisms to Control the Cast Microstructure in Al Based Alloys - 390 and Wrought Alloys (Ph.D. Thesis)*. 2005, Worcester Polytechnic Institute, USA.
138. Jong-Kyu, B., Hae-Wook, K., *Effect of Squeeze Cast Process Parameters on Fluidity of Hypereutectic Al-Si Alloy*. J. Mater. Sci. Technol. , 2008. **24**(1): p. 7-11.
139. Chen, L., Wang, D., Che, X. and Li, F., *Low-Cycle Fatigue Behavior of Permanent Mold Cast and Die-Cast Al-Si-Cu-Mg Alloys*. China Foundry, 2012. **9**(1): p. 39-42.
140. Patel, J.B., Liu, Y. Q., Shao, G. and Fan, Z., *Rheo-Processing of an Alloy Specifically Designed for Semi-Solid Metal Processing Based on the Al-Mg-Si System*. J. Mater. Sci. Eng. A, 2008. **476**(1-2): p. 341-349.
141. Ittipon, D., *Semi-Solid Processing of Hypereutectic Al-Si Alloys (Ph.D. Thesis)*. 1996, Massachusetts Institute of Technology, USA.
142. Saha, D., Apelian, D., Dadgupta, R. *SSM Processing of Hypereutectic Al-Si Alloy*. in *Proc of the 8th inter conf on semi-Solid Processing of Alloys and composites*. 2004. Limassol.
143. Birol, Y., *Cooling Slope Casting and Thixoforming of Hypereutectic A390 Alloy*. J. Mater. Proc. Technol., 2008. **207**(1-3): p. 200-203.
144. Wang, H., Ning, Z. L., Yao, X. D., Davidson, C. J. and StJohn, D., *Thixotropic Structure Formation in A390 Hypereutectic Al-Si Alloy*, in *Proc of the 8th inter conf on semi-Solid Processing of Alloys and composites*. 2004: Limassol. p. 553-561.
145. Hogg, S.C., Atkinson, H. V. and Kapranos, P., *Semi-Solid Rapid Compression Testing of Spray-Formed Hypereutectic Al-Si Alloys*. Metallurgical and Materials Transactions A, 2004. **35**(3): p. 899-910.

146. Hogg, S.C., Lambourne, A., Ogilvy, A. and Grant, P. S., *Microstructural Characterisation of Spray Formed Si-30Al for Thermal Management Applications*. Scripta Materialia, 2006. **55**(1): p. 111-114.
147. Ohmi, T., Kudoh, M. and Ohsasa, K., *Effect of Casting Condition on Refinement of Primary Crystals in Hypereutectic Al-Si Alloy Ingots Produced by Duplex Casting Process*. J. Japan Inst. Metals, 1992. **56**(9): p. 1064-1071.
148. Ohmi, T., Nakadera, K. and Kudoh, M., *Modification of Hypereutectic Al-Si Alloys by the Duplex Casting Process with Addition of Na and P*. J. Japan Inst. Light Metals, 1992. **42**(3): p. 132-137.
149. Volmer, M., Weber , A., (1925) 277, J. Phys. Chem., 1925. **119**: p. 227.
150. Doutre, D., Hay, G. and Wales, P., *Semi-Solid Concentration Processing in Metallic Alloys , US Patent No. 6,428,636* 2002.
151. <http://www.ingot.alcan.com/ingot/AlcanAluIngot.nsf>
152. Tebib, M., Morin, J. B., Ajersch, F. and Grant Chen, X., *Semi-Solid Processing of Hypereutectic A390 Alloys using Novel Rheoforming Process*. Trans. Nonferrous Metals Soc. China, 2010. **20**(9): p. 1743-1748.
153. Association, A., *Standard Test Procedure for Aluminum Alloy Grain Refiners: TP-1*. 1987, The Aluminium Association, Washington DC.
154. Do, Y.R., Dwight, K. and Wold, A., *Crystal Growth and Characterization of the Solid Solutions  $(ZnS)_{1-x}(CuMS_2)_x$  ( $M = Al$ ,  $In$ , or  $Fe$ )*. J. Chem. Mater., 1992. **4**(5): p. 1014-1017.
155. She, Y., Yang, J. and Qiu, K., *Synthesis of ZnS Nanoparticles by Solid-Liquid Chemical Reaction with ZnO and  $Na_2S$  under Ultrasonic*. Trans. Nonferrous Metals Soc. China 2010. **20**: p. 211-215.
156. Lewis, A.E., *Review of Metal Sulphide Precipitation*. Hydrometallurgy, 2010. **104** (2): p. 222-234.
157. Pennors, A., Samuel, A. M. and Dothy, H. W., *Precipitation of  $\beta$ - $Al_5FeSi$  Iron Intermatallic in Al-6% Si-3.5% Cu (319) Type Alloys: Role of Sr and P*. Trans. AFS, 1998. **106**(98-105 ): p. 251-264.
158. Lewis, J.M., Kydd, R. A. and Boorman, P. M., *A Study of Fluorided Ni-Mo/ $Al_2O_3$  Catalysts in Cumene Conversion and Thiophene HDS Reactions*. J. Catalysis, 1989. **120**(2): p. 413-420.
159. Morales, A., Ramírez de Agudelo, M. M. and Hernández, F., *Adsorption Mechanism of Phosphorus on Alumina*. Appl. Catalysis, 1988. **41**(15 July ): p. 261-271.

160. Ohmi, T., Nakadera, K. and Kudoh, M., *Undercooling and Solidification Behavior of Fluid Clumps of Second-Poured Melt of Hypereutectic Al-Si Alloy in Duplex Casting Process*. J. Japan Inst. Light Metals, 1994. **44**(2): p. 91-96.
161. Gill, R., *Modern Analytical Geochemistry: An Introduction to Quantitative Chemical Analysis for Earth, Environmental and Materials Scientist*. 1997, Harlow, England: Wesley Longman Ltd.
162. Goodhew, P.J., Humphreys, F. J. and Beanland, R., *Electron Microscopy and Analysis, 3<sup>rd</sup> Edition*. 2001: Taylor and Francis.
163. Qiao, J., Liu, X., and Bian, X., *Relationship between Microstructures and Contents of Ca/P in Near-Eutectic Al-Si Piston Alloys*. J. Mater. Lett., 2005. **59**(14-15): p. 1790-1794.
164. Mayuki, M., *Sources of Phosphorus and Shrinkage Characteristics of Al-Si Alloy*. J. Japan Foundry Eng. Soc., 2002. **74**(6): p. 383-387.
165. Al-Helal, K., Stone, I. C. and Fan, Z., *Simultaneous Primary Si Refinement and Eutectic Modification in Hypereutectic Al-Si Alloys*. Trans. Indian Inst. Metals, 2012. **65**(6): p. 663-667.
166. Kobayashi, K., Hogan, L. M., *Fivefold Twinned Silicon Crystals Grown in an Al-16wt%Si Melt*. J. Phil. Mag. A, 1979. **40**(3): p. 399-407.
167. Delhez, R., Keijser, T. H., Mittemeijer, E. J., Mourik, P., Pers, N. M., Katgerman, L. and Zalm, W. E., *Structural Inhomogeneities of Al/Si Alloys Rapidly Quenched from the Melt*. J. Mater. Sci., 1982. **17**(10): p. 2887-2894.
168. Wang, W., Bian, X., Qin, J. and Syliusarenko, S. I., *The Atomic-Structure Changes in Al-16 Pct Si Alloy above the Liquidus*. Metall. Mater. Trans. A 2000. **31**(9): p. 2163-2168.
169. Calvo-Dahlborg, M., Popel, P. S., Kramer, M. J., Besser, M., Morris, J. R. and Dahlborg, U., *Superheat-Dependent Microstructure of Molten Al-Si Alloys of Different Compositions Studied by Small Angle Neutron Scattering*. J. Alloys Compd., 2013. **550**(15 February): p. 9-22.
170. Bernal, J.D., *Geometrical Approach to the Structure of Liquids*. Nature, 1959. **183**(17 January ): p. 141-147.
171. Xu, C.L., Wang, H. Y., Liu, C. and Jiang, Q. C., *Growth of Octahedral Primary Silicon in Cast Hypereutectic Al-Si Alloys*. J. Cryst. Growth, 2006. **291**(2): p. 540-547.
172. Wang, R.Y., Lu, W.H. and Hogan, L.M., *Twin Related Silicon Crystal in Al-Si Alloys and Their Growth Mechanism*. J. Mater. Sci. Technol., 1995. **11**(5): p. 441-449.

173. Wang, R.Y., Lu, W. H. and Hogan, L. M., *Faceted Growth of Silicon Crystals in Al-Si Alloys*. Metall. Mater. Trans. A, 1997. **28**(5): p. 1233-1243.
174. Hellawell, A., *The Growth and Structure of Eutectics with Silicon and Germanium*. Progress Mater. Sci., 1970. **15**(1): p. 3-78.
175. Wagner, R.S., *On the Growth of Germanium Dendrites*. Acta Metall. Mater., 1960. **8**(1): p. 57-60.
176. Crosley, P.B., Mondolfo, L. F., *The Modification of Aluminum-Silicon Alloys*. Mod. Cast., 1966. **46**(March): p. 89-100.
177. Li, J.H., Schumacher, P., *Effect of Y Addition and Cooling Rate on Refinement of Eutectic Si in Al-5wt%Si Alloys*. Int. J. Cast Met. Res., 2012. **25**(6): p. 347-357.
178. Jenkinson, D.C., Hogan, L. M., *The Modification of Aluminium-Silicon Alloys with Strontium*. J. Cryst. Growth, 1975. **28**(2): p. 171-187.
179. Schlesinger, M.E., *The Thermodynamic Properties of Phosphorus and Solid Binary Phosphides*. Chem. Rev. , 2002. **102**(11): p. 4267-4301.
180. Alapati, S.V., Johnson, J. K. and Sholl, D. S., *Identification of Destabilized Metal Hydrides for Hydrogen Storage Using First Principles Calculations*. J. Phys. Chem. B, 2006 **110**(17): p. 8769-8776.
181. Al-Helal, K., Stone, I. C. and Fan, Z., *Effect of Ca Level on the Formation of Silicon Phases during Solidification of Hypereutectic Al-Si Alloys*. Mater. Sci. Forum, 2013. **765**: p. 117-122.
182. Daniels, E.J., Bonsignore, P. V. in *Light Metals Conference*. 1995. Warrendale, PA: Metals and Materials Society/AIME.
183. Hekmat-Ardakan, A., Ajersch, F., *Microstructure Modification of Al-17%Si Alloy by Addition of Mg*. J. Mater. Sci., 2011. **46**(7): p. 2370-2378.
184. Sainz, M.A., Mazzoni, A. D., Aglietti, E. F. and Caballero, A., *Thermochemical Stability of Spinel ( $MgO \cdot Al_2O_3$ ) under Strong Reducing Conditions*. Mater. Chem. Phys., 2004. **86**(2-3): p. 399-408.
185. Shou-Yong, J., Li-Bin, L., Ning-Kang, H., Jin, Z. and Yong, L. , *Investigation on Lattice Constants of Mg-Al Spinels*. J. Mater. Sci. Lett. , 2000. **19**(3): p. 225-227.
186. Tsumura, Y., *Effect of 20 Adding Elements on Silumin*. J. Japan Inst. Light Metals 1955. **1955**(17): p. 51-70.
187. Bührer, W., Bill, H., *Lattice Dynamics of  $Na_2S$* . J. Phys. C: Solid State, 1980. **13**(50): p. 5495-5504.

188. Wang, J., Zhang, Y., Feng, C., Li, J. and Li, G., *Adsorption Capacity for Phosphorus Comparison among Activated Alumina, Silica Sand and Anthracite Coal*. J. Water Resource and Protection, 2009. **4**: p. 260-264.
189. Zhang, L., Hong, S., He, J., Gan, F. and Ho, Y., *Isotherm Study of Phosphorus Uptake from Aqueous Solution Using Aluminum Oxide*. Clean-Soil, Air, Water 2010. **38**(9): p. 831-836.
190. Hurley, T.J., Atkinson, R.G. , *Effects of Modification Practice on Aluminum A356 Alloys*. AFS Trans., 1985. **93**(85-39): p. 291-296.
191. Jones, W.R.D., Bartlett, W.L., *The Viscosity of Aluminium and Binary Aluminium Alloys*. J. Inst. Metals, 1952. **81**(11): p. 145-152.
192. Dai, H., Du, J., Wang, Li, Peng, C. and Liu, X., *First-Principle Study of the Al/Pt Interfacial Adhesion*. Physica B: Condensed Matter., 2010. **405**(2): p. 573-578.